Malarial Parasite Infection Compromises Gastrointestinal Defenses Against Enteric Pathogens

By

GREGORY THOMPSON WALKER
DISSERTATION

Submitted in partial satisfaction of the requirements for the degree of

DOCTOR OF PHILOSOPHY

in

Microbiology

in the

OFFICE OF GRADUATE STUDIES

of the

UNIVERSITY OF CALIFORNIA

DAVIS

Approved:

Renée Tsolis PhD, Chair

Charles Bevins MD PhD

Stephen McSorley PhD

Committee in Charge

2021

ACKNOWLEDGEMENTS

I would like to start by acknowledge the many, many people who in some way contributed to making this work possible.

First, I want to show my appreciation for all the scientists who have mentored and guided me to this point. My dissertation mentor Dr. Renée Tsolis, for bringing me into the lab, challenging me to pursue the questions I believed were important and supporting my research plans- even as the answers proved less obvious than we had initially hoped. Dr. Andreas Bäumler, for involving me in collaborations beyond the scope of this work that have further shaped my research interests. My committee, Dr. Charles Bevins and Dr. Stephen McSorley, for their insights and suggestions that helped guide my studies, and their support of me as a scientist. My first P.I.s, Dr. Jennifer Lewis and Dr. Scott Dawson, for emboldening me to consider pursuing research in the first place. And finally, my amazing colleagues and friends from the Tsolis and Bäumler labs, for their energy, their insights, their willingness to always help out, and their ability to make my time working in the lab wonderful.

Additionally, thank you to my friends and family who have supported me through this PhD journey. My family, especially my parents Tim and Victoria and sister Allie, for always offering love and encouragement. And my friends outside academia, particularly Amy, Christie, Clara, Derek, Jake, Janice, Joe, Jonathan, Kat, Larry, Louisa, Mandy, Meeza, Nic, Reid and Rizal- for keeping me sane, laughing, and always being there for each other. I am so grateful for all you have done, especially through this past year.

DEDICATION

This work is dedicated to the teachers who nurtured my curiosity for discovering the stories of biology and a passion for science.

And to the memory of my friend Jonathan, who was always excited to learn something new.

Table of Contents:

Abstract

Though generally associated with the etiology of gastroenteritis, non-typhoidal *Salmonella* (NTS) serovars such as *Salmonella enterica* serovar Typhimurium are also frequently linked to disseminated infections in sub-Saharan Africa, commonly referred to as invasive NTS disease (iNTS). Epidemiological evidence has identified malaria in children as a significant risk factor for the development of iNTS. Prior studies discovered that *Plasmodium* infections in mice can transiently alter the commensal microbial flora and increase the initial colonization of enteric *S.* Typhimurium infections. In order to better understand how malaria impacts susceptibility to enteric pathogens, I further assessed the effects of *Plasmodium yoelii* infection on the mouse intestine. Although my studies confirmed that *P. yoelii* infection could impact the gut microbiota, changes in abundance of microbial taxa were not obviously correlated with increasing implantation levels of *S.* Typhimurium. Rather, *P. yoelii* was found to induce hypochlorhydria dependent on TNF-α signaling that impairs gastric defense against orally inoculated *S.* Typhimurium. Additionally, my investigation found that levels of endogenous *Enterobacteriaceae*, particularly *Escherichia coli*, consistently increase in the intestines during *P. yoelii* infection. Neither reduction in gastric acid alone nor *E. coli* utilization of increased levels of inflammation-associated nitrate could explain the bloom. However, a similar outgrowth of intestinally colonized avirulent *S.* Typhimurium was dependent on *acrAB*, vital components of a multidrug efflux pump (AcrAB-TolC) common to Enterobacteriaceae that is known to provide bile acid resistance. I determined that both *P. yoelii* infection and induction of hemolysis alone impacted the intestinal bile composition, and phenylhydrazine-induced hemolysis was sufficient to stimulate the *E. coli* expansion. The hemolysis-associated *E. coli* bloom was also dependent on functional siderophore uptake systems, as a *tonB* mutant did not expand and was outcompeted by wildtype *E. coli* in mice that were treated with phenylhydrazine. Together, these data suggest that both hemolysis-associated shifts in the gut metabolome and the immune

response to the *Plasmodium* parasite contribute to enhanced susceptibility to *S.* Typhimurium implantation and colonization. My work highlights the critical role of oft-overlooked non-immunological antibacterial defenses in resisting enteric colonization and illustrates how *Plasmodium* can impact unexpected aspects of physiology that influence susceptibility to secondary infections.

Chapter 1

Factors contributing to invasive bacterial infection by non-typhoidal *Salmonella*

Introduction: *Salmonella enterica*

Salmonella enterica (subsp. *enterica*) is a species of Gram-negative, motile gastrointestinal and intracellular pathogens of the family *Enterobacteriaceae* generally associated with foodborne illness in humans. A close relative of the common intestinal inhabitant/pathogen *Escherichia coli* (diverging approximate 100 million years ago) (*1, 2*), *S. enterica* has evolved into numerous, genetically divergent serovars defined by their expression of outer membrane antigens that are broadly grouped based on typical disease presentation in otherwise healthy populations (*3*).

The typhoidal serovars, including *S. enterica* serovar Typhi (*S.* Typhi) and the Paratyphi A, B, and C serovars are the causative agents of enteric (sometimes known as typhoid or paratyphoid) fever (*4-7*). These serovars are strictly adapted to causing disease in humans (*7, 8*). During infection, typhoidal *Salmonella* invades the host from the intestine, disseminating via the blood and lymph to systemic tissues (spleen, liver, and bone marrow) with apparently minimal activation of the host's innate inflammatory defenses. Immune detection of the pathogen in these extraintestinal sites then results in the characteristic enteric fever, which can take weeks to resolve (*5*). A small proportion (less than 5%) of *S.* Typhi-infected hosts develop a chronic carriage of the bacteria in their gallbladder, serving as a reservoir for the pathogen where it can intermittently seed the intestinal lumen and be shed in feces for continued transmission to new hosts (*7*).

The remainder of serovars are broadly categorized as non-typhoidal *Salmonella* (NTS) and account for the vast majority of *Salmonella* infections worldwide (*6*). In contrast to typhoidal serovars, NTS are zoonotic generalists, with a breadth of mammalian and avian reservoirs (*9*).

In healthy populations, these NTS infections cause a severe inflammation in the intestinal lining known as gastroenteritis, which results in a rapid onset of symptoms including diarrhea and cramping (*3*). Reasons for this strikingly distinct presentation have been linked to genetic differences found between typhoidal and NTS strains. Many differences found in typhoidal varieties are adaptations to a "stealthier" lifestyle in humans, including the acquisition of the *viaB* locus-encoded Vi polysaccharide capsule (*10-15*) and reduced expression of virulence factors easily recognized by host cells as pathogen-associated molecular patterns (PAMPs), such as flagellin, to limit detection of extraintestinal by the immune system (*16, 17*). Despite sharing many genetic signatures contributing to invasiveness, the typhoidal and paratyphoidal serovars do not actually form an evolutionary clade separate from the non-typhoidal serovars, and rather seem to have evolved these similar adaptations to a host-restricted invasive lifestyle through convergent genome degradation and horizontal gene transfer (*6, 18*).

The most common NTS infections in humans involve the serovars *S.* Typhimurium and *S.* Enteritidis, though other serovars have also been linked to gastroenteritis outbreaks (*19, 20*). While the majority of infections with NTS serovars worldwide cause gastroenteritis, a small but notable share of NTS infections result in an extraintestinal disease. These so-called invasive NTS (iNTS) infections cause bacteremia or meningitis that is significantly more lethal than typical gastroenteritis (*21-24*). While iNTS infections are thought to make up less than 2.0% of the 94-155 million annual NTS infections that cause disease worldwide, iNTS-associated bacteremia likely accounts for more than half of all NTS-associated deaths, with an estimated 63,000 to 681,000 from NTS bacteremia versus 56,000 to 155,000 from gastroenteritis (*6, 25, 26*). This corresponds to a high apparent mortality rate of approximately 20% overall for NTS bacteremia, compared to the less than 0.2% mortality from gastroenteritis and less than 4.0% mortality for enteric fevers.

Globally, invasive NTS is typically associated with immunocompromised populations (*25*). In high income settings, risk factors include old age (>65 years), chronic disease, gastric

hypochlorhydria, and the use of immunosuppressive drugs including corticosteroids and chemotherapy (*26*). However, iNTS disproportionately impacts populations in sub-Saharan Africa, with over 1.9 million of the 3.4 million annual cases and an estimated 390,000 of the 681,000 deaths in 2010 originating there (*25, 26*). Epidemiological surveillance in Africa has pointed to a number of additional risk factors and comorbidities that seem to make iNTS disease hyperendemic in the region (*27*). In these studies, invasive NTS was most predominant in young children (< 2 years old) and HIV-infected adults (*25, 28-30*). Within the younger population, primary risk factors for iNTS include malnutrition, HIV infection, and malaria (*31-33*). In addition to these immunocompromising conditions, bloodstream isolates of the non-typhoidal serovars infecting patients with sepsis in Africa have been investigated and found to be phylogenetically distinct from NTS serovars more associated with gastroenteritis in the rest of the world. Of particular note are isolates of the sequence type (ST)313, a set of *S.* Typhimurium forming a clade of lineages with notable genetic alterations compared to the ST19 serovars common to gastroenteritis outbreaks. These ST313 isolates appear to have largely evolved in Africa (*34, 35*) and along with acquiring resistance to multiple antibiotics, display numerous signs of adaptation to an invasive or potentially host-restricted lifestyle (*36*), with genomic changes often echoing alterations associated with typhoidal serovars (*37, 38*). Yet, it is uncertain to what degree this genetic divergence in African NTS serovars reflects active evolution towards a more invasive human pathogen versus genomic degradation due to lack of selection for gastroenteritis-associated pathology over decades of passage through immunocompromised hosts.

In the past 20 years, researchers have investigated how these various risk factors- including HIV (*39*), malnutrition (*40*), malaria and other anemias (*41*), as well as serovar adaptations associated with iNTS disease (*26, 42*)- can impact the progression of non-typhoidal *Salmonella* infections in animal and *in vitro* models. These studies provide insights that may allow for improved or context-dependent interventions against iNTS. The goal of this chapter is

to summarize and review how these potential mechanisms may alter the course of a non-typhoidal *Salmonella* infection to result in an invasive bacterial infection, rather than gastroenteritis, with a primary focus on the impacts of malaria on *S.* Typhimurium strains.

How iNTS risk factors can exacerbate extraintestinal NTS

To better understand how immunocompromising conditions associated with iNTS disease impact the outcome of infection, it is useful to consider the course of a standard NTS infection such as *S.* Typhimurium that results in gastroenteritis in otherwise healthy human populations. Potential effects of the risk factors on the immune system that can interfere with the response to invading NTS will then be discussed.

NTS infection in the healthy host

Non-typhoidal *Salmonella* is primarily transmitted via the fecal-oral route and colonizes the ileal and colonic lumen and mucosae to cause disease. As such, it must survive both environmentally, and through a gauntlet of innate host defenses throughout the stomach and small intestine, then overcome colonization resistance provided by the endogenous intestinal microbiota in order for an infection to successfully implant in the gut. *S.* Typhimurium achieves this outcome through engineering of their new gastrointestinal ecosystem, exploiting host responses of intestinal inflammation to generate new growth niches it can use to compete with the local microbial community.

To this end, the critical virulence factors used by *S.* Typhimurium for pathogenesis are a pair of type-III secretion systems (T3SS-1 and T3SS-2) that enable the pathogen to directly interact with host cells. T3SS-1, encoded by the *Salmonella* pathogenicity island 1 (SPI-1) locus, allows for invasion of the intestinal epithelium (*43*). The T3SS-2, encoded by SPI-2, is involved in survival outside of the gut in host cells, particularly phagocytes (*44*). Both systems secrete effector proteins encoded by their respective loci that are injected into the host cell's

cytosol to induce functions. The T3SS-1 effectors induce uptake of the pathogen by epithelial cells (*45*), while T3SS-2 effectors generally promote intracellular replication and the spread of NTS through host tissues, allowing for significant dissemination in some animal reservoirs (*43*). These secretion systems and effectors are necessary for NTS to produce substantial intestinal inflammation through manipulation of the host cytokine response (*46*).

In the prototypical infection, *S.* Typhimurium travels through Microfold (M) cells in the Peyer's patches of the ileal epithelium to the lamina propria using its T3SS effectors, where it either reaches the bloodstream or is engulfed by local dendritic cells and macrophages. These APCs detect *S.* Typhimurium PAMPs, including LPS and lipoprotein, triggering TLR-receptor mediated MYD88 signaling and NF-κB-dependent production of pro-inflammatory cytokines such as IL-1β, IL-18, and critically, IL-23. IL-23 signals to local cells, including CD4+ Th17 cells, to stimulate the release of IL-17 and IL-22 (*47*). IL-17 and IL-22 signaling on epithelial cells induces the release of CXC chemokines, which attracts neutrophils to the intestine that release antimicrobial proteins and phagocytose *Salmonella*, using oxidative bursts via NADPH oxidase to kill the pathogen (*48*) and potentially generating neutrophil extracellular traps (NETs) (*49*). However, these host immune responses seemingly meant to clear out *Salmonella* end up doing more harm than good, impairing critical members of the colonic microflora and interfering with colonization resistance against *Salmonella* in the intestinal lumen (*50*). This pattern of epithelial invasion, pathogen recognition, and immune cell recruitment to the intestine resulting in diarrhea ultimately benefits *Salmonella* through the generation of numerous growth niches that non-typhoidal serovars like *S.* Typhimurium has evolved to make use of (discussed below). The inflammatory response promotes massive expansion of *Salmonella* population, enhancing continued transmission to subsequent hosts (*51*).

Impacts of iNTS risk factors on the mucosal and systemic NTS immune response

Significant research *in vitro* and work modeling co-morbidities using mice and non-human primates has suggested mechanistic interactions that help explain how the various epidemiologically associated risk factors for iNTS disease can actually enhance the likelihood and severity of extraintestinal infections with the pathogen.

Malaria is the disease caused by bloodborne infections of the parasite *Plasmodium*, the leading cause of parasitic deaths (*52*) and endemic in sub-Saharan Africa. The parasite is transmitted from host to host by bites of the *Anopheles* mosquito, which can ingest *Plasmodium* when it feeds on an infected animal. In the mosquito, the parasite localizes to the salivary glands, where sporozoites can be injected into the skin of a new host via the mosquito's saliva (*53*). *Plasmodium* parasites then travel through the blood to the liver, replicating and maturing into schizonts inside hepatocytes for a short time (1-3 weeks) before rupturing the cells and re-entering the bloodstream as infectious merozoites, beginning the erythrocytic stage of infection. Here, the merozoites re-enter circulation and infect red blood cells (RBCs), differentiating into ring-stage trophozoites, multiplying into schizonts and rupturing the cells, which release the matured merozoites that can go on to infect more RBCs. This cycle can generate a profound anemia that, along with the buildup of parasite waste (hemozoin), lysed RBC fragments, and localized inflammatory responses to parasitized RBCs sequestered in tissue vasculature, results in widespread pathologies and symptomatic disease. These symptoms typically include the characteristic relapsing fever, headaches and joint paint, vomiting, and jaundice, but infections can also develop dangerous complications including severe malarial anemia, acute respiratory distress syndrome, cerebral malaria, and organ failure (*54*).

The impact of concurrent *Plasmodium* infection on the severity and lethality of *S.* Typhimurium has long been appreciated (*55*), but more recent studies using mouse models of *Plasmodium-Salmonella* co-infection have pointed to specific host-parasite interactions that disrupt intestinal barrier functions and blunt the immune response to NTS (reviewed extensively by Mooney *et al* (*41*)). While human malaria involves the parasite species *P. falciparum, P.*

vivax, P. ovale, P. malariae, and *P. knowlesi* (*53*), these species will not cause symptomatic disease in mice so rodent *Plasmodium* species such as *P. berghei, P. chabaudi,* and *P. yoelii* are used to model blood stage disease and complications of *Plasmodium* infection (*56, 57*). Mice co-infected with *P. yoelii* and *S.* Typhimurium displayed higher systemic *Salmonella* burdens (*58-61*) due to multiple related mechanisms. *P. yoelii* infection was associated with ileal mast cell recruitment and heightened plasma histamine levels that increased intestinal permeability (*60, 62*). Increased ileal mast cell counts and histamine levels were also confirmed in *P. fragile*-infected rhesus macaques (*62*), suggesting normal barrier functions to systemic bacterial infections can be impaired by malaria. A separate study utilizing the ligated ileal loops from the rhesus macaques found the mucosal response to *S.* Typhimurium was blunted by *Plasmodium*, with reduced pathology and expression of inflammatory cytokines IL-8, IL-17, and IFNγ in response to the bacteria (*63*). In a secondary line of evidence using mice, this inhibition of *S.* Typhimurium-induced inflammation was linked to increased expression of the immunomodulatory cytokine IL-10 as part of the response to *Plasmodium*, as IL-10 antibody blockade during parasite infection could rescue inflammatory signaling and limited *Salmonella* dissemination (*63*). IL-10 signaling also seems to inhibit systemic limitation of *S.* Typhimurium by myeloid cells (*61*). Additionally, hemolysis that occurs during *Plasmodium* infection may partially explain the increased burden in systemic tissues (*58, 64*). This could be specifically linked to heme degradation by heme oxygenase (HO-1) generating carbon monoxide and biliverdin that inhibit neutrophil oxidative burst (*59*). Additionally, iron accumulation in macrophages during *Plasmodium*-associated hemolysis was found to promote growth of intracellular *Salmonella* and blunted bactericidal capacity (*65*). As induction of IL-10 and HO-1 during hemolysis are also common aspects of malaria in human populations (*66-68*), these findings could represent shared mechanisms contributing to increased invasion and inability to appropriately control extraintestinal NTS during malaria.

While malaria is associated with one type of anemia that has been directly implicated in iNTS, additional anemias are actually fairly common in Africa and have been linked to bacteremia as well (*69-71*). Sickle cell anemia is a chronic hemolytic anemia caused by a point mutation in the hemoglobin gene, resulting in polymerization of hemoglobin when bound to oxygen that produces the elongated "sickled" RBC with impaired vascular flow that result in occlusion, ischemia, and intravascular hemolysis (*72, 73*). HO-1 activation in children with sickle cell anemia has been shown to impair neutrophil oxidative burst, potentially enhancing NTS extraintestinal survival in a similar manner to malaria (*74*). In a rarer set of inherited hemoglobin disorders, the thalassemias- particularly β-thalassemia- anemia onsets due to genetic alterations or absence of the β-globin chain (*75*). Thalassemias are also associated with enhanced risk for developing bacteremia (*71*), and a knockout mouse model of thalassemia was more susceptible to *S.* Typhimurium and *Listeria monocytogenes* infections (*76*). This link was hypothesized to be due to tissue iron overload, a consistent feature of thalassemias (*71*). Additionally, transfusions in thalassemia patients may result in secondary iron overload that can promote bacteremia, as iron fortification has been associated with enhancement of extraintestinal infections (*77, 78*).

It is unclear to what degree nutritional iron deficiencies, a major cause of anemia, contribute to or actually protect from invasive infections (*79*). However, other forms of malnutrition have been consistently positively associated with severe NTS infection (*21, 23, 80*), though mechanistic studies to define this interaction are lacking. Presumably, one factor could be that immune development and maintenance depends on proper nutrition (*81*). One study found that a protein-deficient diet in mice (modeling kwashiorkor) reduced survival during *S.* Typhimurium challenge (*82*). At the level of micronutrient malnourishment, vitamin A is known to be important for functional innate and adaptive immunity (*83*) and is a common deficiency in children in sub-Saharan Africa (*84*). A diet lacking vitamin A was found to exacerbate disseminated *S.* Typhimurium infections in mice, and vitamin A supplementation in deficient

mice improved outcomes (*40*), suggesting that critical vitamin deficiencies could contribute to malnourishment-associated iNTS. Intriguingly, recent research has suggested that malnutrition can also worsen pathologies associated with other risk factors. Malnourished mice on a low protein, zinc- and iron-deficient diet displayed slightly more resilience to a *P. chabaudi* infection, but also showed increased levels of intestinal inflammatory markers and reduced intestinal barrier function (*85*) than with infection or malnutrition alone, indicating multiple risk factors can combine to even further amplify risk for iNTS infections. Ultimately, more research will be needed to identify specific nutrient deficiencies that alter NTS infection outcomes.

As its name implies, the human immunodeficiency virus (HIV) leads to severe immunocompromise and is associated with the majority of iNTS cases in African adults (*26*). The virus targets CD4 receptor-expressing cells- primarily CD4+ T cells, but also some populations of monocytes and macrophages, inducing their severe depletion in infected hosts (*86*). This could clearly limit the capacity of the immune system to clear extraintestinal *Salmonella*, but additionally has been found to curb the mucosal immune response. In a SIV-infected rhesus macaque model, CD4+ Th17 cells in the intestinal mucosa were depleted, which are critical for producing IL-17 and IL-22 during *S.* Typhimurium infection for neutrophil recruitment that limits systemic invasion (*39*). Furthermore, mucosal tissues during SIV infection show a dampened expression of pattern recognition receptors (PRRs), particularly TLR4, which could reduce innate detection of *S.* Typhimurium PAMPs by SIV- or HIV-infected hosts (*87*).

The reduced ability for NTS to generate significant intestinal inflammation in the immunocompromised host prevents significant gastroenteritis and may have helped select for alterations in local NTS strains circulating in Africa with a reduced capacity for immune activation and competition in the intestinal lumen and a greater aptitude for invasive infection. African *S.* Typhimurium ST313 bloodstream isolates show significant genomic change relative to ST19 strains associated with most gastroenteritis worldwide. The primary virulence determinant promoting the broad success of ST313 seems to be multi-drug resistance (*36*).

Sampling of NTS associated with bloodstream infections from multiple sites in Africa since 1966 shows that replacement of ST19 isolates with ST313 isolates corresponded most strongly with the acquisition of antimicrobial resistance to chloramphenicol by the ST313 lineage II (L2) (*88*). Chloramphenicol resistance is associated with acquisition of the *cat* resistance gene, encoded on the virulence plasmid pSLT-BT, but isolates from ST313 L2 also display resistances to other common first-line antibiotics including to ampicillin, trimethoprim/sulfamethoxazole, and streptomycin (*34, 89, 90*). With this resistance factor, significant genome degradation and host adaptation could occur.

In infection studies using the isolates, representative ST313 isolates have been shown to cause less intestinal inflammation and do more poorly in the gut than ST19 strains in chickens and macaques (*91, 92*). *In vitro* macrophage infections and transcriptomic profiling suggests this phenotype may be due to reduced expression of immunogenic flagellin (*fliC*) or the SPI-1 effector *sopE2* (*42*). This latter alteration seemed to correspond with the finding that ST313 isolates were less invasive of epithelial cells, indicating alternate mechanisms of invasion associated with iNTS risk factors- for example, loss of epithelial barrier functions with malaria or HIV- could be sufficient. Despite reduced epithelial cell invasion, ST313 isolates were found to disseminate more rapidly out of the intestine in chicken and mouse models of infection (*91-93*). This may be due in part to the pseudogenization of the SPI-2 effector *sseI* in ST313 speeding up D23580 dissemination inside infected immune cells (*38*), since functional *sseI* has been shown to interfere with migration patterns of infected cells to lymph nodes (*94*).

Exciting recent work has also uncovered changes that could actually contribute to increased systemic survival and immune evasion by disseminating ST313 isolates. Hammarlöf and colleagues found a SNP in the promoter of the gene *pgtE* that results in increased expression of the protease by the ST313 isolate D23580. PgtE helps *S.* Typhimurium degrade complement components deposited on the bacteria in the blood. Increasing PgtE levels thus reduces complement-based killing and immune activation, promoting serum resistance (*95*).

The finding strongly suggests that ST313 isolates are being selected for improved extraintestinal survival. However, it is important to note that while research has suggested ST313 isolates are perhaps less inflammatory in animal models and cultured cells, the ST313 lineage is still capable of causing diarrhea and gastroenteritis in otherwise healthy humans (*96, 97*), suggesting only partial transition to an extraintestinal pathogenic lifestyle. In fact, a separate lineage of ST313 has been identified circulating in the United Kingdom and is not associated with systemic disease (*98*). This, more than most other evidence, is a sign of the significance of the immunocompromising risk factors in the actual development of iNTS disease.

How iNTS risk factors can impact innate & intrinsic intestinal defense

While significant research has indicated mechanisms by which the host response to malaria and other iNTS risk factors results in immunomodulation and immunocompromise that promotes iNTS, a subset of work has additionally suggested that some aspects of these comorbidities could be altering the gut environment prior to NTS infection, possibly benefitting the initial colonization and intestinal competition of the ingested pathogen (*99*). These factors may be useful for colonization of hosts by the *S.* Typhimurium ST313 isolates deficient in triggering inflammatory responses for intestinal growth, by enhancing both the establishment and transmission of NTS infections in the gut.

The Stomach: First Line of Defense

In foodborne bacterial infections, gastric acid provides a frontline defense against ingested pathogens reaching the intestines (*100, 101*). While it also promotes proper digestion and mineral absorption, the killing of microbes by gastric acid has long been an appreciated effect (*102-104*) and is potentially the factor that most strongly selected for high gastric acidity (*105*). The human stomach naturally harbors few bacteria (< 10^4 per mL content) (*106*), predominantly due to the strongly acidic environment of the lumen (pH < 3). Abnormally low

levels of gastric acid secretion (hypochlorhydria) or the absence of secretions (achlorhydria) has been consistently associated with overgrowth of gastric bacteria and shifts in intestinal microbial communities (*107-109*).

Production of low pH in the gastric lumen is the duty of corpus-associated parietal cells, which use a specialized H+,K+-ATPase (ATP4A/B) proton pump to actively secrete hydrochloric acid (HCl) into the stomach when stimulated, killing the vast majority of ingested bacteria (*101, 103*). Secretion can be inhibited pharmacologically via blockade of stimulation (e.g. histamine H2 receptor antagonists) or direct interference with the ATPase using proton pump inhibitors (PPIs) such as omeprazole. The use of PPIs has been associated with enhanced likelihood of enteric pathogen infections (*110-112*), including *Salmonella* (*113, 114*). Interestingly, *Salmonella* and *E. coli* genomes encode pH-response regulation systems governed by Fur, OmpR, PhoP and RpoS that enable acid tolerance, with additional acid resistance mechanisms in *E. coli* (*115*). However, these are perhaps most useful for survival in moderately acidic environments (pH > 3.0), rather than the comparatively extreme pH in the stomach. Consistent with this supposition, mouse models have provided evidence that *Enterobacterales* including *S.* Typhimurium are sensitive to killing by stomach acid, and inhibition of acid secretion enhances pathogen survival and intestinal implantation (*101*).

PPIs are unlikely to be as widely prescribed in sub-Saharan Africa as in Western countries (*116, 117*). Still, considering this clear link between stomach acidity and the likelihood of intestinal infection, iNTS risk factors negatively impacting gastric acid levels could promote co-infection with NTS and potentially other acid-sensitive intestinal pathogens. It has also been found that HIV may exacerbate *Helicobacter pylori*-associated hypochlorhydria through increased induction of gastritis (*118*). Additionally, our own research suggests that the host immune response during *Plasmodium* infection in mice results in a reduction in gastric acidity that promotes implantation of secondary bacterial infection in the gut (currently unpublished results; see Chapter 3). This finding suggests parasite-associated hypochlorhydria could

promote human-to-human transmission in malaria-endemic populations, without the need for *Salmonella* to generate significant gastroenteritis for growth. Conversely, work on other frequent causes of anemia in Africa has indicated that sickle cell disease is not associated with reduced gastric acid secretion in response to histamine stimulation (*119*). Still, the overall prevalence of hypochlorhydria in populations at high risk for iNTS is uncertain.

Some studies have indicated that starvation is associated with achlorhydria (*120*), which tracks with research on how macronutrient detection in the stomach and small intestine influences proton pump-activation signaling (*103*). Interestingly, chronic hypochlorhydria and achlorhydria have been shown to promote certain forms of malnutrition. Chronic hypochlorhydria is associated with small intestinal bacterial overgrowth (SIBO), which can divert energy from food to bacterial metabolism instead of host metabolism (*121*). Additionally, achlorhydria has been identified as a cause of iron deficiency (*122*). Although low gastric acidity has long been associated with “pernicious” anemia (vitamin B12 deficiency) (*123*), this is presumably not a causal relationship, but separate symptoms resulting from gastritis and destruction of parietal cells that secrete both HCl and intrinsic factor into the stomach, allowing for proper absorption of B12 (*124*).

In addition to the potential of malaria or HIV-associated gastritis to promote pathogen survival through the stomach, the representative ST313 isolate D23580 has been shown to be slightly more acid-tolerant than ST19 strain SL1344 in an *in vitro* tolerance comparison (increased survival after pH 3.5 exposure). This could suggest adaptation to higher levels of acid, though the associated mechanism was not explored (*93*). However, in our hands D23580 displayed approximately equivalent survival in low pH as the ST19 strain IR715 (ATCC 14028s), with minimal survival of either strain after 1 hour of incubation at pH 3 or below (unpublished findings). Altogether, currently known phenotypic differences in ST313 do not particularly suggest adaptations that significantly impact gastric survival.

The Small Intestine: Antimicrobials Abound

Once it was reaching the small intestine, *Salmonella* encounters what could be a more hospitable environment than the stomach, with a generally less acidic pH but similarly low levels of competing microbes, and an abundance of proteins and simple monosaccharides and disaccharides yet to be absorbed (*106, 125, 126*). However, the small intestine also has numerous host-derived habitat filters that select for the established microbiota and limit colonization of pathogen. For many bacteria, these filters could include the fairly oxygenated lumen that inhibits strict anaerobes, though NTS are facultative anaerobes and thrive in higher oxygen environments (*127*). Another selective pressure in the small intestine is the high concentrations of bile acids secreted from the gallbladder into the duodenum to aid in digestion of fats (*128*). Bile acids are amphipathic cholesterol-derived molecules that destabilize bacterial cell membranes; thus, growth in content with extreme bile acid levels requires significant mechanisms of efflux for resistance. Many *Enterobacteriaceae*, such as NTS and *E. coli*, encode efflux pump systems (e.g., AcrAB-TolC) that provide relatively high levels of tolerance to bile acids (*129*), particularly relative to taxa that dominate the colonic microbiota. As such, factors that most limit *Salmonella* colonization of the upper small intestine (duodenum and jejunum) seem to be the high levels of antimicrobial peptides (AMPs), such as lysozyme and the alpha-defensins secreted by Paneth cells in the crypts, which saturate the mucus layer to create a barrier between the lumen and epithelium that limits bacterial invasion (*128*). Moreover, the rapid transit of contents through the duodenum and jejunum can make it difficult for bacteria to get a foothold (*130*), though the flagellated motility of *Salmonella* likely helps it overcome this for trafficking to M cells in the ileum (*131, 132*).

Investigations characterizing variability and impacts of disease on the microbiota and metabolite composition of the human small intestine have been limited, largely due to inaccessibility and invasiveness necessary for sampling (*133, 134*). However, recent mouse studies have better characterized potential effects of *Plasmodium* infection on these sites that

could influence NTS infection. The upper GI tract of C57BL/6 mice infected with *P. berghei* ANKA displayed severe pathology, including increased gas retention, a shortened small intestine, and enlarged goblet cells (*135*). This phenotype of inflammatory markers in the small intestine during *P. berghei* infection was confirmed by another study, as well as detecting shorted villi and increased mucus layers associated with the parasite (*136*). *Plasmodium*-associated inflammation in the gut, despite being an extraintestinal pathogen, could provide an early benefit to colonizing *Salmonella* that relies on inducing inflammation to succeed in the lumen. Similar markers of altered small intestine barrier function, including atrophied microvilli, have been associated with HIV infection (*137*). Additionally, mice infected with *P. yoelii* 17XNL (a strain less associated with severe pathology) found alterations in the metabolite profile throughout the intestines of the mice during infection, including changes in the composition of the bile acid pool (*138*). Changes in bile acids in other models of infection have shown benefits to colonization of NTS serovars, including acute administration of a high fat diet (*129*) and *Salmonella* inflammation in a streptomycin-treated model of colitis (*139*). These studies were generally associated with an increase in the abundance of bile acids in the gut, as *Salmonella* is strongly resistant and outcompetes much of the commensal microbiota in bile-rich environments (*129, 140*). It is less clear whether total bile acid levels increase with malaria, or if merely the relative amounts of various conjugated varieties are altered. Compositional changes to the bile acid pool have been linked to susceptibility to various other enteric pathogens, such as *C. difficle* (*141*). Additionally, bile acids are involved in regulating expression of *S.* Typhimurium virulence genes, repressing invasion of host cells (*142, 143*). As the observed alterations were associated with liver damage (where bile acids are synthesized from cholesterol before being stored in the gallbladder), it would be reasonable to assume the changes could actually be reducing overall bile levels as well, further prompting NTS invasion of the co-infected host.

Circulating bile acid levels have also been shown to be impacted by severe acute malnutrition (*144*). This could indicate reduced bile acid production in the liver, as bile acids

negatively regulate synthesis by farnesoid X receptor signaling on hepatocytes. Conversely, plasma bile acid pool composition was shown to be altered in HIV-infected patients (*145*). Further research may help glean whether these observed changes correspond with differences in the intestinal pool.

Outside of bile acids, alterations in AMP production or function could impact *Salmonella* killing in immunocompromised hosts. Notably, influenza virus infections in mice were linked with dysbiosis and enhanced *Salmonella* colonization due to type I interferon inhibition of antimicrobial peptide activity (*146*). This finding suggests viral infections limiting immune activation to NTS could enhance its survival. One sign that differences in AMP may be impacted in at-risk populations is a study on mutations in the ST313 *macAB* genes, encoding components of a macrolide efflux pump (MacAB-TolC) regulated by PhoP that is associated with antimicrobial peptide resistance in Gram-negative bacteria (*147*). The mutations in *macAB* reduce resistance to the peptide C18G and reduce fitness of the ST313 isolate in the gut of resistant mice. This could be the result of reduced selection for AMP resistance in a host with reduced AMP levels. However, that might again be an extraintestinal adaptation, indicating the strains are escaping the gut before AMP resistance becomes a relevant aspect of selection. Future work characterizing the impact of comorbidities on host production of AMPs would be useful, as AMPs also significantly contribute to colonization resistance by helping shape the microbiota, and loss of some AMPs has been associated with various disease states, such as a reduction in α-defensin levels in ileal Chron's disease (*148, 149*).

The Colon: Shaping Microbiota-associated Colonization Resistance

Compared to the upper GI tract, our understanding of the ecosystem in the large intestine, and how host defenses and colonization resistance provided by the endogenous microbiota there influence enteric infection outcomes, has been extensively studied and reviewed (*50, 125, 150-156*). Relative to the rest of the gut, the colon is relatively nutrient-poor

and hypoxic, yet contains a large microbial community (10^{10}-10^{12} CFU/mL) mostly composed of members of the *Firmicutes*, *Bacteroidetes*, *Actinobacteria* and *Proteobacteria* phyla (*106, 126, 130*). As hosts to these microbes, it seems humans have evolved to select for a fairly stable community that can provide defense against various pathogens via direct and indirect mechanisms (*50*). Significant disruption of the "balanced" community structure- a state commonly referred to as dysbiosis- can result in a loss of colonization resistance and is linked with numerous disorders. Large swaths of research on how colonization resistance can be overcome has focused on how insults to the microbiota- including poor diet (*157*), antibiotic use (*158*), and intestinal inflammatory disorders (*159, 160*)- foster dysbiosis that promotes growth of pathogens and endogenous microbes whose expansion can cause disease (*161*).

Unlike opportunistic infections, the SPI-associated virulence systems of *Salmonella* allow it to naturally overcome the colonization resistance derived from the microbiota at homeostasis to cause disease (*50*). However, this still requires sufficient amounts of ingested *Salmonella* to reach the ileum and colon (an "infectious dose"), and different microbial community structures can impact the necessary infectious dose (*162, 163*). For example, the microbiota after treatment with the antibiotic streptomycin is associated with significantly reduced colonization resistance against *Salmonella* (*164*). In some of these cases, the changes in the community structure due to exogenous insult mimic shifts observed during inflammation caused by NTS pathogenesis (*127*), indicating shared mechanisms predisposing the host to *Salmonella* expansion in the lumen. For example, high-fat diets, antibiotics, and DSS-induced colitis have all been shown to shift the microbiota and influence colonocyte metabolism to increase levels of respiratory electron acceptors (such as nitrate, tetrathionate, and oxygen) in the lumen that allow *Enterobacteriaceae* and other *Enterobacterales* capable of using them to flourish (reviewed in (*50*) and (*165*)). Factors like these can actually limit the necessity for pathogen-associated virulence, as the groundwork of shifting the gut environment to provide

competitive nutrient or respiratory niches for *Salmonella* to thrive has already been done, thus removing the burden of ecosystem engineering from *Salmonella*.

Moreover, some members of the microbiome can produce metabolites or antimicrobial compounds that directly inhibit competing pathogens. For example, the short-chain fatty acid (SCFA) propionate produced by mouse *Bacteroides* species was shown to inhibit *Salmonella* colonization (*166*). It has also been shown that bile acid dehydroxylation by *Clostridium scindens* in the gut produces a novel bile acid that inhibits pathogenic *Clostridium difficile* (*141*). One can imagine numerous additional similar interactions occurring *in vivo* that are yet to be discovered, where presence or absence of a microbe with specific metabolic properties greatly influences colonization resistance. Risk factors altering the microbiota in a manner that depletes bacteria critical for resistance could foster enhanced host colonization by pathogens like NTS.

In mice, *P. yoelii* and severe infection with *P. berghei* has been linked to large intestinal inflammatory pathology and dysbiotic shifts in the fecal microbiome (*136, 167*). In one of the studies, germfree mice that were given a fecal microbiota transplant from *P. yoelii*-infected mice showed increased *S.* Typhimurium implantation oral challenge compared to mice receiving a transplant from healthy mice (*167*), providing evidence that parasite-induced dysbiosis might actually underly increased intestinal implantation of NTS during malaria. However, this finding was based on a small experiment (3 mice per treatment), so further evidence could elucidate the degree to which dysbiosis during *Plasmodium* infection actually reduces colonization resistance against *S.* Typhimurium.

While both studies found significant inflammatory markers in the intestines of susceptible *Plasmodium* infected mice, neither was able to definitely determine how the infection in the blood produced dysbiosis in the gut, though additional research has confirmed that *Plasmodium* infection can alter both the microbiota and the intestinal metabolic profile in mice (*138*). Remarkably, this latter study was following up observations that differences in the microbiota of mice from different vendors seems to result in significantly different profiles of *P. yoelii* infection

severity (*168*), though currently the precise mechanisms are unknown (*169, 170*). Earlier work from Yilmaz et al., however, reported that a specific member of the human microbiota (α-gal-expressing *E. coli* O86:B7) could promote immunity against *Plasmodium* infection in the skin, limiting transmission (*171*). Together, these data indicate that reciprocal interactions can exist between *Plasmodium* infection and the gut microbiota in animals.

One important caveat to these studies is that the majority of malaria-associated iNTS disease occurs in very young children, and the natural microbiota of the adult laboratory mouse (> 8 weeks old) does not actually resemble that of human infants (*172*). The infant microbiota is typically dominated by members of the phylum *Actinobacteria* (*Bifidobacterium* species) and *Enterobacteriaceae*, which is thought to provide niche pre-emption to pathogenic enteric bacteria and guide the maturation of the microbiota to the adult stage (*151, 173*). In contrast, the mouse fecal microbiota is mostly made up of anaerobic Firmicutes and Bacteroidetes, closer in composition to the mature community in humans (*106*). Unfortunately, few studies have been undertaken to determine whether (and in what way) malaria could impact the gut microbiota in affected children. One recent analysis tracking Kenyan infants found little impact of malaria on the fecal microbiome (*174*). However, febrile participants were immediately provided treatment when malaria was suspected, limiting the severity of *Plasmodium* infections, which could reduce observable differences. More research is needed to more thoroughly understand the impacts of malaria on the developing microbiota. To that end, it might also be informative to investigate the impact of *Plasmodium* in an ex-germfree mouse model with a defined microbiota with composition closer to that of an infant, and how infection might impact the maturation of the microbiota.

One aspect of severe malaria that might influence the microbiota is the significant hemolysis that can generate anemia. The presence of anemia in infants and children in Kenya has been correlated to differences in the gut microbiota composition (*175*). It was found that in infants, anemia was associated with a reduction in pathogenic E. coli, while this correlation was

reversed in older children. Additionally, increased *C. difficile* was associated with anemia in both age groups, as well as reduced butyrate- a SCFA involved in colonocyte metabolism, regulating inflammation, and maintenance of intestinal hypoxia that limits facultative anaerobe blooms in the gut (*176*). Conversely, iron supplementation has also been associated with dysbiosis, increasing inflammatory markers (fecal calprotectin) and *E. coli* abundance (*177*). This actually suggests that host adaptations to iron deficiency may involve cellular iron sequestration from potential pathogens.

Invasive NTS risk factors outside of malaria have also been linked to significant changes in the gut microbiota. On the whole, studies have found HIV is associated with increased levels of *Enterobacteriaceae* and reduced levels of the SCFA-producing *Lachnospiraceae* (phylum *Firmicutes*) (*178*), shifts that resemble those associated with inflammation and *Plasmodium* infection in mice. Intriguingly, reduced levels of *Bacteroides* have also often been reported, which could benefit *Salmonella* colonization through reduction in propionate levels (*166*). These changes might also be linked with reduced PRR expression in intestinal tissues impacting commensal training of host mucosal immunity, which was observed in SIV-infected macaques (*87*). Moreover, although it successfully suppresses circulating viremia and has been linked with reduced incidence of HIV-linked iNTS disease (*179*), antiretroviral therapy does not seem sufficient to fully correct these intestinal dysbiosis (*87, 137*), likely due to a continued depletion of mucosal CD4+ T cells- though probiotic use has shown beneficial effects in improving barrier functions and reducing inflammation.

While a so-called “Western” diet high in fat and simple sugars has been repeatedly linked to dysbiosis and susceptibility to enteric pathogen colonization (*129, 180-185*), analysis of the microbiota of malnourished populations also offers insights into the influence of nutrition and the development of the microbiota. Children in Bangladesh with severe acute malnutrition displayed reduced diversity and immaturity in their fecal microbiota relative to healthy children, characterized by an overabundance of *Enterobacteriaceae* species (*186*). Food intervention

reduced *Enterobacteriaceae* levels and enriched for previously depleted *Lactobacillus* and *Bifidobacterium* species, indicating nutritional status can significantly shape the microbiota. Furthermore, it has been shown that acute anorexic responses to infection can alter the microbiota, often through the enrichment of species less dependent on dietary carbohydrates for their metabolism, such as the mucin-degrading *Akkermansia muciniphila* (*187*). While some studies have associated abundance of this species with a healthy gut microbiota (*188, 189*), *A. muciniphila* blooms in the absence of significant dietary fiber intake can be a marker for mucus barrier degradation and dysfunction, thus promoting mucosal pathogen colonization (*181*). Interestingly, presence of *A. muciniphila* was shown to promote *S.* Typhimurium pathology and dissemination in a gnotobiotic mouse model (*190*), evidence that *A. muciniphila* is not always protective of the host.

Finally, ST313 isolates show reduced capacity to colonize the gut of some animal models. As previously described, this has been linked to reduced expression of flagellin and the SPI-1 gene *sopE2* (*42, 91*). These alterations may be signs that the preferred host for ST313 does not require as much induction of inflammation for gut colonization. In accordance with this hypothesis, characterizations of the representative ST313 lineage II isolate D23580 have suggested a loss or reduced expression of genes involved in carbon utilization, including systems for using allantoin, tartrate, and melibiose (*37, 191*). Of particular note, allantoin is a reported inflammatory marker in IBD (*192*). Melibiose has been shown to accumulate in the mouse gut during *S.* Typhimurium infection (*193*) and melibiose utilization genes of a ST19 strain were upregulated in the gut during chicken infections (*194*). These findings suggest those carbon sources could be useful for *S.* Typhimurium growth in the inflamed gut, and loss of the ability to use them effectively could indicate extraintestinal or potentially anthropogenic adaptation (*36*). Additionally, a *S.* Enteritidis strain isolated from iNTS infections displayed altered carbon and nitrogen source utilization when compared to a gastroenteritis-linked isolate (*195*). This could be a sign that metabolic alterations are a feature shared by invasive African

NTS isolates more generally, suggesting the risk factors associated with Africa could be driving genomic adaptations outside of the well-characterized ST313 lineages.

Emergence of the chloramphenicol-resistant ST313 Lineage II (L2) in the 1970s and their rapid supplantation of the ST313 Lineage I (L1) corresponded with the broad adoption of chloramphenicol as the drug of choice for bacterial infections in Africa (*35*). Strikingly, reduction of chloramphenicol use has been temporally linked with the emergence of a new lineage of ST313 (L3) lacking chloramphenicol resistance, but which shows increased accumulation of genomic alterations in loci predicted to be associated with extraintestinal infection (*88*). On the other hand, another ST313 lineage (L2.1) with added resistance to the third-generation cephalosporin ceftriaxone, ciprofloxacin, and azithromycin (though not all three together) has been detected at some sites in sub-Saharan Africa (*196*), corresponding to the increased use of these drugs for iNTS (*88*). These L2.1 isolates also show genomic alterations associated with increased invasive potential relative to ST19, ST313 L1, and ST313 L2 clones, including the further loss of the flagellin *fljB* gene (*196*). African *S.* Enteritidis bloodstream isolates have also shown acquisition of drug resistances. One representative isolate was found to have a pSENV-derived plasmid encoding nine antimicrobial resistance genes (*195*). Ultimately, these adaptations could allow the resistant NTS strains to easily outcompete a microbiota concurrently being depleted or inhibited through treatment with an antibiotic that the ST313 strain can resist, allowing for degradation of pathways useful in outcompeting the healthy microbiota.

Conclusions and Future Perspectives

It has long been appreciated in mouse models of *Plasmodium* infection and chemically-induced hemolytic anemia that the treatments can enhance the lethality of non-typhoidal *Salmonella* infections (*55, 64*). Recognition of the influence of immunocompromising HIV infection on invasive bacterial infections (IBIs) emerged nearly concurrently with awareness of the AIDS epidemic (*197-199*). And while our understanding of how different forms of

malnutrition encourage specific IBIs is still in its nascency, it is well known that nutritional status and resistance to infection are closely tied (*200*).

These risk factors can effectively turn intestinal NTS strains into opportunistic invasive infections, significantly less dependent on a robust virulence system to succeed in the host. The typical cycle of NTS growth and transmission depends on the pathogen hijacking host immune responses to gain a foothold in the intestine, resulting in gastroenteritis. It is little surprise, then, that regularly encountering hosts suffering immunocompromise that interfere with this cycle could drive the generation of strains such as the ST313 clade, better suited to alternative infection lifestyles. In fact, the major determinant of the dominance of ST313 is likely its broad antibiotic resistance, with other genomic changes perhaps being useful in actually limiting immunocompromised host mortality once the pathogen has disseminated. Too lethal an interaction would lead to dead-end hosts and ultimately be selected against.

Although the iNTS burden in sub-Saharan Africa is significant, it only makes up ~17% of detected bacteremias (*201*), indicating the impact of comorbidities like malaria, malnutrition, and HIV predispose to additional infections via more diverse mechanisms than *Salmonella*-specific interactions. Studies in mouse *Plasmodium* infection models have suggested the parasite can enhance IBIs with *Streptococcus pneumoniae*, *Listeria monocytogenes*, and potentially enteropathogenic/enterohemorrhagic *E. coli* (as modeled by *Citrobacter rodentium*) (*202, 203*). This multi-bacterial susceptibility is concerning, as pathobionts with significant antimicrobial resistance, such as carbapenem-resistant *Enterobacteriaceae*, are disseminating worldwide (*204*), and could rapidly dominate the invasive-infection landscape. Additionally, although we are beginning to clarify mechanisms by which single immunocompromising factors can influence the development of iNTS, the mixed presence of such comorbidities is a common occurrence in at-risk populations (*205-208*) and have been shown capable of amplifying detrimental effects on the host to that could promote iNTS (*85*). Better understanding of how various risk factors work together could also help design rational treatments to limit IBIs.

It seems the best way to reduce IBIs will be to focus efforts on treating the underlying conditions. Invasive NTS vaccines are in development, but many of the risk factors can compromise of vaccine-based immunity (*201, 209*). Devising appropriate treatments for acquired anemias that don't actually promote the potential of IBIs may prove difficult (*78, 210*), but antiretroviral therapy for HIV and reducing malarial transmission have been effective in reducing the incidence of secondary iNTS disease (*26, 80*), suggesting funding such approaches would be a reasonable way to reduce the burden of invasive bacterial infections.

REFERENCES

1. R. F. Doolittle, D. F. Feng, S. Tsang, G. Cho, E. Little, Determining divergence times of the major kingdoms of living organisms with a protein clock. *Science* **271**, 470-477 (1996).
2. J. N. V. Martinson, S. T. Walk, Escherichia coli Residency in the Gut of Healthy Human Adults. *EcoSal Plus* **9**, (2020).
3. O. Gal-Mor, E. C. Boyle, G. A. Grassl, Same species, different diseases: how and why typhoidal and non-typhoidal Salmonella enterica serovars differ. *Front Microbiol* **5**, 391 (2014).
4. C. M. Parry, T. T. Hien, G. Dougan, N. J. White, J. J. Farrar, Typhoid fever. *N Engl J Med* **347**, 1770-1782 (2002).
5. M. Raffatellu, R. P. Wilson, S. E. Winter, A. J. Baumler, Clinical pathogenesis of typhoid fever. *J Infect Dev Ctries* **2**, 260-266 (2008).
6. H. Hiyoshi, C. R. Tiffany, D. N. Bronner, A. J. Baumler, Typhoidal Salmonella serovars: ecological opportunity and the evolution of a new pathovar. *FEMS Microbiol Rev* **42**, 527-541 (2018).

7. J. B. A, J. Hill, J. B. C, J. P. A, Host restriction, pathogenesis and chronic carriage of typhoidal Salmonella. *FEMS Microbiol Rev*, (2021).
8. J. Song *et al.*, Absence of TLR11 in Mice Does Not Confer Susceptibility to Salmonella Typhi. *Cell* **164**, 827-828 (2016).
9. N. S. Galbraith, Studies of human Salmonellosis in relation to infection in animals. *Vet Rec* **73**, 1296-1303 (1961).
10. M. Raffatellu *et al.*, The Vi capsular antigen of Salmonella enterica serotype Typhi reduces Toll-like receptor-dependent interleukin-8 expression in the intestinal mucosa. *Infect Immun* **73**, 3367-3374 (2005).
11. M. Raffatellu *et al.*, The capsule encoding the viaB locus reduces interleukin-17 expression and mucosal innate responses in the bovine intestinal mucosa during infection with Salmonella enterica serotype Typhi. *Infect Immun* **75**, 4342-4350 (2007).
12. R. P. Wilson *et al.*, The Vi-capsule prevents Toll-like receptor 4 recognition of Salmonella. *Cell Microbiol* **10**, 876-890 (2008).
13. T. Haneda *et al.*, The capsule-encoding viaB locus reduces intestinal inflammation by a Salmonella pathogenicity island 1-independent mechanism. *Infect Immun* **77**, 2932-2942 (2009).
14. R. P. Wilson *et al.*, The Vi capsular polysaccharide prevents complement receptor 3-mediated clearance of Salmonella enterica serotype Typhi. *Infect Immun* **79**, 830-837 (2011).
15. T. Wangdi *et al.*, The Vi capsular polysaccharide enables Salmonella enterica serovar typhi to evade microbe-guided neutrophil chemotaxis. *PLoS Pathog* **10**, e1004306 (2014).
16. S. E. Winter, M. Raffatellu, R. P. Wilson, H. Russmann, A. J. Baumler, The Salmonella enterica serotype Typhi regulator TviA reduces interleukin-8 production in intestinal epithelial cells by repressing flagellin secretion. *Cell Microbiol* **10**, 247-261 (2008).

17. S. E. Winter *et al.*, Salmonella enterica Serovar Typhi conceals the invasion-associated type three secretion system from the innate immune system by gene regulation. *PLoS Pathog* **10**, e1004207 (2014).

18. M. McClelland *et al.*, Comparison of genome degradation in Paratyphi A and Typhi, human-restricted serovars of Salmonella enterica that cause typhoid. *Nat Genet* **36**, 1268-1274 (2004).

19. S. M. Jajere, A review of Salmonella enterica with particular focus on the pathogenicity and virulence factors, host specificity and antimicrobial resistance including multidrug resistance. *Vet World* **12**, 504-521 (2019).

20. X. Li *et al.*, Spatial Epidemiology of Salmonellosis in Florida, 2009-2018. *Front Public Health* **8**, 603005 (2020).

21. A. J. Brent *et al.*, Salmonella bacteremia in Kenyan children. *Pediatr Infect Dis J* **25**, 230-236 (2006).

22. K. H. Keddy *et al.*, Clinical and Microbiological Features of Salmonella Meningitis in a South African Population, 2003-2013. *Clin Infect Dis* **61 Suppl 4**, S272-282 (2015).

23. E. Muthumbi *et al.*, Invasive Salmonellosis in Kilifi, Kenya. *Clin Infect Dis* **61 Suppl 4**, S290-301 (2015).

24. G. B. D. N.-T. S. I. D. Collaborators, The global burden of non-typhoidal salmonella invasive disease: a systematic analysis for the Global Burden of Disease Study 2017. *Lancet Infect Dis* **19**, 1312-1324 (2019).

25. T. T. Ao *et al.*, Global burden of invasive nontyphoidal Salmonella disease, 2010(1). *Emerg Infect Dis* **21**, (2015).

26. J. J. Gilchrist, C. A. MacLennan, Invasive Nontyphoidal Salmonella Disease in Africa. *EcoSal Plus* **8**, (2019).

27. J. Lessler, A. S. Azman, H. S. McKay, S. M. Moore, What is a Hotspot Anyway? *Am J Trop Med Hyg* **96**, 1270-1273 (2017).

28. M. Seydi, M. Soumare, A. I. Sow, B. M. Diop, P. S. Sow, [Current aspects of Salmonella bacteremia cases in the Ibrahima Diop Mar Infectious Diseases clinic, Fann National Hospital Center (Senegal)]. *Med Mal Infect* **35**, 23-27 (2005).

29. J. A. Berkley *et al.*, Bacteremia among children admitted to a rural hospital in Kenya. *N Engl J Med* **352**, 39-47 (2005).

30. F. Marks *et al.*, Incidence of invasive salmonella disease in sub-Saharan Africa: a multicentre population-based surveillance study. *Lancet Glob Health* **5**, e310-e323 (2017).

31. S. M. Graham, A. L. Walsh, E. M. Molyneux, A. J. Phiri, M. E. Molyneux, Clinical presentation of non-typhoidal Salmonella bacteraemia in Malawian children. *Trans R Soc Trop Med Hyg* **94**, 310-314 (2000).

32. R. N. Bronzan *et al.*, Bacteremia in Malawian children with severe malaria: prevalence, etiology, HIV coinfection, and outcome. *J Infect Dis* **195**, 895-904 (2007).

33. H. M. Biggs *et al.*, Invasive Salmonella infections in areas of high and low malaria transmission intensity in Tanzania. *Clin Infect Dis* **58**, 638-647 (2014).

34. R. A. Kingsley *et al.*, Epidemic multiple drug resistant Salmonella Typhimurium causing invasive disease in sub-Saharan Africa have a distinct genotype. *Genome Res* **19**, 2279-2287 (2009).

35. C. K. Okoro *et al.*, Intracontinental spread of human invasive Salmonella Typhimurium pathovariants in sub-Saharan Africa. *Nat Genet* **44**, 1215-1221 (2012).

36. K. L. Lokken, G. T. Walker, R. M. Tsolis, Disseminated infections with antibiotic-resistant non-typhoidal Salmonella strains: contributions of host and pathogen factors. *Pathog Dis* **74**, (2016).

37. C. K. Okoro *et al.*, Signatures of adaptation in human invasive Salmonella Typhimurium ST313 populations from sub-Saharan Africa. *PLoS Negl Trop Dis* **9**, e0003611 (2015).

38. S. E. Carden *et al.*, Pseudogenization of the Secreted Effector Gene sseI Confers Rapid Systemic Dissemination of S. Typhimurium ST313 within Migratory Dendritic Cells. *Cell Host Microbe* **21**, 182-194 (2017).

39. M. Raffatellu *et al.*, Simian immunodeficiency virus-induced mucosal interleukin-17 deficiency promotes Salmonella dissemination from the gut. *Nat Med* **14**, 421-428 (2008).

40. A. R. Stull-Lane *et al.*, Vitamin A supplementation boosts control of antibiotic-resistant Salmonella infection in malnourished mice. *PLoS Negl Trop Dis* **14**, e0008737 (2020).

41. J. P. Mooney, L. J. Galloway, E. M. Riley, Malaria, anemia, and invasive bacterial disease: A neutrophil problem? *J Leukoc Biol* **105**, 645-655 (2019).

42. S. Carden, C. Okoro, G. Dougan, D. Monack, Non-typhoidal Salmonella Typhimurium ST313 isolates that cause bacteremia in humans stimulate less inflammasome activation than ST19 isolates associated with gastroenteritis. *Pathog Dis* **73**, (2015).

43. D. L. LaRock, A. Chaudhary, S. I. Miller, Salmonellae interactions with host processes. *Nat Rev Microbiol* **13**, 191-205 (2015).

44. E. Jennings, T. L. M. Thurston, D. W. Holden, Salmonella SPI-2 Type III Secretion System Effectors: Molecular Mechanisms And Physiological Consequences. *Cell Host Microbe* **22**, 217-231 (2017).

45. M. Raffatellu *et al.*, SipA, SopA, SopB, SopD, and SopE2 contribute to Salmonella enterica serotype typhimurium invasion of epithelial cells. *Infect Immun* **73**, 146-154 (2005).

46. S. Hapfelmeier *et al.*, The Salmonella pathogenicity island (SPI)-2 and SPI-1 type III secretion systems allow Salmonella serovar typhimurium to trigger colitis via MyD88-dependent and MyD88-independent mechanisms. *J Immunol* **174**, 1675-1685 (2005).

47. I. Godinez *et al.*, Interleukin-23 orchestrates mucosal responses to Salmonella enterica serotype Typhimurium in the intestine. *Infect Immun* **77**, 387-398 (2009).

48. M. Valeri, M. Raffatellu, Cytokines IL-17 and IL-22 in the host response to infection. *Pathog Dis* **74**, (2016).

49. K. W. Chen *et al.*, Noncanonical inflammasome signaling elicits gasdermin D-dependent neutrophil extracellular traps. *Sci Immunol* **3**, (2018).

50. A. W. L. Rogers, R. M. Tsolis, A. J. Baumler, Salmonella versus the Microbiome. *Microbiol Mol Biol Rev* **85**, (2021).

51. T. D. Lawley *et al.*, Host transmission of Salmonella enterica serovar Typhimurium is controlled by virulence factors and indigenous intestinal microbiota. *Infect Immun* **76**, 403-416 (2008).

52. W. H. Organization, "WHO Global Malaria Programme," (World Health Organization, Geneva, Switzerland, 2016).

53. B. Nadjm, R. H. Behrens, Malaria: an update for physicians. *Infect Dis Clin North Am* **26**, 243-259 (2012).

54. C. Coban, M. S. J. Lee, K. J. Ishii, Tissue-specific immunopathology during malaria infection. *Nat Rev Immunol* **18**, 266-278 (2018).

55. D. Kaye, J. G. Merselis, Jr., E. W. Hook, Influence of Plasmodium berghei infection on susceptibility to salmonella infection. *Proc Soc Exp Biol Med* **120**, 810-813 (1965).

56. T. J. Lamb, D. E. Brown, A. J. Potocnik, J. Langhorne, Insights into the immunopathogenesis of malaria using mouse models. *Expert Rev Mol Med* **8**, 1-22 (2006).

57. R. Stephens, R. L. Culleton, T. J. Lamb, The contribution of Plasmodium chabaudi to our understanding of malaria. *Trends Parasitol* **28**, 73-82 (2012).

58. C. M. Roux *et al.*, Both hemolytic anemia and malaria parasite-specific factors increase susceptibility to Nontyphoidal Salmonella enterica serovar typhimurium infection in mice. *Infect Immun* **78**, 1520-1527 (2010).

59. A. J. Cunnington, J. B. de Souza, M. Walther, E. M. Riley, Malaria impairs resistance to Salmonella through heme- and heme oxygenase-dependent dysfunctional granulocyte mobilization. *Nat Med* **18**, 120-127 (2011).

60. J. Y. Chau *et al.*, Malaria-associated L-arginine deficiency induces mast cell-associated disruption to intestinal barrier defenses against nontyphoidal Salmonella bacteremia. *Infect Immun* **81**, 3515-3526 (2013).

61. K. L. Lokken *et al.*, Malaria parasite infection compromises control of concurrent systemic non-typhoidal Salmonella infection via IL-10-mediated alteration of myeloid cell function. *PLoS Pathog* **10**, e1004049 (2014).

62. R. A. Potts *et al.*, Mast cells and histamine alter intestinal permeability during malaria parasite infection. *Immunobiology* **221**, 468-474 (2016).

63. J. P. Mooney *et al.*, The mucosal inflammatory response to non-typhoidal Salmonella in the intestine is blunted by IL-10 during concurrent malaria parasite infection. *Mucosal Immunol* **7**, 1302-1311 (2014).

64. D. Kaye, E. W. Hook, The Influence of Hemolysis on Susceptibility to Salmonella Infection: Additional Observations. *J Immunol* **91**, 518-527 (1963).

65. K. L. Lokken, A. R. Stull-Lane, K. Poels, R. M. Tsolis, Malaria Parasite-Mediated Alteration of Macrophage Function and Increased Iron Availability Predispose to Disseminated Nontyphoidal Salmonella Infection. *Infect Immun* **86**, (2018).

66. M. Walther *et al.*, HMOX1 gene promoter alleles and high HO-1 levels are associated with severe malaria in Gambian children. *PLoS Pathog* **8**, e1002579 (2012).

67. I. A. Clark, M. M. Awburn, C. G. Harper, N. G. Liomba, M. E. Molyneux, Induction of HO-1 in tissue macrophages and monocytes in fatal falciparum malaria and sepsis. *Malar J* **2**, 41 (2003).

68. W. L. Mandala *et al.*, Cytokine Profiles in Malawian Children Presenting with Uncomplicated Malaria, Severe Malarial Anemia, and Cerebral Malaria. *Clin Vaccine Immunol* **24**, (2017).

69. T. N. Williams *et al.*, Bacteraemia in Kenyan children with sickle-cell anaemia: a retrospective cohort and case-control study. *Lancet* **374**, 1364-1370 (2009).

70. L. H. Richards, J. Howard, J. L. Klein, Community-acquired Salmonella bacteraemia in patients with sickle-cell disease 1969-2008: a single centre study. *Scand J Infect Dis* **43**, 89-94 (2011).

71. W. Wanachiwanawin, Infections in E-beta thalassemia. *J Pediatr Hematol Oncol* **22**, 581-587 (2000).

72. G. J. Kato, M. H. Steinberg, M. T. Gladwin, Intravascular hemolysis and the pathophysiology of sickle cell disease. *J Clin Invest* **127**, 750-760 (2017).

73. G. J. Lonergan, D. B. Cline, S. L. Abbondanzo, Sickle cell anemia. *Radiographics* **21**, 971-994 (2001).

74. C. Evans *et al.*, Impairment of neutrophil oxidative burst in children with sickle cell disease is associated with heme oxygenase-1. *Haematologica* **100**, 1508-1516 (2015).

75. A. T. Taher, D. J. Weatherall, M. D. Cappellini, Thalassaemia. *Lancet* **391**, 155-167 (2018).

76. N. M. Ampel, D. B. Van Wyck, M. L. Aguirre, D. G. Willis, R. A. Popp, Resistance to infection in murine beta-thalassemia. *Infect Immun* **57**, 1011-1017 (1989).

77. A. Atamna *et al.*, Chronic use of oral iron supplements is associated with poor clinical outcomes in patients with gram-negative bacteremia. *Eur J Clin Microbiol Infect Dis* **38**, 689-693 (2019).

78. J. H. Cross *et al.*, Oral iron acutely elevates bacterial growth in human serum. *Sci Rep* **5**, 16670 (2015).

79. F. A. Jonker, M. Boele van Hensbroek, Anaemia, iron deficiency and susceptibility to infections. *J Infect* **69 Suppl 1**, S23-27 (2014).

80. N. A. Feasey *et al.*, Modelling the Contributions of Malaria, HIV, Malnutrition and Rainfall to the Decline in Paediatric Invasive Non-typhoidal Salmonella Disease in Malawi. *PLoS Negl Trop Dis* **9**, e0003979 (2015).

81. S. Maggini, A. Pierre, P. C. Calder, Immune Function and Micronutrient Requirements Change over the Life Course. *Nutrients* **10**, (2018).

82. M. D. Peck, G. F. Babcock, J. W. Alexander, The role of protein and calorie restriction in outcome from Salmonella infection in mice. *JPEN J Parenter Enteral Nutr* **16**, 561-565 (1992).

83. C. B. Stephensen, Vitamin A, infection, and immune function. *Annu Rev Nutr* **21**, 167-192 (2001).

84. G. A. Stevens *et al.*, Trends and mortality effects of vitamin A deficiency in children in 138 low-income and middle-income countries between 1991 and 2013: a pooled analysis of population-based surveys. *Lancet Glob Health* **3**, e528-536 (2015).

85. N. J. Murr *et al.*, Plasmodium chabaudi Infection Alters Intestinal Morphology and Mucosal Innate Immunity in Moderately Malnourished Mice. *Nutrients* **13**, (2021).

86. S. Lucas, A. M. Nelson, HIV and the spectrum of human disease. *J Pathol* **235**, 229-241 (2015).

87. T. W. Glavan *et al.*, Gut immune dysfunction through impaired innate pattern recognition receptor expression and gut microbiota dysbiosis in chronic SIV infection. *Mucosal Immunol* **9**, 677-688 (2016).

88. C. V. Pulford *et al.*, Stepwise evolution of Salmonella Typhimurium ST313 causing bloodstream infection in Africa. *Nat Microbiol* **6**, 327-338 (2021).

89. J. A. Crump, R. S. Heyderman, A Perspective on Invasive Salmonella Disease in Africa. *Clin Infect Dis* **61 Suppl 4**, S235-240 (2015).

90. L. M. Kalonji *et al.*, Invasive Salmonella Infections at Multiple Surveillance Sites in the Democratic Republic of the Congo, 2011-2014. *Clin Infect Dis* **61 Suppl 4**, S346-353 (2015).

91. B. N. Parsons *et al.*, Invasive non-typhoidal Salmonella typhimurium ST313 are not host-restricted and have an invasive phenotype in experimentally infected chickens. *PLoS Negl Trop Dis* **7**, e2487 (2013).

92. G. Ramachandran *et al.*, Virulence of invasive Salmonella Typhimurium ST313 in animal models of infection. *PLoS Negl Trop Dis* **11**, e0005697 (2017).

93. J. Yang *et al.*, Characterization of the Invasive, Multidrug Resistant Non-typhoidal Salmonella Strain D23580 in a Murine Model of Infection. *PLoS Negl Trop Dis* **9**, e0003839 (2015).

94. L. M. McLaughlin *et al.*, The Salmonella SPI2 effector SseI mediates long-term systemic infection by modulating host cell migration. *PLoS Pathog* **5**, e1000671 (2009).

95. D. L. Hammarlof *et al.*, Role of a single noncoding nucleotide in the evolution of an epidemic African clade of Salmonella. *Proc Natl Acad Sci U S A* **115**, E2614-E2623 (2018).

96. B. Paglietti *et al.*, Diversity among human non-typhoidal salmonellae isolates from Zimbabwe. *Trans R Soc Trop Med Hyg* **107**, 487-492 (2013).

97. S. Kariuki, R. S. Onsare, Epidemiology and Genomics of Invasive Nontyphoidal Salmonella Infections in Kenya. *Clin Infect Dis* **61 Suppl 4**, S317-324 (2015).

98. P. M. Ashton *et al.*, Public health surveillance in the UK revolutionises our understanding of the invasive Salmonella Typhimurium epidemic in Africa. *Genome Med* **9**, 92 (2017).

99. M. M. Ippolito, J. E. Denny, C. Langelier, C. L. Sears, N. W. Schmidt, Malaria and the Microbiome: A Systematic Review. *Clin Infect Dis* **67**, 1831-1839 (2018).

100. S. A. Sarker, K. Gyr, Non-immunological defence mechanisms of the gut. *Gut* **33**, 987-993 (1992).

101. S. M. Tennant *et al.*, Influence of gastric acid on susceptibility to infection with ingested bacterial pathogens. *Infect Immun* **76**, 639-645 (2008).

102. A. F. Hurst, The Clinical Importance of Achlorhydria. *Br Med J* **2**, 665-669 (1934).

103. A. C. Engevik, I. Kaji, J. R. Goldenring, The Physiology of the Gastric Parietal Cell. *Physiol Rev* **100**, 573-602 (2020).

104. L. P. Garrod, A study on the bactericidal power of hydrochloric acid and of gastric juice. *St. Bartholomew Hosp. Rep.* **72**, 145–167 (1939).

105. D. E. Beasley, A. M. Koltz, J. E. Lambert, N. Fierer, R. R. Dunn, The Evolution of Stomach Acidity and Its Relevance to the Human Microbiome. *PLoS One* **10**, e0134116 (2015).

106. D. Avelar Rodriguez, P. M. Ryan, E. M. Toro Monjaraz, J. A. Ramirez Mayans, E. M. Quigley, Small Intestinal Bacterial Overgrowth in Children: A State-Of-The-Art Review. *Front Pediatr* **7**, 363 (2019).

107. R. W. Stockbruegger, Bacterial overgrowth as a consequence of reduced gastric acidity. *Scand J Gastroenterol Suppl* **111**, 7-16 (1985).

108. F. Imhann *et al.*, Proton pump inhibitors affect the gut microbiome. *Gut* **65**, 740-748 (2016).

109. E. I. Levy, D. M. Hoang, Y. Vandenplas, The effects of proton pump inhibitors on the microbiome in young children. *Acta Paediatr* **109**, 1531-1538 (2020).

110. A. Minalyan, L. Gabrielyan, D. Scott, J. Jacobs, J. R. Pisegna, The Gastric and Intestinal Microbiome: Role of Proton Pump Inhibitors. *Curr Gastroenterol Rep* **19**, 42 (2017).

111. A. Trifan *et al.*, Proton pump inhibitors therapy and risk of Clostridium difficile infection: Systematic review and meta-analysis. *World J Gastroenterol* **23**, 6500-6515 (2017).

112. G. C. Cook, Infective gastroenteritis and its relationship to reduced gastric acidity. *Scand J Gastroenterol Suppl* **111**, 17-23 (1985).

113. R. Freeman *et al.*, Association between use of proton pump inhibitors and non-typhoidal salmonellosis identified following investigation into an outbreak of Salmonella Mikawasima in the UK, 2013. *Epidemiol Infect* **144**, 968-975 (2016).

114. H. H. Wu *et al.*, Association between recent use of proton pump inhibitors and nontyphoid salmonellosis: a nested case-control study. *Clin Infect Dis* **59**, 1554-1558 (2014).

115. J. P. Audia, C. C. Webb, J. W. Foster, Breaking through the acid barrier: an orchestrated response to proton stress by enteric bacteria. *Int J Med Microbiol* **291**, 97-106 (2001).

116. I. Forgacs, A. Loganayagam, Overprescribing proton pump inhibitors. *BMJ* **336**, 2-3 (2008).

117. B. T. Batuwitage, J. G. Kingham, N. E. Morgan, R. L. Bartlett, Inappropriate prescribing of proton pump inhibitors in primary care. *Postgrad Med J* **83**, 66-68 (2007).

118. J. Geraghty *et al.*, Helicobacter pylori, HIV and Gastric Hypochlorhydria in the Malawian Population. *PLoS One* **10**, e0132043 (2015).

119. L. Wosornu, F. I. Konotey-Ahulu, Gastric acid secretion in sickle-cell anaemia. *Gut* **12**, 197-199 (1971).

120. P. Kelly, Starvation and Its Effects on the Gut. *Adv Nutr*, (2020).

121. S. A. Sarker, T. Ahmed, H. Brussow, Hunger and microbiology: is a low gastric acid-induced bacterial overgrowth in the small intestine a contributor to malnutrition in developing countries? *Microb Biotechnol* **10**, 1025-1030 (2017).

122. A. L. Betesh, C. A. Santa Ana, J. A. Cole, J. S. Fordtran, Is achlorhydria a cause of iron deficiency anemia? *Am J Clin Nutr* **102**, 9-19 (2015).

123. R. W. Stockbruegger *et al.*, Pernicious anaemia, intragastric bacterial overgrowth, and possible consequences. *Scand J Gastroenterol* **19**, 355-364 (1984).

124. R. Oh, D. L. Brown, Vitamin B12 deficiency. *Am Fam Physician* **67**, 979-986 (2003).

125. J. M. Pickard, G. Nunez, Pathogen Colonization Resistance in the Gut and Its Manipulation for Improved Health. *Am J Pathol* **189**, 1300-1310 (2019).

126. E. T. Hillman, H. Lu, T. Yao, C. H. Nakatsu, Microbial Ecology along the Gastrointestinal Tract. *Microbes Environ* **32**, 300-313 (2017).

127. F. Rivera-Chavez *et al.*, Depletion of Butyrate-Producing Clostridia from the Gut Microbiota Drives an Aerobic Luminal Expansion of Salmonella. *Cell Host Microbe* **19**, 443-454 (2016).

128. M. S. Kennedy, E. B. Chang, The microbiome: Composition and locations. *Prog Mol Biol Transl Sci* **176**, 1-42 (2020).

129. S. Y. Wotzka *et al.*, Escherichia coli limits Salmonella Typhimurium infections after diet shifts and fat-mediated microbiota perturbation in mice. *Nat Microbiol* **4**, 2164-2174 (2019).

130. G. P. Donaldson, S. M. Lee, S. K. Mazmanian, Gut biogeography of the bacterial microbiota. *Nat Rev Microbiol* **14**, 20-32 (2016).

131. B. Stecher *et al.*, Flagella and chemotaxis are required for efficient induction of Salmonella enterica serovar Typhimurium colitis in streptomycin-pretreated mice. *Infect Immun* **72**, 4138-4150 (2004).

132. B. Stecher *et al.*, Motility allows S. Typhimurium to benefit from the mucosal defence. *Cell Microbiol* **10**, 1166-1180 (2008).

133. S. El Aidy, B. van den Bogert, M. Kleerebezem, The small intestine microbiota, nutritional modulation and relevance for health. *Curr Opin Biotechnol* **32**, 14-20 (2015).

134. M. J. Claesson, A. G. Clooney, P. W. O'Toole, A clinician's guide to microbiome analysis. *Nat Rev Gastroenterol Hepatol* **14**, 585-595 (2017).

135. M. Shimada *et al.*, Upper gastrointestinal pathophysiology due to mouse malaria Plasmodium berghei ANKA infection. *Trop Med Health* **47**, 18 (2019).

136. T. Taniguchi *et al.*, Plasmodium berghei ANKA causes intestinal malaria associated with dysbiosis. *Sci Rep* **5**, 15699 (2015).

137. C. D'Angelo, M. Reale, E. Costantini, Microbiota and Probiotics in Health and HIV Infection. *Nutrients* **9**, (2017).

138. J. E. Denny *et al.*, Differential Sensitivity to Plasmodium yoelii Infection in C57BL/6 Mice Impacts Gut-Liver Axis Homeostasis. *Sci Rep* **9**, 3472 (2019).

139. R. W. Crawford *et al.*, Very long O-antigen chains enhance fitness during Salmonella-induced colitis by increasing bile resistance. *PLoS Pathog* **8**, e1002918 (2012).

140. J. R. Sistrunk, K. P. Nickerson, R. B. Chanin, D. A. Rasko, C. S. Faherty, Survival of the Fittest: How Bacterial Pathogens Utilize Bile To Enhance Infection. *Clin Microbiol Rev* **29**, 819-836 (2016).

141. C. G. Buffie *et al.*, Precision microbiome reconstitution restores bile acid mediated resistance to Clostridium difficile. *Nature* **517**, 205-208 (2015).

142. C. R. Eade *et al.*, Bile Acids Function Synergistically To Repress Invasion Gene Expression in Salmonella by Destabilizing the Invasion Regulator HilD. *Infect Immun* **84**, 2198-2208 (2016).

143. A. M. Prouty, J. S. Gunn, Salmonella enterica serovar typhimurium invasion is repressed in the presence of bile. *Infect Immun* **68**, 6763-6769 (2000).

144. L. Zhang *et al.*, Impaired Bile Acid Homeostasis in Children with Severe Acute Malnutrition. *PLoS One* **11**, e0155143 (2016).

145. M. McRae *et al.*, Plasma bile acid concentrations in patients with human immunodeficiency virus infection receiving protease inhibitor therapy: possible implications for hepatotoxicity. *Pharmacotherapy* **30**, 17-24 (2010).

146. E. Deriu *et al.*, Influenza Virus Affects Intestinal Microbiota and Secondary Salmonella Infection in the Gut through Type I Interferons. *PLoS Pathog* **12**, e1005572 (2016).

147. J. D. Honeycutt *et al.*, Genetic variation in the MacAB-TolC efflux pump influences pathogenesis of invasive Salmonella isolates from Africa. *PLoS Pathog* **16**, e1008763 (2020).

148. J. Wehkamp *et al.*, Reduced Paneth cell alpha-defensins in ileal Crohn's disease. *Proc Natl Acad Sci U S A* **102**, 18129-18134 (2005).

149. C. L. Bevins, N. H. Salzman, Paneth cells, antimicrobial peptides and maintenance of intestinal homeostasis. *Nat Rev Microbiol* **9**, 356-368 (2011).

150. E. E. Olsan *et al.*, Colonization resistance: The deconvolution of a complex trait. *J Biol Chem* **292**, 8577-8581 (2017).

151. Y. Litvak *et al.*, Commensal Enterobacteriaceae Protect against Salmonella Colonization through Oxygen Competition. *Cell Host Microbe* **25**, 128-139 e125 (2019).

152. F. Rivera-Chavez, C. A. Lopez, A. J. Baumler, Oxygen as a driver of gut dysbiosis. *Free Radic Biol Med* **105**, 93-101 (2017).

153. M. Raffatellu *et al.*, Lipocalin-2 resistance confers an advantage to Salmonella enterica serotype Typhimurium for growth and survival in the inflamed intestine. *Cell Host Microbe* **5**, 476-486 (2009).

154. B. Stecher, The Roles of Inflammation, Nutrient Availability and the Commensal Microbiota in Enteric Pathogen Infection. *Microbiol Spectr* **3**, (2015).

155. S. Kim, A. Covington, E. G. Pamer, The intestinal microbiota: Antibiotics, colonization resistance, and enteric pathogens. *Immunol Rev* **279**, 90-105 (2017).

156. Q. R. Ducarmon *et al.*, Gut Microbiota and Colonization Resistance against Bacterial Enteric Infection. *Microbiol Mol Biol Rev* **83**, (2019).

157. S. Bibbo *et al.*, The role of diet on gut microbiota composition. *Eur Rev Med Pharmacol Sci* **20**, 4742-4749 (2016).

158. J. Ramirez *et al.*, Antibiotics as Major Disruptors of Gut Microbiota. *Front Cell Infect Microbiol* **10**, 572912 (2020).

159. D. D. Eichele, K. K. Kharbanda, Dextran sodium sulfate colitis murine model: An indispensable tool for advancing our understanding of inflammatory bowel diseases pathogenesis. *World J Gastroenterol* **23**, 6016-6029 (2017).

160. A. K. DeGruttola, D. Low, A. Mizoguchi, E. Mizoguchi, Current Understanding of Dysbiosis in Disease in Human and Animal Models. *Inflamm Bowel Dis* **22**, 1137-1150 (2016).

161. C. D. Shelton, M. X. Byndloss, Gut Epithelial Metabolism as a Key Driver of Intestinal Dysbiosis Associated with Noncommunicable Diseases. *Infect Immun* **88**, (2020).

162. E. M. Velazquez *et al.*, Endogenous Enterobacteriaceae underlie variation in susceptibility to Salmonella infection. *Nat Microbiol* **4**, 1057-1064 (2019).

163. S. Brugiroux *et al.*, Genome-guided design of a defined mouse microbiota that confers colonization resistance against Salmonella enterica serovar Typhimurium. *Nat Microbiol* **2**, 16215 (2016).

164. A. M. Spees *et al.*, Streptomycin-induced inflammation enhances Escherichia coli gut colonization through nitrate respiration. *mBio* **4**, (2013).

165. R. M. Tsolis, A. J. Baumler, Gastrointestinal host-pathogen interaction in the age of microbiome research. *Curr Opin Microbiol* **53**, 78-89 (2020).

166. A. Jacobson *et al.*, A Gut Commensal-Produced Metabolite Mediates Colonization Resistance to Salmonella Infection. *Cell Host Microbe* **24**, 296-307 e297 (2018).

167. J. P. Mooney *et al.*, Inflammation-associated alterations to the intestinal microbiota reduce colonization resistance against non-typhoidal Salmonella during concurrent malaria parasite infection. *Sci Rep* **5**, 14603 (2015).

168. N. F. Villarino *et al.*, Composition of the gut microbiota modulates the severity of malaria. *Proc Natl Acad Sci U S A* **113**, 2235-2240 (2016).

169. J. M. Stough *et al.*, Functional Characteristics of the Gut Microbiome in C57BL/6 Mice Differentially Susceptible to Plasmodium yoelii. *Front Microbiol* **7**, 1520 (2016).

170. S. Chakravarty, R. K. Mandal, M. L. Duff, N. W. Schmidt, Intestinal short-chain fatty acid composition does not explain gut microbiota-mediated effects on malaria severity. *PLoS One* **14**, e0214449 (2019).

171. B. Yilmaz *et al.*, Gut microbiota elicits a protective immune response against malaria transmission. *Cell* **159**, 1277-1289 (2014).

172. C. Milani *et al.*, The First Microbial Colonizers of the Human Gut: Composition, Activities, and Health Implications of the Infant Gut Microbiota. *Microbiol Mol Biol Rev* **81**, (2017).

173. M. A. Underwood, J. B. German, C. B. Lebrilla, D. A. Mills, Bifidobacterium longum subspecies infantis: champion colonizer of the infant gut. *Pediatr Res* **77**, 229-235 (2015).

174. R. K. Mandal *et al.*, Longitudinal Analysis of Infant Stool Bacteria Communities Before and After Acute Febrile Malaria and Artemether-Lumefantrine Treatment. *J Infect Dis* **220**, 687-698 (2019).

175. D. J. Paganini, T.; Cercamondi, C.; Kujinga, P.; Moretti, D.; Zimmermann, M., Anemia and iron status are predictors of gut microbiome composition and metabolites in infants and children in rural Kenya. *FASEB J. Conf. Exp. Biol* **30**, (2016).

176. M. X. Byndloss *et al.*, Microbiota-activated PPAR-gamma signaling inhibits dysbiotic Enterobacteriaceae expansion. *Science* **357**, 570-575 (2017).

177. T. Jaeggi *et al.*, Iron fortification adversely affects the gut microbiome, increases pathogen abundance and induces intestinal inflammation in Kenyan infants. *Gut* **64**, 731-742 (2015).

178. I. Vujkovic-Cvijin, M. Somsouk, HIV and the Gut Microbiota: Composition, Consequences, and Avenues for Amelioration. *Curr HIV/AIDS Rep* **16**, 204-213 (2019).

179. N. A. Feasey *et al.*, A reduction in adult blood stream infection and case fatality at a large African hospital following antiretroviral therapy roll-out. *PLoS One* **9**, e92226 (2014).

180. P. J. Turnbaugh *et al.*, The effect of diet on the human gut microbiome: a metagenomic analysis in humanized gnotobiotic mice. *Sci Transl Med* **1**, 6ra14 (2009).

181. M. S. Desai *et al.*, A Dietary Fiber-Deprived Gut Microbiota Degrades the Colonic Mucus Barrier and Enhances Pathogen Susceptibility. *Cell* **167**, 1339-1353 e1321 (2016).

182. S. Devkota *et al.*, Dietary-fat-induced taurocholic acid promotes pathobiont expansion and colitis in Il10-/- mice. *Nature* **487**, 104-108 (2012).

183. L. A. David *et al.*, Diet rapidly and reproducibly alters the human gut microbiome. *Nature* **505**, 559-563 (2014).

184. T. Sen *et al.*, Diet-driven microbiota dysbiosis is associated with vagal remodeling and obesity. *Physiol Behav* **173**, 305-317 (2017).

185. A. Agus *et al.*, Western diet induces a shift in microbiota composition enhancing susceptibility to Adherent-Invasive E. coli infection and intestinal inflammation. *Sci Rep* **6**, 19032 (2016).

186. S. Subramanian *et al.*, Persistent gut microbiota immaturity in malnourished Bangladeshi children. *Nature* **510**, 417-421 (2014).

187. L. Labarta-Bajo *et al.*, CD8 T cells drive anorexia, dysbiosis, and blooms of a commensal with immunosuppressive potential after viral infection. *Proc Natl Acad Sci U S A* **117**, 24998-25007 (2020).

188. K. Zhou, Strategies to promote abundance of Akkermansia muciniphila, an emerging probiotics in the gut, evidence from dietary intervention studies. *J Funct Foods* **33**, 194-201 (2017).

189. M. C. Dao *et al.*, Akkermansia muciniphila and improved metabolic health during a dietary intervention in obesity: relationship with gut microbiome richness and ecology. *Gut* **65**, 426-436 (2016).

190. B. P. Ganesh, R. Klopfleisch, G. Loh, M. Blaut, Commensal Akkermansia muciniphila exacerbates gut inflammation in Salmonella Typhimurium-infected gnotobiotic mice. *PLoS One* **8**, e74963 (2013).

191. R. Canals *et al.*, Adding function to the genome of African Salmonella Typhimurium ST313 strain D23580. *PLoS Biol* **17**, e3000059 (2019).

192. R. Schicho *et al.*, Quantitative metabolomic profiling of serum, plasma, and urine by (1)H NMR spectroscopy discriminates between patients with inflammatory bowel disease and healthy individuals. *J Proteome Res* **11**, 3344-3357 (2012).

193. B. L. Deatherage Kaiser *et al.*, A Multi-Omic View of Host-Pathogen-Commensal Interplay in Salmonella-Mediated Intestinal Infection. *PLoS One* **8**, e67155 (2013).

194. P. C. Harvey *et al.*, Salmonella enterica serovar typhimurium colonizing the lumen of the chicken intestine grows slowly and upregulates a unique set of virulence and metabolism genes. *Infect Immun* **79**, 4105-4121 (2011).

195. N. A. Feasey *et al.*, Distinct Salmonella Enteritidis lineages associated with enterocolitis in high-income settings and invasive disease in low-income settings. *Nat Genet* **48**, 1211-1217 (2016).

196. S. Van Puyvelde *et al.*, An African Salmonella Typhimurium ST313 sublineage with extensive drug-resistance and signatures of host adaptation. *Nat Commun* **10**, 4280 (2019).

197. E. J. Bottone, G. P. Wormser, F. P. Duncanson, Nontyphoidal Salmonella bacteremia as an early infection in acquired immunodeficiency syndrome. *Diagn Microbiol Infect Dis* **2**, 247-250 (1984).

198. J. L. Jacobs, J. W. Gold, H. W. Murray, R. B. Roberts, D. Armstrong, Salmonella infections in patients with the acquired immunodeficiency syndrome. *Ann Intern Med* **102**, 186-188 (1985).

199. M. A. Fischl, G. M. Dickinson, C. Sinave, A. E. Pitchenik, T. J. Cleary, Salmonella bacteremia as manifestation of acquired immunodeficiency syndrome. *Arch Intern Med* **146**, 113-115 (1986).

200. P. Katona, J. Katona-Apte, The interaction between nutrition and infection. *Clin Infect Dis* **46**, 1582-1588 (2008).

201. R. Balasubramanian *et al.*, The global burden and epidemiology of invasive non-typhoidal Salmonella infections. *Hum Vaccin Immunother* **15**, 1421-1426 (2019).

202. C. L. Harding, N. F. Villarino, E. Valente, E. Schwarzer, N. W. Schmidt, Plasmodium Impairs Antibacterial Innate Immunity to Systemic Infections in Part Through Hemozoin-Bound Bioactive Molecules. *Front Cell Infect Microbiol* **10**, 328 (2020).

203. L. I. Dos Santos *et al.*, Disrupted Iron Metabolism and Mortality during Co-infection with Malaria and an Intestinal Gram-Negative Extracellular Pathogen. *Cell Rep* **34**, 108613 (2021).

204. R. F. Potter, A. W. D'Souza, G. Dantas, The rapid spread of carbapenem-resistant Enterobacteriaceae. *Drug Resist Updat* **29**, 30-46 (2016).

205. K. A. Trott *et al.*, Evidence for an increased risk of transmission of simian immunodeficiency virus and malaria in a rhesus macaque coinfection model. *J Virol* **85**, 11655-11663 (2011).

206. P. E. Brentlinger *et al.*, Practical Management of HIV-Associated Anemia in Resource-Limited Settings: Prospective Observational Evaluation of a New Mozambican Guideline. *AIDS Res Hum Retroviruses* **32**, 12-25 (2016).

207. D. Das *et al.*, Complex interactions between malaria and malnutrition: a systematic literature review. *BMC Med* **16**, 186 (2018).

208. M. D. Herrero, P. Rivas, N. I. Rallon, G. Ramirez-Olivencia, S. Puente, HIV and malaria. *AIDS Rev* **9**, 88-98 (2007).

209. J. P. Mooney *et al.*, Transient Loss of Protection Afforded by a Live Attenuated Non-typhoidal Salmonella Vaccine in Mice Co-infected with Malaria. *PLoS Negl Trop Dis* **9**, e0004027 (2015).

210. M. J. Murray, A. B. Murray, M. B. Murray, C. J. Murray, The adverse effect of iron repletion on the course of certain infections. *Br Med J* **2**, 1113-1115 (1978).

Chapter 2

Surveying the impact of *Plasmodium yoelii* infection on the mouse intestine and colonization resistance

Gregory T. Walker[1], Connor R. Tiffany[1], Guiyan Yang[1,2], and Renée M. Tsolis[1]

[1]Department of Medical Microbiology and Immunology; University of California, Davis, Davis, CA 95616, USA

[2]College of Veterinary Medicine, China Agricultural University, Beijing 100193, China

ABSTRACT

Infection with malarial parasite is a significant risk factor to severe non-typhoidal *Salmonella* (NTS) disease. Research using mouse models has suggested that severe *Plasmodium* infection can also alter the composition of the fecal gut microbiota in a manner that reduces colonization resistance against NTS. Here, we expanded these observations throughout the initial two weeks of *Plasmodium* infection. We determined that after approximately 1 week, *Plasmodium* infected mice develop increased abundance of commensal *E. coli* when it is present in the gut, indicating that changes to the environment impacting *Enterobacteriaceae* members can occur by this point of the infection. We further assessed the potential of various microbial taxa and metabolic niches modulated by parasite infection at that timepoint to influence colonization resistance against NTS. Finally, we evaluated whether certain metabolism-associated enzymes encoded by the NTS genome are necessary for the pathogen to benefit from the *Plasmodium*-associated implantation boost.

INTRODUCTION

Most mucosal tissues and the skin are microbe-rich environments (*1*), colonized with flora that provide some level of colonization resistance that limit the incursion of bacterial pathogens and prevent infection of the healthy host (*2*). Significant disruptions in the “balanced” composition of the microbiota, known as dysbiosis, have been associated with increased risk of many diseases (*3*). Antibiotics in particular are known to often result in dysbiosis that significantly inhibits the ability of the microbiota to provide the sufficient colonization resistance limiting infection many bacterial pathogens (*4*). One popular model of non-typhoidal *Salmonella* colitis in mice actually uses pretreatment of the animals with the antibiotic streptomycin prior to infection with NTS to greatly enhance the colonization and inflammatory potential of the pathogen in the gut (*5, 6*), potentially through depletion of critical members of the microbiota (*7*).

In recent years, the field of microbiota research and 16S rRNA profiling of the variation of the bacterial microbiota in health and disease states has flourished in popularity (*8*). Investigators have uncovered that factors such as diet and genetics, that shape the microbial flora and promote differential disease outcomes (*9-13*). Additionally, concurrent or recent infection with many pathogens- including viruses (*14, 15*) and intestinal parasites such as *Toxoplasma gondii* (*16*) and *Giardia* (*17*)- have been shown to impact the composition of the microbiota. We recently reported that infection with the malarial parasite *Plasmodium* can modulate the host's intestinal microbiota (*18, 19*). This finding was somewhat surprising, as unlike *Toxoplasma* or *Giardia*, *Plasmodium* infection occurs primarily in the blood, liver, and spleen tissues (*20*), and the parasite does not directly interact with the contents of the human gut. Thus, it seemed likely the parasite was influencing the gut microbiota indirectly, either via localized immune responses against sequestered parasitized blood cells in the gut tissue vasculature (*18*) or generalized systemic immune responses that happen to alter gastrointestinal physiology (*21*).

Moreover, we found that this *Plasmodium*-altered microbiota was associated with boosted intestinal colonization of the NTS serovar *S.* Typhimurium, independent of *S.* Typhimurium-associated T3SS virulence, though the underlying mechanisms remained poorly understood. The findings present a potential public health concern, as malaria is also a known risk factor for the development of invasive NTS bacteremia disease (*22*). Thus, the collective effect of *Plasmodium* could be both potentiating the transmission of NTS while also increasing the odds of bacteremia, making NTS infections both more likely and more lethal in malaria-endemic regions. Here, we further explored the changes occurring in the intestinal environment of mice throughout early blood-stage *Plasmodium* infections to elucidate potential microbial and/or metabolic changes that might benefit *Salmonella* and closely related bacterial species.

RESULTS AND DISCUSSION

Plasmodium infection induces microbiota alterations in C57BL/6J mice

As our previous study was focused on characterizing the changes to the microbiota of a single set of mice infected with *Plasmodium*, we first wanted to confirm the previous findings while expanding our observations to better understand how the early course of *Plasmodium* infection influences the composition of the intestinal microbiota. To do this, two strains of 8-week-old mice (C57BL/6J and CBA/J) were injected with rodent *Plasmodium* parasite *P. yoelii nigeriensis* (*Pyn*)-infected blood or mock-infected with control blood from otherwise healthy mice (*n* = 6 mice per group, outlined in Fig. 2.1A). Prior to infection and over the following two weeks (at 3, 7, 10, and 14 days after infection), fecal samples were collected for 16s rRNA sequencing and mice were monitored for symptoms of illness (weight loss) and the development of parasitemia through tail blood sampling. Around 6 days post-parasite inoculation (dpp), the C57BL/6J mice infected with *Pyn* began to lose substantial amounts of weight (Fig. 2.1B), corresponding with an early spike in the parasite burden (Fig. 2.1C). By the end of the sampling period at 14 dpp, all *Pyn*-infected mice had developed significant splenomegaly and anemia relative to the mock-infected control animals (Fig. 2.1D and 2.1E). Additionally, there was a mild but not significant trend towards a shorter colon length in the infected mice (Fig 2.1F), a sign of intestinal inflammation that can occur with severe parasite infection (*19*).

Fecal pellets from all mice at days 0, 3, 7, 10, and 14 post-inoculation were flash frozen at collection, prior to bacterial DNA extraction and 16S rRNA sequencing. Echoing findings of earlier reports (*18, 19, 23*), this analysis found moderate modulation of the fecal microbiota composition during early *Plasmodium* infection of the C57BL/6J mice (Fig. 2.2-2.4 and Table 2.1). At the highest level of bacterial classification, mock-infected mice appeared to more stably maintain their starting microbiota, while *Pyn* infection resulted in a mix of changes at the different sampling timepoints. For example, early on in *Pyn* infection (3 dpp) there was a trend towards increasing relative abundance of the phyla *Verrucomicrobia* and *Actinobacteria*,

compared to mock-infected mice, where these phyla were comparatively stable throughout the observation period (Fig. 2.2A). The trend in *Verrucomicrobia* appears to arise from the genus *Akkermansia* (Table 2.1), likely the species *Akkermansia muciniphila*, a common member of the human intestinal microbiota. This species is known for breaking down and using host mucins for energy (*24*). A high abundance of *A. muciniphila* is associated with positive health outcomes, including a reduced risk of obesity (*25, 26*). However, when consuming diets low in fiber, *A. muciniphila* can also significantly degrade the mucus barrier and promote host susceptibility to enteric pathogens (*13*). It has also been shown that *A. muciniphila* blooms in response to viral-linked anorexia (*27*). Ultimately, the increased abundance could be a signal of reduced food intake leading to relatively improved competition by host-provided mucin-degrading *A. muciniphila* against the microbiota members depending on regular food and dietary fiber for energy. Alternately, *Plasmodium* infection could cause an acute release in mucus by goblet cells into the gut, perhaps via stimulation by histamine released from mast cells in response to the parasite (*21, 28*).

The 3 dpp boost in *Actinobacteria* seems to be due to the maintained abundance of the order *Coriobacteriales* coupled with a relative increase in the genus *Bifidobacterium* (family *Bifidobacteriaceae*, order *Bifidobacteriales*; Table 2.1). *Bifidobacterium* include many species of bacteria thought to be beneficial to the proper structure of the microbiome through their unique carbohydrate metabolism breaking down complex polysaccharides intro simpler sugars to cross-feed other microbial flora (*29*). Some strains of *Bifidobacterium,* including *B. longum* and *B. infantis,* have even been used as probiotics to treat diarrheal and inflammatory bowel diseases (*29*). This increased abundance could represent an actual metabolic niche opening early in *Pyn* infection that *Bifidobacterium* can expand to occupy, or potentially *Bifidobacterium* levels are actually stable, and the increased relative abundance solely represents a reduction in other taxa (e.g. *Firmicutes*).

The enrichment in low abundance taxa at 3 dpp seems to come at the expense of the phylum *Firmicutes*, which was concurrently reduced in *Pyn*-infected mice while remaining consistently high in the control mice (Fig 2.2A). However, at later time points of *Pyn* infection the *Firmicutes* rebound, while the *Verrucomicrobia* and *Actinobacteria* increased at 3 dpp subside to pre-infection levels (Fig 2.2A). Magnifying the analysis to lower classification levels clarifies that the reduction in the abundance of the *Firmicutes* was predominantly due to a relative drop in members of the family *Lachnospiraceae* (class *Clostridia*, order *Clostridiales*, Fig. 2.2B and 2.2C, Table 2.1), which includes critical butyrate producers (*30*) that help maintain gut hypoxia (*7*). This taxon then expanded to pre-infection levels by 7 dpp but was found at lower abundance at 10 dpp and 14 dpp, mirroring previous findings at 10 dpp (*18*). The higher abundance of *Firmicutes* was maintained after 7 dpp through increased abundance of the class *Bacilli* (order *Lactobacillales*). These trends in the *Clostridiales* and *Lactobacillales* levels at later timepoints were actually largely shared in the mock-infected mice too, though this group started with a lower relative abundance of *Clostridiales* (Fig. 2.2C). Considered as a whole, this suggests that husbandry effects could be relevant to the observed changes in the abundance of Firmicutes members in the *Pyn* group later on in infection.

To better assess what observed differences in microbiota composition were most likely to be (1) associated with *Pyn* infection, and (2) not just due to general shifts in the communities from shared husbandry practices, we compared the relative abundance of each detected taxon between the Mock-infected and *Pyn*-infected groups at each collection timepoint (Welch's *t*-test) as well as pairwise comparisons of each taxa's abundance between every *Pyn*-infected mouse before and during infection (Paired *t*-test). We list taxa that showed statistically significantly different ($P < 0.05$) relative abundances by both comparisons in Table 2.1. Notably, the 3 dpp timepoint featured the vast majority of composition differences by this measure (both increased and decreased abundance); the only other taxon found with statistically significantly different abundance at a different time point was an increased relative abundance of an unclassified

member of the family *Porphyromonadaceae* (order *Bacteroidales*) at 10 dpp (Table 2.1), which does generally track with our previous findings of increased *Bacteroidales* at 10 dpp (*18*).

To better understand what aspect of the comparison was leading to so few definable changes, we generated volcano plots to visually represent the overall magnitude of changes in taxa abundance with their degree of significance by these statistical comparisons (Fig. 2.3). By this measure, it is clear that there were already a number of differences between the microbiota of the groups of otherwise healthy mice prior to *Pyn* or mock infection (Fig. 2.3A), which could make it more difficult to pick out taxa that made relevant changes. Though every time point assessed actually displayed a number of taxa diverging from 0 dpp in the paired comparisons of *Pyn*-infected mice (Fig. 2.3B-D), only at 3 dpp was there also multiple taxa with matching significant differences when compared to the Mock-infected mice. Surprisingly, at the 7 dpp and 10 dpp timepoints it appears that the overall composition of the microbiota of *Pyn*-infected mice actually more closely resembles their mock-infected counterparts than their own microbiota prior to infection (Fig 2.3C and 2.3D). Overall, this suggests that the important *Pyn*-associated shifts in composition may be difficult to discern with this small of a sample size and such variability in the pre-infection microbiota.

Microbiota shifts with *Pyn* infection of CBA/J mice mirror C57BL/6J mice

Next, we wondered whether the severe malarial infection associated with the C57BL/6J-*Pyn* model was necessary, or if other mouse strains more “tolerant” to infection with the parasite would also present with microbiota shifts (*19*). To determine how consistent the microbiota changes during *Plasmodium* infection we observed are across genetic backgrounds, we sought to compare the general trends in C57BL/6J mice to changes that occur during parasite infection of more resistant CBA/J mice. While they are also an inbred strain, CBA/J mice are genetically distinct from the C57BL/6J strain in numerous ways. Critically, CBA/J mice maintain a fully-functioning *Nramp1* gene, which is known to provide improved resistance against many

intracellular pathogens (such as *Salmonella*) through metal withholding in macrophages phagolysosomes (*31*). *Nramp1* is also necessary for iron recycling by macrophages during hemolytic anemia (*32*), which could lead to a buildup in systemic tissues that negatively influences disease outcomes. We had noticed that CBA/J mice appear less susceptible to suffering severe morbidity from *P. yoelii nigeriensis* infection (Fig. 2.1B, Right Panel), although other aspects characteristic of the disease (including splenomegaly and anemia) still occur (Fig. 2.1C and 2.1D). Prior research has suggested that mice resistant to severe malarial disease may develop milder intestinal pathology and dysbiosis than susceptible strains (*19*). Thus, we hypothesized that the *Pyn*-infected CBA/J mice might not show alterations in their fecal microbiota, or that alterations that occur might be different than in C57BL/6J mice.

Remarkably, general trends in the microbiota of CBA/J mice closely mirror those observed in the C57BL/6J mice (Fig 2.4A and 2.4B). Like the C57BL/6J mice, the CBA/J mice also show a relatively increased abundance of *Verrucomicrobia* (genus *Akkermansia*) and *Bifidobacteriaceae* (genus *Bifidobacterium*) at 3 dpp that returned to low levels thereafter (Fig. 2.4B, Right Panel). Likewise, the CBA/J microbiota at 3 dpp showed reduced *Lachnospiraceae*, which increased significantly (above 0 dpp levels) at 7 dpp before showing reductions at 10 dpp and 14 dpp largely through an increase in *Lactobacillaceae* (Fig. 2.4B, Right Panel). Additionally, the mock-infected CBA/J mice generally showed more consistent levels of the various families of *Firmicutes* throughout the experiment (Fig. 2.4B, Left Panel), compared to the C57BL/6J mock-infected mice that displayed notable enrichment of *Lachnospiraceae* at 7 dpp and *Lactobacillaceae* at 10 dpp and 14 dpp (Fig 2.4A, Left Panel). This suggests that these shared shifts in the microbiota composition between CBA/J and C57BL/6J mice are a characteristic feature of the responses to *Plasmodium* infection and not simply husbandry effects, and that the noted variability in the mock-infected C57BL/6J microbiota is noise that potentially obscures relevant effects of the parasite.

Intriguingly, later time points in all sets of mice were associated with slightly increased alpha-diversity (intra-sample diversity) in the fecal microbiota, as we could sometimes detect over twice as many distinct OTUs as early in the infection (Fig. 2.4C and 2.4D), though there was little difference between the mock- and *Pyn*-infected groups by this measure. This might indicate changes in husbandry impacted the microbiota of these mice, whether through handling-based stress allowing low-abundance taxa to expand, or via introduction of outside microbes to the mice. In either scenario, such taxa were still maintained as very low-abundance members of their respective microbial communities (<1% relative abundance). Overall, these data suggest that *Pyn*-associated shifts in the gut microbiota are not solely attributable to the genetics of C57BL/6J mice, as they paralleled changes in the infected CBA/J mice.

Comparing microbiota alterations after 10 days of *Plasmodium* infection

In our previous report (*18*), we focused attention on the microbiota shifts that were detectable at 10 dpp. While we concluded that *Plasmodium* induced numerous changes to the microbiota in those experiments, we had found fewer significant changes at the matching time point in this follow-up work (Table 2.1). However, we also used a significantly lower parasite dose when infecting these mice (10-fold fewer parasite-infected RBCs), to limit the potential for severe weight loss and mortality during the experiment. This lower infectious dosage could cause a less severe disease with reduced capacity to transform the gut environment or change the timing of when certain changes arise during the infection. Still, when considered as a whole, the microbiota does appear to change form multiple times during early *Plasmodium* infection compared to healthy mice (Fig. 2.2), and we even see a shift in the 10 dpp populations when plotted using non-metric multidimensional scaling (Fig. 2.5A). To further assess the validity of our previous findings, we homed in on mice at the 10 dpp time point, and individually reassessed taxa that we had observed changing significantly in the prior study. The primary significant change found at 10 dpp in the current study was an increase in the abundance of an

Unclassified genus of the *Bacteroidetes* family *Porphyromonadaceae* (Table 2.1 and Fig. 2.5B). In the overall context, it is clear that this trend was also dependent on a concurrent reduction of the taxa in mock-infected animals (Fig 2.5B). However, abundance of members of the genus still trended in opposite directions in the mock and *Pyn* groups, suggesting that *Plasmodium* had a greater impact on this *Porphyromonadaceae* than the shift that naturally occurred in the healthy mice.

Our previous work had noted that some of the most interesting changes were in the relative reduction of *Firmicutes* and relative increase in *Bacteroidetes*, the two dominant phyla making up the healthy mouse microbiota (*33*). When considering these taxa individually, these trends hold in same direction for this study (Fig. 2.5C and 2.5D), though both taxa are still highly abundant. On a finer level, we also still see reductions in the relative abundance of the genus *Ruminococcus* (Fig. 2.5E), though abundance levels were significantly lower than previously observed (1.0% previously versus less than 0.1% in these mice). This finding was of potential interest, as a loss of *Firmicutes* of the class *Clostridia* has been associated with dysbiosis and reduced colonization resistance against non-typhoidal *Salmonella* species (*7*). Many members of this taxa, especially of the families *Lachnospiraceae* and *Ruminococcaceae* are known as important producers of butyrate (*34*), a SCFA produced by dietary fiber degradation and used by epithelial cells lining the colon as a primary source of energy. Metabolism of butyrate into acyl-CoA chains by colonocytes is achieved via beta-oxidation, a process that also consumes most oxygen reaching these cells. This breakdown of butyrate keeps the colonic epithelium strongly hypoxic and the lumen nearly anoxic, benefitting the commensal anaerobes (*35*). When butyrate levels are severely depleted- such as during antibiotic treatment (*7*) or severe inflammation inhibiting the commensal butyrate producers (*36*)- colonocytes may switch their metabolism away from oxygen-heavy beta oxidation, allowing diffusion of oxygen across the epithelium to oxygenate the colon (*37*). This provides a new growth niche benefitting facultative anaerobes, such as *Salmonella* and endogenous *Enterobacterales* like *E. coli* (*35*).

We reasoned that if the microbiota changes during *Plasmodium* infection were a sign of reduced intestinal butyrate, it might explain the depleted colonization resistance of NTS. Remarkably, butyrate levels measured in the cecal contents of *Pyn*-infected mice at 10 dpp were found to be approximately half the concentration in healthy mice (Fig. 2.5F). Other SCFAs, including acetate and propionate, also trended toward lower concentrations, and lactate levels were also slightly reduced (Fig. 2.5F), suggesting alterations to the metabolome co-occurring with the microbiota changes. This difference in SCFAs signified that altered colonocyte metabolism could play a role in *Pyn*-associated loss of colonization resistance. Additionally, although it was not severely depleted, propionate produced by *Bacteroides* species has been linked with inhibiting *Salmonella* in the gut (*38*), suggesting an alternate SCFA mechanism that could contribute.

To determine whether *Pyn* infection results in a loss of colonic hypoxia that could benefit colonizing *Salmonella*, we treated mice with the hypoxia-probing dye pimonidazole (PMDZ) at 10 dpp, 1 hour prior to euthanizing the animals. This hypoxia marker binds to thiol-containing proteins in very low oxygen environments (pO_2 < 10 mmHg) (*39, 40*), including the healthy intestinal epithelial border (*7*). Formalin-fixed, paraffin-embedded cecal tissues collected at necropsy were immunofluorescently stained for PMDZ (primary antibody: mouse anti-PMDZ; secondary: goat anti-mouse-Cy3-conjugated) and counterstained with DAPI for cell nuclei detection. Although we expected reduced PMDZ signal in cells lining the lumen of *Pyn*-infected mice (indicating increased epithelial oxygenation), we instead observed at least equivalent staining in mock and *Pyn*-infected mice at 10 dpp (Fig. 2.5G), which suggests increased oxygenation of the lumen at this time point is not likely to be occurring. As controls, tissues from healthy mice not administered PMDZ, and tissues from PMDZ-treated animals but not exposed to the secondary fluorescent antibody were also assessed and displayed significantly less signal (Fig. 2.5G, Right Panels), indicating the fluorescence was specific to the hypoxia probe and not autofluorescence of the tissues. Although these findings appear to counter to the lower levels of

butyrate, that 2-fold reduction is actually relatively minor compared to the massive (1000-fold) depletion following streptomycin treatment (*7*). We actually see somewhat greater tissue hypoxia in the *Pyn*-infected mouse tissues, which could be a result of the reduced oxygen carrying capacity due to the severe malarial anemia caused by the parasite (*41*).

Overall, these results suggest that many of the shifts in the gut microbiota associated with *Pyn* infection of C57BL/6J mice are broadly consistent in their direction, if not necessarily in degree. Additionally, while some of these alterations may be linked to differences in the abundance of metabolite such as SCFAs, it is unclear how much these subtle differences impact host physiology.

Intestinal *E. coli* (when present) blooms during *Plasmodium* infection

While these findings may represent microbiota changes that truly occur during severe clinical infections with *Plasmodium*, one potentially critical factor is missing from the C57BL/6J and CBA/J models: these mice lack any naturally occurring culturable commensal *Enterobacteriaceae,* such as *E. coli.* This is by design, as The Jackson Laboratory has screened out these potential pathobionts from their specific pathogen-free (SPF) mouse stocks (*42*). However, it is known that species like *E. coli* are ubiquitous (though typically low-abundance) members of human microbial flora (*43*), and potentially provide some degree of colonization resistance in the gut against related pathogens like *Salmonella* via metabolic niche pre-emption (*12, 42*). Thus, we hypothesized that if a commensal *Enterobacteriaceae* such as *E. coli* was present in the gut during *Pyn* infection it would actually derive a growth benefit through the same metabolic components benefitting *Salmonella* Typhimurium.

To test this, we experimentally infected C57BL/6N mice acquired from Charles River Laboratory with *Pyn. Enterobacteriaceae* naturally occur as part of the intestinal flora of these mice (*42*), including culturable *E. coli*, allowing for *Plasmodium*'s influence on these bacterial populations in the feces to be easily assessed over the course of infection. *Plasmodium*

infection resulted in a significantly increased abundance of commensal *E. coli* in these mice, with a peak of 1000-fold increase over pre-infection *E. coli* levels (Fig. 2.6A and 2.6B). Intriguingly, this increase in *E. coli* was most prominent at 7 dpp after beginning to onset around 5 dpp, and was maintained at higher levels than pre-infection and mock-infected controls through 14 dpp. A similar pattern also occurred in C57BL/6J mice that were pre-colonized with a mouse commensal *E. coli* JB2 (*44*) for 3 weeks prior to *Pyn* infection (Fig. 2.6C and 2.6D). Prior research indicated that the composition of the gut microbiota can influence parasite burden and infection outcomes (*45*), but both *E. coli* models developed significant parasite burdens (Fig 2.6E), comparable both to each other and to infection in mice lacking *E. coli* (Fig. 2.1C), signifying overall similar courses of infection.

The time points found to be associated with increased *E. coli* abundance do not neatly correlate temporally with changes previously observed in the rest of the microbiota. Most of the microbiota alterations were transient, arising at 3 dpp and subsiding by 7 dpp (Fig. 2.4A and Table 2.1). It may be that the changes seen at 3 dpp lead to the environment that allows *Enterobacteriaceae* to flourish, but that in the absence of *Enterobacteriaceae* to occupy the niche the microbiota composition returns to the former state. Alternately, the microbiota changes with *Plasmodium* may just be a marker of other host associated changes to the gut environment that are more important to enhanced Salmonella colonization than the specific differences in the microbiota.

We hypothesized that the bloom in *E. coli* marks the onset of impaired colonization resistance during *Plasmodium* infection. To test this hypothesis, we challenged mice with *S.* Typhimurium lacking functioning type-III secretion systems (T3SS)-1 and -2 (IR715 *invA spiB phoN*::Cm^{R}*)* earlier in the course of *Pyn* infection and assessed the fecal burden 24 hours later. *Pyn*-infected mice challenged at 6 dpp were colonized to significantly higher levels the next day than mock-infected mice at the same time point (Fig. 2.6F). Earlier infection (3 dpp) showed trends towards higher burdens as well, but with less consistency than the 6 dpp time point. Both

groups showed similar patterns of parasitemia (Fig. 2.6G), though parasitemia still increased past the 3 dpp time point. Overall, these data suggest that *Pyn* abrogates colonization resistance against *S.* Typhimurium and *E. coli* by around 6 dpp. This time typically follows an early peak of parasite infection in the model around 5 dpp (Fig. 2.6E), which could be relevant to the changes.

Finally, it is known that commensal or probiotic *E. coli* can provide some degree of colonization resistance to mice against *S.* Typhimurium (*42, 46*). As *E. coli* blooms during *Pyn* infection correlated with the timing of onset of increased *S.* Typhimurium implantation, we questioned whether the presence of *E. coli* in the microbial flora would be sufficient to prevent enhanced *Salmonella* levels in co-infected mice. C57BL/6N mice from Charles River Laboratory with natural *E. coli* were infected with *Pyn* or control blood, and challenged with *S.* Typhimurium (IR715 *invA spiB phoN*::Cm^R) at 6 dpp for 24 hours. By 6 dpp, fecal *E. coli* had bloomed in 4 of the 6 *Pyn*-infected mice (Fig. 2.6H), with comparatively no change in *E. coli* levels in mock-infected animals (Fig. 2.6I). At 24 hpi, *S*. Typhimurium had still colonized to significantly higher levels in the *Pyn*-infected mice compared to the mock-infected controls (Fig. 2.6J), despite the presence of endogenous *E. coli*. This finding implies that either the *Pyn* infection creates a large enough niche for both strains to grow to similarly high levels, or that separate niches are opened at the same time that allow for both *E. coli* blooms and enhanced *S.* Typhimurium implantation. In either case, it seems that increased *E. coli* loads and susceptibility to enhanced *S.* Typhimurium are highly correlated during *Pyn*-infection, as the mice that did not show *E. coli* blooms also presented with significantly lower *S.* Typhimurium burdens than the remainder of the group (Fig. 2.6J).

Pyn-linked microbiota alterations correlating with higher *S.* Typhimurium loads

Our findings suggested that the degree of *S.* Typhimurium susceptibility in a *Pyn*-infected mouse might correlate directly with the composition of the intestinal environment. Our

prior studies also suggested the parasite-altered microbiota was at least partially sufficient to explain enhanced *S.* Typhimurium implantation (*18*). Germ-free mice given a fecal microbiota transplant from *Plasmodium*-infected mice prior to *S.* Typhimurium challenge displayed enhanced *S.* Typhimurium colonization as well, suggesting the *Pyn*-associated microbiota (rather than the parasite or host immune response) was important to influencing *S.* Typhimurium colonization (*18*). Therefore, we hypothesized that the NTS acquires a growth advantage in the intestines of *Plasmodium*-infected animals from microbiota and metabolic alterations in the gut environment that introduce a new niche for boosted NTS growth.

In order to characterize changes in the intestinal environment during infection that were both associated with *Pyn* and also likely to explain the differential Salmonella colonization we observe, we collected fecal pellets for both 16S rRNA sequencing and untargeted metabolomics analysis from mock- and *Pyn*-infected mice immediately prior to oral *S.* Typhimurium challenge, then assessed *Salmonella* burden 24 later (outlined in Fig. 2.7A). As usual, *Pyn*-infected mice lost weight (Fig. 2.7B) and developed significant detectable parasitemia by 6 dpp (Fig. 2.7C). *S.* Typhimurium loads from *Pyn*-infected mice were on average 100-fold higher than mock infected mice (Fig. 2.7D), and the overall range of *S.* Typhimurium levels between the two groups varied from less than 10^5 to nearly 10^9 CFU/g colon content, providing a large scope to compare and correlate notable changes in microbial taxa and metabolite abundance.

While the overall microbiota structure had not shifted significantly from pre-infection composition relative to the mock-infected controls (Fig. 2.7E), individual taxa clearly appeared to be impacted by *Pyn* infection at 6 dpp (Fig. 2.8A and 2.8B). Of particular note is a relative reduction in the abundance of *Lactobacillus* at 6 dpp, which made up a significant proportion of the 16S reads in all the mice at 6 dpp (Fig. 2.8B). It also appears that various Clostridia, including *Lachnospiraceae* and *Ruminococcaceae*, were enriched at 6 dpp, particularly an Unclassified genus of *Lachnospiraceae* and a minor increase *Clostridium* cluster XIVa, a set of species known for butyrate production (*47*). Additionally, we also see a relatively increased

abundance of *Akkermansia*, which previously had been enriched at 3 dpp but were no longer at 7 dpp (Fig. 2.4A and Table 2.1). Overall, there were some notable shifts in specific taxa during *Pyn* infection by 6 dpp, which might help explain the boost to *Enterobacteriaceae* during infection that onsets around this point.

To better highlight microbial taxa that correlate strongest with the increased colonization of *S.* Typhimurium, we plotted the nonlinear regression of the Log_{10}(Relative Abundance) of every detected genus-level OTU in both the mock and *Pyn* groups at 6 dpp against that mouse's associated colonic *S.* Typhimurium burden the next day. Few taxa strongly correlated ($R^2 \geq 0.30$) over the whole range of *S.* Typhimurium burdens detected in the mice. Of those that did, higher *Akkermansia*, *Parasutterella* (Class *Betaproteobacteria*, Order *Burkholderiales*), and *Bifidobacterium* abundance at 6 dpp was generally associated with higher *S.* Typhimurium the next day (Fig. 2.9A), while an unclassified *Lachnospiraceae*, *Senegalinassilia* (Class *Actinobacteria*, Order *Coriobacteriales*), and *Prevotella* (Class *Bacteroidia*, Order *Bacteroidales*) were associated with lower *S.* Typhimurium colonization (Fig. 2.9B).

However, for the hypothesis that it is *Pyn*-associated changes to the taxa driving the boosted *Salmonella* growth to hold true, the correlation must also be nearly as strong (or stronger) in the *Pyn* group alone. By this measure, *Akkermansia, Parasutterella,* and the unclassified Lachnospiraceae genus either do not correlate, or in the case of *Akkermansia*, show the reverse trend when considering the *Pyn* group alone (Fig. 2.9A and 2.9B, red lines), indicating they are not likely to be contributing to the enhanced *Salmonella* colonization in those mice. Of the remaining taxa, although *Bifidobacterium* correlates decently well with *Salmonella* burden ($R^2 = 0.2920$, Fig. 2.9A, Right Panel), it does not appear to actually be strongly influenced by *Pyn* infection at this time point (Fig. 2.9C), compared to *Akkermansia* and *Parasutterella*. Similarly, *Senegalimassilia* abundance is not strongly impacted by the parasite (Fig. 2.9D), suggesting these correlations may simply be statistical noise. This left only *Prevotella*, which was both reduced with *Pyn* infection (Fig. 2.9D) and trended with the

Salmonella numbers (Fig. 2.9B, Right Panel). *Prevotella* is a member of the *Bacteroidales* order that has been positively associated with dietary fiber intake (*48*), but was not directly associated with inhibiting *Salmonella* colonization in past studies (*38*). Though it is found at very low abundance in these mice (0.01-0.1%), its reduction, like the increase in *Akkermansia*, could be a sign of reduced dietary fiber availability to the intestinal microbiota at this point of *Pyn* infection. Taken together, these data indicate that the microbial changes that occur by 6 dpp during *Pyn* infection do not appear to strongly correlate with the heightened susceptibility to *S.* Typhimurium infection that onsets at this time.

Intestinal metabolome changes with malaria cannot explain boosted *Enterobacteriaceae*

While we found few microbiota changes during *Pyn* infection that could potentially directly account for the loss in colonization resistance alone, we hypothesized that perhaps as a whole, changes to the gut environment could be impacting the metabolome in the intestinal lumen in a manner that the compositional changes to the microbial flora would not account for. To test this, we homogenized fecal pellet samples collected from the mice in the previous experiment in sterile water. We then centrifuged the samples to pellet bacteria and debris and submitted the supernatant samples for untargeted metabolomics analysis (GC-TOF MS) to assess the relative abundance of water-soluble metabolites generally available for *Salmonella* to use in the lumen.

The screen detected 261 discernable metabolites in the samples (92 known, 169 unknown). As a whole, the metabolite profiles of mock- and *Pyn*-infected mice were largely similar at 0 dpp and 6 dpp, with largely overlapping in the groups by principal component analysis (Fig. 2.10A). To assess whether specific metabolites were impacted by *Plasmodium* infection, we compared the differences between metabolites in the mock versus *Pyn* groups at the different time points, and within the mock and *Pyn* groups from pre-infection to 6 dpp (Fig. 2.10B-E). Unlike the microbiota profiles, there appeared to be minimal significant and

substantial (>2-fold) difference in detected metabolites between the mouse groups prior to infection (Fig. 2.10B). Still, few metabolites appeared to differ between the groups at 6 days of infection, and those that did show large changes were unknowns that did not allow for further hypothesis generation (Fig. 2.10C). Yet, within the infected mice a subset of metabolites was found to be consistently changed at 6 dpp that did not change within the mock-infected mice (Fig. 2.10D and 2.10E). Xanthine, ornithine, lysine, and three unknown metabolites were significantly and substantially increased in the feces at 6 dpp, while lactic acid and an additional unknown metabolite were concurrently reduced (Fig. 2.10E). It is unclear if these changes are relevant to *Salmonella* colonization, as their relative concentrations did not actually correlate with pathogen load either (data not shown). Taken together, these data do not indicate that many significant changes to the primary intestinal metabolome are occurring during early *Pyn* infection that could account for the enhanced *Salmonella* or *E. coli* colonization potential around 6-7 dpp. However, as the metabolomics was limited to water-soluble free metabolites not associated with larger particles that pellet during centrifugation, many potential targets could have been missed. Further studies should be undertaken to better characterize the full effect of *Plasmodium* infection on the intestinal environment.

Increased respiratory growth cannot explain boosted *S.* Typhimurium with malaria

As the gut microbiota and metabolomics analyses failed to generate specific targets in that might explain the *Pyn*-linked susceptibility to *Enterobacteriaceae* colonization, we next considered metabolic niches known to benefit *Salmonella* and other *Enterobacteriaceae* that might not be detectable by mass spectrometry. One way that *Salmonella* and *E. coli* differ from much of the commensal microbiota is through to encoding a number of respiratory reductases and oxidases that allow for enhanced growth with a variety of anaerobic and aerobic electron acceptors (*49-53*). For instance, it has been shown that during inflammation *Salmonella* requires its tetrathionate reductase locus (*ttr*) to gain a growth benefit from the tetrathionate that

is generated from respiratory bursts of white blood cells oxidizing thiosulfate (*49*). Additionally, *Salmonella* infection stimulates epithelial cells in the colon to generate nitric oxide via inducible nitric oxide synthase (iNOS). This nitric oxide can then be oxidized to nitrate in the inflamed intestine, which intestinal *Salmonella* or *E. coli* can use for respiratory growth via their nitrate reductases (*50, 51*).

Since *Pyn* infection was associated with an increased inflammatory tone of the intestines in our previous study (*18*), we hypothesized that this parasite-associated inflammation could be increasing anaerobic respiratory electron acceptor levels in the gut, thereby creating a respiratory growth niche for *Salmonella*. To test this, we performed a competitive *Salmonella* infection experiment at 6 dpp. Mice were given an oral infection of equal amounts (approximately $5x10^8$ CFU each) of a wildtype *S.* Typhimurium (IR715) and an isogenic *moaA* mutant, and the fecal burden of each strain was assessed the following day (Fig. 2.11A). MoaA is the first enzyme for catalyzing molybdopterin cofactor biosynthesis, a necessary component for the function of both nitrate and tetrathionate respiratory reductases as well as enzymes for using DMSO or TMAO; the *moaA* mutant is therefore deficient in using these anaerobic electron acceptors for enhanced growth (*52*). Although the wildtype *S.* Typhimurium colonized the *Pyn*-infected mice to significantly higher levels than mock-infected mice (Fig. 2.11B, Left Panel), the *moaA* mutant generally colonized the mice equally well, with little competitive defect and no difference in the competitive index (Wildtype/mutant ratio in the feces, corrected to the inoculum ratio) between the mock- and *Pyn*-infected groups (Fig. 2.11B, Right Panel). To confirm that the T3SS virulence of wildtype Salmonella was not influencing the intestinal environment to somehow compensate for the *moaA* mutant, we also assessed competition of the *moaA* mutant in an *invA spiB* (T3SS-1/2 deficient) background. Still, no significant colonization deficiency was found in the *moaA* mutant in either group, indicating that anaerobic respiration of the inflammatory byproducts nitrate and tetrathionate was dispensable for enhanced colonization during *Pyn* infection (Fig. 2.11C).

Next, we wanted to confirm that oxygen was not a significant contributor to the enhanced *S.* Typhimurium colonization. As *Salmonella*-associated intestinal inflammation has been shown to be sufficient in reducing intestinal hypoxia alone (*7*), we generated a double cytochrome oxidase mutant (*cydAB cyxAB*) deficient in aerobic respiration using the *invA spiB* background for competitive infection. The mutant did display reduced colonization relative to the oxidase-containing strain (Fig. 2.11D, Left Panel), suggesting oxygen-based respiration is driving some portion of the overall *S.* Typhimurium levels. However, the defect was the same size in mock-infected mice (Fig. 2.11D, Right Panel), confirming that boosted growth via respiration of oxygen was not associated with the increased implantation during *Pyn* infection at this time point.

Salmonella has also been shown to grow using hydrogen (H_2) as an energy source via a set of hydrogenases (predominantly *hyb*) (*53*). Thus, we hypothesized that changes in the microbiota with *Pyn* infection might increase access to hydrogen for enhanced *S.* Typhimurium growth. However, competition against a triple-hydrogenase knockout mutant (*hya hyb hyd*) indicated that while the hydrogenase mutant was deficient in colonization (Fig. 2.11E, Left Panel), *Pyn* infection actually reduced the competitive defect. This suggests that hydrogen was actually less important for colonizing *Pyn*-infected mice at 6 dpp.

Outside of respiratory growth, access to metals needed for survival in the host gut- in particular iron- contributes to competition between many bacterial species (*54*). As *Plasmodium* infection results in significant hemolysis (Fig. 2.1E), we hypothesized that this might increase access to iron (potentially hemoglobin-bound) in the gut. Interestingly, we found lipocalin-2 levels were slightly increased in the cecal contents of *Pyn*-infected mice (Fig. 2.11F), suggesting the mice may be attempting to sequester iron from microbes in the intestine (*55*). However, a *S.* Typhimurium iron uptake mutant (*tonB feoB*) (*56*) displayed even less of a competitive defect than in mock-infected mice, despite significantly higher bacterial burden overall (Fig. 2.11G). This suggested that differential iron access during *Plasmodium* infection was not critical in

driving boosted *S.* Typhimurium levels at 6 dpp. Taken together, these results suggest that many of the mechanisms by which *S.* Typhimurium typically gains a competitive advantage in the mammalian gut over time are not important contributors to the initial increased implantation of the pathogen that can occur during early *Pyn* infection.

Conclusions

From our experiments following up on the observations in Mooney et al. (*18*), we confirmed that *Pyn* infection promotes characteristic shifts in the composition of the mouse intestinal microbiota (Fig. 2.4). Some of these changes, such as the increased abundance of *Akkermansia* and concurrent reductions in fiber-degrading bacteria, may be side effects of the acute anorexic response that occurs early in the *Plasmodium* infection (*27*). Potentially more important is the enrichment in *E.* coli, if it is present in the gut, beginning around 1 week of parasite infection (Fig. 2.6). Moreover, minor changes in the composition of the gut metabolome could also be observed (Fig. 2.10). However, these changes in the intestinal environment were not significantly correlated with the enhanced non-typhoidal *Salmonella* colonization witnessed in *Pyn* co-infected mice (Fig. 2.9). One caveat to this and all 16S rRNA profiling and untargeted metabolomics studies is that our data is compositional (*57*), and only indicates the relative abundance of different bacterial taxa and metabolites in the gut. Thus, this type of analysis might easily miss large shifts in the absolute amounts of certain factors that are actually driving the differences between groups. Potentially, a targeted screen for certain metabolites known to benefit *S.* Typhimurium competition and growth in the gut (such as bile acids (*12*) or 1,2-propanediol (*52*)) would more clearly elucidate the impact of *Plasmodium* on this complex environment.

Additionally, these findings seem to contradict our previous report, which found the *Pyn*-associated microbiota underlies *Salmonella* colonization differences (*18*). However, we have altered the infection here- using a lower parasite dose and focusing on the microbiota

associated with a different time point- to a degree that direct comparisons to the previous report may be invalid. It is not obvious whether a fecal microbiota transfer from *Pyn*-infected mice at 6 dpp to germ-free animals would be sufficient to promote higher *S.* Typhimurium loads than FMT from control mice. Nevertheless, this study suggests that such *Plasmodium*-associated microbiota changes may not be strictly necessary for enhanced Salmonella colonization. The overall composition of the microbiota has changed little by 6 dpp (Fig. 2.7E), despite these mice being significantly more susceptible to *S.* Typhimurium by this time point (Fig. 2.6F and 2.7D). Rather, the changes we see seem to be a symptom of other parasite-associated alterations in the environment that may be differentially impacting both the microbial composition and *Salmonella* loads. Further studies to better characterize the differential impact of FMT from healthy and *Pyn*-infected animals to germfree mice would be useful in defining what microbiota changes, if any, are biologically significant to altered colonization resistance during infection.

MATERIALS AND METHODS

Animal experiments. All animal experiments were approved by the Institution of Animal Care and Use Committee at the University of California, Davis. 6 to 8 week-old female C57BL/6J mice (stock no. 000664) and CBA/J (stock no. 000656) were purchased from The Jackson Laboratory. For experiments requiring animals with naturally occurring *E. coli*, 6 to 8 week-old female C57BL/6NCrl mice were purchased from Charles River Laboratory. For generating *Plasmodium* parasitized blood stocks, CD-1 mice were purchased from Charles River Laboratory. Mice were housed under specific pathogen-free conditions and used for experiments at 8 to 11 weeks of age with at least 4 mice in each group.

***Plasmodium* infections**. *Plasmodium yoelii nigeriensis* (*Pyn*) parasite stock was obtained from the Malaria Research and Reference Reagent Resource (MRRRR) and was maintained and

expanded by passage through CD-1 mice. Blood from multiple CD-1 mice infected with parasite was collected by cardiac puncture, pooled, and mixed 1:2 (vol/vol) with freezing solution (10% glycerol and 90% Alsever's solution [Sigma-Aldrich]) for storage in liquid nitrogen. For mock infections, blood was collected from uninfected CD-1 mice and similarly preserved.

For infections, parasitized blood stocks were diluted to $4x10^7$ parasite-infected red blood cells (iRBCs)/mL with 0.9% saline and mice were inoculated intraperitoneally (ip) with 0.1 mL of diluted parasitized blood. For mock infections, uninfected control blood was diluted with an equivalent volume of saline, and 0.1 mL was injected ip into the mice. Parasite infection was tracked through a combination of weight loss, blood cell counts, and parasite burden in the blood. For circulating blood cell counts, tail blood was diluted 1:1000 in PBS and cell concentration was assessed using a hemocytometer or TC20™ Automated Cell Counter (Bio-Rad Laboratories, Inc.). Counts were normalized to the average counts from the mock-treated animals collected and measured at the same time to allow for improved comparisons of anemia across groups. Parasitemia was determined by examination of Giemsa-stained (Harleco) thin blood smears from tail blood to enumerate the percentage of red blood cells containing detectable *Pyn* parasites.

Fecal microbiota analysis by 16S rRNA sequencing. For 16S rRNA analysis of the intestinal microbiota throughout infection, fecal pellets from all mice at indicated time points were collected fresh and flash frozen in liquid nitrogen, then stored at -80°C. Whole pellets were submitted to SeqMatic (Fremont, CA) for bacterial DNA extraction, library preparation and Illumina MiSeq analysis of the 16S rRNA locus amplicons collection. Phylogenetic analysis of the 16S rRNA sequences was accomplished using the Qiime pipeline (Version 1.9.0) with the GreenGenes 16s Reference Database (gg_13_8_otus) and a 97% species match threshold to cluster operational taxonomic units (OTUs) for further analysis. Initial assessment of the microbiota and NMDS plots comparing groups were generated using R open-source software

(www.r-project.org) and the packages Phyloseq and Gggplot. Significant differences in the Log-normalized relative abundance of OTUs between the Mock-infected and *Pyn*-infected groups at each collection timepoint were determined by Welch's *t*-test on each taxa at each time point (0, 3, 7, and 10 dpp), and significant changes within *Pyn*-infected animals were determined by Paired *t*-tests on the Log-normalized abundance at each time point of interest versus 0 dpp. Statistics were analyzed and abundance data plotted in Prism 9 (GraphPad).

Metabolomics of intestinal content. Targeted measurement of intestinal SCFA concentrations in cecal content was performed using an ultra-high performance liquid chromatography triple quadrupole mass spectrometer (UHPLC-QqQ-MS) on treated supernatant from samples homogenized in nanopure water, as previously described (*37*).

Untargeted metabolomic screen of fecal content at 0 and 6 dpp was performed by the West Coast Metabolomics Center (Davis, CA). Samples were submitted as supernatant of fecal pellets homogenized in ultrapure water, then centrifuged to limit analysis to soluble components. Samples were assessed by gas chromatography-Time-of-Flight Mass Spectrometry (GC-TOF MS) to detect components of primary metabolism, including: carbohydrates and sugar phosphates, amino acids, hydroxyl acids, free fatty acids, purines, pyrimidines, aromatics, and exposome-derived chemicals. Maximum peak heights of detected metabolites were used for relative quantification. Principal component analysis was performed using R open-source software and comparisons between groups were made using Welch's and Paired *t*-tests on Log-normalized abundances (as with OTUs) in GraphPad Prism.

Bacterial strains. A complete list of *Salmonella* and *E. coli* strains used in this study can be found in Table 2.2. Unless otherwise indicated, bacteria were routinely grown on LB agar or MacConkey agar plates and cultured aerobically at 37°C in lysogeny broth (LB) supplemented with antibiotics at the following concentrations for selection when appropriate: nalidixic acid (Nal), 0.05 mg/mL; carbenicillin (Carb), 0.1 mg/mL; kanamycin (Kan), 0.1 mg/mL;

chloramphenicol (Cm), 0.03 mg/mL. The mouse commensal *E. coli* JB2 was a generous gift from Dr. Manuela Raffatellu (*44*).

Construction of most mutant *S.* Typhimurium strains used in this study has been described in prior work (Table 2.2). To construct the double cytochrome oxidase mutant *S.* Typhimurium *invA spiB cydAB cyxAB* (GTW47, IR715 Δ*invA* Δ*spiB phoN*::KSAC Δ*cydAB cyxAB*::*bla*), approximately 500 bp regions upstream and downstream of the *cyxAB* and *cydAB* regions of IR715 were PCR amplified with extended primers for Gibson assembly and cloned into the SalI restriction site of the plasmid pRDH10 with an XbaI restriction site added between the flanking regions to create plasmids pGW14 (*cyxAB* flanking regions) and pGW15 (*cydAB* flanking regions). The *bla* resistance cassette from the KSAC plasmid was PCR amplified with XbaI sites added at the ends. The *bla* cassette, pGW14 and pGW15 were digested with XbaI and the *bla* cassette was ligated in between the flanking regions to generate pGW19 and pGW18, respectively. *E. coli* S17-1 λ*pir* was transformed with the plasmids and selected on LB+Cm+Carb for plasmid backbone and *bla* cassette insertion, and proper fragment insertions were confirmed by restriction digestion and PCR. Strains containing the proper pGW18 plasmid were used for conjugation with FF459 (IR715 Δ*invA* Δ*spiB phoN*::KSAC), then selection for Kan^R $Carb^R$ and sucrose selection to select for loss of the integrated plasmid, generating strain GTW42. For the clean *cydAB* deletion, GTW42 was then conjugated with *E. coli* S17-1 λ*pir containing pGW15 and selected for* Kan^R Cm^R $Carb^S$*, and resulting colonies were put through sucrose selection and selected for* Kan^R Cm^S *to confirm loss of the integrated plasmid, generating strain GTW45 (IR715* Δ*invA* Δ*spiB* Δ*cydAB phoN::*KSAC). GTW45 was then conjugated with *E. coli* S17-1 λ*pir* containing pGW19 and selected for Kan^R $Carb^R$ Cm^S then put through sucrose selection to confirm loss of the integrated plasmid, generating strain GTW47. For each S. Typhimurium mutant (GTW42, GTW45, and GTW47), insertions and deletions were confirmed by PCR amplification.

Mutants in *moaA (FF310 and FF312)* were generated by conjugation and sucrose selection of pRDH10 plasmids containing *moaA* flanking regions with a Kanamycin-resistance KSAC cassette inserted between into IR715 (wildtype) and IR715 Δ*invA* Δ*spiB* (SPN487) respectfully.

Bacterial inoculation and colonization readouts. To prepare inocula, *S.* Typhimurium or *E. coli* colonies grown on selective agar plates were inoculated into LB with appropriate selection antibiotics and incubated at 37°C with shaking (200 rpm) overnight (14-20 hrs). Overnight cultures were centrifuged (10 min, 4000*g*, 4°C) and bacterial pellets washed with fresh LB. Pellets were resuspended in LB and adjusted to the appropriate bacterial concentration (based on optical density) for infections. For single-strain infections, mice were gavaged with 0.1 mL of *S.* Typhimurium at approximately $1x10^{10}$ colony forming units (CFU)/mL. For competitive infections, the strains were prepared separately, adjusted to $1x10^{10}$ CFU/mL, then mixed 1:1 (vol/vol) and inoculated as 0.1 mL by oral gavage. Inocula were serially diluted and plated for CFU to confirm accuracy of the concentration and the input strain ratio for competitive infection calculations. Mice were euthanized at the indicated time points or when they became moribund. Mice euthanized early due to health concerns were excluded from analysis.

Fecal pellets or intestinal contents (approximately 20-100 mg) from mice were collected at indicated time points into 1-2 mL PBS and homogenized by vortex (3-10 m). Homogenates were serially diluted in PBS and plated on appropriate selective agar to assess CFU loads. If no *S.* Typhimurium could be recovered post-challenge, the load was set to the detection limit for statistical comparisons (100 CFU/g intestinal content). In the competitive infections, intestinal content was plated on separate media selecting for each inoculated strain (wildtype and mutant strain), and competitive index was calculated as the wild-type:mutant load, corrected for the input ratio of the inoculum.

Hypoxia staining of intestinal tissues. Mice were treated with 60mg/kg of pimonidazole (PMDZ) HCl, i.p. (Hypoxyprobe) one hour before euthanasia. Colon and cecal samples were collected and fixed in 10% buffered formalin for 24 hours and 70% ethanol for a week. Tissues were paraffin-embedded, and sections were deparaffinized in xylenes and hydrated in 95-70% ethanol to be processed for immunofluorescence imaging. Bound PMDZ was detected with mouse anti-PMDZ IgG1 (MAb 4.3.11.3) overnight and stained with Cy-3 conjugated goat anti-mouse antibody (Jackson ImmunoResearch Laboratories) for 1 hour. Samples were counterstained with DAPI (1 µg/mL in water) and preserved using SlowFace Gold mount. Representative images were obtained using a Zeiss Axiovert 200 M fluorescent microscope (20x objective) with an appropriate fluorescence brightness used for all samples based on untreated controls (No PMDZ).

Lipocalin-2 measurement. Lipocalin-2 concentrations in cecal content were detected in homogenized sample supernatant using the DuoSet ELISA kit (R&D Systems).

Statistical analyses. The investigators were not blinded to animal allocation during experiments and outcome assessment, except for histopathology analysis. Sample sizes were estimated on the basis of effect sizes in previous studies. All analyses were performed using Prism 9 (GraphPad Software, La Jolla, CA). The limit of detection while plating for *S.* Typhimurium loads was set to 100 CFU/g content, and the number of CFU per gram intestinal content was Log10 transformed to normalize the data for statistical analysis. Significant differences in groups of Log-normalized data (CFUs, competitive indices, relative abundance of OTUs) were determined by unpaired *t* tests with Welch's correction, or Paired *t*-tests for comparisons within animals over time. Significant differences between groups in their competitive indices and other measures not log-normalized prior to comparison (body weight changes, spleen weights, blood cell counts, parasite burden, and intestinal Lcn2) were

determined by Mann-Whitney tests. In all comparisons, $P < 0.05$ was considered statistically significant.

Software. The following software was used: Microsoft Excel for Mac, Prism 9 for macOS (GraphPad Software), and R open-source software (www.r-project.org) with the packages Phyloseq and Gggplot.

REFERENCES

1. C. Human Microbiome Project, Structure, function and diversity of the healthy human microbiome. *Nature* **486**, 207-214 (2012).
2. J. M. Pickard, M. Y. Zeng, R. Caruso, G. Nunez, Gut microbiota: Role in pathogen colonization, immune responses, and inflammatory disease. *Immunol Rev* **279**, 70-89 (2017).
3. M. Levy, A. A. Kolodziejczyk, C. A. Thaiss, E. Elinav, Dysbiosis and the immune system. *Nat Rev Immunol* **17**, 219-232 (2017).
4. M. P. Francino, Antibiotics and the Human Gut Microbiome: Dysbioses and Accumulation of Resistances. *Front Microbiol* **6**, 1543 (2015).
5. M. Bohnhoff, B. L. Drake, C. P. Miller, Effect of streptomycin on susceptibility of intestinal tract to experimental Salmonella infection. *Proc Soc Exp Biol Med* **86**, 132-137 (1954).
6. M. Barthel *et al.*, Pretreatment of mice with streptomycin provides a Salmonella enterica serovar Typhimurium colitis model that allows analysis of both pathogen and host. *Infect Immun* **71**, 2839-2858 (2003).

7. F. Rivera-Chavez *et al.*, Depletion of Butyrate-Producing Clostridia from the Gut Microbiota Drives an Aerobic Luminal Expansion of Salmonella. *Cell Host Microbe* **19**, 443-454 (2016).
8. J. Pollock, L. Glendinning, T. Wisedchanwet, M. Watson, The Madness of Microbiome: Attempting To Find Consensus "Best Practice" for 16S Microbiome Studies. *Appl Environ Microbiol* **84**, (2018).
9. A. A. Kolodziejczyk, D. Zheng, E. Elinav, Diet-microbiota interactions and personalized nutrition. *Nat Rev Microbiol* **17**, 742-753 (2019).
10. R. D. Hills, Jr. *et al.*, Gut Microbiome: Profound Implications for Diet and Disease. *Nutrients* **11**, (2019).
11. J. K. Goodrich *et al.*, Human genetics shape the gut microbiome. *Cell* **159**, 789-799 (2014).
12. S. Y. Wotzka *et al.*, Escherichia coli limits Salmonella Typhimurium infections after diet shifts and fat-mediated microbiota perturbation in mice. *Nat Microbiol* **4**, 2164-2174 (2019).
13. M. S. Desai *et al.*, A Dietary Fiber-Deprived Gut Microbiota Degrades the Colonic Mucus Barrier and Enhances Pathogen Susceptibility. *Cell* **167**, 1339-1353 e1321 (2016).
14. E. Deriu *et al.*, Influenza Virus Affects Intestinal Microbiota and Secondary Salmonella Infection in the Gut through Type I Interferons. *PLoS Pathog* **12**, e1005572 (2016).
15. R. Correa *et al.*, Gut microbiota modulation induced by Zika virus infection in immunocompetent mice. *Sci Rep* **11**, 1421 (2021).
16. E. Prandovszky *et al.*, Toxoplasma gondii-Induced Long-Term Changes in the Upper Intestinal Microflora during the Chronic Stage of Infection. *Scientifica (Cairo)* **2018**, 2308619 (2018).

17. A. Riba *et al.*, Disturbed gut microbiota and bile homeostasis in Giardia-infected mice contributes to metabolic dysregulation and growth impairment. *Sci Transl Med* **12**, (2020).

18. J. P. Mooney *et al.*, Inflammation-associated alterations to the intestinal microbiota reduce colonization resistance against non-typhoidal Salmonella during concurrent malaria parasite infection. *Sci Rep* **5**, 14603 (2015).

19. T. Taniguchi *et al.*, Plasmodium berghei ANKA causes intestinal malaria associated with dysbiosis. *Sci Rep* **5**, 15699 (2015).

20. T. Brugat *et al.*, Sequestration and histopathology in Plasmodium chabaudi malaria are influenced by the immune response in an organ-specific manner. *Cell Microbiol* **16**, 687-700 (2014).

21. J. Y. Chau *et al.*, Malaria-associated L-arginine deficiency induces mast cell-associated disruption to intestinal barrier defenses against nontyphoidal Salmonella bacteremia. *Infect Immun* **81**, 3515-3526 (2013).

22. T. S. Nyirenda, W. L. Mandala, M. A. Gordon, P. Mastroeni, Immunological bases of increased susceptibility to invasive nontyphoidal Salmonella infection in children with malaria and anaemia. *Microbes Infect* **20**, 589-598 (2018).

23. J. E. Denny *et al.*, Differential Sensitivity to Plasmodium yoelii Infection in C57BL/6 Mice Impacts Gut-Liver Axis Homeostasis. *Sci Rep* **9**, 3472 (2019).

24. M. Derrien, E. E. Vaughan, C. M. Plugge, W. M. de Vos, Akkermansia muciniphila gen. nov., sp. nov., a human intestinal mucin-degrading bacterium. *Int J Syst Evol Microbiol* **54**, 1469-1476 (2004).

25. C. Depommier *et al.*, Supplementation with Akkermansia muciniphila in overweight and obese human volunteers: a proof-of-concept exploratory study. *Nat Med* **25**, 1096-1103 (2019).

26. Q. Zhou *et al.*, Gut bacteria Akkermansia is associated with reduced risk of obesity: evidence from the American Gut Project. *Nutr Metab (Lond)* **17**, 90 (2020).

27. L. Labarta-Bajo *et al.*, CD8 T cells drive anorexia, dysbiosis, and blooms of a commensal with immunosuppressive potential after viral infection. *Proc Natl Acad Sci U S A* **117**, 24998-25007 (2020).

28. D. Hayashi *et al.*, Role of histamine and its receptor subtypes in stimulation of conjunctival goblet cell secretion. *Invest Ophthalmol Vis Sci* **53**, 2993-3003 (2012).

29. A. O'Callaghan, D. van Sinderen, Bifidobacteria and Their Role as Members of the Human Gut Microbiota. *Front Microbiol* **7**, 925 (2016).

30. H. J. Flint, S. H. Duncan, K. P. Scott, P. Louis, Links between diet, gut microbiota composition and gut metabolism. *Proc Nutr Soc* **74**, 13-22 (2015).

31. D. E. Brown *et al.*, Salmonella enterica causes more severe inflammatory disease in C57/BL6 Nramp1G169 mice than Sv129S6 mice. *Vet Pathol* **50**, 867-876 (2013).

32. S. Soe-Lin *et al.*, Nramp1 promotes efficient macrophage recycling of iron following erythrophagocytosis in vivo. *Proc Natl Acad Sci U S A* **106**, 5960-5965 (2009).

33. R. E. Ley *et al.*, Obesity alters gut microbial ecology. *Proc Natl Acad Sci U S A* **102**, 11070-11075 (2005).

34. N. T. Baxter *et al.*, Dynamics of Human Gut Microbiota and Short-Chain Fatty Acids in Response to Dietary Interventions with Three Fermentable Fibers. *mBio* **10**, (2019).

35. A. W. L. Rogers, R. M. Tsolis, A. J. Baumler, Salmonella versus the Microbiome. *Microbiol Mol Biol Rev* **85**, (2021).

36. M. A. Borton *et al.*, Chemical and pathogen-induced inflammation disrupt the murine intestinal microbiome. *Microbiome* **5**, 47 (2017).

37. M. X. Byndloss *et al.*, Microbiota-activated PPAR-gamma signaling inhibits dysbiotic Enterobacteriaceae expansion. *Science* **357**, 570-575 (2017).

38. A. Jacobson *et al.*, A Gut Commensal-Produced Metabolite Mediates Colonization Resistance to Salmonella Infection. *Cell Host Microbe* **24**, 296-307 e297 (2018).

39. N. Terada, N. Ohno, S. Saitoh, S. Ohno, Immunohistochemical detection of hypoxia in mouse liver tissues treated with pimonidazole using "in vivo cryotechnique". *Histochem Cell Biol* **128**, 253-261 (2007).

40. S. Kizaka-Kondoh, H. Konse-Nagasawa, Significance of nitroimidazole compounds and hypoxia-inducible factor-1 for imaging tumor hypoxia. *Cancer Sci* **100**, 1366-1373 (2009).

41. N. R. Brand, R. O. Opoka, K. E. Hamre, C. C. John, Differing Causes of Lactic Acidosis and Deep Breathing in Cerebral Malaria and Severe Malarial Anemia May Explain Differences in Acidosis-Related Mortality. *PLoS One* **11**, e0163728 (2016).

42. E. M. Velazquez *et al.*, Endogenous Enterobacteriaceae underlie variation in susceptibility to Salmonella infection. *Nat Microbiol* **4**, 1057-1064 (2019).

43. P. B. Eckburg *et al.*, Diversity of the human intestinal microbial flora. *Science* **308**, 1635-1638 (2005).

44. J. Behnsen *et al.*, The cytokine IL-22 promotes pathogen colonization by suppressing related commensal bacteria. *Immunity* **40**, 262-273 (2014).

45. N. F. Villarino *et al.*, Composition of the gut microbiota modulates the severity of malaria. *Proc Natl Acad Sci U S A* **113**, 2235-2240 (2016).

46. E. Deriu *et al.*, Probiotic bacteria reduce salmonella typhimurium intestinal colonization by competing for iron. *Cell Host Microbe* **14**, 26-37 (2013).

47. P. Van den Abbeele *et al.*, Butyrate-producing Clostridium cluster XIVa species specifically colonize mucins in an in vitro gut model. *ISME J* **7**, 949-961 (2013).

48. P. Kovatcheva-Datchary *et al.*, Dietary Fiber-Induced Improvement in Glucose Metabolism Is Associated with Increased Abundance of Prevotella. *Cell Metab* **22**, 971-982 (2015).

49. S. E. Winter *et al.*, Gut inflammation provides a respiratory electron acceptor for Salmonella. *Nature* **467**, 426-429 (2010).

50. S. E. Winter *et al.*, Host-derived nitrate boosts growth of E. coli in the inflamed gut. *Science* **339**, 708-711 (2013).

51. C. A. Lopez, F. Rivera-Chavez, M. X. Byndloss, A. J. Baumler, The Periplasmic Nitrate Reductase NapABC Supports Luminal Growth of Salmonella enterica Serovar Typhimurium during Colitis. *Infect Immun* **83**, 3470-3478 (2015).

52. F. Faber *et al.*, Respiration of Microbiota-Derived 1,2-propanediol Drives Salmonella Expansion during Colitis. *PLoS Pathog* **13**, e1006129 (2017).

53. L. Maier *et al.*, Microbiota-derived hydrogen fuels Salmonella typhimurium invasion of the gut ecosystem. *Cell Host Microbe* **14**, 641-651 (2013).

54. C. A. Lopez, E. P. Skaar, The Impact of Dietary Transition Metals on Host-Bacterial Interactions. *Cell Host Microbe* **23**, 737-748 (2018).

55. X. Xiao, B. S. Yeoh, M. Vijay-Kumar, Lipocalin 2: An Emerging Player in Iron Homeostasis and Inflammation. *Annu Rev Nutr* **37**, 103-130 (2017).

56. K. L. Lokken, A. R. Stull-Lane, K. Poels, R. M. Tsolis, Malaria Parasite-Mediated Alteration of Macrophage Function and Increased Iron Availability Predispose to Disseminated Nontyphoidal Salmonella Infection. *Infect Immun* **86**, (2018).

57. G. B. Gloor, J. M. Macklaim, V. Pawlowsky-Glahn, J. J. Egozcue, Microbiome Datasets Are Compositional: And This Is Not Optional. *Front Microbiol* **8**, 2224 (2017).

FIGURES AND TABLES

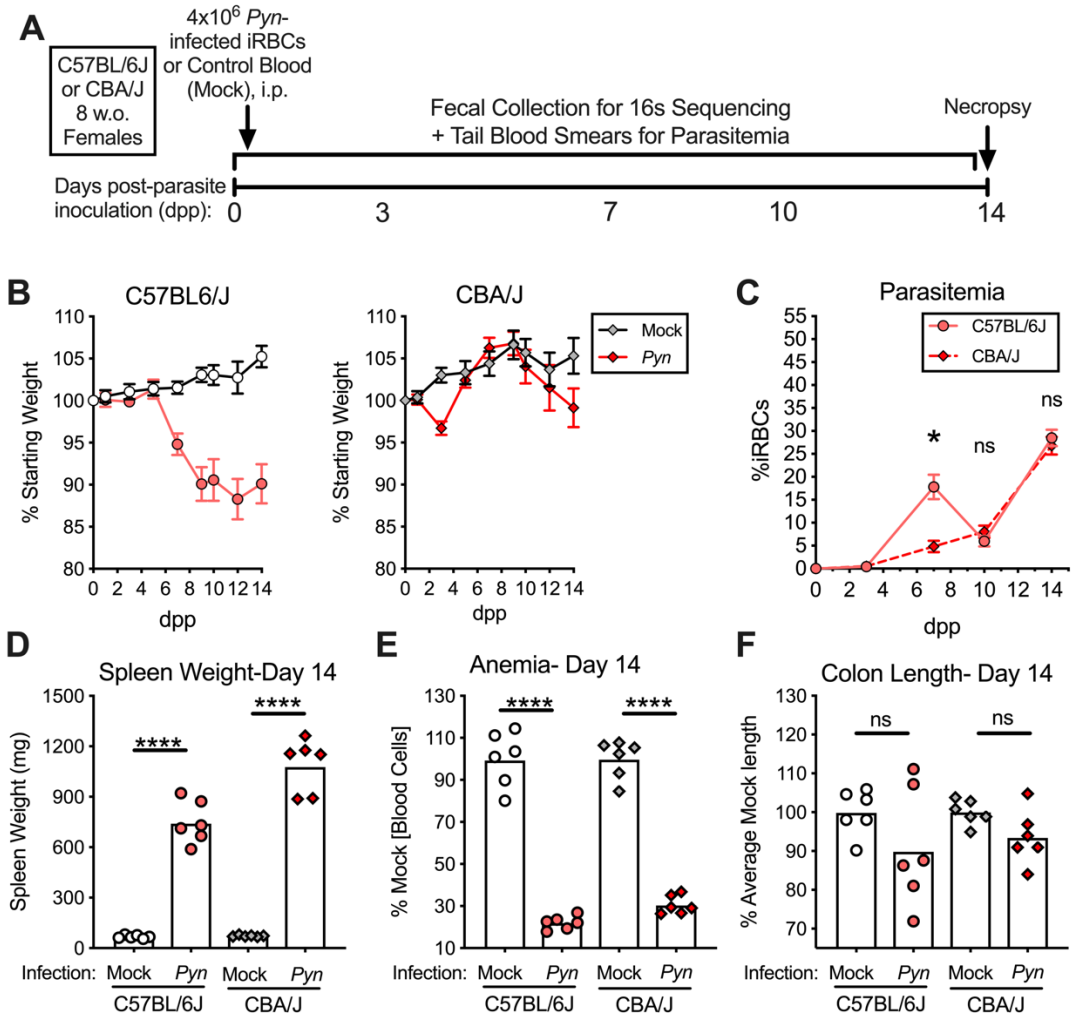

Figure 2.1. Experimental outline and comparison of the response to *P. yoelii nigeriensis* infection in C57BL/6J and CBA/J mice. (A) Schematic outlining the infection and sampling experiment used for data in Figs. 2.1-2.5. Groups of C57BL/6J and CBA/J mice (*n* = 6 per group) were infected with 4x10^6 *Pyn*-infected mouse RBCs or an equal volume of saline-diluted mouse control blood. Prior to infection and on days 3, 7, 10, and 14 post-infection (dpp), feces were collected for 16s rRNA sequence analysis and microbial community profiling. (B) Body weight fluctuations throughout infections. (C) Parasitemias (circulating concentration of *Pyn*-iRBCs) throughout infections. (D) Spleen weight at 14 dpp. (E) Blood cell counts at 14 dpp,

normalized to the average counts in mock-infected mice. (F) Colon length at 14 dpp, normalized to average length in mock-infected mice.

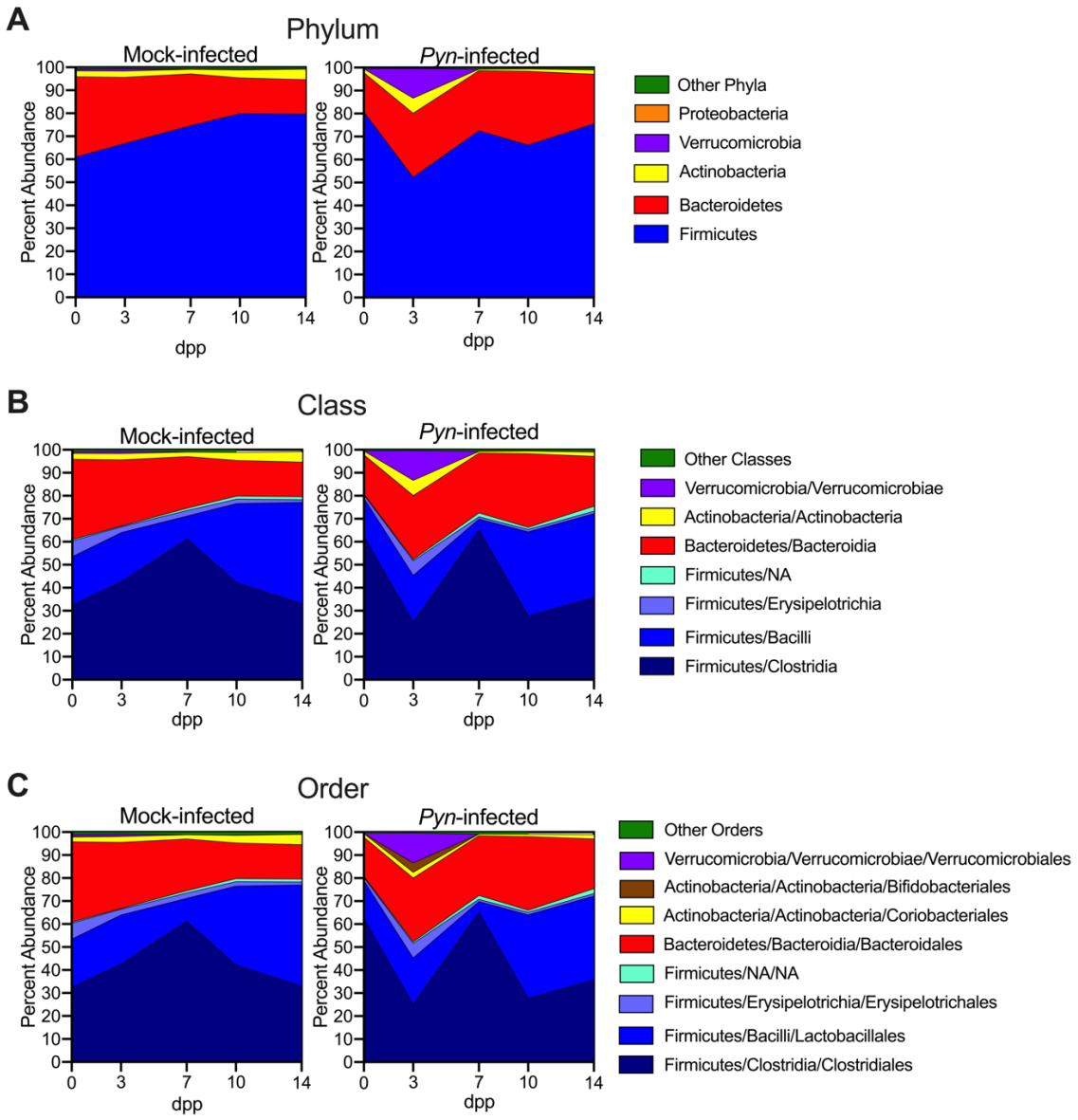

Figure 2.2. OTU abundance at different taxonomic hierarchies in the feces of C57BL/6J mice during *Pyn* infection. Fluctuations in relative abundance of the most abundant bacterial taxa based on assigned OTUs from 16s rRNA sequencing in C57BL/6J mice at the (A) Phylum,

(B) Class, and (C) Order level. The relative amount of each OTU at a time point is based on the average abundance of the taxon in that group of mice (mock- or *Pyn*-infected).

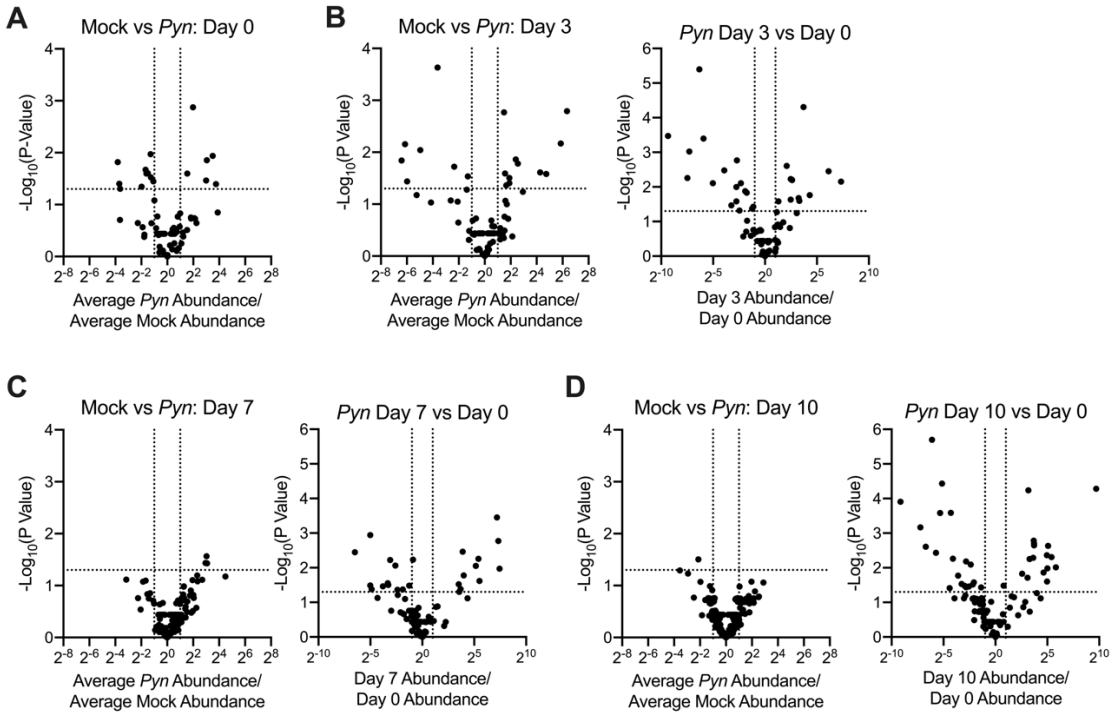

Figure 2.3. Volcano plot comparisons of genus-level microbial variation in mock and *Pyn*-infected mice (related to Table 2.1). Plots comparing the overall abundance of genus-level OTUs between indicated groups, compared to the statistical significance of the difference between the groups. (A and Left Panels of B-D) Significance was determined by Welch's t-test on Log_{10}-normalized relative abundances of taxa when comparing time-matched mock and *Pyn*-infected groups. (B-D, Right Panels) Significance was determined by Paired t-test on Log_{10}-normalized relative abundances of taxa in *Pyn*-infected mice at indicated time points compared to pre-infection (Day 0) levels. Each dot represents a single detected genus. Horizontal dotted lines represent P = 0.05; vertical lines represent 2-fold difference.

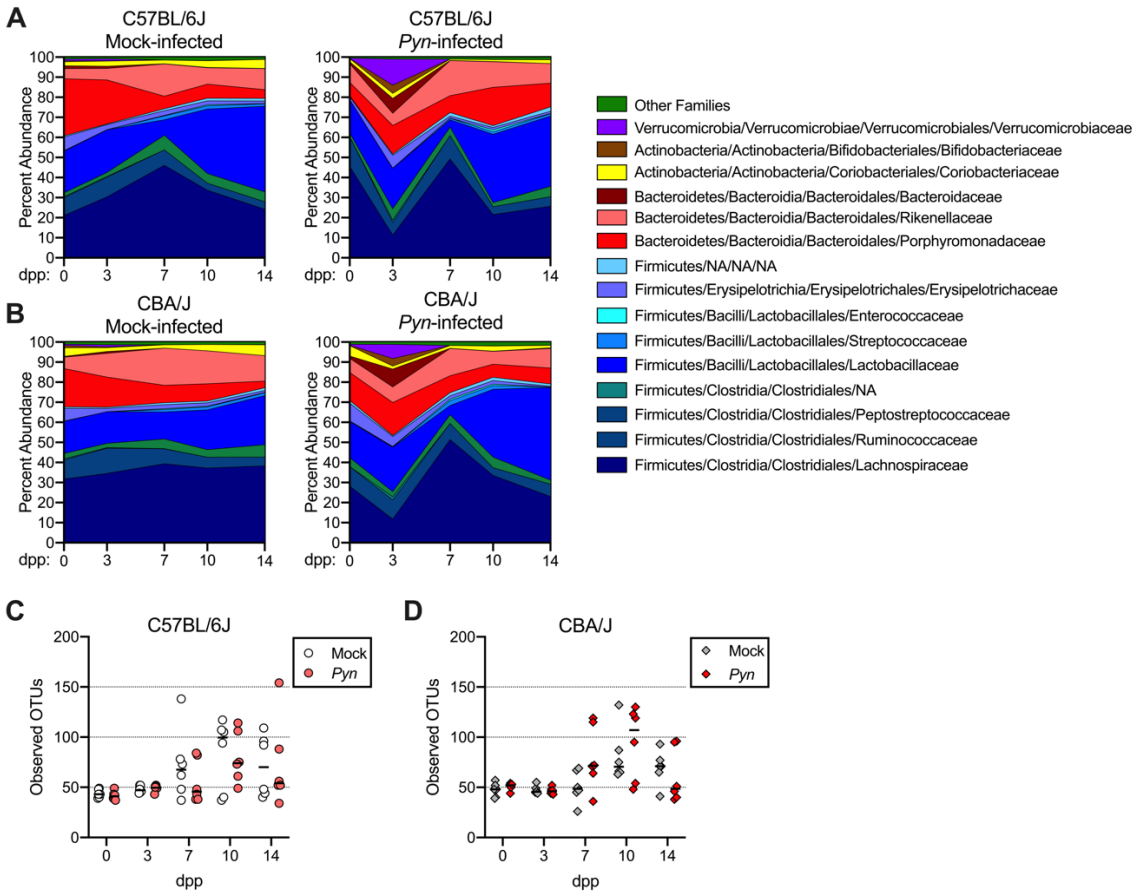

Figure 2.4. Comparison of family-level microbiota shifts during *Pyn* infection in C57BL/6J and CBA/J mice. (A and B) Fluctuations in relative abundance of the most abundant bacterial taxa based on assigned OTUs from 16s rRNA sequencing in C57BL/6J mice at the Family level in (A) C57BL/6J and (B) CBA/J mice. The relative amount of each OTU at a time point is based on the average abundance of the taxon in that group of mice (mock- or *Pyn*-infected). (C and D) Alpha-diversity as measured by the number of OTUs detected in the feces of individual mice at each time point in (C) C57BL/6J and (D) CBA/J mice. White circles or grey diamonds: Mock-infected mice; Light red circles or dark red diamonds: *Pyn*-infected. Lines represent the geometric means.

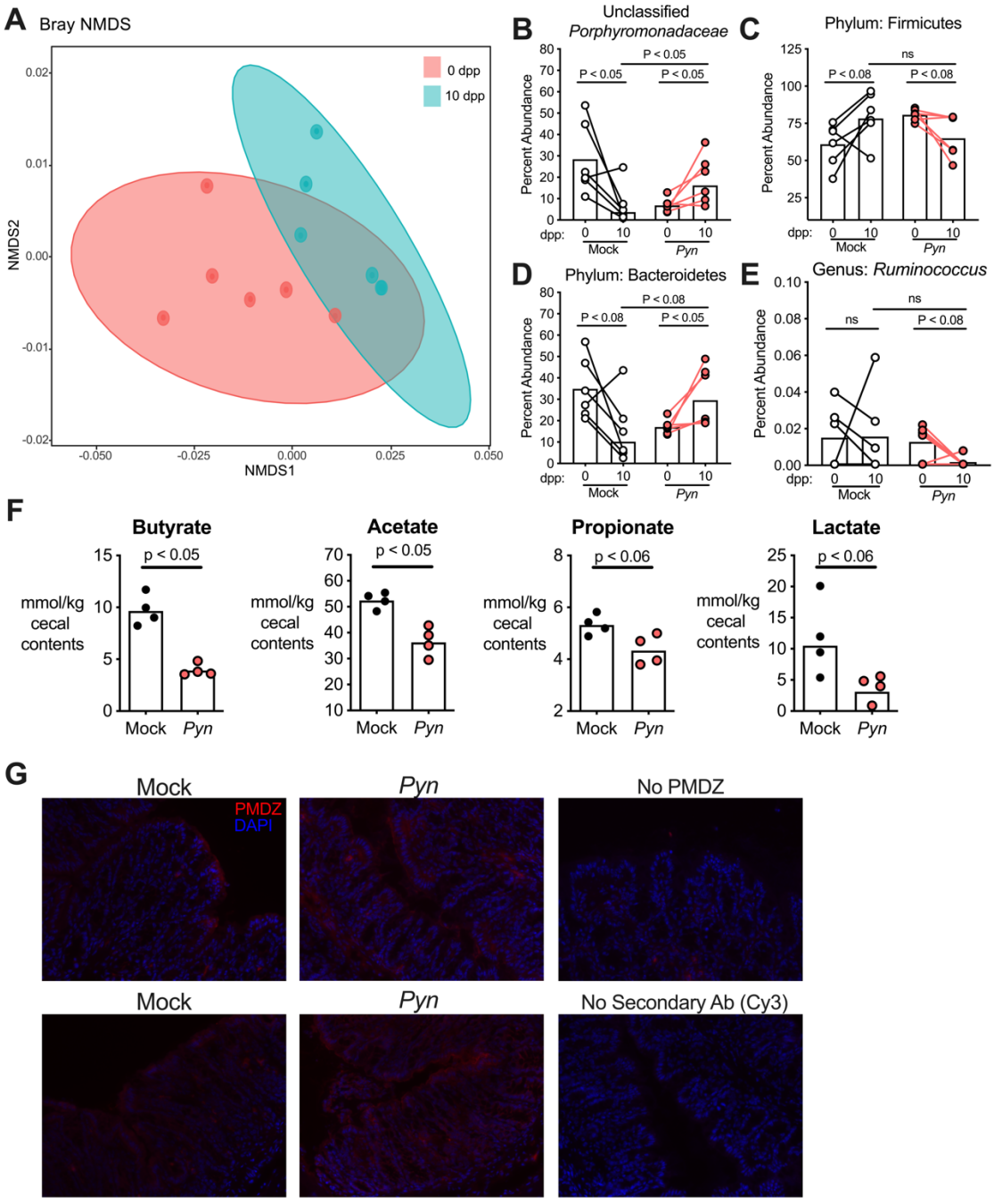

Figure 2.5. Characterizing gut microbial and metabolic alterations at 10 dpp. (A) NMDS plot indicating general shifts in the bacterial populations of *Pyn*-infected mice from 0 dpp to 10 dpp. (B-E) Relative abundance of (B) an unclassified genus of *Porphyromonadaceae*, (C) *Firmicutes*, (D) *Bacteroidetes*, and (E) *Ruminococcus* at 0 and 10 dpp in mock- and *Pyn* infected mice. Symbols represent abundance in individual mice, with connected symbols

representing abundances of the taxon from the same mouse at 0 and 10 dpp. (F) In a separate experiment, SCFA and lactate levels were measured in the cecal content of mock- and *Pyn*-infected mice euthanized at 10 dpp. Levels of butyrate, acetate, propionate and lactate were somewhat reduced at 10 dpp. (G) Hypoxia-stained cecal tissues of Mock (left images), *Pyn*-infected (middle images) and control mock-infected tissues not treated with the hypoxyprobe PMDZ (upper right image) or treated with PMDZ but not stained with the secondary fluorescence antibody to detect the probe (lower right image). Images were taken with the 20x objective on the Zeiss Axiovert 200 M fluorescent microscope. Red fluorescence indicated PMDZ binding to proteins in the tissue, which requires local hypoxia (pO_2 < 10 mmHg); blue fluorescence is DAPI counterstain (nuclei).

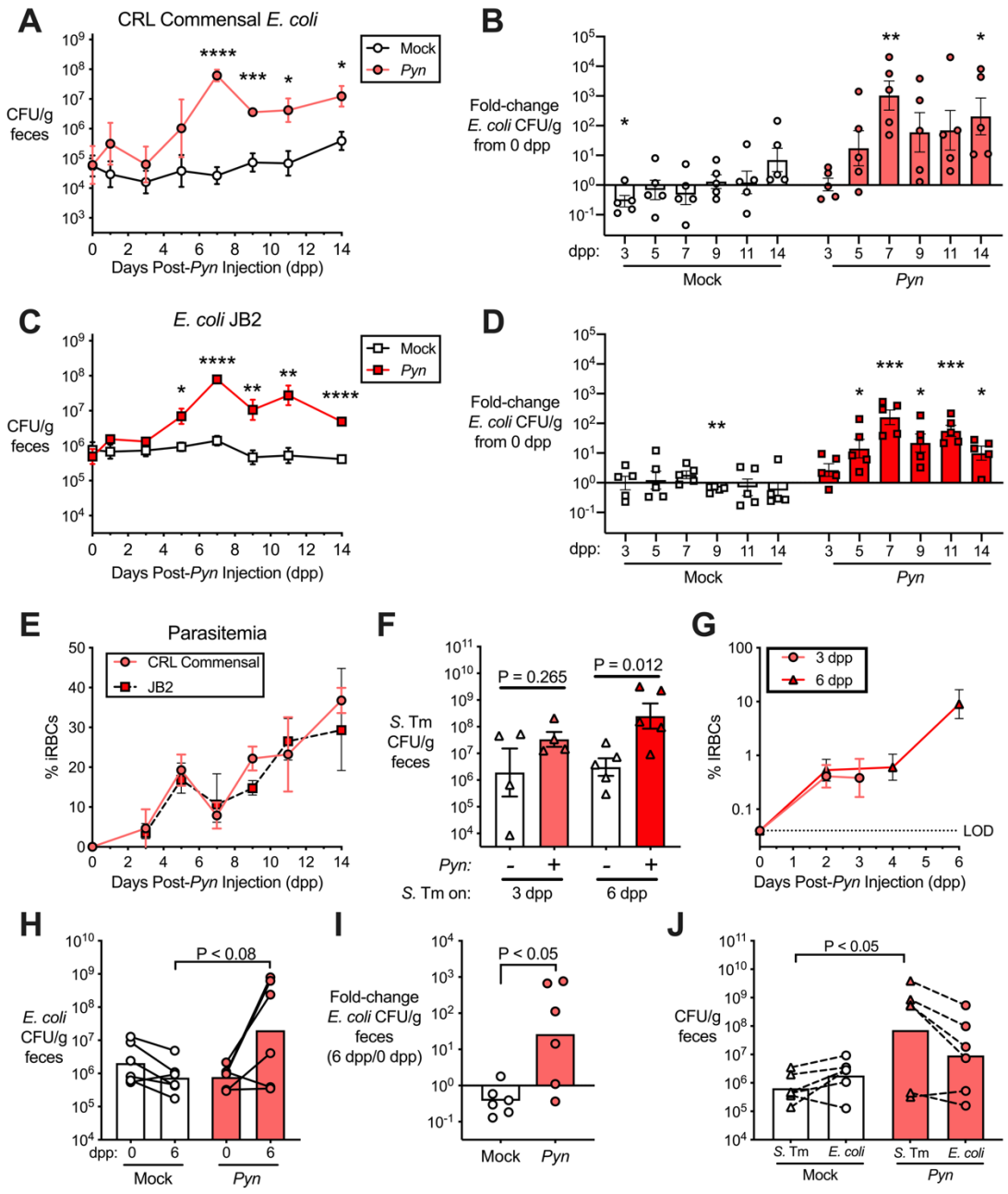

Figure 2.6. Characterization of changes in commensal *E. coli* burden during *Pyn* infection. (A) *E. coli* abundance in feces of C57BL/6NCrl mice throughout mock (white symbols) and *Pyn* (red symbols) infection. (B) Fold-change in fecal *E. coli* abundance from pre-infection (0 dpp) at indicated time points. (C) *E. coli* JB2 abundance in feces of C57BL/6J mice (colonized with JB2 3 weeks prior to infection) throughout mock (white symbols) and *Pyn* (red symbols) infection. (D) Fold-change in fecal *E. coli* JB2 abundance from pre-infection (0 dpp) at

indicated time points. (E) Parasite burdens from *Pyn*-infected C57BL/6NCrl mice (light red circles) and C57BL/6J mice colonized with JB2 (dark red squares). (F) *S.* Typhimurium *invA spiB* Cm^R burden 24 hours after challenge of mock (-) and *Pyn*-infected (+) mice at 3 dpp or 6 dpp. (G) Parasite burden of mice from (F) prior to *S*. Typhimurium challenge. (H) Relative endogenous *E. coli* levels in the feces of C57BL/6NCrl mice before (0 dpp) and during (6 dpp) *Pyn* infection. (I) Fold-change in endogenous *E. coli* in the feces of mice from (H). (J) *S.* Typhimurium *invA spiB* Cm^R 24 hpi from mice in (H and I) challenged at 6 dpp, paired with matching *E. coli* levels at the same time point (7 dpp). Symbols in (A, C, E, and G) indicate geometric mean of n = 5 mice/group. Symbols in (B, D, F, H, I, and J) represent data from individual mice; bars represent the mean ± SEM of Log_{10}-normalized data. Significance between mock- and *Pyn*-infected groups at different time points were determined by Welch's *t*-test. Significance of fold-change in *E. coli* levels of groups at different time points (B and D) was determined by one-sample *t*-test of Log_{10}-normalized values compared to a hypothetical mean of 0 (indicating 1-fold).

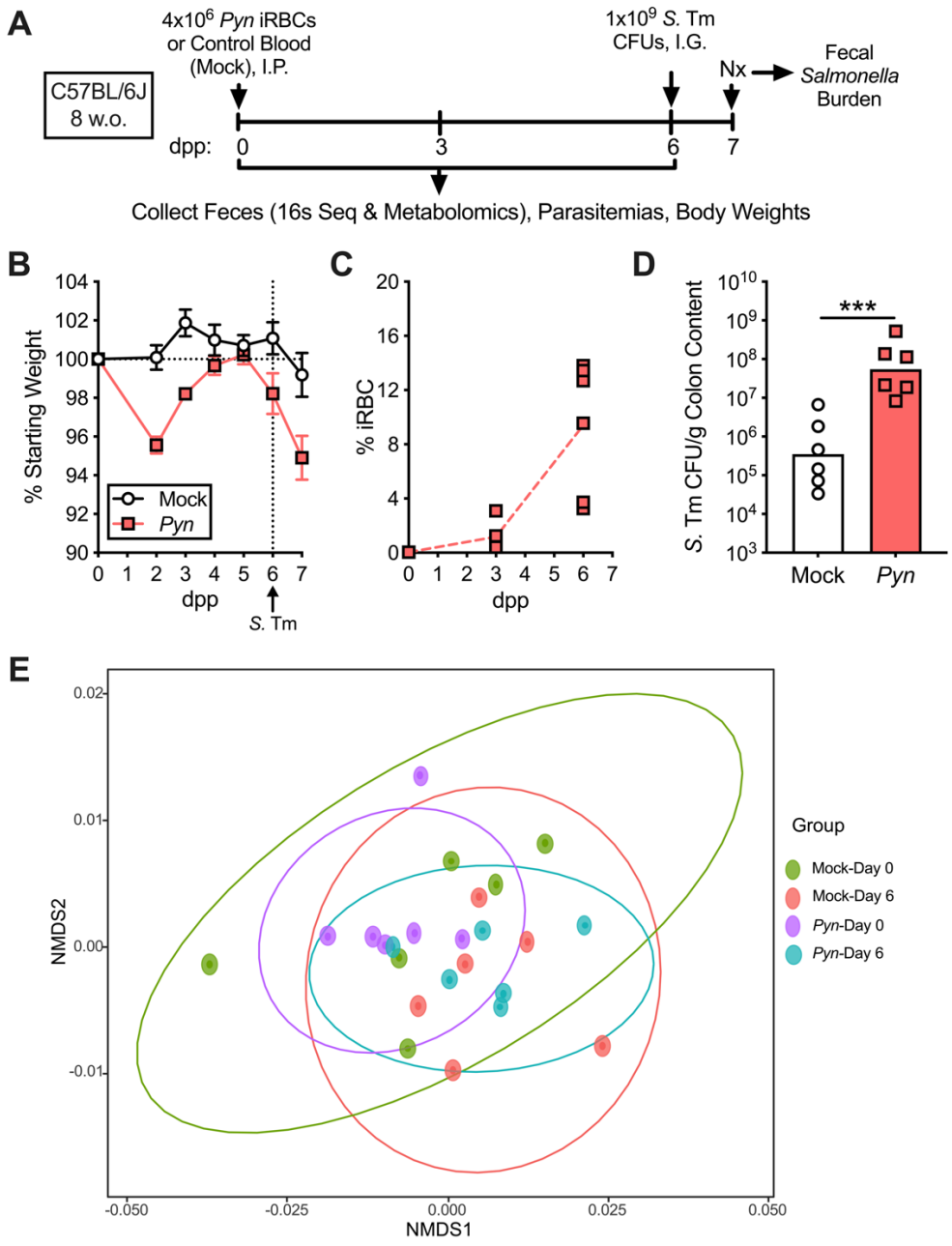

Figure 2.7. Experiment to correlate changes in the gut environment during *Pyn* infection with enhanced *S.* Typhimurium colonization. (A) Schematic outlining the infection experiment for data presented in Figs. 2.7-2.10. Groups of C57BL/6J mice (*n* = 6 per group) were infected with 4x10^6 *Pyn* iRBCs or mock-infected an equal volume of control mouse blood. Prior to infection (0 dpp) and at 6 dpp, feces were collected for 16s rRNA sequence analysis and microbial community profiling, as well as untargeted metabolomics analysis by GC-TOF

MS. After collection at 6 dpp, mice were challenged with an oral gavage of $1x10^9$ CFU *S.* Typhimurium (*S.* Tm) *invA spiB* Kan^R and 24 hpi intestinal *S.* Typhimurium burden was determined by plating contents for CFUs. (B) Body weight fluctuations throughout infections (vertical line indicates timing of *S*. Typhimurium gavage). (C) Parasitemias throughout the *Pyn* infections. (D) *S.* Typhimurium burden 24 hpi (on 7 dpp). (E) NMDS plot comparing microbiota changes in the mock- and *Pyn*-infected groups at 0 and 6 dpp. ***P ≤ 0.001.

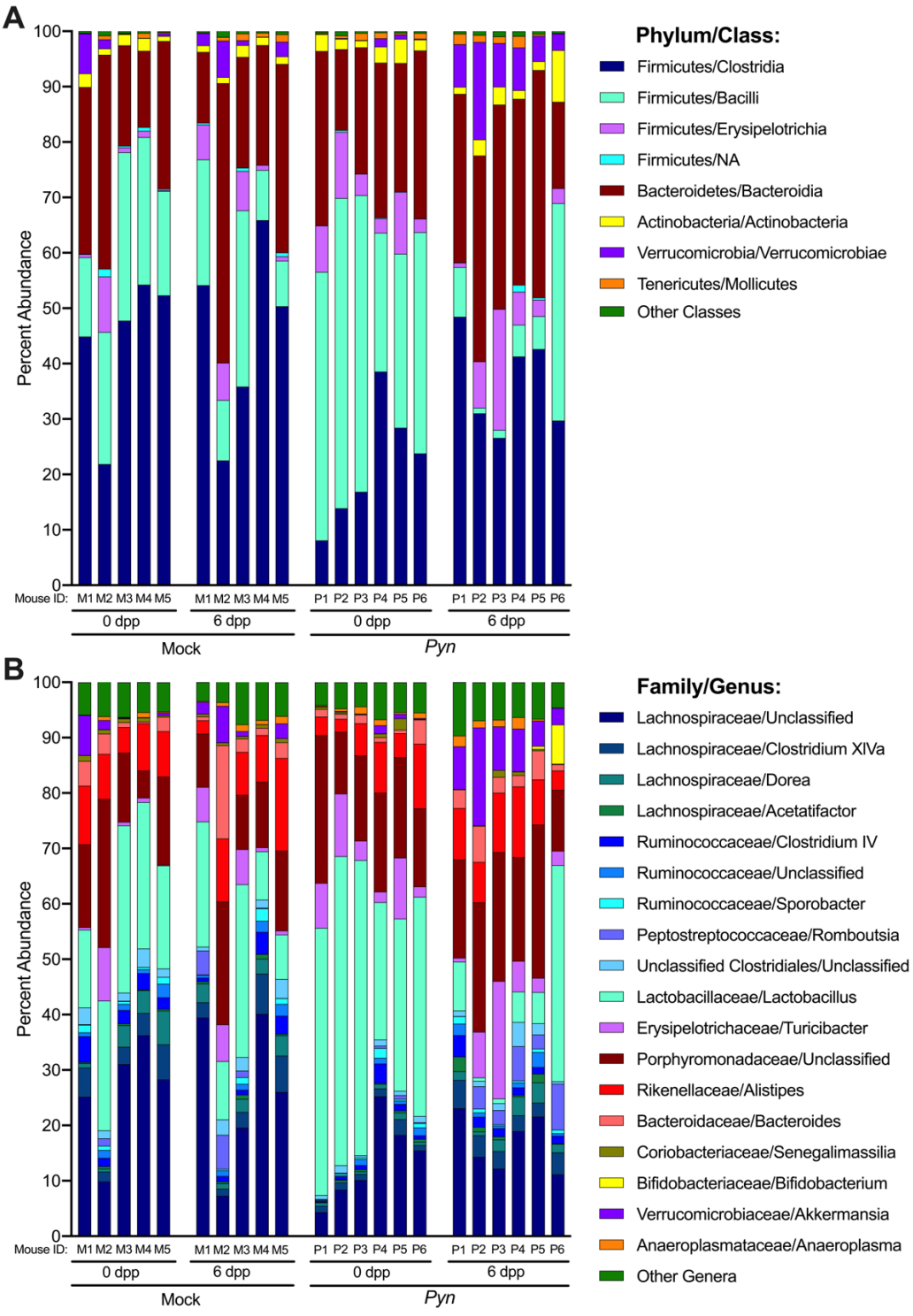

Figure 2.8. Microbiota shifts in individual mice at day 6 of *Pyn* infection. (A and B) Bars representing microbiota composition by major taxa in mock- and *Pyn*-infected mice at indicated time points (0 or 6 dpp) the (A) Class and (B) Genus levels. Each bar represents measurements

from an individual mouse (mock M1-M5 and *Pyn* P1-P6). One mock mouse was excluded from the analysis for poor read abundance in the sample at 0 dpp, but was included in further analyses for 6 dpp abundance.

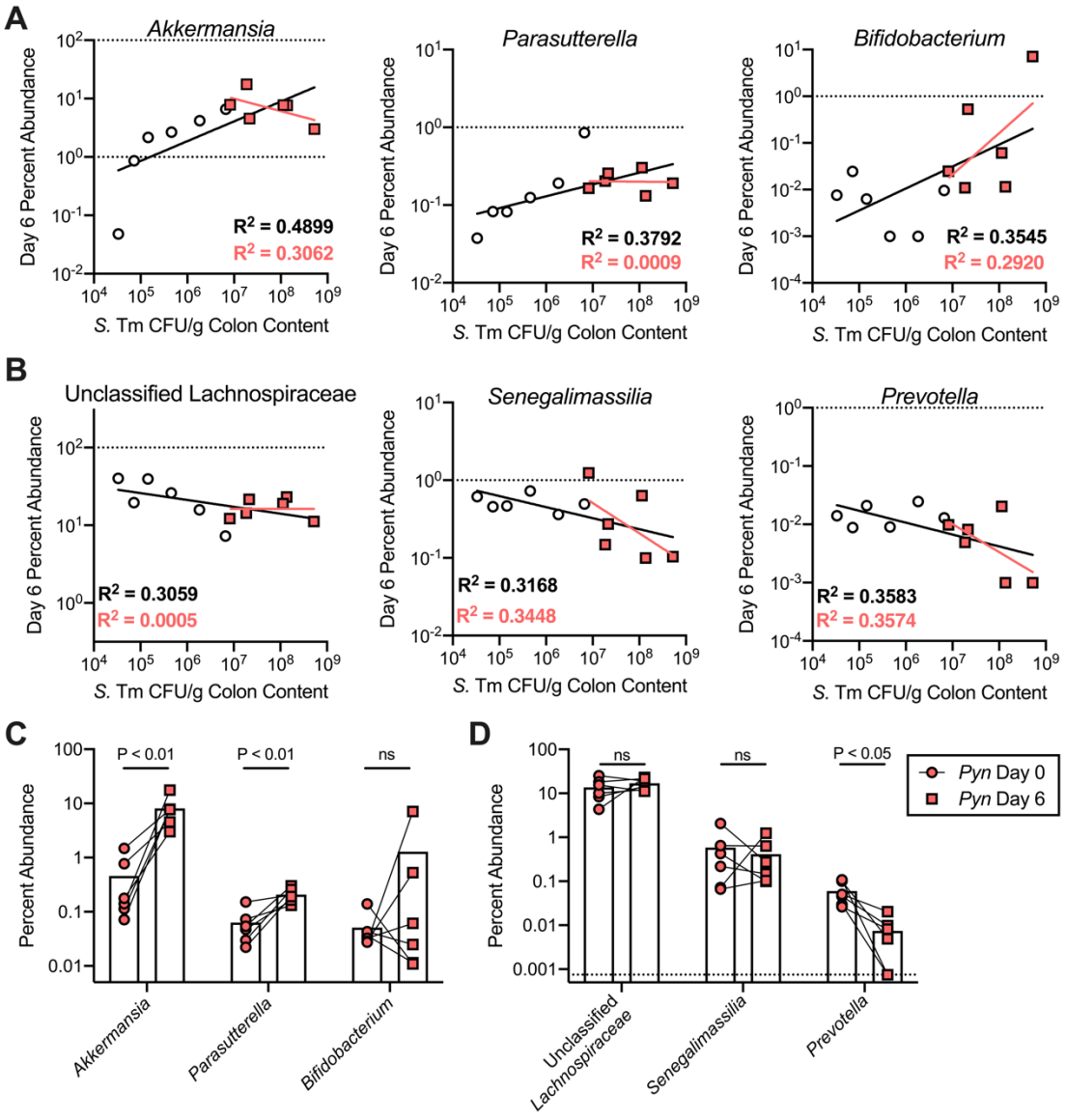

Figure 2.9. Fecal microbiota changes at 6 dpp with the strongest correlations to next-day fecal *S.* Typhimurium levels. (A and B) Scatter plots showing the microbial taxa (indicated) whose 6 dpp relative abundance showed the strongest correlation with *S.* Typhimurium (*S.* Tm) loads over both groups of mice (mock and *Pyn*-infected). (A) Taxa positively correlated with *S.*

Tm levels. (B) Taxa negatively correlated with *S.* Tm levels. White circles indicate data from mock mice; red squares are data from *Pyn*-infected. The black line and R^2 values represent the linear regression of data from both sets of mice analyzed together; the red line and R^2 values represent the linear regression of the *Pyn* group analyzed on its own. (C and D) Paired comparisons from 0 dpp and 6 dpp of the relative abundance of the taxa in *Pyn*-infected mice from (A and B). R^2 was calculated in Prism 9.0 using simple linear regression on Log_{10}-normalized *S.* Tm levels (CFU/g content) plotted against the Log_{10}-normalized relative abundance of OTUs detected in the samples. Symbols represent data from individual mice; in (C and D), bars represent the mean of Log_{10}-normalized abundance.

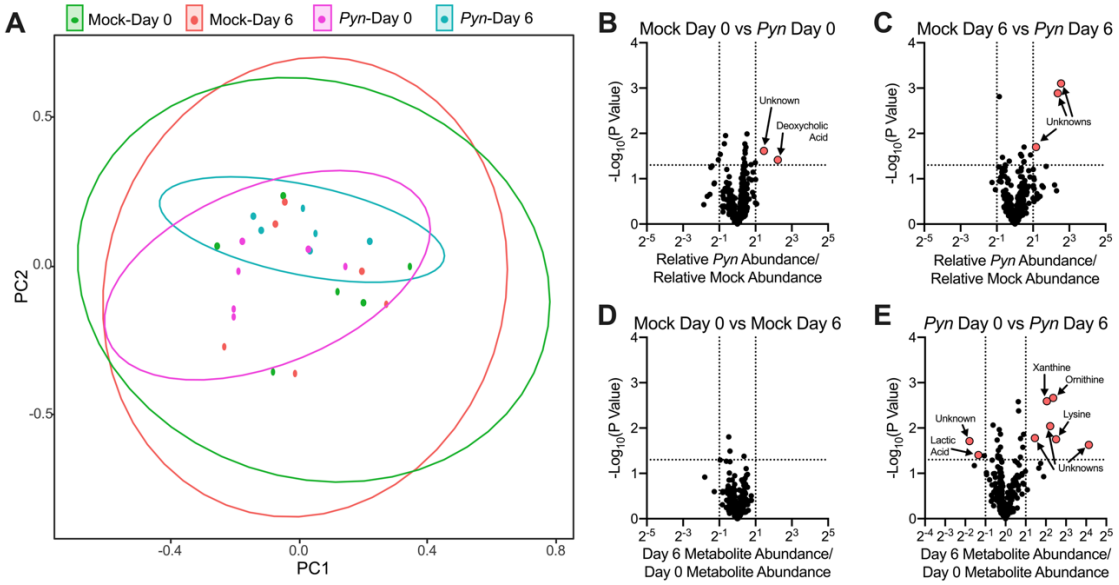

Figure 2.10. Comparison of fecal metabolomic profiles during *Pyn* infection. (A) Principal component analysis of the fecal metabolomic profiles from mock- and *Pyn*-infected mice at 0 dpp and 6 dpp. (B) Volcano plot comparing the average fold-difference in different metabolite abundance between the groups of mice prior to infection. (C) Volcano plot comparing the average fold-difference in different metabolite abundance between the mock and *Pyn* groups at 6 dpp. (D) Volcano plot comparing the average fold-difference in different metabolite abundance

within the mock group, between 0 dpp and 6 dpp. (E) Volcano plot comparing the average fold-difference in different metabolite abundance within the *Pyn*-infected group, between 0 dpp and 6 dpp. (A) Symbols represent profiles of individual mice, and circles represent the 95% confidence of the group. (B-E). Each dot represents the fold-difference in a single detected metabolite. Horizontal dotted lines represent P = 0.05; vertical lines represent 2-fold difference. Metabolites displaying highly significant (P < 0.05 by Welch's or paired *t*-test) differences with a > 2-fold difference are indicated by red circles and identified with arrows.

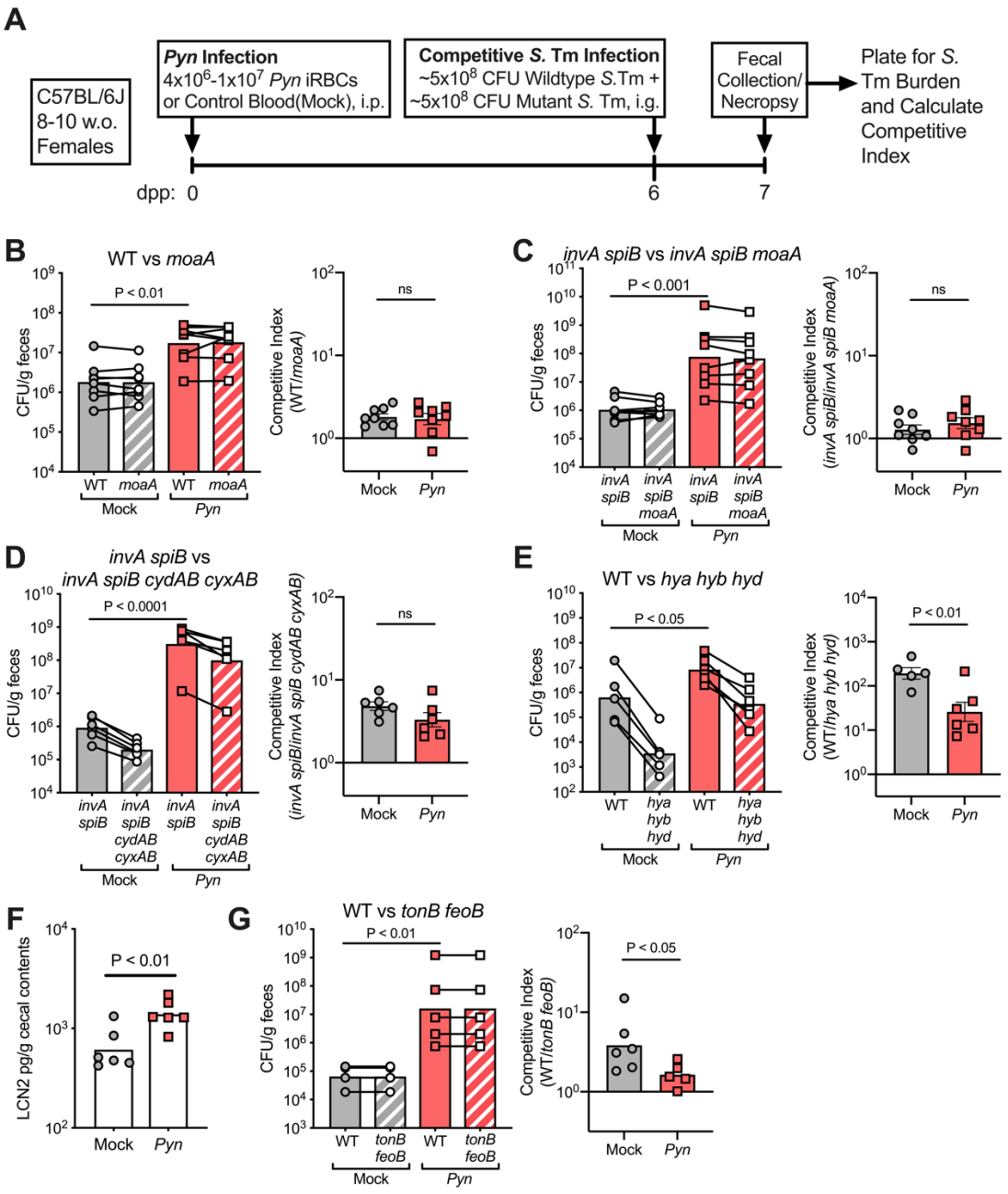

Figure 2.11. Enhanced *S.* Typhimurium intestinal colonization at day 6 of *Pyn* infection is not dependent on respiration of nitrate, tetrathionate, oxygen or hydrogen, or due to increased iron availability. (A) Schematic outlining the timing of infection experiments for data presented (B-G). Groups of C57BL/6J mice (*n* = 5-8 per group) were infected with *Pyn* iRBCs or mock-infected an equal volume of control mouse blood. At 6 dpp, mice were challenged by oral gavage with a competitive infection of approximately 5x10^8 CFU of an *S.* Typhimurium (*S.* Tm)

mutant deficient in uptake or utilization of various metabolites known to benefit for intestinal growth, and $5x10^8$ CFU of an otherwise isogenic strain with the functional (wildtype) gene. Fecal samples collected 24 hours later were plated on selective agar to count and compare CFU loads of each strains to assess the competitive advantage provided by the wild-type gene in mock versus *Pyn*-infected animals. (B) Relative loads of *S.* Typhimurium IR715 (WT) versus an isogenic *moaA* mutant, and competitive index for *moaA* in the colon (WT/mutant levels in feces relative to WT/mutant levels in the inoculum) at 24 hpi in the mock and *Pyn*-infected mice. (C) Relative loads of *S.* Typhimurium *invA spiB* versus an isogenic *moaA* mutant (*invA spiB moaA*), and competitive index in the colon for *moaA* at 24 hpi in an *invA spiB* background, in the mock and *Pyn*-infected mice. (D) Relative loads of *S.* Typhimurium *invA spiB* Cm^R (*invA spiB*) versus an isogenic *cydAB cyxAB* mutant (*invA spiB cydAB cyxAB*), and competitive index in the colon for *cydAB cyxAB* at 24 hpi in the mock and *Pyn*-infected mice. (E) Relative burdens of *S.* Typhimurium Cm^R (WT) versus a triple-hydrogenase mutant (*hya hyb hyd*), and competitive index in the colon for the hydrogenase mutant at 24 hpi, in the mock and *Pyn*-infected mice. (F) Cecal levels of Lipocalin-2 at 6 dpp measured by ELISA. (G) Relative loads of *S.* Typhimurium (WT) versus a *tonB feoB* iron uptake mutant (*tonB feoB*), and competitive index in the colon for the iron mutant at 24 hpi in the mock and *Pyn*-infected mice. (B-G) Comparisons between mock and *Pyn*-infected groups were made by Welch's *t*-test on Log_{10}-normalized data, with P-values indicated.

Level	Classification	% Abundance			P-value	
		Pyn Day 0	*Pyn* Day 3	Mock Day 3	*Pyn* D0 vs *Pyn* D3	Mock D3 vs *Pyn* D3
INCREASED AT DAY 3						
Phylum	Verrucomicrobia	0.064	10.139	0.817	< 0.0001	0.0002
Class	Erysipelotrichia	0.728	5.710	1.248	0.0209	0.0196
Class	Verrucomicrobiae	0.064	10.139	0.817	< 0.0001	0.0002
Order	Erysipelotrichales	0.728	5.710	1.248	0.0209	0.0196
Order	Verrucomicrobiales	0.064	10.139	0.817	< 0.0001	0.0002
Order	Bifidobacteriales	0.029	1.734	0.020	0.0044	0.0144
Family	Unclassified Clostridiales	1.888	4.490	1.824	0.0314	0.0291
Family	Bacteroidaceae	0.843	5.532	0.088	0.0018	0.0364
Family	Erysipelotrichaceae	0.728	5.710	1.248	0.0209	0.0196
Family	Verrucomicrobiaceae	0.064	10.139	0.817	< 0.0001	0.0002
Family	Bifidobacteriaceae	0.029	1.734	0.020	0.0044	0.0144
Family	Clostridiaceae I	0.002	0.387	0.005	0.0012	0.0070
Genus	Unclassified Clostridiales	1.888	4.490	1.824	0.0314	0.0291
Genus	*Bacteroides*	0.843	5.532	0.088	0.0018	0.0364
Genus	*Turicibacter*	0.597	5.631	1.106	0.0257	0.0189
Genus	*Akkermansia*	0.064	10.139	0.817	< 0.0001	0.0002
Genus	*Bifidobacterium*	0.029	1.734	0.020	0.0044	0.0144
Genus	*Clostridium*	0.002	0.387	0.005	0.0012	0.0070
REDUCED AT DAY 3						
Phylum	Tenericutes	0.220	0.013	0.215	0.0206	0.0211
Class	Mollicutes	0.220	0.011	0.215	0.0241	0.0245
Order	Anaeroplasmatales	0.220	0.011	0.215	0.0241	0.0245
Family	Lachnospiraceae	45.186	7.565	28.054	0.0090	0.0287
Family	Anaeroplasmataceae	0.220	0.011	0.215	0.0241	0.0245
Genus	Unclassified Lachnospiraceae	28.973	5.214	19.454	0.0114	0.0314
Genus	*Clostridium XlVa*	8.362	0.887	3.312	0.0032	0.0395
Genus	*Flavonifractor*	2.754	0.648	1.925	0.0030	0.0257
Genus	*Oscillibacter*	1.272	0.098	0.512	0.0003	0.0138
Genus	*Acetatifactor*	1.453	0.240	0.758	0.0068	0.0435
Genus	*Senegalimassilia*	0.792	0.323	0.903	0.0219	0.0017
Genus	*Stomatobaculum*	0.789	0.005	0.286	0.0027	0.0068
Genus	*Anaeroplasma*	0.220	0.011	0.215	0.0241	0.0245
Genus	*Clostridium XlVb*	0.179	0.003	0.209	0.0026	0.0016
Level	Classification	% Abundance			P-value	
		Pyn Day 0	*Pyn* Day 10	Mock Day 10	*Pyn* D0 vs *Pyn* D10	Mock D10 vs *Pyn* D10
INCREASED AT DAY 10						
Genus	Unclassified Porphyromonadaceae	6.209	16.144	3.708	0.031	0.0169

Table 2.1. OTUs with significant changes during *Pyn* infection.

Name in this study	Strain Designation	Genotype	Source or Reference
S. Typhimurium IR715	IR715	Naladixic acid-resistant derivative of ATCC 14028	PMID: 7868611
S. Typhimurium Kan^R	AJB715	IR715 *phoN*::KSAC	PMID: 12540539
S. Typhimurium *invA spiB*	SPN487	IR715 Δ*invA* Δ*spiB*	PMID: 23637594
S. Typhimurium Cm^R	FF176	IR715 *phoN*::*Tn10d-Cm*	PMID: 27309805
S. Typhimurium *invA spiB* Cm^R	FF183	IR715 Δ*invA* Δ*spiB phoN*::*Tn10d-Cm*	PMID: 27309805
S. Typhimurium *invA spiB* Kan^R	FF459	Δ*invA* Δ*spiB phoN*::KSAC	This study
S. Typhimurium *moaA*	FF310	IR715 *moaA*::KSAC	This study
S. Typhimurium *invA spiB moaA*	FF312	IR715 Δ*invA* Δ*spiB moaA*::KSAC	This study
S. Typhimurium *invA spiB cydAB cyxAB*	GTW47	IR715 Δ*invA* Δ*spiB phoN*::KSAC Δ*cydAB cyxAB*::*bla* ($Carb^R$)	This Study
S. Typhimurium *hya hyb hyd*	JSG321	ATCC 14028 ΔSTM3147-STM3150 ΔSTM1538-STM1539 ΔSTM1786-STM1787	PMID: 15501756
S. Typhimurium *tonB feoB*	GTW48	JK1128 *tonB*::Kan^R *feoB*::$Carb^R$	PMID: 29986892
Escherichia coli JB2	JB2	Endogenous *E. coli* strain isolated from laboratory mice	PMID: 24508234

Table 2.2. Bacterial strains used in this study.

Chapter 3

Malaria parasite infection compromises colonization resistance to an enteric pathogen by reducing gastric acidity*

Gregory T. Walker,[1] Guiyan Yang,[1,2] Julia Y. Tsai,[1,3] Jorge L. Rodriguez,[1] Bevin C. English,[1] Franziska Faber,[1,4] Lattha Souvannaseng,[1,5,6] Brian P. Butler,[6] and Renée M. Tsolis[1]

[1]Department of Medical Microbiology & Immunology, School of Medicine, University of California Davis, Davis, California, United States of America

[2]College of Veterinary Medicine, China Agricultural University, Beijing 100193, China

[3]School of Veterinary Medicine, University of California Davis, Davis, California, United States of America

[4]Institute for Molecular Infection Biology (IMIB), Faculty of Medicine, University of Würzburg, D-97080 Würzburg, Germany

[5]Mouse Biology Program, University of California Davis, Davis, California, United States of America

[6]Department of Pathobiology, School of Veterinary Medicine, St. George's University, Grenada, West Indies

*A version of this Chapter has been accepted for publication as a manuscript by *Science Advances*.

ABSTRACT

Infection with malaria parasites weakens colonization resistance against *Salmonella enterica* serovar (*S.*) Typhimurium, as indicated by increased shedding of the pathogen with the feces. *S.* Typhimurium is a member of the *Enterobacterales*, a taxon that increases in abundance when the colonic microbiota is disrupted or the colonic mucosa is inflamed. However, here we show that infection of mice with *Plasmodium yoelii* enhances fecal shedding of *S.* Typhimurium not by altering the environment in the colon, but by weakening host control in the upper gastrointestinal tract. *P. yoelii*-infected mice exhibited a considerably higher gastric pH than healthy mice. Exogenous stimulation of gastric acid secretion during *Plasmodium yoelii* infection restored stomach acidity and colonization resistance, demonstrating that *P. yoelii*-induced hypochlorhydria increases the gastric survival of *S.* Typhimurium. Furthermore, blockade of parasite-induced TNF-α signaling was sufficient to prevent an increase in gastric pH and enhance *S.* Typhimurium colonization during *P. yoelii* infection. Collectively, these data suggest that the abundance in the fecal microbiota of facultative anaerobic bacteria, such as *S.* Typhimurium, can be increased by suppressing antibacterial defenses in the upper gastrointestinal tract, such as gastric acid.

INTRODUCTION

Facultative anaerobic bacteria of the order *Enterobacterales* (*ord. nov.* (*1*)) are minority species commonly present in the fecal microbiota of healthy adults (*2*). An expansion of this taxon in the fecal microbiota is a signature of dysbiosis (*3*), which is associated with a disruption of the colonic microbiota by antibiotics (*4*) or linked to inflammation of the colon in patients with ulcerative colitis (*5*) or colorectal cancer (*6*). Pathogenic members of the *Enterobacterales*, such as *S.* Typhimurium, *Citrobacter rodentium* or *Yersinia enterocolitica*, use their virulence factors to trigger colitis, thereby altering the intestinal environment to increase the availability of

respiratory electron acceptors, which fuel pathogen growth to escalate fecal shedding (*7-11*). Infection of mice with the parasite *Toxoplasma gondii* triggers intestinal inflammation and bacterial dysbiosis characterized by an expansion of commensal *Enterobacterales* in the fecal microbiota (*12, 13*). *T. gondii* infection induces a dysbiosis dominated by *Enterobacterales* by triggering an influx of macrophages, which produce nitric oxide that is converted in the gut lumen into nitrate, thereby fueling growth of commensal *Enterobacterales* through nitrate respiration (*14*).

We recently reported that infection with a malaria parasite, *Plasmodium yoelii*, increases the abundance of *S.* Typhimurium in the fecal microbiota of mice (*15*), which might contribute to the increased risk of malaria patients to develop invasive bloodstream infections with non-typhoidal *Salmonella* serotypes, such as *S.* Typhimurium (*16, 17*). Infection of mice with *Plasmodium yoelii* triggers expression of inflammatory cytokines and inflammatory infiltrates of macrophages and T cells in the cecal mucosa (*15*), but it remains unknown whether parasite-induced intestinal inflammation is responsible for increasing fecal shedding of *S.* Typhimurium during co-infection. Here, we utilized a co-infection model to interrogate potential interactions by which malaria increases susceptibility to intestinal colonization by *Salmonella*.

RESULTS

Plasmodium yoelii infection increases intestinal colonization of *S.* Typhimurium

In experimental malaria models such as *Plasmodium yoelii nigeriensis* (henceforth referred to as *P. yoelii*), infection of mice can alter the gut environment (*15, 18*) and reduce colonization resistance against *S.* Typhimurium (*15, 19*). However, at later time points after infection, *S.* Typhimurium can overcome colonization resistance because its virulence factors, two type III secretion systems (T3SS-1 and T3SS-2), trigger intestinal inflammation (*9*). To disentangle the contribution of concurrent malaria from the contribution of *S.* Typhimurium

virulence factors to weakening colonization resistance, groups of mice were infected with the *S.* Typhimurium wild type or an *invA spiB* mutant that lacks T3SS-1 (due to a mutation in *invA*) and T3SS-2 (due to a mutation in *spiB*) at various time points following *P. yoelii* inoculation (outlined in Fig. 3.1A). When challenged at 6 days post-*P. yoelii* injection (dpp) or later, a *S.* Typhimurium *invA spiB* colonized the ceca and colons of *P. yoelii*-infected mice at 10- to 100-fold higher levels than in control mice (Fig. 3.1B, 3.1C, and 3.S1A). This was independent of *S.* Typhimurium virulence, as both wild-type and the *invA spiB* mutant displayed enhanced colonization (Fig. 3.S1B). The 6 dpp time point correlated with a peak in parasite expansion in the blood (Fig. 3.S2A). By this time, mice infected with *P. yoelii* had consistently developed severe anemia (Fig. 3.S2B) and showed substantial weight loss (Fig. 3.S2C), while splenomegaly increased steadily throughout the parasite infection (Fig. 3.S2D). Therefore, 6 days following *P. yoelii* inoculation was determined to be the earliest reliable time point to interrogate underlying causes of the malaria-associated defect in colonization resistance and was used as the primary model in subsequent experiments.

Impact of nitrate- and oxygen-associated growth on boosting *S.* Typhimurium colonization

Since macrophages recruited during *T. gondii* parasite infection fuel growth of commensal *Enterobacterales* through nitrate respiration (*14*) and previous work shows that *P. yoelii* infection also recruits macrophages to the cecal mucosa (*15*), we hypothesized that concurrent malaria might increase the luminal availability of nitrate to fuel a *S.* Typhimurium expansion. To test this idea, we compared the fitness of the *S.* Typhimurium wild type with a mutant lacking nitrate reductase activity (*napA narG narZ cyxA* mutant) by infecting mice with a 1:1 mixture of both strains. Surprisingly, genetic ablation of nitrate respiration did not reduce the fitness of *S.* Typhimurium in *P. yoelii*-infected mice (Fig. 3.1D and 3.1E), despite increased

intestinal burden overall in the co-infected group. This finding indicated that nitrate utilization was dispensable for increased fecal recovery of *S.* Typhimurium during concurrent malaria.

Alternatively, it has been shown that inflammation also benefits *S.* Typhimurium via increasing the bioavailability of oxygen. Depletion of *Clostridia*, either through *S.* Typhimurium virulence-associated inflammation or antibiotic administration, results in decreased microbiota production of the short chain fatty acid butyrate, which typically fuels epithelial colonocytes responsible for maintaining luminal hypoxia (*9*). Reduced butyrate availability switches colonocyte primary metabolism away from oxygen-intensive breakdown of SCFAs, allowing increased diffusion of oxygen into the colonic lumen. This provides an additional respiratory electron acceptor for growth of facultative anaerobes such as *Salmonella* and *E. coli* using cytochrome oxidases (*9, 20, 21*). As our previous work found that *P. yoelii* infection can impact the microbiota, including a relative reduction in *Clostridia* in the feces (*15*), we hypothesized this could be opening the oxygen respiratory niche in the colon and promoting *Salmonella* growth. To test this idea, we compared the fitness of the *S.* Typhimurium wild type with a mutant lacking the high-affinity cytochrome *bd* oxidase (*cydA* mutant). However, although *cydA* provided an approximately 10-fold fitness advantage in *P. yoelii*-infected mice, a similar fitness advantage was observed in mice not exposed to *P. yoelii* (Fig. 3.1F and 3.1G), suggesting that increased oxygenation of the intestinal lumen in co-infected mice did not contribute to the heightened *S.* Typhimurium levels. Overall, these results indicate that increased access to respiratory electron acceptors was not a major contributing factor to the defect in colonization resistance during *P. yoelii* infection.

P. yoelii infection does not rapidly increase intestinal *S.* Typhimurium replication

The absence of *Plasmodium*-enhanced respiratory growth defects led us to question whether reduced colonization resistance was actually coupled with more rapid growth of *S.* Typhimurium in co-infected mice. To evaluate this, mice were inoculated with *S.* Typhimurium

carrying the lactose-addicted plasmid pAM34 (*22*), which allows for the short-term assessment of bacterial growth in low-lactose environments such as the adult mouse intestine (*23*). At 24 h post-challenge, *S.* Typhimurium populations throughout the gut exhibited equivalent replication rates in both *P. yoelii* co-infected and mock-infected mice, despite increased bacterial burdens in the co-infected group (Fig. 3.2A and 3.2B). Intriguingly, we found that *S.* Typhimurium colonization was already greater in co-infected mice by 4 h post-challenge, also independent of the *in vivo* growth rate (Fig. 3.2C and 3.2D). This rapid difference in *S.* Typhimurium loads without a concomitant increase in replication indicated that boosted growth of the bacteria is not responsible for the enhanced colonization of *P. yoelii*-infected mice.

P. yoelii infection impacts gastric antibacterial defense

Since differences in *S.* Typhimurium loads arose rapidly after bacterial inoculation of mice, we hypothesized that *P. yoelii* infection may compromise intrinsic “bottleneck” defenses against bacterial colonization that act early following pathogen ingestion. As we also observed that co-infected mice often exhibited higher *S.* Typhimurium levels throughout the upper gastrointestinal tract (Fig. 3.S3A), it seemed likely that loss of colonization resistance against *S.* Typhimurium in co-infected mice could be occurring in the stomach or small intestine.

One of the most severe initial bottlenecks against colonization by many enteric pathogens is imposed by the highly acidic (pH 1.5-3) environment encountered in the stomach (*24*). While *S.* Typhimurium thrives at neutral pH (*25*), it is capable of surviving short-term (60 min) exposure to acidity as low as pH 4 *in vitro* (Fig. 3.3A). However, inoculated bacteria are rapidly killed at pH 3.5 or lower, with no bacteria recovered from exposure to media at pH 2.5 or below (Fig. 3.3A). A similar degree of acid sensitivity is shared by many *Enterobacterales*, including both pathogenic and non-pathogenic varieties (Fig. 3.S4A-E). This finding corroborates previous work indicating *S.* Typhimurium and other enteric pathogens are highly susceptible to killing by the acid levels present in the stomach (*24*). Thus, deficiencies in

maintaining gastric acidity could result in greater survival of ingested *S.* Typhimurium into the intestines.

When measuring the acidity of the stomach lumen directly using a pH-sensing microelectrode, *P. yoelii* infection was associated with a significantly higher gastric pH (mean pH = 4.02 $\pm$ 1.07) compared to mock-infected mice (mean pH = 2.46 $\pm$ 0.32) by 6 dpp (Fig. 3.3B). Onset of hypochlorhydria during *P. yoelii* infection correlated with the loss of colonization resistance, as it was not detectable in mice earlier than 6 dpp (Fig. 3.S3B). Stomachs of mice at 6 dpp were generally smaller than mock-infected controls (Fig. 3.S5A), likely resulting in part from reduced food consumption (Fig. 3.S5B) that paralleled observed weight loss patterns during parasite infection (Fig. 3.S2C). As meal intake can be stimulatory for gastric acid secretion (*26*), we predicted that the observed pH differences were a result of acute reductions in food intake during malaria. Fasting mock-infected mice overnight was sufficient to reduce stomach weight (Fig. 3.S5C), but did not alter the gastric pH of the fasted mice compared to fed mice with *ad libitum* food access (Fig. 3.S5D). Fasting also did not normalize colonization resistance against inoculated *S.* Typhimurium between fasted mock- and *P. yoelii*-infected mice (Fig. 3.S5E), suggesting that more than acute decreases in food intake during *P. yoelii* infection is necessary to explain the defects in gastric acidity and susceptibility to *S.* Typhimurium colonization.

Malaria-induced reduction in gastric acidity impacts *S.* Typhimurium colonization

We next wanted to determine whether the observed hypochlorhydria is actually responsible for the increased survival of co-infected *S.* Typhimurium. Gastric acid secretion is normally regulated through a combination of stimulatory and inhibitory signaling to gastric parietal cells, leading to translocation of the gastric proton pump to the apical membrane and active acid secretion into gastric lumen (*26*). One of the most potent pro-secretion signals is histamine, released locally by enterochromaffin-like cells in the gastric glands, binding parietal cell H2 receptors (H2R) (*26*). To assess whether the high gastric pH during *P. yoelii* infection

was responsible for the defect in colonization resistance, mice were treated with the specific H2R agonist dimaprit dihydrochloride to stimulate gastric acid secretion 1 h prior to *S.* Typhimurium challenge. H2R agonist administration acutely reduced the stomach pH in *P. yoelii*-infected animals to mock-infected levels (Fig. 3.3C). Furthermore, H2R stimulation in *P. yoelii*-infected mice rescued colonization resistance against *S.* Typhimurium (Fig. 3.3D and 3.3E) without impacting other aspects of the parasite infection, including parasitemia (Fig. 3.S6A) and anemia (Fig. 3.S6B).

In complementary experiments, mice were treated with the proton pump inhibitor omeprazole to block acid secretion into the stomach lumen prior to *S.* Typhimurium challenge. Omeprazole treatment in control mice resulted in a rise in both the gastric pH (Fig. 3.3F) and *S.* Typhimurium burden (Fig. 3.3G and 3.3H) relative to vehicle-treated mice, as has been previously observed (*24*). However, omeprazole administration in *P. yoelii*-infected animals did not further increase *S.* Typhimurium loads over *P. yoelii*-infected mice given the vehicle (Fig. 3.3G and 3.3H) and had no impact on measures of parasite infection severity (Fig. 3.S6C-D). This suggests that the effect of *P. yoelii* infection alone on stomach pH was sufficient to maximally benefit inoculated bacteria in better surviving the gastric environment. Collectively, these data indicate that reduced gastric acidity in *P. yoelii*-infected mice contributes to their increased susceptibility to *S.* Typhimurium infection, as the parasite-associated hypochlorhydria is necessary for boosted survival of inoculated bacteria in the stomach, which in turn promotes intestinal colonization.

Altered expression of gastric signaling peptides during malaria

To explore potential mechanisms underlying the rise in gastric pH, we analyzed the effect of *P. yoelii* on the expression of genes associated with regulation of acid secretion by parietal cells in the stomach (*26*). Notably, in the stomach tissues of *P. yoelii*-infected mice expression of the parietal-stimulatory hormone gastrin (*Gast*) was reduced 2- to 4-fold (Fig. 3.4A), while transcripts for

the inhibitory hormone somatostatin (*Sst)* were increased nearly 2-fold relative to mock (Fig. 3.4B). This result suggested that alterations in typical signaling mechanisms governing acid secretion could be contributing to hypochlorhydria.

Parietal cells utilize specialized H^+,K^+-ATPases (ATP4) concentrated intracellularly on tubulovesicles that localize apically when stimulated to actively secrete protons into the stomach lumen, generating the low pH (*26, 27*). Intriguingly, expression of genes encoding the proton pump (*Atp4a/b*) was slightly reduced in the stomach during malaria, with *Atp4b* notably reduced 2-fold relative to mock mice (Fig. 3.4C and 3.4D). Gastric acid secretion is not typically regulated by altering the expression of proton pump components, so we explored whether this reduction in transcript abundance instead paralleled a reduction in parietal cell abundance, the primary cells expressing *Atp4a/b*. Blinded histopathology of hematoxylin and eosin (H&E)-stained gastric tissues was imaged by light microscopy (Fig. 3.S7A) as well as fluorescence imaging (Fig. 3.S7B) to more accurately quantify highly eosinophilic cells. Eosin is autofluorescent and parietal cells stain strongly with eosin compared to other cell populations in the gastric mucosa; thus, large autofluorescent cells in H&E-stained gastric tissue sections are mostly parietal cells (*28*). We compared eosin-stained cell counts between mock and *P. yoelii*-infected animals in the gastric tissues as a proxy to estimate parietal cell abundance (workflow provided in Fig. 3.S7C). However, this analysis found no discernable difference in the overall parietal cell abundance in gastric tissues during malaria (Fig. 3.4E), suggesting that elevated pH may result from reduced mRNA abundance of genes encoding the proton pump in the stomachs of *Plasmodium*-infected animals.

Proinflammatory signaling during malaria reduces gastric acidity

We next investigated how the immune response to *P. yoelii* may be impacting gastric acid production. In the course of assessing gastric gene expression, we observed elevated transcripts for the inflammatory cytokine tumor necrosis factor (TNF-α, encoded by *Tnf*) in the stomach tissue of *P. yoelii* infected mice (Fig. 3.4F). TNF-α treatment was reported to reduce

secretagogue responses by rabbit parietal cells (*29*) and TNF-α administration induced apoptosis of rat parietal cells (*30*). Moreover, it is known that both clinical and experimental malaria can be associated with elevated circulating TNF-α (*31-33*), a response that is thought to help control parasite replication (*31, 34*) but can also be associated with severe or cerebral malaria (*32, 33, 35*). In line with these findings, circulating TNF-α was also higher with *P. yoelii* infection than in control mice (Fig. 3.5A). Thus, we hypothesized that TNF-α responses to the parasite might be interfering with gastric acid secretion.

In mice treated with TNF-α neutralizing antibody, mock- and *P. yoelii*-infected groups displayed equivalent gastric pH (Fig. 3.5B and Fig. 3.S8A), suggesting that TNF-α signaling is necessary for development of hypochlorhydria with *P. yoelii*. In the context of *S.* Typhimurium, TNF-α blockade also equalized initial (3 hpi) colonization between mock- and *P. yoelii*-infected mice (Fig. 3.5C and Fig. 3.S8B), compared to groups treated with an isotype control. Longer challenge time points were not assessed, as TNF-α responses are also necessary for appropriate host defenses to limit systemic *S.* Typhimurium infection (*36, 37*). Despite TNF-α blockade, mice infected with *Plasmodium* still developed anemia (Fig. 3.5D) and displayed even greater circulating parasitemia (Fig. 3.5E). This latter impact on parasite burden is actually evidence of effective antibody blockade, as early TNF-α responses to *Plasmodium* are associated with limiting parasite replication in the host (*34, 35*). TNF-α blockade did not significantly affect food consumption or weight loss in infected mice, compared with isotype-treated controls (Fig. 3.S8C-E). *P. yoelii*-infected mice given anti-TNF-α antibody still showed an increase in gastric TNF-α transcripts (Fig. 3.S8F), but TNF-α blockade led to a reduction of pro-IL-1β expression (Fig. 3.S8G), indicating a potential dampening of the pro-inflammatory cytokine response. Overall, these results link pro-inflammatory TNF-α responses by the host during *P. yoelii* infection with loss of the intrinsic gastric acid defense, thereby increasing susceptibility to secondary infection by enteric pathogens.

DISCUSSION

The expansion of facultative anaerobic bacteria in the fecal microbiota has been associated with disruption of the colonic microbiota by antibiotics (*4*) and additionally can occur during inflammation of the colon in patients with ulcerative colitis (*5*) or colorectal cancer (*6*). While in these instances, increase in the relative abundance of facultative anaerobes such as *Enterobacterales* has been linked to alterations in the colonic environment, our results demonstrate that changes to stomach acid, an antimicrobial defense of the upper GI tract, can affect the composition of the fecal microbiota. Thus, our findings on how malaria impacts colonization resistance to *S.* Typhimurium, a foodborne microbe, have implications for understanding factors affecting the composition of the microbiota in the lower GI tract, as assessed by fecal microbiota profiling. For example, abundance of bacteria from the oral cavity in the fecal microbiota has been linked to multiple pathogenic processes throughout the digestive tract. Increased prevalence of oral bacteria such as *Fusobacterium* has been found in the fecal microbiota of patients with systemic inflammation caused by inflammatory bowel disease (*38*), liver cirrhosis (*39*), and HIV infection (*5*). This spread of oral bacteria to other sites in the digestive tract is clinically important, especially since some members of the oral microbiota have been linked to colonic (*40*) and pancreatic cancers (*41*). Notably, patients with both AIDS (*42*) and liver cirrhosis (*43*) exhibit hypochlorhydria, though the underlying mechanisms are unknown. Our results suggest that in addition to lowering the barrier to enteric pathogen colonization, inflammation-induced hypochlorhydria may also contribute to spread of oral microbiota to other sites in the digestive tract. Therefore, interpretation of alterations to the fecal microbiota may need to consider habitat filters in the upper GI tract, such as the acidic barrier of the stomach.

Susceptibility to enteric pathogen infection is regulated by both host- and microbiota-associated defenses. Host physiology and immunity influence the distinct habitats of the gastrointestinal tract, thereby filtering for the most suitable microbial communities throughout

(*21, 44*). The microbiota then serves, in part, to resist pathogen colonization by training host immunity and pre-empting access to resource and nutrient niches necessary for potential pathogens to thrive in the gut (*44-46*). However, many enteric pathogens have evolved virulence systems to avert microbiota-mediated colonization resistance by engineering novel growth niches to bloom in the intestine (*7, 47*). Such mechanisms still typically require sufficient quantities of the pathogen to reach the lower intestines in order to trigger a significant host response to alter the gut environment (*48, 49*). Given this limitation, intrinsic host defenses that rapidly restrict survival of ingested microbes- particularly in the upper G.I. tract- are necessary to maintain maximal defense against infection. This type of resistance is largely provided by the innate production and secretion of compounds with antibacterial properties, such as host-derived antimicrobial peptides (*45*), various components of bile (*23, 45*), and gastric acid (*24, 50*). It is ultimately the combined gauntlet of antimicrobial defenses and nutrient limitation that must be avoided or averted by pathogens to infect the host and cause disease.

Our prior research showed that mice infected with *Plasmodium,* a pathogen that replicates in the bloodstream during the erythrocytic infection state, display remarkably increased susceptibility to colonization by non-typhoidal *Salmonella* (*15*). The findings presented here advance our understanding of how malaria affects colonization resistance to pathogens by linking the boosted implantation of *Salmonella* to a previously unreported, prolonged reduction in gastric acidity associated with inflammatory signaling during infection with the malarial parasite.

Low stomach pH in healthy animals serves as a significant bottleneck in the colonization of many bacterial pathogens (*24*), including *S.* Typhimurium and related bacteria (Fig. 3.3A and Fig. 3.S4A-E). Drugs impacting gastric acidity in humans, such as proton pump inhibitors, have been noted as risk factors that can both alter the gut microbiome and increase susceptibility to intestinal infection with pathogens including *Salmonella, Campylobacter* and *Clostridioides difficile (45, 51-54)*. In our model, high stomach pH during malaria was associated with

increased *S.* Typhimurium abundance post-infection, and exogenous stimulation of gastric acid secretion prior to *S.* Typhimurium inoculation rapidly restored resistance to colonization, demonstrating that parasite-induced hypochlorhydria was responsible for increased susceptibility to the secondary infection.

Typically, parietal cells in the gastric glands are stimulated by a combination of histamine, gastrin, and acetylcholine released from nearby cells, leading to apical translocation of the parietal's H^+/K^+-ATPase proton pump, thereby allowing active acid secretion into the stomach lumen (*26*). Somatostatin serves as the major hormonal inhibitor of gastric acid secretion via direct action on parietal cells and indirectly through inhibition of histamine release by enterochromaffin-like cells. Supporting the notion that *Plasmodium* infection alters normal signaling for gastric acid release, we found increased somatostatin and reduced gastrin expression in gastric tissues from parasite-infected mice (Fig. 3.4A and 3.4B), which suggests reduced parietal cell stimulation as a mechanism underlying elevated gastric pH. This mechanism is consistent with our findings that parietal cell abundance was unchanged (Fig. 3.4E) and that stimulation with an H2R agonist resulted in acid production (Fig. 3.3D).

In the context of gastric *Helicobacter pylori* infection, local production of pro-inflammatory cytokines, including TNF-α, can influence and inhibit gastric acid secretion by parietal cells (*26, 29, 55*). Our results extend this concept to a parasite infection, as antibody blockade of TNF-α signaling during *Plasmodium* infection was sufficient to maintain normal gastric acidity (Fig. 3.5B) and colonization resistance (Fig. 3.5C). TNF-α is known to also be involved in both mouse and human innate immune responses to malaria (*33, 56*) and appears to contribute to limiting parasite replication in host cells (*34*), supporting our data that indicates mice treated with TNF-α blocking antibody develop higher circulating parasitemia (Fig. 3.5E). This inflammatory cytokine response may represent a shared mechanism between our model and susceptibility to disseminated salmonellosis associated with human malaria. It remains

unclear whether the hypoacidic environment could actually be impacting the rest of the microbiota, either directly or indirectly (e.g. through altered digestion or vitamin availability), to produce the shifts in the microbial community composition observed previously (*15, 19*), or whether these changes are the result of additional gastrointestinal impacts of *Plasmodium* infection.

In sub-Saharan Africa, malaria is associated with a higher risk for systemic non-typhoidal *Salmonella* infections in children (*16, 17, 57*). While prior work in mouse models helped illuminate how elements of the immune response to *Plasmodium* can promote systemic infections by *S.* Typhimurium (*58, 59*), our current findings suggest the additional mechanism of *Plasmodium*-associated hypochlorhydria by which underlying malaria increases susceptibility to colonization by *S.* Typhimurium. This generalized reduction in initial bacterial killing could particularly benefit the multi-drug resistant ST313 isolates currently circulating in Africa, which exhibit genomic degradation and reduced capacity for inflammatory activation (*57*). Induction of inflammation is well recognized as part of the usual NTS strategy for colonizing the host (*7-9, 44, 47*), but avirulent *S.* Typhimurium incapable of inducing a significant intestinal inflammatory response displayed equivalent colonization enhancement by *P. yoelii* (Fig. 3.S1B). This suggests that in the context of malaria, reduced killing of the bacteria in the stomach and upper intestines could compensate for genetic deficits in NTS pathogenesis identified in the currently circulating strains. Moreover, malaria-associated suppression of colonization resistance could help clarify why such apparent deficits are not eliminated by selective pressure in the region, allowing development towards an extraintestinal pathogenic lifestyle and ultimately increasing the odds of the high-risk bloodstream NTS infections.

MATERIALS AND METHODS

Mice and experimental co-infection model. 6- to 8-week-old female C57BL/6J mice (stock no. 000664) were purchased from The Jackson Laboratory for infection experiments. For generating *Plasmodium* parasitized blood stocks, CD-1 mice were purchased from Charles River Laboratory. Mice were housed under specific pathogen-free conditions and used for experiments at 8 to 11 weeks of age. For most experiments, at least 5 mice were used in each group, with multiple cages of mice (2 to 5 mice per cage) used for each group to limit the possibility of cage effects. All animal experiments were approved by the Institution of Animal Care and Use Committee at the University of California, Davis.

***Plasmodium* infections**. *Plasmodium yoelii nigeriensis* parasite stock was obtained from the Malaria Research and Reference Reagent Resource (MRRRR) and was maintained and expanded by passage through CD-1 mice. Blood from multiple CD-1 mice infected with parasite was collected by cardiac puncture, pooled, and mixed 1:2 (vol/vol) with freezing solution (10% glycerol and 90% Alsever's solution [Sigma-Aldrich]) for storage in liquid nitrogen. For mock infections, blood was collected from uninfected CD-1 mice and similarly preserved.

C57BL/6J mice were infected with *P. yoelii* parasite upon reaching 8 to 11 weeks of age. Parasitized blood stocks were diluted to $1x10^8$ parasite-infected red blood cells (iRBCs)/mL with 0.9% saline. Mice were then inoculated intraperitoneally (ip) with 0.1 mL of diluted parasitized blood. For mock infections, uninfected control blood was diluted with an equivalent volume of saline, and 0.1 mL was injected ip into the mice. Parasite infection was tracked through a combination of weight loss, food consumption, blood cell counts, and parasite burden in the blood. Anemia (reduced circulating blood cell counts) and parasite burden were assessed from blood collected from tail snips. For circulating blood cell counts, tail blood was diluted 1:1000 in PBS and cell concentration was assessed using a TC20™ Automated Cell Counter (Bio-Rad Laboratories, Inc.). Counts were normalized to the average counts from the mock-treated animals collected and measured at the same time. Parasitemia was determined by examination

of Giemsa-stained (Harleco) thin blood smears to enumerate the percentage of red blood cells containing detectable *P. yoelii* parasites.

***Salmonella* strains.** A complete list of *Salmonella* strains used in this study can be found in Table 3.S1. Unless otherwise indicated, bacteria were routinely grown on LB agar or MacConkey agar plates and cultured aerobically at 37°C in lysogeny broth (LB) supplemented with antibiotics at the following concentrations for selection when appropriate: nalidixic acid (Nal), 0.05 mg/mL; carbenicillin (Carb), 0.1 mg/mL; kanamycin (Kan), 0.1 mg/mL; chloramphenicol (Cm), 0.03 mg/mL. Construction of most mutant strains used in this study has been described in prior work (*9, 60*). *S.* Typhimurium *invA spiB* Kan^R (FF459, IR715 Δ*invA* Δ*spiB phoN*::KSAC) was generated by P22 transduction of *phoN*::KSAC from IR715 *phoN*::KSAC into IR715 Δ*invA* Δ*spiB* (SPN487), in the manner previously described for the production of *S.* Typhimurium *invA spiB* Cm^R (FF183) (*60*). *S.* Typhimurium *invA spiB* Cm^R + pAM34 (GTW58) was produced by transforming the plasmid pAM34 (*22*) into FF183 by heat-shock, and maintained through culturing in LB with carbenicillin and 1 mM isopropyl β- d-1-thiogalactopyranoside (IPTG).

***Salmonella* infection and colonization readouts.** Single colonies of *S.* Typhimurium grown on selective agar plates were inoculated into LB supplemented with the appropriate antibiotics for selection and incubated with shaking (200 rpm) at 37°C for 14-18 hours. Cultures were pelleted by centrifugation (10 min, 4000*g*, 4°C) and washed with sterile LB without antibiotics. Pelleted *S.* Typhimurium was resuspended in LB and adjusted to the appropriate bacterial density for infections. For single-strain infections, mice were inoculated orally by a pipette tip with 0.02 mL of *S.* Typhimurium at a density of approximately $5x10^{10}$ colony forming units (CFU)/mL. This high inoculum dose was used to help limit variability in colonization between mice in the groups,

and to reduce non-detection of *Salmonella* in some mice that can occur at lower doses for a more accurate comparison of intestinal burden. For competitive infections, the strains were prepared separately, adjusted to $1x10^{10}$ CFU/mL, then mixed 1:1 (vol/vol) and inoculated as 0.1 mL by oral gavage. Inocula were serially diluted and plated for CFU to confirm accuracy of the concentration and the input strain ratio for calculations in competitive infections. *S.* Typhimurium inoculations occurred in the morning, between 06:00 and 12:00. Mice were euthanized at the indicated time points or when they became moribund. Mice euthanized early due to health concerns were excluded from analysis.

Intestinal contents (approximately 20-100 mg) of euthanized mice were collected from the relevant portions of the intestines into 1-2 mL PBS and homogenized by vortex. Samples were then serially diluted in PBS and plated on appropriate selective agar to assess CFU loads. If no *S.* Typhimurium could be recovered post-challenge, the load was set to the detection limit for statistical comparisons (100 CFU/g intestinal content). In the *S.* Typhimurium challenges lasting 4 hours or less, mice were excluded from the analysis if *S.* Typhimurium could be detected in the small intestine but no CFUs were detected in the cecal or colon content, indicating the inoculum had not yet reached the large intestine at the point of collection. In that case, using the detection limit as the CFU load in the cecum or colon for statistical analysis would be inaccurate. In the competitive infections, intestinal content was plated on media selecting for both inoculated strains (LB + nalidixic acid) as well as the mutant strain alone (LB + chloramphenicol). Wild-type *S.* Typhimurium (IR715) burden was determined by subtraction of the mutant numbers from the overall (LB + nalidixic acid) numbers, and competitive index was calculated as the wild-type:mutant load, corrected for the input ratio of the inoculum.

***In vivo* pAM34 growth assays.** To compare the approximate *in vivo* rate of *S.* Typhimurium in *P. yoelii*-infected and mock-infected animals, mice were perorally inoculated with $1x10^9$ CFU *S.* Typhimurium *invA spiB* Cm^R + pAM34 (GTW58). As has been previously described (*22*),

replication of the pAM34 plasmid is under control of the LacI repressor region which allows it to be replicated and maintained by *Salmonella* when grown in high concentrations of lactose or a lactose analog such as IPTG, but cannot replicate and is rapidly lost as the bacteria divide in low-lactose environments such as the adult mouse. Thus, loss of the plasmid at a population level correlates with the overall replication of the bacteria in the low-lactose environment, which allows for assessment of the replication rate (*23*).

To prepare inocula of *S.* Typhimurium *invA spiB* Cm^R + pAM34, single colonies grown on LB supplemented with carbenicillin (0.1 mg/mL) and 1 mM IPTG (for plasmid maintenance) were inoculated into LB broth (supplemented with IPTG alone) and incubated with shaking (200 rpm) at 37°C for 12 hours. Then, the plasmid was diluted to better assess the early replication rate by subculturing the inoculum (1:100) in fresh LB without IPTG and allowed to grow for an additional 3 hours prior to harvesting the bacteria by centrifugation and infecting the mice perorally, as previously described. Immediately following infection of the mice, the inoculum was serially diluted in PBS and plated on MacConkey and MacConkey+Carbenicillin+1 mM IPTG to quantify the ratio of pAM34-containing *S.* Typhimurium to the total inoculated *S.* Typhimurium count. At 4 or 24 hours post- inoculation, mice were euthanized, and intestinal contents were collected and plated on MacConkey and to quantify *S.* Typhimurium burden and determine the fraction of the population maintaining pAM34. In parallel to the mouse infections, serial dilutions of the inoculum were cultured in LB for an additional 4 to 24 hours, then plated on MacConkey and MacConkey + Carb + IPTG to generate a standard curve correlating population-level pAM34 plasmid loss to number of replications, as has been previously described (*23*).

***In vitro* pH bacterial survival assays.** To assess bacterial sensitivity to low pH, PBS was acidified to different pH levels between 2 and 5 with hydrochloric acid and aliquoted into separate tubes. *S.* Typhimurium *invA spiB* Kan^R and strains of *Escherichia coli* strain Nissle 1917, *Escherichia coli* O157:H7 EDL933 (ATCC 43895), *Citrobacter rodentium* DBS100 (ATCC

51459), *Shigella flexneri* M90T (ATCC BAA-2402), *Yersinia enterocolitica subsp. enterocolitica* (ATCC 700823) were grown overnight in LB broth and prepared for inoculating mice as described above, except washed and resuspended using PBS instead of LB, to an OD_{600} of 1.0, and plated for quantification of initial CFUs. The inoculum was then diluted 1:100 into the different low-pH PBS tubes and incubated at 37°C with shaking for 1 hour. Samples were serially diluted in fresh PBS (pH 7.4) and plated on MacConkey agar to quantify remaining bacterial concentrations.

Gastric pH assessment. Following euthanasia, stomachs of mice were removed from the body cavity. The microelectrode PH-N and reference probes (Unisense) were immediately inserted into the untreated gastric antral lumen for assessment of pH, and measurements on the Unisense Microsensor Multimeter (in mV) were recorded and converted to pH values using a standard curve generated from concurrent readings of reference standards at pH 2, 4, and 7. The probes were rinsed with 70% ethanol and distilled water between measurements.

Histamine H2 Receptor agonist (dimaprit) administration. Mice were inoculated with *P. yoelii*-infected or control blood as previously described. In the morning of day 6 post-infection, mice received a single dose of the histamine H2 receptor (H2R) agonist dimaprit dihydrochloride (Tocris Bioscience) or a mock treatment with the vehicle. Dimaprit was administered intraperitoneally as 0.1 mL of 40 mg/mL dimaprit dihydrochloride dissolved in sterile saline, and the vehicle (saline) was administered in an equivalent volume. 1 hour later, mice were challenged with *S.* Typhimurium for 4 hours, then assessed for gastric pH and intestinal *S.* Typhimurium burden.

Omeprazole administration. Mice were inoculated with *P. yoelii*-infected or control blood as previously described. In the afternoon on days 3, 4, and 5 post-infection, mice began receiving

daily treatments with either the proton pump inhibitor omeprazole (Sigma-Aldrich) or a mock treatment with the vehicle. Omeprazole was administered intraperitoneally as 0.1 mL of a 30 mg/mL suspension in 1% Tween-80 (Sigma-Aldrich) in dPBS (Gibco), and vehicle was administered in an equivalent volume. At 6 dpp, mice were challenged with *S.* Typhimurium for 24 hours then assessed for gastric pH and intestinal *S.* Typhimurium burden.

Anti-TNF-α antibody administration. Mice were inoculated with *P. yoelii*-infected or control blood as previously described. On days 3 and 5 post-infection, mice received a dose of either Ultra-LEAF™ Purified anti-mouse TNF-α antibody (Clone: MP6-XT22, BioLegend, Inc.) or Ultra-LEAF™ Purified Rat IgG1, κ isotype control antibody (BioLegend, Inc.). Both antibodies were diluted to 2 mg/mL in dPBS (Gibco) and administered as 0.25 mL per mouse, intraperitoneally, for a dose of 0.5 mg/mouse (approximately 25 mg/kg body weight). At 6 dpp, mice were either euthanized for relevant measurements, or challenged with *S.* Typhimurium for 3 hours, then euthanized for gastric pH and intestinal *S.* Typhimurium burden.

RNA extraction and real-time PCR expression analyses. Following lumen content removal, tissues were snap frozen in liquid nitrogen at necropsy and stored at -80°C. RNA was isolated from tissues using Tri-Reagent (Molecular Research Center). Briefly, whole tissues were suspended in Tri-Reagent and homogenized by glass bead-beating for 1 minute, then treated with chloroform and centrifuged to separate the phases. The aqueous phase was removed and mixed with 95% ethanol, then applied to a silica membrane column (EconoSpin™, Epoch Life Science) and washed with 3M sodium acetate. The column was treated with PureLink™ DNase (Invitrogen) to remove genomic DNA contamination, washed twice with 10 mM HEPES in 70% ethanol, and RNA was eluted in RNase-free water for quantification.

For analysis of mRNA expression, 1 µg of total RNA per sample was reverse-transcribed into cDNA in a 50 µL reaction using MultiScribe™ Reverse Transcriptase (ThermoFisher

Scientific), and 4 µL of the resulting cDNA was used for each real-time reaction. Real-time PCR was performed using SYBR green (Applied Biosystems) on a ViiA 7 Real-Time PCR System (Applied Biosystems) using primers listed in Table 3.S2. Data was analyzed using the comparative threshold cycle method in QuantStudio™ Real-Time PCR System (Applied Biosystems), with target gene expression levels normalized to *Actb* RNA levels in the same sample and represented as fold-change over the average expression in mock-infected animals.

Gastric histopathology. At necropsy, stomachs were flayed open along the lesser curvature and samples of the greater curvature approximately 5 mm wide at the midline were collected from the forestomach to pyloric sphincter, as described by Sigal *et al.* (*61*), and embedded in paraffin to generate longitudinal sections. 5 µm-thick tissue sections were cut from formalin-fixed paraffin-embedded tissues and hematoxylin and eosin stained by the UC Davis Veterinary Pathology Laboratory. Blinded images of stained slides were taken as both bright-field (20x) and autofluorescence (40x, RFP channel, Excitation: 531/40, Emission: 593/40) scans using an EVOS™ FL imaging microscope (ThermoFisher Scientific) for general histopathological assessment as well as highly eosinophilic (autofluorescent) cell quantification.

To assess eosinophilic cell abundance in the gastric mucosa to estimate parietal cell abundance (*28*), images of glandular/mucosal portions of the tissues distal to the forestomach-corpus junction were bounded manually and the glandular area was measured using ImageJ. Then the images were made binary, holes filled, watershed to separate nearby cell structures, and large particles (radius > 25 µm) were analyzed. As this process often grouped multiple, closely associated parietal cells as single particles (see overlay example in right panel of Fig. 3.S7C), analyzed particles were converted to approximate cell numbers by dividing the particle area in each image by the overall median particle size.

Plasma TNF-α measurements. Blood was collected from mice by cardiac puncture using heparinized needles immediately following death by CO_2 inhalation. The heparinized blood was centrifuged (8000*g* for 4 minutes) and the plasma layer was removed and stored at -80°C for TNF-α measurement using the mouse TNF-α DuoSet® ELISA (R&D Systems, Inc.) according to the manufacturer's instructions.

Statistical analyses. The investigators were not blinded to animal allocation during experiments and outcome assessment, except for histopathology analysis. Sample sizes were estimated on the basis of effect sizes in previous studies. All analyses were performed using Prism 8 (GraphPad Software, La Jolla, CA). The limit of detection while plating for *S.* Typhimurium loads was set to 100 CFU/g content, and the number of CFU per gram intestinal content was Log10 transformed to normalize the data for statistical analysis. Significant differences in Log10-normalized CFU loads, gastric pH, and Log2-normalized mRNA expression data between groups were determined by unpaired *t* tests with Welch's correction. Significant differences in CFU loads of competing *S.* Typhimurium strains in the same animal were determined by paired *t* tests. Significant differences between groups in their competitive indices and other measures not log-normalized prior to comparison (body weight changes, spleen and stomach weights, blood cell counts, parasite burden, and circulating TNF-α) were determined by Mann-Whitney tests. In all comparisons, $P < 0.05$ was considered statistically significant.

Software. The following software was used: Microsoft Excel for Mac, Prism 8 for macOS (GraphPad Software), QuantStudio™ Real-Time PCR System Version 1.3 (Applied Biosystems), EVOS™ FL Auto 2 Imaging System (ThermoFisher Scientific), ImageJ/FIJI Version 2.0.0-rc-69/p1.520 (https://imagej.net/Fiji/Downloads) (*62, 63*).

REFERENCES

1. M. Adeolu, S. Alnajar, S. Naushad, S. G. R, Genome-based phylogeny and taxonomy of the 'Enterobacteriales': proposal for Enterobacterales ord. nov. divided into the families Enterobacteriaceae, Erwiniaceae fam. nov., Pectobacteriaceae fam. nov., Yersiniaceae fam. nov., Hafniaceae fam. nov., Morganellaceae fam. nov., and Budviciaceae fam. nov. *Int J Syst Evol Microbiol* **66**, 5575-5599 (2016).
2. C. Human Microbiome Project, Structure, function and diversity of the healthy human microbiome. *Nature* **486**, 207-214 (2012).
3. N. R. Shin, T. W. Whon, J. W. Bae, Proteobacteria: microbial signature of dysbiosis in gut microbiota. *Trends in biotechnology* **33**, 496-503 (2015).
4. E. J. Vollaard, H. A. Clasener, A. J. Janssen, Co-trimoxazole impairs colonization resistance in healthy volunteers. *J Antimicrob Chemother* **30**, 685-691 (1992).
5. S. C. Lee, L. L. Chua, S. H. Yap, T. F. Khang, C. Y. Leng, R. I. Raja Azwa, S. R. Lewin, A. Kamarulzaman, Y. L. Woo, Y. A. L. Lim, P. Loke, R. Rajasuriar, Enrichment of gut-derived Fusobacterium is associated with suboptimal immune recovery in HIV-infected individuals. *Sci Rep* **8**, 14277 (2018).
6. J. C. Arthur, E. Perez-Chanona, M. Muhlbauer, S. Tomkovich, J. M. Uronis, T. J. Fan, B. J. Campbell, T. Abujamel, B. Dogan, A. B. Rogers, J. M. Rhodes, A. Stintzi, K. W. Simpson, J. J. Hansen, T. O. Keku, A. A. Fodor, C. Jobin, Intestinal inflammation targets cancer-inducing activity of the microbiota. *Science* **338**, 120-123 (2012).
7. S. E. Winter, P. Thiennimitr, M. G. Winter, B. P. Butler, D. L. Huseby, R. W. Crawford, J. M. Russell, C. L. Bevins, L. G. Adams, R. M. Tsolis, J. R. Roth, A. J. Baumler, Gut inflammation provides a respiratory electron acceptor for Salmonella. *Nature* **467**, 426-429 (2010).

8. C. A. Lopez, F. Rivera-Chavez, M. X. Byndloss, A. J. Baumler, The Periplasmic Nitrate Reductase NapABC Supports Luminal Growth of Salmonella enterica Serovar Typhimurium during Colitis. *Infect Immun* **83**, 3470-3478 (2015).

9. F. Rivera-Chavez, L. F. Zhang, F. Faber, C. A. Lopez, M. X. Byndloss, E. E. Olsan, G. Xu, E. M. Velazquez, C. B. Lebrilla, S. E. Winter, A. J. Baumler, Depletion of Butyrate-Producing Clostridia from the Gut Microbiota Drives an Aerobic Luminal Expansion of Salmonella. *Cell Host Microbe* **19**, 443-454 (2016).

10. K. Kamdar, S. Khakpour, J. Chen, V. Leone, J. Brulc, T. Mangatu, D. A. Antonopoulos, E. B. Chang, S. A. Kahn, B. S. Kirschner, G. Young, R. W. DePaolo, Genetic and Metabolic Signals during Acute Enteric Bacterial Infection Alter the Microbiota and Drive Progression to Chronic Inflammatory Disease. *Cell Host Microbe* **19**, 21-31 (2016).

11. C. A. Lopez, B. M. Miller, F. Rivera-Chavez, E. M. Velazquez, M. X. Byndloss, A. Chavez-Arroyo, K. L. Lokken, R. M. Tsolis, S. E. Winter, A. J. Baumler, Virulence factors enhance Citrobacter rodentium expansion through aerobic respiration. *Science* **353**, 1249-1253 (2016).

12. M. Raetz, S. H. Hwang, C. L. Wilhelm, D. Kirkland, A. Benson, C. R. Sturge, J. Mirpuri, S. Vaishnava, B. Hou, A. L. Defranco, C. J. Gilpin, L. V. Hooper, F. Yarovinsky, Parasite-induced TH1 cells and intestinal dysbiosis cooperate in IFN-gamma-dependent elimination of Paneth cells. *Nature immunology* **14**, 136-142 (2013).

13. L. M. Haag, A. Fischer, B. Otto, R. Plickert, A. A. Kuhl, U. B. Gobel, S. Bereswill, M. M. Heimesaat, Intestinal microbiota shifts towards elevated commensal Escherichia coli loads abrogate colonization resistance against Campylobacter jejuni in mice. *PloS one* **7**, e35988 (2012).

14. S. Wang, A. El-Fahmawi, D. A. Christian, Q. Fang, E. Radaelli, L. Chen, M. C. Sullivan, A. M. Misic, J. A. Ellringer, X. Q. Zhu, S. E. Winter, C. A. Hunter, D. P. Beiting, Infection-

Induced Intestinal Dysbiosis Is Mediated by Macrophage Activation and Nitrate Production. *mBio* **10**, (2019).

15. J. P. Mooney, K. L. Lokken, M. X. Byndloss, M. D. George, E. M. Velazquez, F. Faber, B. P. Butler, G. T. Walker, M. M. Ali, R. Potts, C. Tiffany, B. M. Ahmer, S. Luckhart, R. M. Tsolis, Inflammation-associated alterations to the intestinal microbiota reduce colonization resistance against non-typhoidal Salmonella during concurrent malaria parasite infection. *Sci Rep* **5**, 14603 (2015).
16. T. T. Ao, N. A. Feasey, M. A. Gordon, K. H. Keddy, F. J. Angulo, J. A. Crump, Global burden of invasive nontyphoidal Salmonella disease, 2010(1). *Emerg Infect Dis* **21**, (2015).
17. E. N. Takem, A. Roca, A. Cunnington, The association between malaria and non-typhoid Salmonella bacteraemia in children in sub-Saharan Africa: a literature review. *Malar J* **13**, 400 (2014).
18. J. E. Denny, J. B. Powers, H. F. Castro, J. Zhang, S. Joshi-Barve, S. R. Campagna, N. W. Schmidt, Differential Sensitivity to Plasmodium yoelii Infection in C57BL/6 Mice Impacts Gut-Liver Axis Homeostasis. *Sci Rep* **9**, 3472 (2019).
19. T. Taniguchi, E. Miyauchi, S. Nakamura, M. Hirai, K. Suzue, T. Imai, T. Nomura, T. Handa, H. Okada, C. Shimokawa, R. Onishi, A. Olia, J. Hirata, H. Tomita, H. Ohno, T. Horii, H. Hisaeda, Plasmodium berghei ANKA causes intestinal malaria associated with dysbiosis. *Sci Rep* **5**, 15699 (2015).
20. Y. Litvak, K. K. Z. Mon, H. Nguyen, G. Chanthavixay, M. Liou, E. M. Velazquez, L. Kutter, M. A. Alcantara, M. X. Byndloss, C. R. Tiffany, G. T. Walker, F. Faber, Y. Zhu, D. N. Bronner, A. J. Byndloss, R. M. Tsolis, H. Zhou, A. J. Baumler, Commensal Enterobacteriaceae Protect against Salmonella Colonization through Oxygen Competition. *Cell Host Microbe* **25**, 128-139 e125 (2019).

21. Y. Litvak, A. J. Baumler, Microbiota-Nourishing Immunity: A Guide to Understanding Our Microbial Self. *Immunity* **51**, 214-224 (2019).

22. D. Gil, J. P. Bouche, ColE1-type vectors with fully repressible replication. *Gene* **105**, 17-22 (1991).

23. S. Y. Wotzka, M. Kreuzer, L. Maier, M. Arnoldini, B. D. Nguyen, A. O. Brachmann, D. L. Berthold, M. Zund, A. Hausmann, E. Bakkeren, D. Hoces, E. Gul, M. Beutler, T. Dolowschiak, M. Zimmermann, T. Fuhrer, K. Moor, U. Sauer, A. Typas, J. Piel, M. Diard, A. J. Macpherson, B. Stecher, S. Sunagawa, E. Slack, W. D. Hardt, Escherichia coli limits Salmonella Typhimurium infections after diet shifts and fat-mediated microbiota perturbation in mice. *Nat Microbiol* **4**, 2164-2174 (2019).

24. S. M. Tennant, E. L. Hartland, T. Phumoonna, D. Lyras, J. I. Rood, R. M. Robins-Browne, I. R. van Driel, Influence of gastric acid on susceptibility to infection with ingested bacterial pathogens. *Infect Immun* **76**, 639-645 (2008).

25. S. Bearson, B. Bearson, J. W. Foster, Acid stress responses in enterobacteria. *FEMS Microbiol Lett* **147**, 173-180 (1997).

26. A. C. Engevik, I. Kaji, J. R. Goldenring, The Physiology of the Gastric Parietal Cell. *Physiol Rev* **100**, 573-602 (2020).

27. M. L. Schubert, Functional anatomy and physiology of gastric secretion. *Curr Opin Gastroenterol* **31**, 479-485 (2015).

28. C. A. Rubio, M. Owston, A. Orrego, E. J. Dick, Jr., A simple method to record parietal cells in the fundic mucosa in baboons. *In Vivo* **24**, 705-707 (2010).

29. I. L. Beales, J. Calam, Interleukin 1 beta and tumour necrosis factor alpha inhibit acid secretion in cultured rabbit parietal cells by multiple pathways. *Gut* **42**, 227-234 (1998).

30. B. Neu, A. J. Puschmann, A. Mayerhofer, P. Hutzler, J. Grossmann, F. Lippl, W. Schepp, C. Prinz, TNF-alpha induces apoptosis of parietal cells. *Biochem Pharmacol* **65**, 1755-1760 (2003).

31. I. C. Hirako, P. A. Assis, N. S. Hojo-Souza, G. Reed, H. Nakaya, D. T. Golenbock, R. S. Coimbra, R. T. Gazzinelli, Daily Rhythms of TNFalpha Expression and Food Intake Regulate Synchrony of Plasmodium Stages with the Host Circadian Cycle. *Cell Host Microbe* **23**, 796-808 e796 (2018).

32. K. E. Lyke, R. Burges, Y. Cissoko, L. Sangare, M. Dao, I. Diarra, A. Kone, R. Harley, C. V. Plowe, O. K. Doumbo, M. B. Sztein, Serum levels of the proinflammatory cytokines interleukin-1 beta (IL-1beta), IL-6, IL-8, IL-10, tumor necrosis factor alpha, and IL-12(p70) in Malian children with severe Plasmodium falciparum malaria and matched uncomplicated malaria or healthy controls. *Infect Immun* **72**, 5630-5637 (2004).

33. W. L. Mandala, C. L. Msefula, E. N. Gondwe, M. T. Drayson, M. E. Molyneux, C. A. MacLennan, Cytokine Profiles in Malawian Children Presenting with Uncomplicated Malaria, Severe Malarial Anemia, and Cerebral Malaria. *Clin Vaccine Immunol* **24**, (2017).

34. L. N. Cruz, Y. Wu, H. Ulrich, A. G. Craig, C. R. Garcia, Tumor necrosis factor reduces Plasmodium falciparum growth and activates calcium signaling in human malaria parasites. *Biochim Biophys Acta* **1860**, 1489-1497 (2016).

35. I. Angulo, M. Fresno, Cytokines in the pathogenesis of and protection against malaria. *Clin Diagn Lab Immunol* **9**, 1145-1152 (2002).

36. P. Everest, M. Roberts, G. Dougan, Susceptibility to Salmonella typhimurium infection and effectiveness of vaccination in mice deficient in the tumor necrosis factor alpha p55 receptor. *Infect Immun* **66**, 3355-3364 (1998).

37. A. Vazquez-Torres, G. Fantuzzi, C. K. Edwards, 3rd, C. A. Dinarello, F. C. Fang, Defective localization of the NADPH phagocyte oxidase to Salmonella-containing phagosomes in tumor necrosis factor p55 receptor-deficient macrophages. *Proc Natl Acad Sci U S A* **98**, 2561-2565 (2001).

38. D. Gevers, S. Kugathasan, L. A. Denson, Y. Vazquez-Baeza, W. Van Treuren, B. Ren, E. Schwager, D. Knights, S. J. Song, M. Yassour, X. C. Morgan, A. D. Kostic, C. Luo, A. Gonzalez, D. McDonald, Y. Haberman, T. Walters, S. Baker, J. Rosh, M. Stephens, M. Heyman, J. Markowitz, R. Baldassano, A. Griffiths, F. Sylvester, D. Mack, S. Kim, W. Crandall, J. Hyams, C. Huttenhower, R. Knight, R. J. Xavier, The treatment-naive microbiome in new-onset Crohn's disease. *Cell Host Microbe* **15**, 382-392 (2014).

39. N. Qin, F. Yang, A. Li, E. Prifti, Y. Chen, L. Shao, J. Guo, E. Le Chatelier, J. Yao, L. Wu, J. Zhou, S. Ni, L. Liu, N. Pons, J. M. Batto, S. P. Kennedy, P. Leonard, C. Yuan, W. Ding, Y. Chen, X. Hu, B. Zheng, G. Qian, W. Xu, S. D. Ehrlich, S. Zheng, L. Li, Alterations of the human gut microbiome in liver cirrhosis. *Nature* **513**, 59-64 (2014).

40. C. L. Sears, W. S. Garrett, Microbes, microbiota, and colon cancer. *Cell Host Microbe* **15**, 317-328 (2014).

41. R. A. Gaiser, A. Halimi, H. Alkharaan, L. Lu, H. Davanian, K. Healy, L. W. Hugerth, Z. Ateeb, R. Valente, C. Fernandez Moro, M. Del Chiaro, M. Sallberg Chen, Enrichment of oral microbiota in early cystic precursors to invasive pancreatic cancer. *Gut* **68**, 2186-2194 (2019).

42. G. Lake-Bakaar, E. Quadros, S. Beidas, M. Elsakr, W. Tom, D. E. Wilson, H. P. Dincsoy, P. Cohen, E. W. Straus, Gastric secretory failure in patients with the acquired immunodeficiency syndrome (AIDS). *Ann Intern Med* **109**, 502-504 (1988).

43. Y. J. Nam, S. J. Kim, W. C. Shin, J. H. Lee, W. C. Choi, K. Y. Kim, T. H. Han, [Gastric pH and Helicobacter pylori infection in patients with liver cirrhosis]. *Korean J Hepatol* **10**, 216-222 (2004).

44. R. M. Tsolis, A. J. Baumler, Gastrointestinal host-pathogen interaction in the age of microbiome research. *Curr Opin Microbiol* **53**, 78-89 (2020).

45. Q. R. Ducarmon, R. D. Zwittink, B. V. H. Hornung, W. van Schaik, V. B. Young, E. J. Kuijper, Gut Microbiota and Colonization Resistance against Bacterial Enteric Infection. *Microbiol Mol Biol Rev* **83**, (2019).

46. M. Sassone-Corsi, M. Raffatellu, No vacancy: how beneficial microbes cooperate with immunity to provide colonization resistance to pathogens. *J Immunol* **194**, 4081-4087 (2015).

47. F. Rivera-Chávez, A. J. Bäumler, The Pyromaniac Inside You: Salmonella Metabolism in the Host Gut. *Annu Rev Microbiol* **69**, 31-48 (2015).

48. M. Bohnhoff, B. L. Drake, C. P. Miller, Effect of streptomycin on susceptibility of intestinal tract to experimental Salmonella infection. *Proceedings of the Society for Experimental Biology and Medicine. Society for Experimental Biology and Medicine (New York, N.Y* **86**, 132-137 (1954).

49. E. M. Velazquez, H. Nguyen, K. T. Heasley, C. H. Saechao, L. M. Gil, A. W. L. Rogers, B. M. Miller, M. R. Rolston, C. A. Lopez, Y. Litvak, M. J. Liou, F. Faber, D. N. Bronner, C. R. Tiffany, M. X. Byndloss, A. J. Byndloss, A. J. Baumler, Endogenous Enterobacteriaceae underlie variation in susceptibility to Salmonella infection. *Nat Microbiol* **4**, 1057-1064 (2019).

50. T. C. Martinsen, K. Bergh, H. L. Waldum, Gastric juice: a barrier against infectious diseases. *Basic Clin Pharmacol Toxicol* **96**, 94-102 (2005).

51. J. Leonard, J. K. Marshall, P. Moayyedi, Systematic review of the risk of enteric infection in patients taking acid suppression. *Am J Gastroenterol* **102**, 2047-2056; quiz 2057 (2007).

52. C. Bavishi, H. L. Dupont, Systematic review: the use of proton pump inhibitors and increased susceptibility to enteric infection. *Aliment Pharmacol Ther* **34**, 1269-1281 (2011).

53. F. Imhann, M. J. Bonder, A. Vich Vila, J. Fu, Z. Mujagic, L. Vork, E. F. Tigchelaar, S. A. Jankipersadsing, M. C. Cenit, H. J. Harmsen, G. Dijkstra, L. Franke, R. J. Xavier, D. Jonkers, C. Wijmenga, R. K. Weersma, A. Zhernakova, Proton pump inhibitors affect the gut microbiome. *Gut* **65**, 740-748 (2016).

54. R. A. Hafiz, C. Wong, S. Paynter, M. David, G. Peeters, The Risk of Community-Acquired Enteric Infection in Proton Pump Inhibitor Therapy: Systematic Review and Meta-analysis. *Ann Pharmacother* **52**, 613-622 (2018).

55. I. T. Padol, R. H. Hunt, Effect of Th1 cytokines on acid secretion in pharmacologically characterised mouse gastric glands. *Gut* **53**, 1075-1081 (2004).

56. K. R. Dobbs, J. N. Crabtree, A. E. Dent, Innate immunity to malaria-The role of monocytes. *Immunol Rev* **293**, 8-24 (2020).

57. J. J. Gilchrist, C. A. MacLennan, Invasive Nontyphoidal Salmonella Disease in Africa. *EcoSal Plus* **8**, (2019).

58. T. S. Nyirenda, W. L. Mandala, M. A. Gordon, P. Mastroeni, Immunological bases of increased susceptibility to invasive nontyphoidal Salmonella infection in children with malaria and anaemia. *Microbes Infect* **20**, 589-598 (2018).

59. J. P. Mooney, L. J. Galloway, E. M. Riley, Malaria, anemia, and invasive bacterial disease: A neutrophil problem? *J Leukoc Biol* **105**, 645-655 (2019).

60. F. Faber, P. Thiennimitr, L. Spiga, M. X. Byndloss, Y. Litvak, S. Lawhon, H. L. Andrews-Polymenis, S. E. Winter, A. J. Baumler, Respiration of Microbiota-Derived 1,2-propanediol Drives Salmonella Expansion during Colitis. *PLoS Pathog* **13**, e1006129 (2017).

61. M. Sigal, M. E. Rothenberg, C. Y. Logan, J. Y. Lee, R. W. Honaker, R. L. Cooper, B. Passarelli, M. Camorlinga, D. M. Bouley, G. Alvarez, R. Nusse, J. Torres, M. R. Amieva, Helicobacter pylori Activates and Expands Lgr5(+) Stem Cells Through Direct Colonization of the Gastric Glands. *Gastroenterology* **148**, 1392-1404 e1321 (2015).

62. J. Schindelin, I. Arganda-Carreras, E. Frise, V. Kaynig, M. Longair, T. Pietzsch, S. Preibisch, C. Rueden, S. Saalfeld, B. Schmid, J. Y. Tinevez, D. J. White, V. Hartenstein, K. Eliceiri, P. Tomancak, A. Cardona, Fiji: an open-source platform for biological-image analysis. *Nat Methods* **9**, 676-682 (2012).

63. J. Schindelin, C. T. Rueden, M. C. Hiner, K. W. Eliceiri, The ImageJ ecosystem: An open platform for biomedical image analysis. *Mol Reprod Dev* **82**, 518-529 (2015).

ACKNOWLEDGEMENTS

General: We thank A. Bäumler (University of California, Davis) for providing *S.* Typhimurium mutants. **Funding:** This work was supported by NIH/National Institute of Allergy and Infectious Disease grants R01AI098078, R01AI112949, R21AI126860. G.W. was also supported by Animal Models of Infectious Diseases Training Program NIH/NIAID grant T32AI060555. G.Y. was supported by a fellowship from the China Scholarship Council. J.T. was supported by the NIH grant T35OD010956. L.S. was supported by a grant from the Postdoctoral Scholars Program at St. George's University. **Author contributions:** Conceived and designed the experiments: G.W. and R.T.; performed the experiments and generated mutant *S.* Typhimurium strains: G.W., G.Y., J.T., J.R., B.E., F.F., and L.S.; analyzed the data: G.W. and B.B.; writing: G.W. and R.T. **Competing interests:** The authors declare that they have no competing interests. **Data and materials availability:** All data needed to evaluate the conclusions in the paper are present in the paper and/or the Supplementary Materials.

FIGURES AND TABLES, INCLUDING SUPPLEMENTARY FIGURES

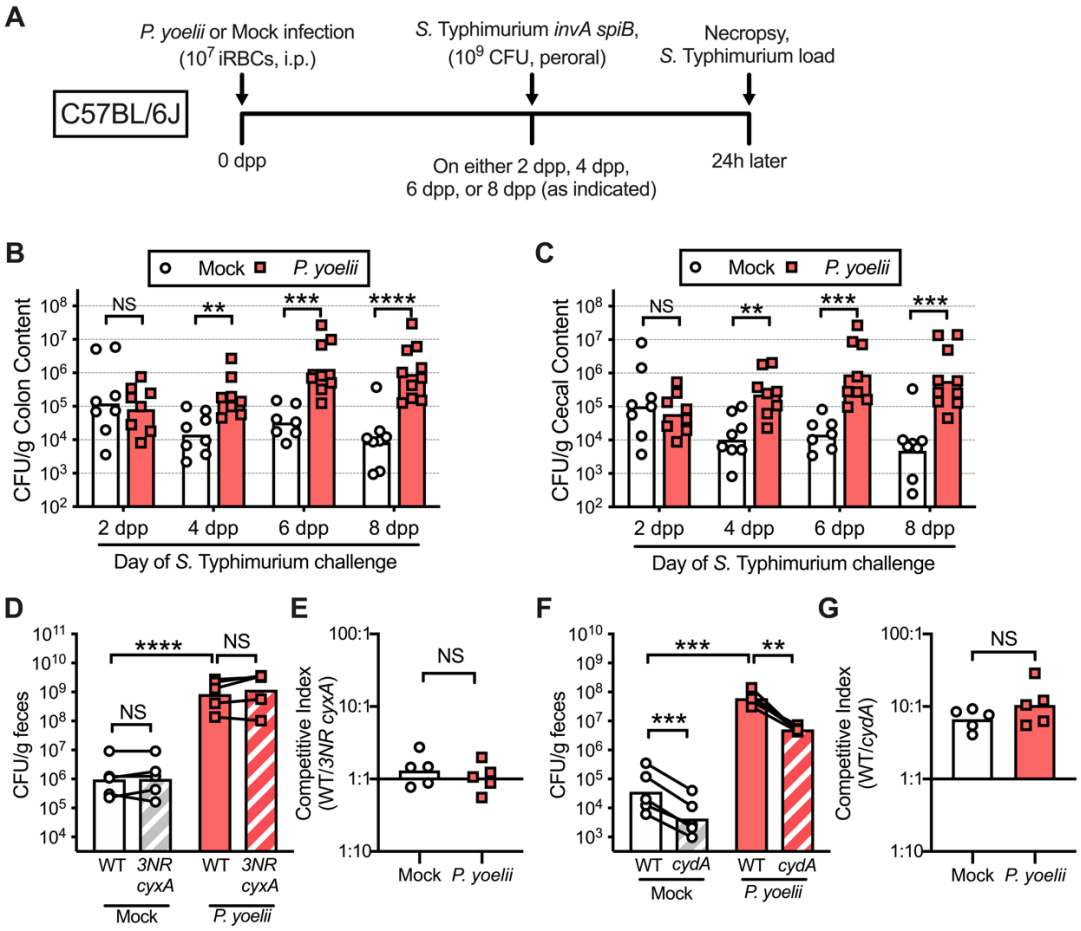

Figure 3.1. Enhanced colonization by *S.* Typhimurium in *P. yoelii*-infected mice is independent of nitrate and oxygen respiratory growth by *Salmonella*. (**A**) Schematic outlining the co-infection model used in (**B**) and **(C**). *Plasmodium yoelii*- and Mock-infected mice were challenged at 2, 4, 6, or 8 days post-infection (as indicated) with 10^9 CFU *Salmonella* Typhimurium *invA spiB* Kan^R (peroral). *Salmonella* loads in the colon (**B**) and cecum (**C**) were determined 24 hours post-*Salmonella* infection. Data pooled from two separate experiments with 3-6 mice per time point (*n* = 7-10 total per group). (**D** to **G**) Mock- and *P. yoelii*-inoculated mice (*n* = 5 per group) were gavaged at 6 dpp with approximately $5x10^8$ CFU wild-type *S.* Typhimurium (WT) and $5x10^8$ CFU of either a *S.* Typhimurium *napA narZ narG cyxA* mutant (*3NR cyxA,* **D** and **E**) or a *S.* Typhimurium

cydA mutant (**F** and **G**). (**D**) Fecal *S.* Typhimurium CFUs and (**E**) competitive indices (WT/*3NR cyxA)* at 24 hpi. (**F**) Fecal *S.* Typhimurium CFUs and (**G**) competitive indices (WT/*cydA)* at 24 hpi. Bars represent the geometric mean. Each symbol or linked pair of symbols represents data from one animal. $^{**}P \leq 0.01$, $^{***}P \leq 0.001$, $^{****}P \leq 0.0001$. NS, not significant.

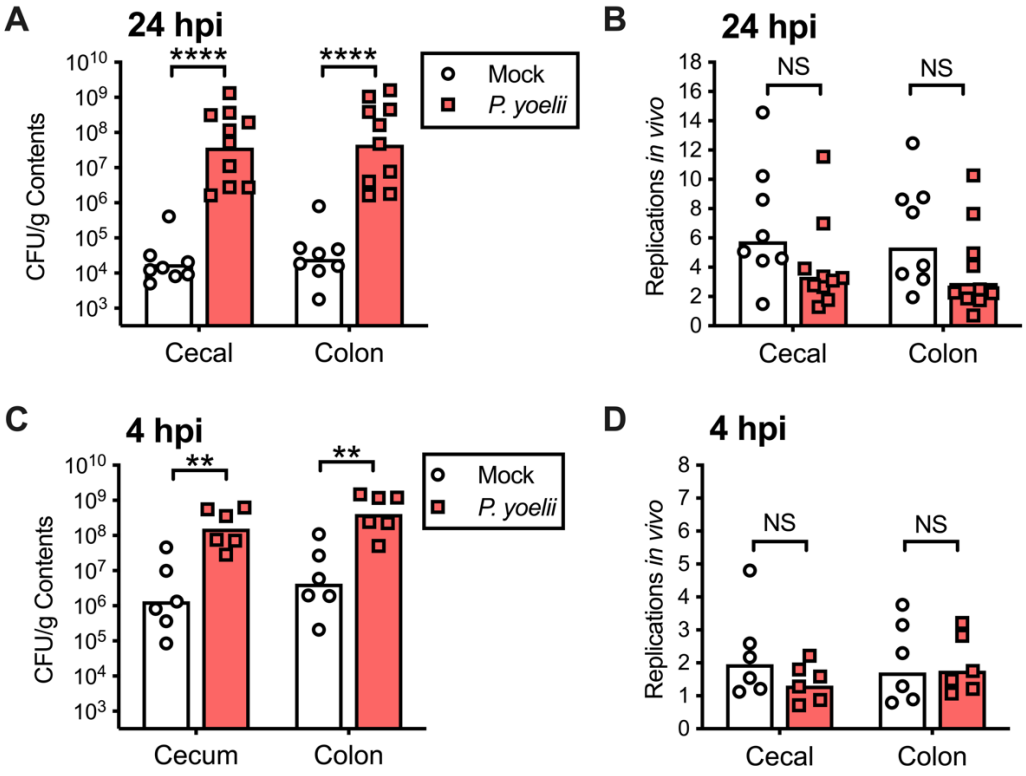

Figure 3.2. *S.* Typhimurium intestinal burden is higher in *Plasmodium* co-infected mice despite equivalent bacterial growth. Mice infected with *P. yoelii* (red squares) or mock-infected (white circles) were challenged at 6 dpp with and oral dose of 10^9 CFU *S.* Typhimurium *invA spiB* Cm^R + pAM34 for assessment of the *in vivo* replication rate of the pathogen. (**A**) *S.* Typhimurium load in the cecal and colon contents 24 hours post-inoculation. (**B**) Generation of the *S.* Typhimurium population based on pAM34 plasmid retention quantified 24 hours post-inoculation. (**C**) *S.* Typhimurium load in the cecal and colon contents 4 hours post-inoculation. (**D**) Generation of the *S.* Typhimurium population based on pAM34 plasmid retention quantified 4 hours post-

inoculation. Data in (A) and (B) are pooled from two separate experiments for a total of *n* = 8 mice in the mock group and *n* = 10 total mice in the *P. yoelii*-infected group. Data in (C) and (D) represent a single experiment with *n* = 6 mice per group. Each symbol represents data from one animal. Bars represent the geometric mean. ***P* ≤ 0.01, *****P* ≤ 0.0001. NS, not significant.

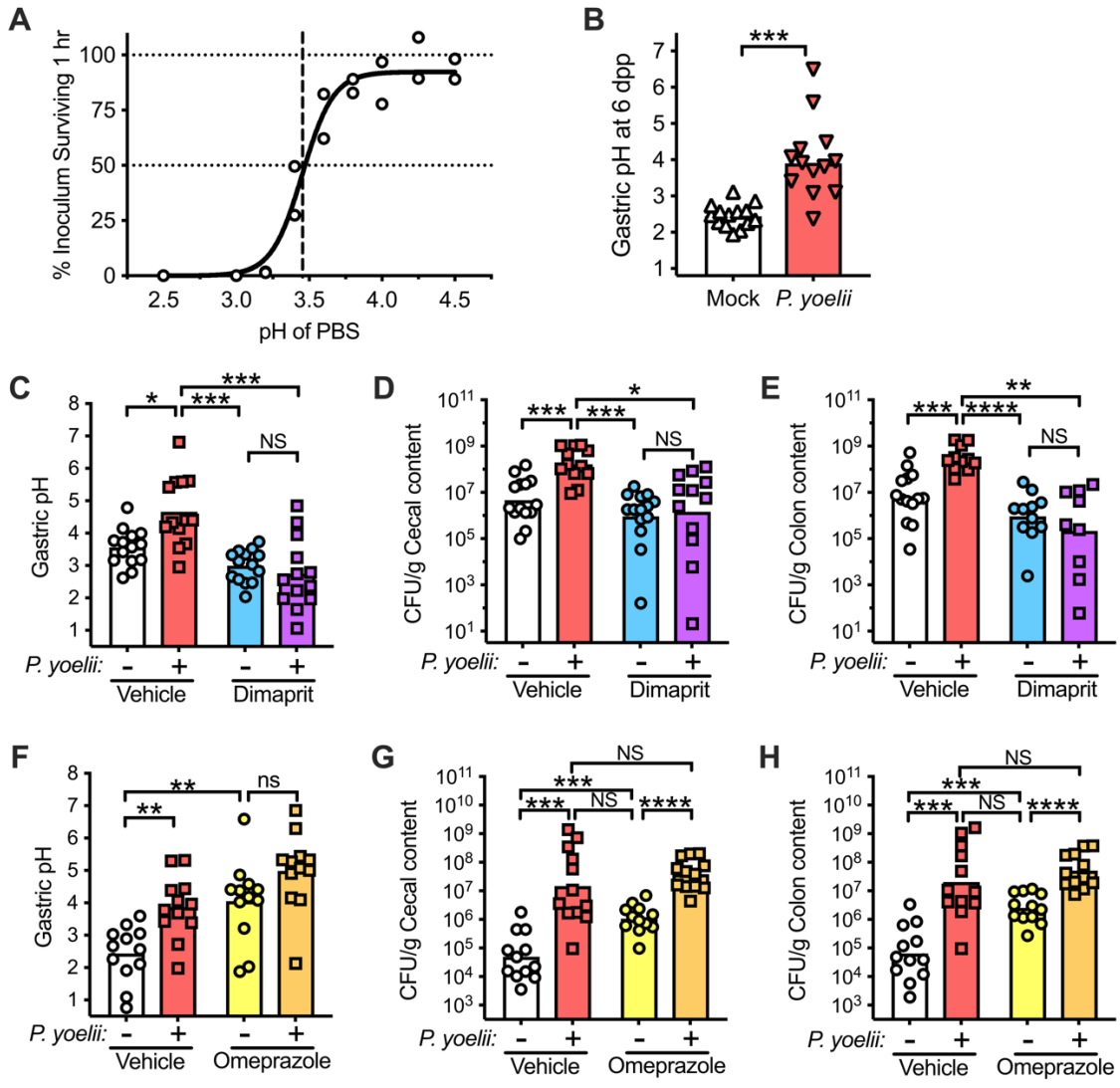

Figure 3.3. *P. yoelii*-infected mice develop hypochlorhydria that impacts colonization of *S.* Typhimurium. (**A**) *S.* Typhimurium survival in PBS at various pHs. Circles represent individual replicates while the curve is the nonlinear regression (4PL). Horizontal lines indicate 100 and 50

percent survival, while the vertical line marks the pH associated with 50 percent survival. (**B**) Gastric pH of mice 6 days post- *P. yoelii* or Mock infection. (**C** to **E**) The stomach pH (**C**), cecal (**D**) and colon (**E**) *S.* Typhimurium loads of *P. yoelii*- and Mock-infected mice treated with Dimaprit or vehicle on 6 dpp, then challenged with *S.* Typhimurium *invA spiB* Kan^R (peroral) for 4 hours. (**F** to **H**) The stomach pH (**F**), cecal (**G**) and colon (**H**) *S.* Typhimurium loads of Mock- and *P. yoelii*-infected mice treated with Omeprazole or vehicle on 3, 4, and 5 dpp and challenged on 6 dpp with *S.* Typhimurium *invA spiB* Kan^R (peroral) for 24 hours. Figures **C** to **H** represent combined data from separate experiments with n = 6-8 mice per group. Bars represent the geometric mean, and symbols represent data from individual mice. *$P \leq 0.05$, **$P \leq 0.01$, ***$P \leq 0.001$, ****$P \leq 0.0001$. NS, not significant.

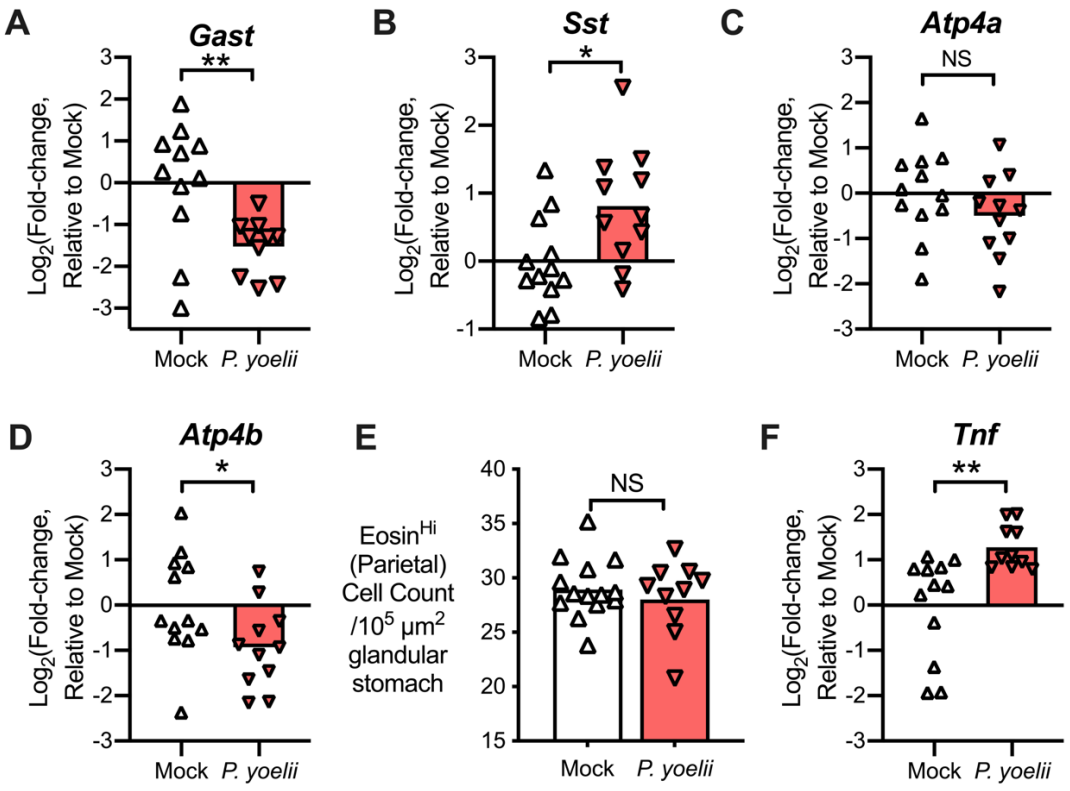

Figure 3.4. *P. yoelii* alters stomach expression of acid secretion and inflammatory signals. Relative expression of the mRNA for the gastric signaling peptides gastrin (**A**, *Gast*), somatostatin

(**B**, *Sst*), parietal cell proton pump subunits ATP4-α (**C**, *Atp4a*) and ATP4-β (**D**, *Atp4b*), and TNF-α (**F**, *Tnf*) in gastric tissues of mock and *P. yoelii*-infected mice at 6 dpp. Gene expression was quantified relative to β-actin and normalized to average mock-infected levels. (**E**) Quantification of highly eosinophilic cells in H&E-stained gastric tissue sections from mock and *P. yoelii*-infected mice at 6 dpp. Bars represent the mean. *$P \leq 0.05$, **$P \leq 0.01$. NS, not significant.

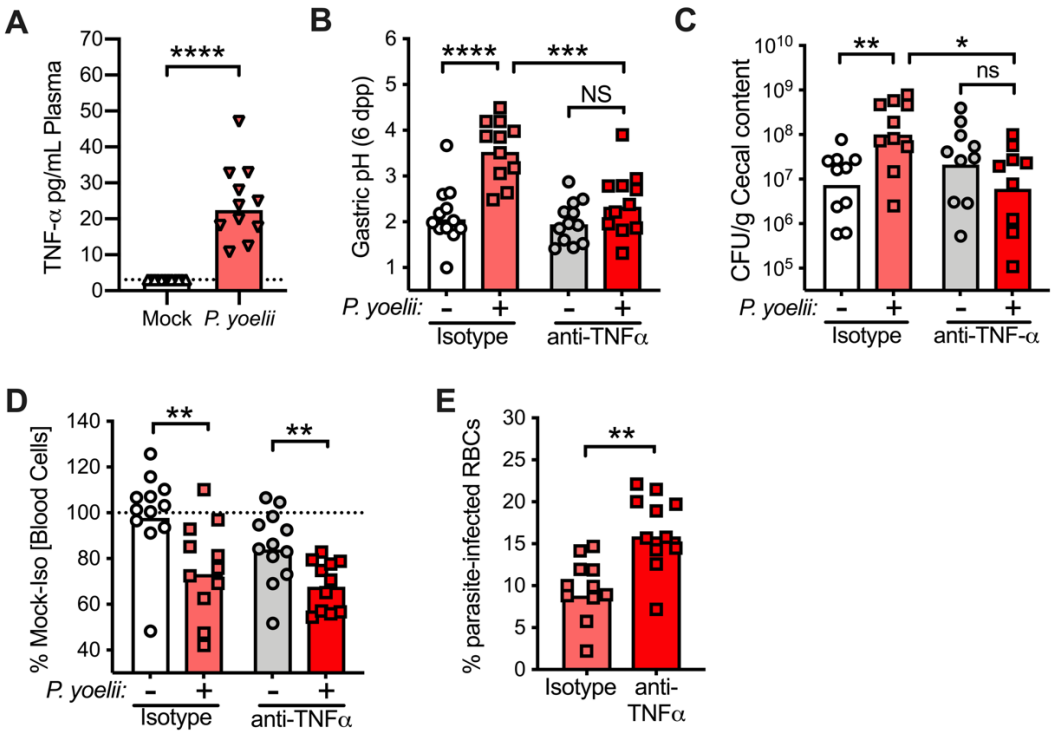

Figure 3.5. TNF-α responses to *P. yoelii* infection induce hypochlorhydria and promote *S.* Typhimurium colonization. (**A**) Circulating TNF-α levels detected in plasma at 6 dpp by ELISA in mock-infected or *P. yoelii*-infected mice. Data represent two separate experiments with n = 5-6 mice in each group. The dotted line represents the limit of detection. (**B** to **E**) On 3 and 5 dpp, mock-infected and *P. yoelii*-infected mice were treated with either anti-mouse TNF-α antibody or an isotype control antibody, and either euthanized at 6 dpp for assessment of the response on measures of parasite infection (**B, D, E**), or challenged at 6 dpp with 10^9 CFU *S.* Typhimurium *invA spiB* Kan^R (oral) to quantify the effect of the treatment on *S.* Typhimurium load at 3 hpi (**C**). Gastric

pH (**B**), cecal *S.* Typhimurium loads (**C**), relative circulating blood cell counts (**D**), and parasitemia (**E**) were determined at necropsy. Data represent three separate experiments with *n* = 3-4 mice per group. Bars represent the mean (B) or the geometric mean (A, C, D, and E). *$P \leq 0.05$, **$P \leq 0.01$, ***$P \leq 0.001$, ****$P \leq 0.0001$. NS, not significant.

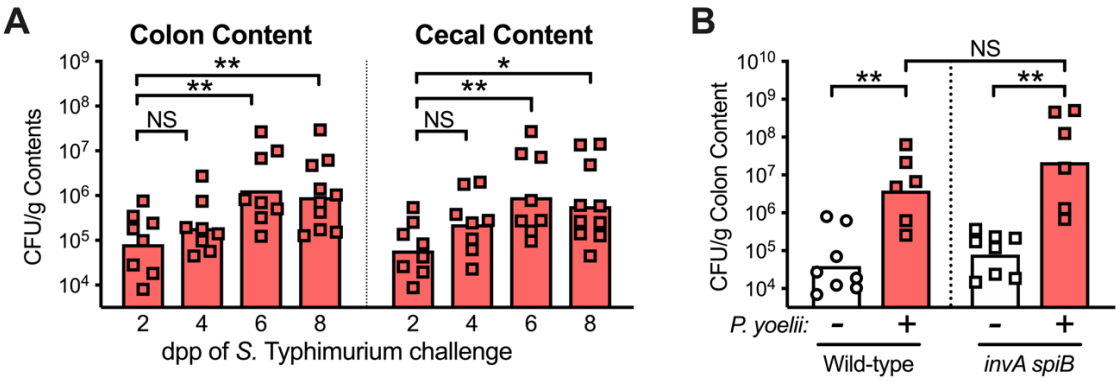

Figure 3.S1. Confirmation of *Salmonella* pathogenicity-independence at 6 dpp. (**A**) Alternative comparison of *S.* Typhimurium CFUs quantified in the *Py*-infected groups from the experiment in Fig. 3.1A-C, demonstrating that inoculating at 6 dpp or later increases *S.* Typhimurium levels over mice infected at 2 dpp, while the 4 dpp load is not significantly higher than 2 dpp. (**B**) *P. yoelii*-infected (red) or control blood-injected (white) mice were challenged orally at 6 dpp with single infections of 10^9 CFU of *S.* Typhimurium Cm^R (Wildtype) or *S.* Typhimurium *invA spiB* Cm^R (*invA spiB*) and colon content was collected 24 hours later to quantify *S.* Typhimurium loads. Bars represent the geometric mean. *$P \leq 0.05$, **$P \leq 0.01$. NS, not significant.

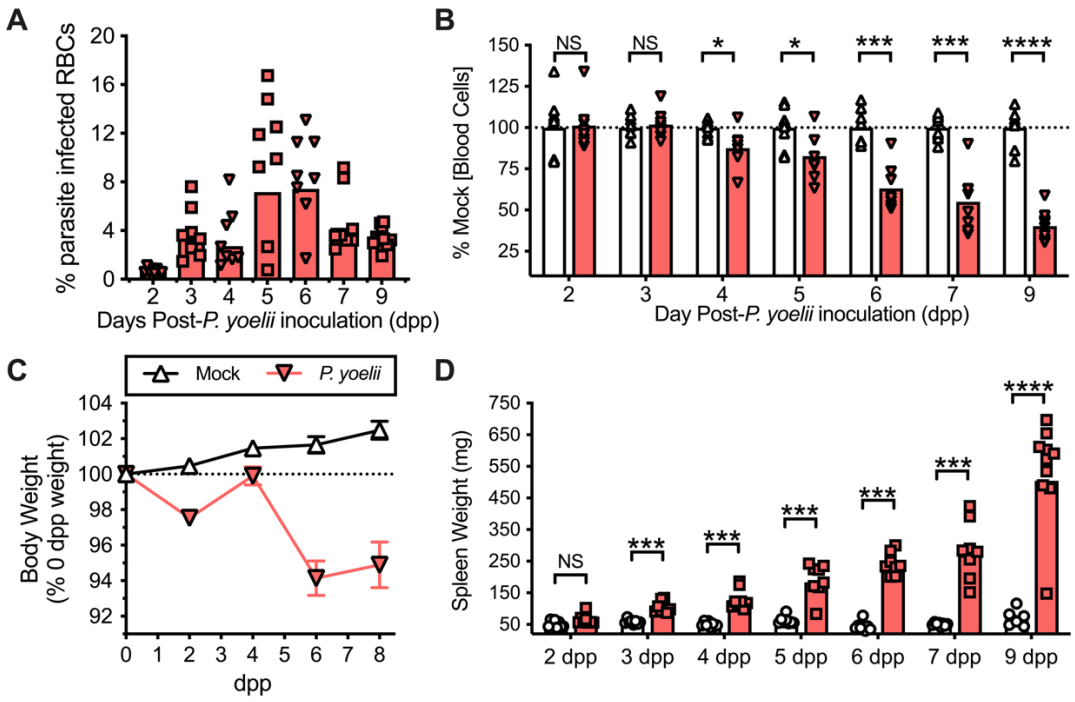

Figure 3.S2. Characterization of the early response to *P. yoelii*. (**A** to **D**) Parasitemias (**A**), circulating blood cell counts (**B**), body weight (**C**), and spleen weight (**D**) were assessed from groups of mock-infected (white) and *P. yoelii*-infected (red) mice at time points corresponding with *S.* Typhimurium infections in Fig. 3.1. Triangles represent data from mice without *S.* Typhimurium co-infection, while squares and circles denote measurements from mice depicted in Fig. 3.1, which had been challenged with an oral inoculation of *S.* Typhimurium *invA spiB* Kan^R 24 hours prior. Dots in (**C**) represent the mean ± SEM (*n* = 24-26 mice per group). Bars in (A, B, and D) represent the geometric mean, while each symbol represents data from one animal; the number of symbols thus indicate the total number of animals (*n*), which ranged from 8-10 mice per group per time point. *P ≤ 0.05, ****P ≤ 0.0001, NS, not significant.

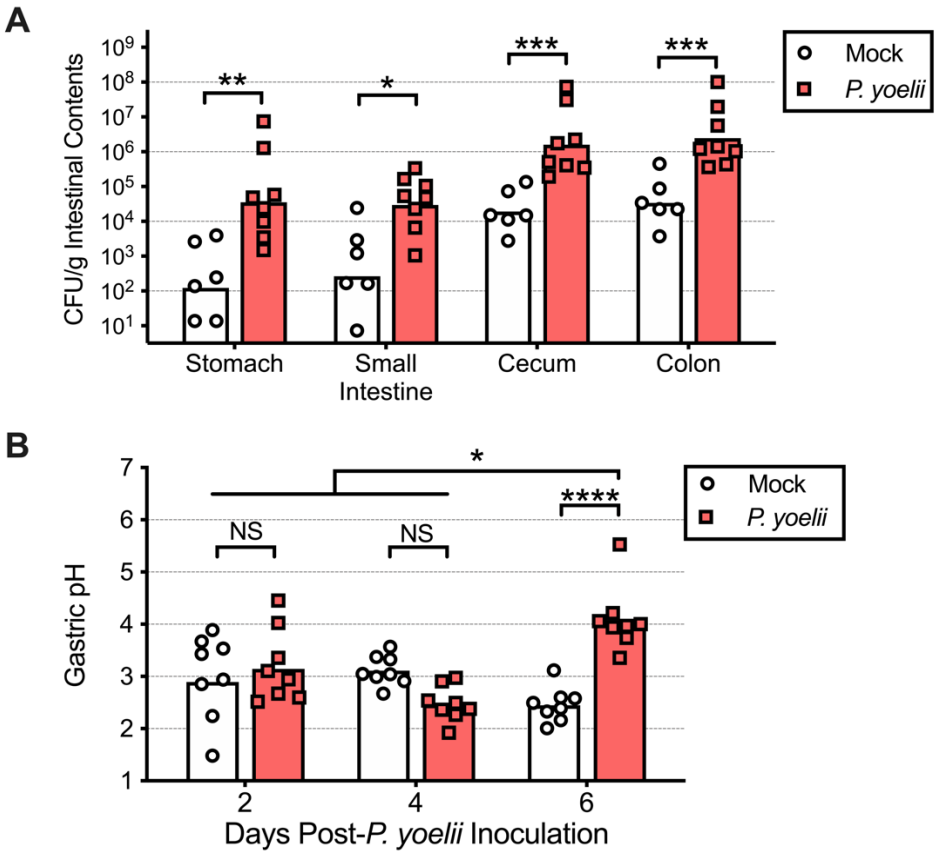

Figure 3.S3. *P. yoelii* infection boosts *Salmonella* levels throughout the gut, and characterization of the onset of hypochlorhydria during malaria. (**A**) *S.* Typhimurium *invA spiB* Kan^R loads recovered from the luminal content in different portions of the gastrointestinal tract 24 hours after oral challenge of mock-infected and *P. yoelii*-infected mice at 6 dpp. (**B**) Gastric pH assessed in sets of mice 2, 4, or 6 days following inoculation with control blood (white) or *P. yoelii* (red). Bars represent the geometric mean (**A**) or mean (**B**). *$P \leq 0.05$, **$P \leq 0.01$, ***$P \leq 0.001$, ****$P \leq 0.0001$. NS, not significant.

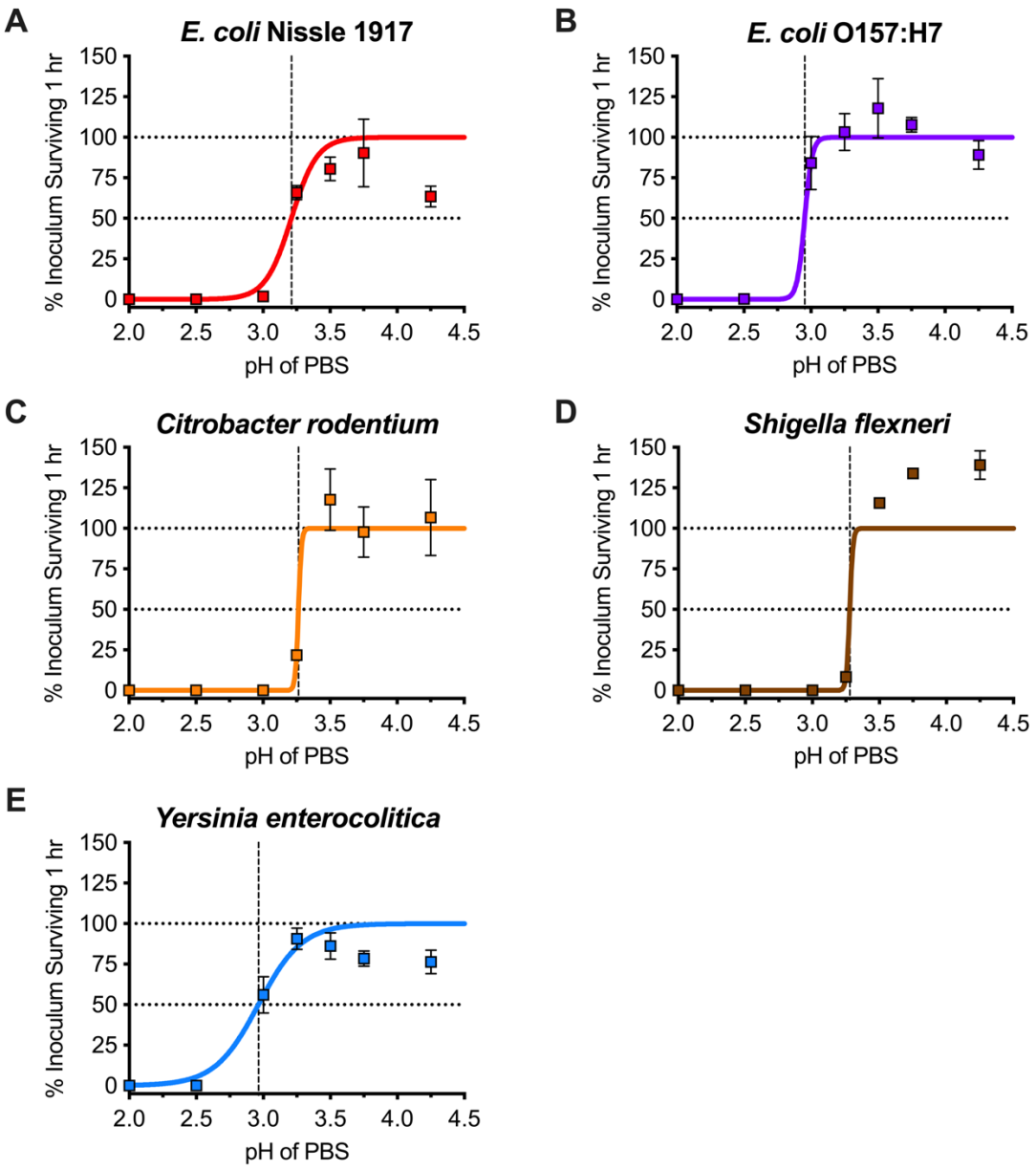

Figure 3.S4. Characterization of various *Enterobacterales* survival after pH shock. (**A-E**) Surviving fraction of various indicated *Enterobacterales* species after *in vitro* inoculation into PBS at various pHs (between 2.0 and 4.5) and incubation for 1 hour at 37°C. Tested strains include (**A**) human commensal/probiotic strain *Escherichia coli* Nissle 1917, (**B**) enterohemorrhagic *E. coli* O157:H7 EDL933, (**C**) mouse pathogen *Citrobacter rodentium* DBS100, (**D**) human enteric pathogen *Shigella Flexneri* M90T, (**E**) non-*Enterobacteriaceae* member of order *Enterobacterales,*

Yersinia enterocolitica subsp. *enterocolitica*. Symbols represent the mean ± SEM of 3 replicates at each pH value, while the sigmoidal curve is the nonlinear regression (4PL) of the data graphed in Prism 8 (GraphPad), constrained to Top = 100 and Bottom = 0. Horizontal dotted lines indicate 100 percent and 50 percent inoculum survival, while the vertical dashed line marks the pH associated with 50 percent inoculum survival *in vitro* (LD_{50}).

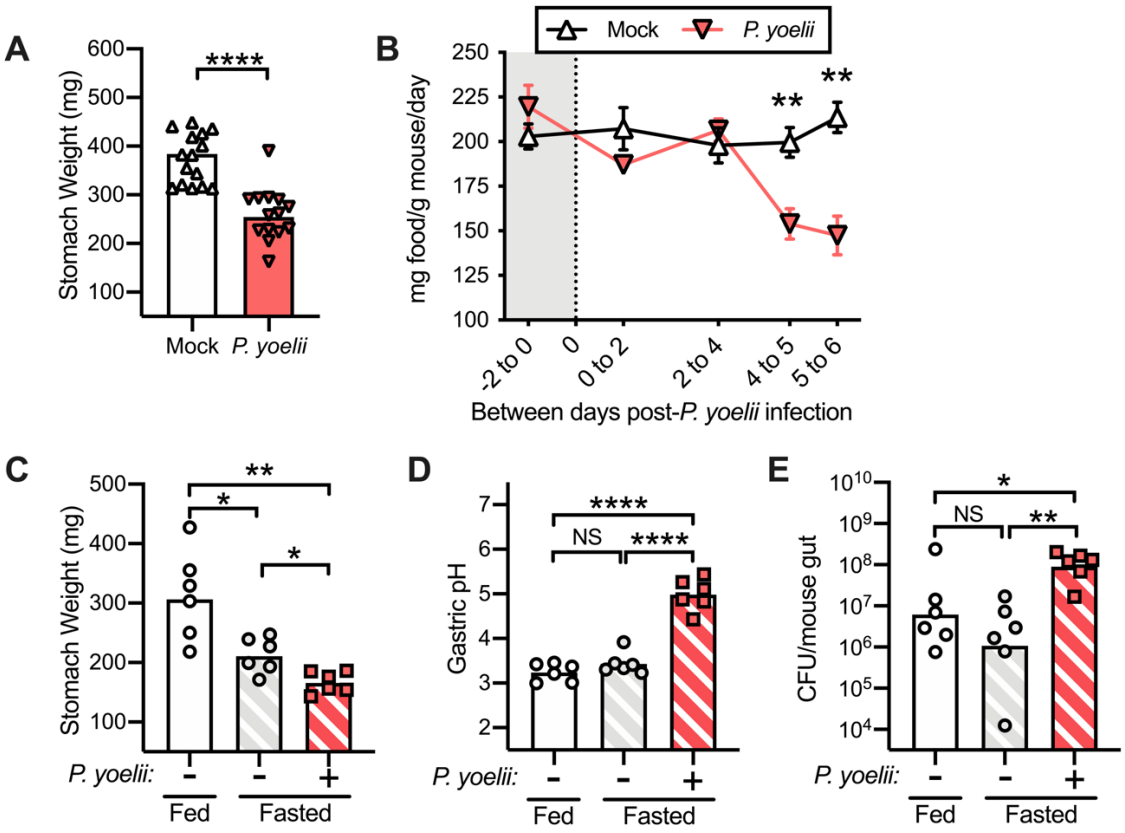

Figure 3.S5. Acute reduction in food intake via overnight fasting is not sufficient to normalize gastric pH or colonization resistance. (**A**) Stomach weights of *P. yoelii* (*P. yoelii:* +) or mock-infected mice (*P. yoelii:* -) at 6 dpp. (**B**) Food intake patterns normalized to mouse weight collected prior to and during parasite infection with food access provided *ad libitum*. Dots and error bars represent the mean ± SEM (*n* = 8 cages per treatment; each cage contained 2 mice). (**C** to **E**) Mice were mock-infected or *P. yoelii*-infected as previously described, then in the afternoon 5 days post-

parasite infection (dpp), food was removed from some of the cages overnight (16 hour fast, groups labeled as “Fasted”) or maintained (“Fed”). The next morning, mice were orally inoculated with 10^9 CFU *S.* Typhimurium *invA spiB* Kan^R and euthanized 1 hour later to assess stomach weights (**C**), gastric pH (**D**), and whole intestinal *S.* Typhimurium burden (**E**). Bars represent the geometric mean. **P* ≤ 0.05, ***P* ≤ 0.01, *****P* ≤ 0.0001. NS, not significant.

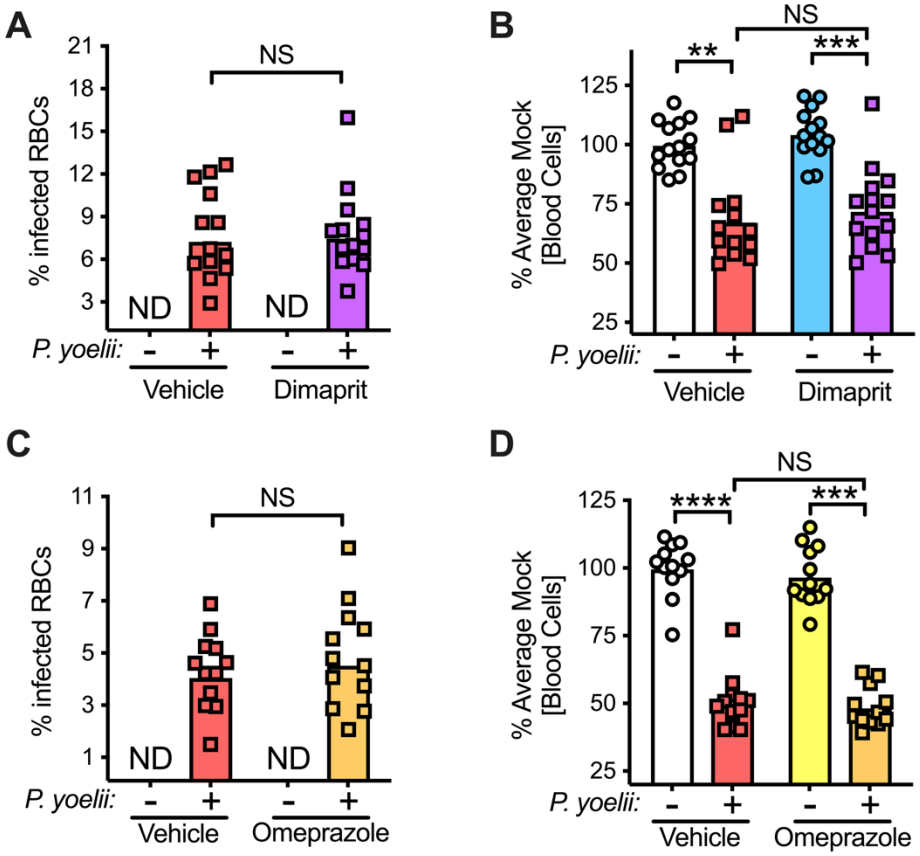

Figure 3.S6. Treatment with omeprazole or dimaprit does not significantly impact measures associated with *P. yoelii* infection severity. Related to Figure 3.3. (**A** and **B**) Parasite burden (A) and blood cell counts (B) at necropsy (7 dpp) from mice in Fig. 3.3C-E. (**C** and **D**) Parasite burden (C) and blood cell counts (D) at necropsy from mice in Fig. 3.3F-H. Bars represent the geometric mean. ***P* ≤ 0.01, ****P* ≤ 0.001, *****P* ≤ 0.0001. NS, not significant. ND, no data collected.

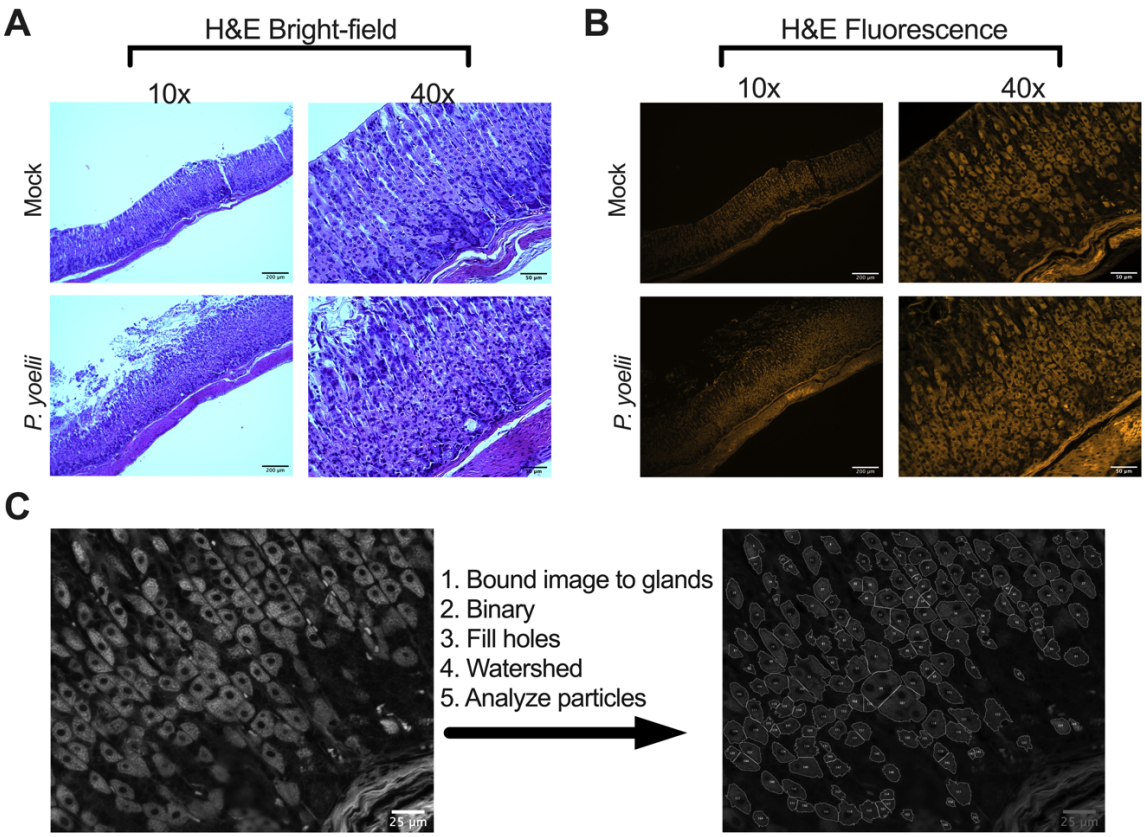

Figure 3.S7. Gastric tissue histopathology and image analysis workflow. (**A**) Representative histopathology of hematoxylin and eosin (H&E)-stained gastric mucosa tissues of mice infected with *P. yoelii* or mock-infected with control blood at 6 dpp. (**B**) Fluorescence images of tissues from (A), highlighting eosin fluorescence under the RFP fluorescence channel (Ex: 531/40 nm, Em: 593/40 nm). (**C**) Scheme for analyzing parietal cell abundance in the gastric corpus mucosa. Because parietal cells stain highly eosinophilic (and are thus autofluorescent) compared to other cells in the gastric mucosa, we utilized fluorescence imaging of H&E stained gastric cross-sections to estimate relative parietal cell counts. Further description of the analysis can be found in the Methods section.

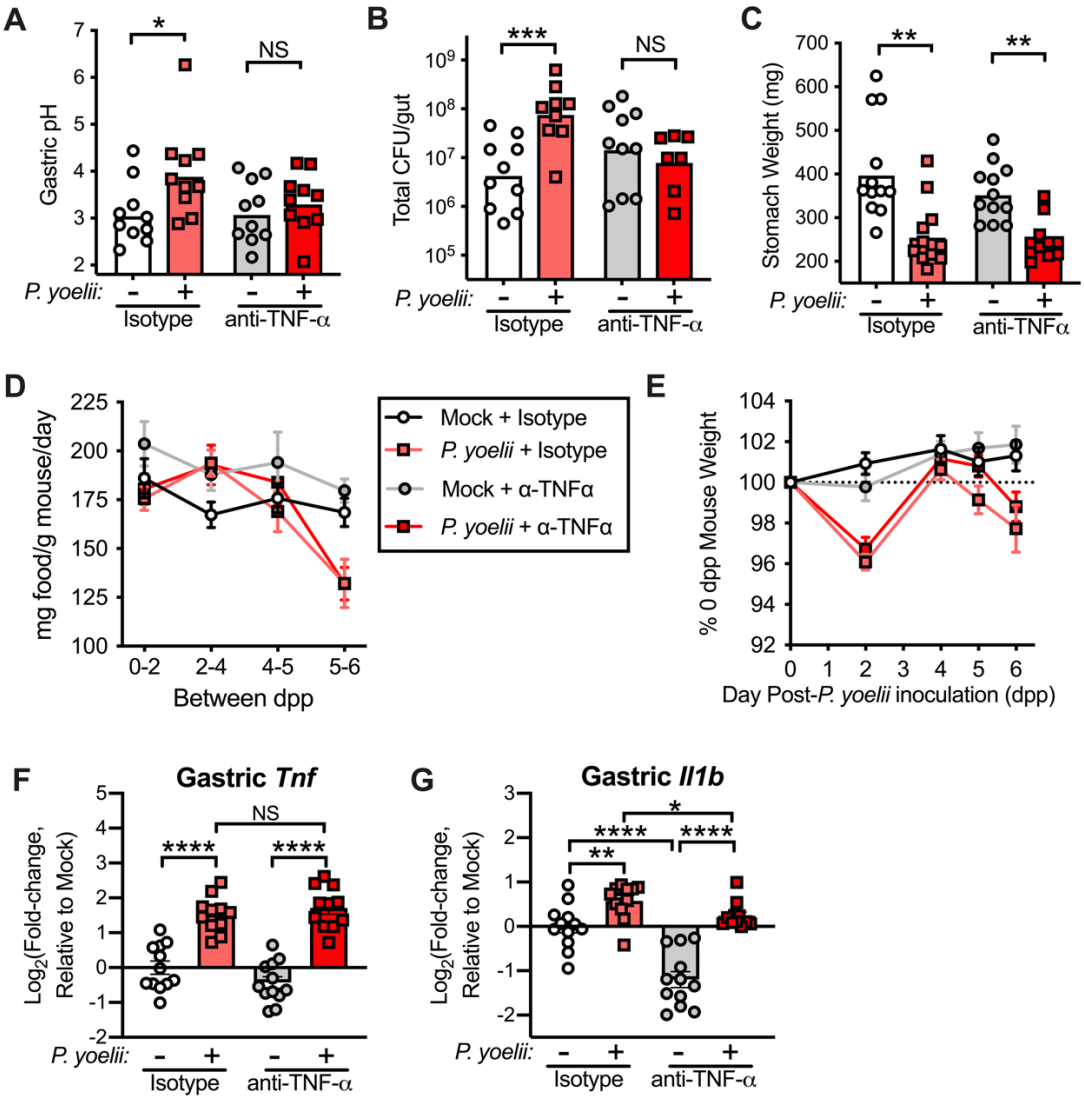

Figure 3.S8. Supplemental data from TNF-α blockade. Related to Figure 3.5. (**A** to **C**) Data from *S.* Typhimurium-infected mice represented in Fig. 3.5C. Gastric pH (**A**), total gastrointestinal CFUs (**B**) and stomach weights (**C**) at necropsy, on 6 dpp and 3 h after oral *S.* Typhimurium *invA spiB* Kan^R inoculation. (**D** and **E**) Food consumption (normalized to mouse weight) (**D**)**,** weight loss (**E**), and gastric tissue expression of *Tnf* (**F**) and *Il1b* (**G**) of mice from experiments in Figure 3.5, treated with control or *P. yoelii*-infected blood and treated with either anti-mouse TNF-α antibody or an isotype control antibody on 3 dpp and 5 dpp. Bars represent the mean (A, F, G) or geometric mean

(B and C). Dots and error bars represent the mean ± SEM. *$P \leq 0.05$, **$P \leq 0.01$, ***$P \leq 0.001$, ****$P \leq 0.0001$. NS, not significant.

***S.* Typhimurium Strains**				
Name in this study	**Desig-nation**	**Genotype**	**Source or Reference**	**Figures using this strain**
S. Typhimurium	IR715	Naladixic acid-resistant derivative of ATCC14028	PMID: 7868611	Fig. 1D-G
S. Typhimurium Kan^R	AJB715	IR715 *phoN*::KSAC	PMID: 12540539	None- Source for *phoN*::KSAC
S. Typhimurium *invA spiB*	SPN487	IR715 Δ*invA* Δ*spiB*	PMID: 23637594	None- Parent strain to FF183 and FF459
S. Typhimurium Cm^R	FF176	IR715 *phoN*::*Tn10d-Cm*	PMID: 27309805	Fig. S1B
S. Typhimurium *invA spiB* Cm^R	FF183	IR715 Δ*invA* Δ*spiB phoN*::*Tn10d-Cm*	PMID: 27309805	Fig. S1B
S. Typhimurium *invA spiB* Kan^R	FF459	Δ*invA* Δ*spiB phoN*::KSAC	This study	Fig. 1B-C; 3A; 3C-H; 5C; S1A; S2A; S2D; S3A; S5; S6; S8A-C
S. Typhimurium *napA narZ narG cyxA*	FR104	IR715 Δ*napA* Δ*narZ narG*::pCAL18 *cyxA*::pPT48	PMID: 27078066	Fig. 1D-E
S. Typhimurium *cydA*	FR103	IR715 *cydA*::pFR9	PMID: 27078066	Fig. 1F-G
S. Typhimurium *invA spiB* Cm^R + pAM34	GTW58	FF183 + plasmid pAM34	This study, PMID: 1937005 (original plasmid)	Fig. 2A-D
Other Bacterial Strains				
Name in this study	**Desig-nation**	**Genotype**	**Source or Reference**	**Figures using this strain**
Escherichia coli Nissle 1917	-	*E. coli* strain isolated in 1917 from human feces	Ardeypharm GmbH	Fig. S4A
Escherichia coli O157:H7	-	EDL933	ATCC 43895	Fig. S4B
Citrobacter rodentium	-	DBS100	ATCC 51459	Fig. S4C
Shigella flexneri	-	Serotype 5a M90T	ATCC BAA-2402	Fig. S4D
Yersinia enterocolitica	-	Subsp. *enterocolitica*	ATCC 700823	Fig. S4E

Table 3.S1. Bacterial strains used in this study.

Gene	Primer Sequence (5’ to 3’)
β-Actin	AGAGGGAAATCGTGCGTGAC
	CAATAGTGATGACCTGGCCGT
Sst	CCACCGGGAAACAGGAACTG
	TTGCTGGGTTCGAGTTGGC
Gast	CGCTCCCAGCTACAGGATG
	GGTCTGCTATGAAGTGTTGAGG
Atp4a	GATGGAGATTAACGACCACCAG
	ACGGGCAAACTTCACATACTC
Atp4b	CAGGAGAAGAAGTCATGCAGC
	GAAACCTGCGTAGTACAGGCT
Tnf	AGCCAGGAGGGAGAACAGAAAC
	CCAGTGAGTGAAAGGGACAGAACC
Il1b	CCTGAACTCAACTGTGAAATGCC
	TCTTTTGGGGTCCGTCAACTTC

Table 3.S2. Primers used for real-time PCR in this study.

Chapter 4

Mechanisms of *Plasmodium*-associated expansion of endogenous *Enterobacteriaceae* populations in the gut

Gregory T. Walker[1] and Renée M. Tsolis[1]

[1]Department of Medical Microbiology and Immunology; University of California, Davis, Davis, CA 95616, USA

ABSTRACT

Plasmodium yoelii infection of mice has been shown to cause marked increases in the levels of endogenous *Enterobacteriaceae* in the gut, though the interactions underlying this phenomenon remained unclear. Here, we assessed potential mechanisms contributing to higher *E. coli* burden during *Plasmodium* infection and chemically induced hemolysis using phenylhydrazine. It was found that neither changes in gastric acidity nor increased luminal nitrate during malaria are sufficient to explain intestinal *E. coli* expansion. However, other aspects of parasite-associated hemolysis, including changes in bile composition and activation of nutritional immunity, were identified as potential contributors to enhanced *Enterobacteriaceae* growth during *Plasmodium* infection. These results suggest that *Enterobacteriaceae* in the gut particularly benefit from the hemolytic anemia that results from *Plasmodium* infection, though other impacts of malaria may have additional effects.

INTRODUCTION

Enterobacteriaceae are a family of *Proteobacteria* of the order *Enterobacterales* that comprises a number of human and animal pathogens and pathobionts, including *Shigella*, *Klebsiella*, *Escherichia coli* and *Salmonella enterica* species (*1*). Although members of this taxon make up only a minor component of the healthy gut microbiota, increased levels of *Enterobacteriaceae* levels are a characteristic of dysbiosis- an “imbalance” in the gut microbiota primarily dominated by obligate anaerobes- that is associated with various disease states (*2-4*). For example, expansion of *Enterobacteriaceae* can be associated with intestinal inflammation that reduces epithelial hypoxia, providing respiratory niches for improved growth of the facultative anaerobic *Enterobacteriaceae* (*5-8*). In recent years, pathogenic infections and pathobiont carriage of carbapenem-resistant *Enterobacteriaceae* species have become an emergent challenge in

healthcare worldwide (*9-11*), so a better understanding of risk factors influencing colonization resistance against *Enterobacteriaceae* is of growing concern.

We had previously found that along with inducing gastric hypochlorhydria that benefits implantation of inoculated enteric bacteria in the intestine, *Plasmodium yoelii nigeriensis* (*Pyn*) infection in mice resulted in increased levels of endogenous *E. coli* after approximately one week of infection (Ch. 2, Fig. 2.5). Although the heightened implantation of the non-typhoidal *Salmonella* serovar *S.* Typhimurium was not dependent on intestinal replication (Ch. 3, Fig. 3.2), the bloom in *E. coli* that already colonize the intestines at lower levels would likely require boosted growth of the bacteria. This suggested the altered intestinal environment does at least boost *E. coli* growth and likely enhances growth of other *Enterobacteriaceae* with shared components of metabolism. Here, we investigate potential mechanisms contributing to the expansion of *Enterobacteriaceae* in the mouse intestine during *Plasmodium* infection.

RESULTS AND DISCUSSION

Hypochlorhydria is insufficient for expansion of endogenous gut *E. coli*

Despite its contribution to improved implantation of enteric bacteria in the gut, we were uncertain whether parasite-associated hypochlorhydria could also be driving improved intestinal growth by *E. coli.* Beginning around 6 days post-parasite injection (dpp), we measured gastric pH levels that consistently trended higher in *Pyn*-infected mice (Fig. 4.1A). Since this timing correlated with *E. coli* blooms in the course of infection (Fig. 4.1B), we hypothesized that the reduced gastric acidity was also somehow boosting downstream growth of *E. coli* in the large intestine. Profiling of drug interactions with gut microbial data suggests that sustained proton pump inhibitor use by humans can reduce gut microbial diversity and lead to dysbiosis (*12, 13*), including enrichment of upper G.I. flora such as *E. coli* and other *Enterobacteriaceae* (*14, 15*), despite the intestine not being the direct target of drugs like omeprazole. It is unclear whether

this is due to downstream effects of reduced acid production in the stomach, or PPIs reaching the lower intestines directly inhibiting other members of the microbiota (*16*), thus improving *E. coli*'s relative competitive advantage throughout the gut.

To test whether the sustained hypochlorhydria could explain the *Enterobacteriaceae* blooms during infection, we treated mice pre-colonized with commensal *E. coli* JB2 with omeprazole for 3-4 days and assessed bacterial loads in the feces (experiments outlined in Fig. 4.2A). We found that no generalized increase/change in the fecal levels of *E. coli* could be detected over this period (Fig. 4.2B and 4.2C), despite significantly higher gastric pH with omeprazole treatment (Fig. 4.2D). Although this data appears to run counter to studies on PPI use and humans (*14*), it may be that the short experimental period did not allow for such enrichment compared to multi-week exposure. However, the changes in gastric pH and *E. coli* abundance with malaria do occur over this short of a time scale (Fig. 4.1). Research has also indicated that sustained omeprazole administration in mice is not sufficient to enhance colonization of some pathogenic bacteria (*Clostridioides difficile)* that are linked to PPI use in humans (*17*), suggesting hypochlorhydria-associated defects in colonization resistance and dysbiosis may require multiple coexisting insults to the gut environment. This experiment thus indicates substantial reduction in gastric acidity alone cannot sufficiently explain the rapid bloom in endogenous *E. coli* in the feces observed in the mice with *Plasmodium* infection.

Impact of alternate malarial parasites on endogenous *E. coli*

To explore potential host-parasite interactions that might clarify why we see *E. coli* bloom in the gut during malaria, we decided to compare the impact of different murine *Plasmodium* strains on intestinal *E. coli*. C57BL/6J mice pre-colonized with *E. coli* JB2 were infected with either *P. yoelii nigeriensis* (*Pyn*), *P. yoelii* 17XNL (*Py*17), *P. berghei* ANKA (*Pb*A), or healthy control blood (mock). These strains of *Plasmodium* are known to result in somewhat different disease severity in depending on the mouse line they infect (*18, 19*). *E. coli* JB2 levels

increased approximately 10-fold over the pre-parasite level within the first 10 days of *Pyn* infection, while little change occurred in *E. coli* levels of mock and *Py*17 mice (Fig 4.3A-C). By contrast, *Pb*A-infected mice showed large increases in *E. coli* burden (10 to 1000-fold, Fig. 4.3D). The infection also resulted in severe weight loss and significant mortality within 6 days (Fig. 4.3E), potentially impacts of cerebral malaria associated with this infection in C57BL/6 mice (*20*). At that point, mice infected with all parasite strains exhibited similar parasite burden (Fig. 4.3F), though the *Pb*A infection did not generate quite the same degree of anemia as either *Pyn* or *Py*17 (Fig. 4.3G). At later points of infection, additional differences between *Pyn* and *Py*17 infections became more apparent: *Pyn* was associated with greater weight loss, higher circulating parasite burdens and lower red blood cell counts by 14 dpp (Fig. 4.3E-G), indicating a more severe infection. Together, these results indicate that more severe/lethal malarial infections may be associated with larger changes in gut *E. coli* levels.

Utilization of host-derived nitrate does not benefit *E. coli* during *Pyn* infection

Dysbiosis has been reported previously with PbA infection, associated with significant intestinal inflammation (*21*). We hypothesized that since severe disease was associated with the increased *E. coli* level, *E. coli* could be growing using nitrate generated in the gut lumen from epithelial or immune cell production of nitric oxygen species (*6*). Although nitrate utilization has been found to be dispensable for *S.* Typhimurium implantation in the gut (Ch. 2, Fig. 2.11), that mechanism was ultimately independent of growth, unlike commensal *E. coli* expansion.

Previous research has indicated that the human probiotic *E. coli* Nissle 1917 (EcN) in the mouse large intestine benefits from inflammation in numerous ways to compete with other *Enterobacteriaceae* (*22-25*), including through host-derived nitrate (*6*). We found that EcN in the gut also benefits from *Pyn* infection relative to colonization of healthy mice (Fig. 4.4A and 4.4B). However, the pattern of change in EcN levels during malaria was somewhat different than that observed for endogenous *E. coli*. In general, EcN dropped to lower levels in mock-infected mice

over the experiment while levels were maintained through *Pyn* infection (Fig. 4.4B), compared to the apparent blooms in JB2 and endogenous *E. coli* in other experiments (Fig. 4.1B). This could be an effect of the different model used in that experiment, giving the inoculation of EcN ($1x10^7$-$1x10^8$ CFU) and the parasite on the same day, compared to pre-colonizing with a higher dose (typically $1x10^9$ CFU) used in the commensal JB2 experiments.

To test whether the higher level of EcN in *Pyn*-infected animals was nitrate-dependent, we performed a competitive infection experiment by inoculating mice with $5x10^8$ CFU each of wildtype EcN and a triple-nitrate reductase mutant of EcN (*ΔnapA ΔnarG ΔnarZ*, ΔNR3) (*22*) one day prior to infection with *Pyn* and tracked the relative competitive advantage of wildtype EcN over EcN ΔNR3 in the intestines. While overall EcN levels trended higher in *Pyn*-infected mice as expected (Fig. 4.4C and 4.4D), the EcN ΔNR3 did not show a significant competitive defect compared to wildtype with either mock or *Pyn* infection (Fig. 4.4E), indicating that nitrate was not specifically benefitting wildtype EcN in the either set of mice.

However, due to the variability in EcN colonization we wanted to confirm that nitrate also does not contribute to the bloom in commensal *E coli* that have established a niche in the gut prior to parasite infection. As activation of host inducible nitric oxide synthase (iNOS) is a major source of increased nitrate during intestinal inflammation (*6, 22, 26*), we assessed the impact of limiting NO production in the gut during *Pyn* infection. In mice given water supplemented aminoguanidine chloride (AG) to inhibit iNOS (1 mg AG/mL water) starting on day 4 of infection, *E. coli* JB2 still showed increased abundance in parasite-infected mice (Fig. 4.5A and 4.5B), to equivalent levels as infected mice given regular drinking water (Fig. 4.5C). Taken together, these data indicate that inflammation-derived nitrate does not provide a significant growth benefit to intestinal *E. coli* during *Pyn* infection.

Altered bile acid composition during malaria may benefit *Enterobacteriaceae*

Next, we considered whether changes to the intestinal environment arising in the small intestine may be benefitting *Enterobacteriaceae* there, and downstream in the colon. Other research has reported fluctuations in the bile acid composition of the small intestinal and cecal luminal contents of mice with malarial parasite infection (*27*), potentially due to parasite interactions with hepatocytes that regulate bile acid secretion into the gallbladder and duodenum (*28*). Since *Enterobacteriaceae* are known to be more resistant to exposure and growth in high levels of bile acids than much of the microbiota (*29-31*), we hypothesized that *Pyn* infection could be altering intestinal bile composition in a manner that gives endogenous *Enterobacteriaceae* like *E. coli* a competitive edge.

We found that total bile acid concentrations in the cecal and small intestinal contents of mice trended higher with *Plasmodium* infection, somewhat correlating with increased *E. coli* JB2 burden (Fig. 4.6A-D). This surprisingly corresponded with a relatively lower levels of liver *Cyp7a1* mRNA (Fig. 4.6E), which encodes a critical enzyme (cholesterol 7 alpha-hydroxylase) that catalyzes an early rate-limiting step in the synthesis of bile acids from cholesterol in hepatocytes (*32*). In theory, lower levels of CYP7A1 should reduce bile acid levels (*33*) (though alternative bile acid synthesis pathways exist), but the reduced expression could also be a sign of higher circulating bile acid levels from uptake of the greater amount of bile acids reaching the terminal small intestine. High levels of serum bile acids are known to inhibit *Cyp7a1* transcription through the farnesoid X receptor (*32, 34*). Strikingly, reduced *Cyp7a1* expression appear to precede higher levels of bile acids being detected in the cecum (Fig. 4.6C) and the development of severe anemia (Fig. 4.6F), but the sharpest changes in *E. coli* levels throughout the gut onset only after significant blood cell loss. Better corresponding with this anemia is an increased concentration in the bile pigment bilirubin (Fig. 4.6G and 4.6H), a breakdown product of biliverdin that is generated from free plasma heme by heme oxygenase-1 (HO-1) that is activated during hemolysis (*35*). This could also be an indicator of generally increased

gallbladder secretions to the small intestines, as bile acids and bile pigments are released together in bile (*36*).

Since *Cyp7a1* expression is generally down with *Plasmodium* infection and overall bile acid levels fluctuate significantly in the small intestine, where the majority of intestinal bile acids are maintained (about 100-fold higher concentrations than in the colon), it is unclear how transient the impact is of bile acid alterations on endogenous *Enterobacteriaceae*. To test whether changes in bile acids during malaria were benefitting *E. coli*, we generated a bile-sensitive mutant lacking a functional multidrug efflux pump AcrAB-TolC (*E. coli* JB2 *acrAB*), which has been shown to contribute to *Enterobacteriaceae's* bile resistance (*31, 37*). The *acrAB* mutant displayed significant deficiencies in growth under high concentrations of the bile acid cholic acid *in vitro* (Fig. 4.7A). However, the mutant was incapable of continuously colonizing mice to detectable levels (Fig. 4.7B), indicating a certain degree of bile resistance may be a necessary component to JB2 colonization of the mouse gut. However, an avirulent *Salmonella* mutant of *acrAB* with similar intolerance to bile acids (Fig. 4.7C) was found to be more capable of somewhat sustained intestinal colonization (Fig. 4.7D). Due to the significant overlap in its core genome and metabolic machinery with *E. coli* (*38, 39*) and lack of significant virulence capacity from Type 3 secretion system inactivation (*40*), we reasoned that this *S.* Typhimurium mutant might allow us to detect whether *acrAB* is important to *Enterobacteriaceae* blooms during malaria. To make this assessment, mice pre-colonized with either *S*. Typhimurium *invA spiB* or the isogenic *acrAB* mutant were co-infected with either *Pyn* or mock-infected (experiment is outlined in Fig. 4.7E). While the *acrAB*-functional strain displayed significantly heightened fecal loads in *Pyn*-infected mice beginning on 7 dpp (Fig. 4.7F), the *acrAB* mutant strain did not exhibit a concurrent expansion (Fig. 4.7G), despite equivalent parasite loads and anemia indicating similar parasite dynamics in the groups (Fig. 4.7H and 4.7I). This finding suggests that the *Pyn*-associated blooms in intestinal *Enterobacteriaceae* are dependent on *acrAB*, and potentially bile acid levels.

To determine whether the differences in intestinal bile during *Plasmodium* infection could be responsible for differential *E. coli* growth, we attempted to perform a competitive growth experiment in intestinal contents *ex vivo*. We collected small intestinal and cecal contents from mock- and *Pyn*-infected mice at 7 dpp, diluted the contents to equivalent concentrations (250 mg/mL) with M9 minimal medium and inoculated the contents with equal amounts of wildtype *E. coli* JB2 and the JB2 *acrAB* mutant. The small intestinal content was highly permissive for wildtype *E. coli* growth (Fig. 4.8A), while the cecal content limited growth (Fig. 4.8B), potentially due to inhibition from the higher concentrations of endogenous microbes in the cecal content. The *acrAB* mutant was comparatively poor at growing in small intestinal content, displaying substantial competitive growth defects that were at least partially rescued by bile sequestration (Fig. 4.8C and 4.8D). Interestingly, infections in small intestinal content of *Pyn*-infected mice exhibited a small but non-significantly higher competitive index between the wildtype and *acrAB* mutant after 4 hour and 20 hours (approximately 2-fold) that was ablated when content was co-incubated with a bile sequestrant (1% cholestyramine resin). Since each set of samples (M9 only and M9 plus bile sequestrant) represented content from an individual mouse, we could calculate the bile-dependent competitive index for samples by normalizing each M9 alone index to its matched sample treated with the resin. This indicated that in the small intestinal lumen of *Pyn*-infected mice, bile contributes more to the growth defect of JB2 *acrAB* (Fig. 4.8E). By contrast, in the cecal content the *acrAB* defect was smaller and similarly sized across all samples, and bile sequestrant had no discernible effect (Fig. 4.8F-H). As the wildtype strain grew poorly in cecal content across all time points (Fig. 4.8B), this defect seems likely to involve initial survival of the inoculated bacteria. Unfortunately, this assay required the whole sample of intestinal content, so quantifications of the bile concentrations present in the samples to correlate the effects was not performed. However, the experiment hints that *E. coli* JB2 could gain a small competitive growth advantage in the small intestines of *Pyn*-infected mice over relatively bile-sensitive members of the microbiota. Future research should determine whether

sequestration of bile acids *in vivo* (*41*) normalizes the differences in wildtype and *acrAB* *Enterobacteriaceae* mutants during *Pyn* infection. When paired with concurrent microbiota shifts observed with malaria (*21, 42*), the relative composition of various bile acid modifications might also be impacted (as has been suggested previously (*27*)), which could further alter *Enterobacteriaceae* growth dynamics. Pathogenesis and gene expression patterns of many bacteria, including *Salmonella,* have been linked to changes in the levels of specific bile acid conjugations in the lumen (*43-45*), which microbiota shifts could also influence (*46, 47*).

Chemically induced hemolysis results in *E. coli* blooms and increased intestinal bile and

One still-unclear factor is how *Plasmodium* infection actually impacts bile acid concentrations. One possibility is that the parasites reaching the liver directly impact hepatocytes, altering their bile synthesis or secretion (*28*). Alternatively, based on the consistent timing of *E. coli* expansion following the first significant drop in blood cell concentration, we contemplated that severe hemolysis could be affecting the interconnected network of the blood, liver, and the gallbladder to alter bile secretions. To test this hypothesis, severe hemolytic anemia without parasite infection was generated in outbred CD-1 mice using phenylhydrazine (PHZ, 0.1 mL of 10 mg/mL in dPBS, i.p.) (*35, 48*). After two days of treatment PHZ-treated mice developed a marked reduction in circulating blood cell numbers to a comparable level as C57BL/6J mice treated in the same way or CD-1 mice after 8 days of *Pyn* infection (Fig. 4.9A). This corresponded with a mildly higher overall concentration of bile acids in the luminal contents of the jejunum of the small intestine (Fig. 4.9B), but not higher levels in the colon content (Fig. 4.9C). Bilirubin levels were also significantly greater in both the jejunal and colon contents (Fig. 4.9D and 4.9E), which had also been observed during *Plasmodium* infection (Fig. 4.6G and 4.6H). Together, these data suggest that hemolysis alone may increase bile acid levels in the small intestine but does not appear to significantly interfere with uptake of bile acids in the ileum.

Despite equivalent bile acid concentrations in the large intestine, the CD-1 mice displayed an increase in fecal *E. coli* loads from PHZ treatment (Fig. 4.9F and 4.9G), and higher levels of *E. coli* were also recovered from the small intestinal lumen after treatment than from vehicle-treated animals (Fig. 4.9H). It could be that bile acid differences in the small intestine are benefitting resistant *E. coli* growth, leading to downstream boosts in the large intestine even without locally higher bile acid concentrations there. In general, though, this experiment indicated that severe hemolysis during *Plasmodium* infection may be sufficient to explain the increases in intestinal *Enterobacteriaceae*, much as it has been shown to benefit extraintestinal *Salmonella* (*35, 49*).

However, *Py*17 infection also causes anemia to a similar degree (Fig. 4.3G) but did not result in a concurrent enrichment of *E. coli.* One effect common to *Pyn* and PHZ treatment but not shared by *Py*17 infection is a significant weight loss (Fig. 4.9I), primarily associated with acute reductions in food and water intake during severe malaria (Ch. 3, Fig 3.S5). Reduced food intake (fasting) has been associated with shifts in the microbiota (*50, 51*), especially enrichment for *Akkermansia muciniphila*, as we see with acute *Pyn* infection (Ch. 2, Fig. 2.4 and 2.8). To assess whether food intake played a significant role in altered *E. coli* loads, JB2-colonized C57BL/6J mice were fasted overnight and fed the next day with equivalent amounts of food as consumed by *Pyn*-infected mice between 6-8 dpp (100 mg/g mouse body weight/day). Fasted mice lost substantial amounts of weight (Fig. 4.10A) and we detected a small, insignificant difference in *E. coli* shedding in the feces (Fig. 4.10B) without changes in gastric pH (Fig. 4.10C), consistent with previous findings on short-term fasting and gastric acidity (Ch. 3, Fig. 3.S5). Thus, it is unclear whether reduced food intake could be involved in boosting *E. coli* loads, but further research could be conducted to draw definitive conclusions.

Inflammation-associated changes to intestinal iron access favors the prepared *E. coli*

Previously, we found that *Pyn* infection can induce intestinal Lipocalin-2 (Lcn2, Ch. 2, Fig. 2.11F), an antimicrobial host protein that is secreted into the gut by neutrophils in the innate inflammatory response to invading pathogens and sequesters iron-bound siderophores away from microbes to limit their growth (*52*). We have also published that *Pyn* infection results in increased expression of calprotectin (*S100a8* and *S100a9* subunits) (*42*), indicating that *Plasmodium* infection can cause intestinal responses that induce nutritional immunity against pathogens (*53, 54*). PHZ treatment was also associated with increased levels of Lcn2 in the cecal content (Fig. 4.9J), which tracks with data suggesting that the protein can be upregulated during anemia (*55*).

We hypothesized that this might enhance competition of *Enterobacteriaceae* that can evade Lcn2 to uptake ferric iron in the inflamed gut using the C-glucosylated form of enterobactin (salmochelin) such as *E. coli* Nissle 1917 (*23, 56*). During PHZ-induced hemolysis, EcN blooms were dependent on access to ferric iron, as a *tonB* mutant deficient in siderophore uptake did not display the same degree of expansion as wildtype EcN with PHZ treatment (Fig. 4.11A-C). In mice co-colonized with EcN wildtype and EcN *tonB* (outlined in Fig. 4.11D), PHZ treatment produced a marked (100-fold) competitive advantage to the wildtype strain by day 2 of treatment (Fig. 4.11E and 4.11F) However, both strains outgrew the wildtype and *tonB* strains on the first day of treatment, suggesting another mechanism early in hemolysis can still benefit EcN in a *tonB*-independent manner. Overall, these data indicate that iron homeostasis in the gut can be impacted by hemolytic anemia, which might influence levels of *Enterobacteriaceae* capable of using siderophores to take advantage better than other microbiota members. We must still determine if *Plasmodium* infection alone is associated with similar changes, but as it appears to also upregulate Lcn2 (Ch. 2, Fig. 2.11) (*57*), it seems possible to be a shared mechanism. It would also be useful to characterize which siderophores are most relevant to this phenotype.

Conclusions and Future Directions

While we had previously observed that endogenous *E. coli* levels in the gut characteristically increase with *Pyn* infection (Ch. 2, Fig. 2.5), it was unclear what aspects of the infection were contributing to the bloom. Here, we found that although increases in gastric pH and *E. coli* burden commonly co-occur during *Pyn* infection (Fig. 4.1), short-term inhibition of gastric acid secretion is not sufficient to significantly increase *E. coli* levels in the colon (Fig. 4.2). The increase was discovered to be somewhat dependent on the parasite strain, as *P. yoelii* 17XNL infection did not boost fecal *E. coli,* while *P. berghei* ANKA-infected mice show sizeable increases in *E. coli* burden prior to succumbing to the infection (Fig. 4.3), suggesting intestinal inflammation could be important to the phenotype (*21, 58*). However, we found that increased anaerobic respiration using nitrate as a respiratory electron acceptor could not explain the *E. coli* outgrowth with *Pyn* infection (Fig. 4.4 and 4.5).

Plasmodium-associated alterations to the composition of the intestinal contents- specifically increased concentrations of bile components (Fig. 4.6)- were assessed as potential benefits to endogenous *E. coli* growth relative to less bile-resistant members of the microbiota (*31*). Using avirulent *S.* Typhimurium mutants, we found that *Pyn* infection can benefit growth of *Enterobacteriaceae* other than *E. coli*, and that the enhanced growth was dependent on the multidrug efflux pump component *acrAB* (Fig. 4.7). Since *acrAB* is necessary for wildtype levels of bile acid resistance (*31, 37*), this suggested that the observed fluctuations in bile acids could be contributing or necessary for expansion of intestinal *Enterobacteriaceae* in the *Pyn*-infected mouse. However, future research could elucidate the ultimate impact of bile acids through concurrent administration of bile acids or use of a bile acid sequestrant such as cholestyramine to normalize bile acid levels in healthy and *Pyn*-infected mice. Furthermore, other *S.* Typhimurium or *E. coli* mutants in bile resistance-associated loci (such as *phoP-phoQ*) could be evaluated (*59*).

Alternately, it remains is unclear what the impact of increased bilirubin levels is on *Enterobacteriaceae*. The general bilirubin increase is likely a byproduct of substantial heme degradation by HO-1 during hemolytic anemia (*60*). Hyperbilirubinemia associated with hemolytic anemia has been linked to the formation of gallstones (*61, 62*) that could serve as sites to nucleate and potentiate the growth of some *Enterobacteriaceae* through biofilm formation (*63-65*). Bile shifts in the small intestine were also inducible by hemolysis alone (Fig. 4.9), suggesting the hypothesis that increased intestinal bile might be a side-effect of massive bilirubin excretion from the gallbladder. We could attempt to limit bilirubin production during infection or anemia with tin-protoporphyrin inhibition of HO-1 (which catalyzes heme degradation to biliverdin) in order to better assess the relative impact of the bile pigments.

Finally, we discovered that maximal *E. coli* expansion during severe hemolysis is dependent on iron siderophore uptake, as a *tonB* mutants in the gut did not expand with PHZ treatment and were outcompeted by the wildtype strain in competitive infections (Fig. 4.11). Recent research using a mouse *Plasmodium chabaudi*/*Citrobacter rodentium* co-infection model has suggested that iron acquisition via the FepA receptor can contribute to enhanced pathogenicity during co-infection (*66*). Our data may help explain this phenomenon, though further research could determine whether the *tonB* deficiency in *Enterobacteriaceae* expansion is shared during *Pyn* infection. Taken together, though, our data indicate that hemolysis-associated alterations to multiple components of the intestinal environment- bile, iron, and perhaps feeding behavior influencing nutrient availability- provide niches that allow for *Enterobacteriaceae* expansion in the gut lumen during severe *Plasmodium* infection.

MATERIALS AND METHODS

Animal experiments. All animal experiments were approved by the Institution of Animal Care and Use Committee at the University of California, Davis. 6 to 8 week-old female C57BL/6J

mice (Stock no. 000664) were purchased from The Jackson Laboratory, while 6 to 8 week-old female C57BL/6NCrl mice and CD-1 mice were purchased from Charles River Laboratory. Mice were housed under specific pathogen-free conditions and used for experiments at 8 to 11 weeks of age with at least 3 mice in each group. In some experiments, chow was withheld overnight to normalize food intake between treatment groups. Mouse weights were tracked following bacterial or parasite infection, and throughout treatment with phenylhydrazine. Mice were routinely euthanized by CO_2 asphyxiation.

***Plasmodium* infections**. Infections with red blood cells containing rodent *Plasmodium* strains *P. yoelii nigerienesis*, *P. yoelii* 17XNL, *P. berghei* ANKA, and mock infections with healthy blood for controls were performed as previously described (Ch. 2, Materials and Methods), except using an infectious dose of $1x10^7$ iRBCs. *P. yoelii* 17XNL and *P. berghei* ANKA parasites were kindly provided by Dr. Shirley Luckhart (University of Idaho). Stocks were passaged through CD-1 mice and maintained as previously indicated (Ch. 2, Materials and Methods). Parasitemia was assessed by counting parasite-infected RBCs from Geimsa (Harleco)-stained thin tail blood smears collected at various points of infection. Hemolytic anemia was tracked via tail blood diluted 1:1000 in PBS using a hemocytometer or TC20™ Automated Cell Counter (Bio-Rad Laboratories, Inc.), with counts normalized to the average counts from the mock-treated animals collected at the same time.

Gastric pH assessment. Gastric pH at necropsy was assessed as described previously (Ch. 3, Materials and Methods). Briefly, microelectrode PH-N and reference probes (Unisense) were inserted into the stomach after confirming death by CO_2 euthanasia for assessment of pH, referenced to measurements from standards at pH 2, 4, and 7. The probes were rinsed with distilled water and 70% ethanol between measurements.

Bacterial strains. All strains used in this study are listed in Table 4.1, except for strains of *E. coli* and other *Enterobacteriaceae* endogenous to Charles River mice, which were detected and quantified from intestinal content on selective MacConkey agar. Colonies that appeared dark pink, indicating lactose-fermenting capability, and non-mucoid and were counted as commensal *E. coli*. Other *E. coli* and *S.* Typhimurium strains were routinely cultured aerobically in LB broth at 37°C as previously described (Ch. 3, Materials and Methods), using LB agar or MacConkey agar plates with appropriate antibiotics (Cm: Chloramphenicol; Kan: Kanamycin; Carb: Carbenicillin) for selection to quantify bacterial loads.

Generation of mutants. Most mutant strains used in this study were generated previously (sources indicated in Table 4.1). The multidrug efflux pump *acrAB* mutants in *E. coli* JB2 and *S.* Typhimurium *invA spiB* were generated using allelic replacement by pRE118. Briefly, 500 bp regions just upstream and downstream of the *acrAB* genes in *S.* Typhimurium and *E. coli* JB2 were amplified by PCR. The *bla* cassette (Ampicillin/Carbenicillin resistance) from KSAC was also amplified. The three PCR products (Upstream flanking region-*bla*-Downstream flanking region) were then inserted into linearized pRE118 by Gibson assembly, generating plasmids pGW22 (for exchange in *S.* Typhimurium) and pGW23 (for exchange in *E. coli* JB2). pGW23 was transformed into JB2 via heat-shock at 42°C and selected for $Carb^R$. Plasmid integration was confirmed by 20% sucrose selection, and double-crossover mutant was confirmed by PCR. pGW22 was transformed by heat-shock into *E. coli* S17-1 λpir, and conjugated with *S.* Typhimurium IR715 *invA spiB phoN*::Cm^R, then selected for Cm^R $Carb^R$. Loss of *acrAB* induces sensitivity to many antibiotics, including chloramphenicol, despite presence of the resistance cassette. So, transconjugants were incubated at 37°C for 2 days to allow for slower growth of mutants. Colonies were picked and patched onto $Carb^R$ for faster growth (since beta-lactamase is secreted, *acrAB* does not impact *bla*-associated resistance) and plasmid integration was confirmed with sucrose selection and PCR.

Colonization of C57BL/6J mice with *Enterobacteriaceae*. Cultures of *E. coli* and avirulent *S.* Typhimurium were grown in LB broth overnight and prepared at various concentrations (CFU/mL) based on optical density. For most single-strain inoculation experiments, cultures were pelleted and resuspended at approximately $1x10^{10}$ CFU/mL for gavage of 0.1 mL or $5x10^{10}$ CFU/mL for oral inoculation of 0.02 mL by pipet tip, in both cases aiming for $1x10^{9}$ CFU/mouse. For competitive inoculations, strains were grown overnight separately, pelleted and resuspended in fresh LB to the appropriate dilutions and mixed 1:1 for inoculation, then diluted in PBS and plated on selective agar to assess relative input index of the inoculum (WT:mutant). In the *E. coli* Nissle 1917 inoculations for experiments in Fig. 4.4, the strains were inoculated by gavage at 0.1 mL of $1x10^{8}$ CFU/mL for single wildtype inoculations and $5x10^{8}$ CFU/mL each for competition between the wildtype and triple nitrate reductase mutant. In some experiments, C57BL/6J mice were "pre-colonized" with *E. coli* or avirulent *S.* Typhimurium before parasite infection, which for some experiments (Fig. 4.5 and Fig. 4.7) consisted of three consecutive days of peroral inoculation with $1x10^{9}$ CFU of the indicated strains to improve the odds of implantation and normalize levels at the start of the experiment. In these instances, the time prior to infection indicates time after the first oral inoculation. In all other experiments, "pre-colonization" was a single dose of the indicated strain 1 to 10 days prior to parasite infection or other experiment treatment.

Assessment of *Enterobacteriaceae* colonization. Fecal pellets were collected from mice at various time points during infections in 1 mL PBS, homogenized by vortex, serially diluted in PBS and plated on selective agar (MacConkey or LB with appropriate antibiotics) to assess *Enterobacteriaceae* loads. In some experiments, content from the cecum or small intestine was collected at necropsy and plated in an equivalent manner.

Omeprazole administration. For inhibition of gastric acid secretion, C57BL/6J mice colonized with *E. coli* JB2 were treated for 3 or 4 consecutive days with either omeprazole (0.1 mL of a 30 mg/mL suspension in 1% Tween-80/dPBS) or mock treated with an equivalent volume of the vehicle, intraperitoneally, as previously described (Ch. 3, Materials and Methods).

Aminoguanidine administration. For inhibition of inducible nitric oxide synthase (iNOS) in the intestines, mice had their drinking water supplemented with 1 mg/mL aminoguanidine chloride as has been previously described (*6*), starting at 4 dpp.

Phenylhydrazine treatment. To induce hemolytic anemia, phenylhydrazine (Sigma) was prepared as a 10 mg/mL solution in sterile Dulbecco's PBS (dPBS), and 0.1 mL was injected intraperitoneally daily, for 2 consecutive days. Control mice were treated with an equal volume of the vehicle alone (dPBS). Mice were tracked twice daily for signs of severe reaction to the chemical.

Total bile acid measurements. Concentrations of total bile acids in the intestinal content were detected in homogenized sample supernatant using the colorimetric Total Bile Acid Assay (CellBioLabs).

Bilirubin measurements. Bilirubin levels in the intestinal content were detected in homogenized sample supernatant using the colorimetric Bilirubin Assay Kit (Sigma-Aldrich).

Lipocalin-2 measurement. Lipocalin-2 concentrations in cecal content were detected in homogenized sample supernatant using the DuoSet ELISA kit (R&D Systems).

Liver *Cyp7a1* expression. Livers from mice were snap frozen in liquid nitrogen at necropsy and stored at -80°C until they could be processed. RNA was isolated from the tissues using Tri-Reagent and cDNA was prepared as 1 µg in a 50 µL reaction as previously described (Ch. 3, Materials and Methods). 4 µL of the resulting cDNA was used for each real-time reaction. Real-time PCR was performed using SYBR green (Applied Biosystems) on a ViiA 7 Real-Time PCR System (Applied Biosystems) using *Cyp7a1* targeting primers (5'-AGCAACTAAACAACCTGCCAGTACTA-3' and 5'-GTCCGGATATTCAAGGATGCA-3') (*67*) and beta-actin (*Actb*) targeting primers (5'- AGAGGGAAATCGTGCGTGAC-3' and 5'-CAATAGTGATGACCTGGCCGT-3') as a reference gene. Data was analyzed using the ddCT method in QuantStudio™ Real-Time PCR System (Applied Biosystems), with target gene expression levels normalized to *Actb* RNA levels in the same sample and represented as the fold-change difference in the average expression of mock-infected animals.

Bile acid sensitivity assay. Mutants in the multidrug efflux pump *acrAB* were assessed for bile acid sensitivity via a minimum inhibitory concentration growth assay. The primary bile acid cholic acid (Sigma) was added to LB at a range of concentrations (0.39 mM to 50 mM) reflecting levels of total bile acids typically found in the small and large intestines of mice. Strains of *acrAB* mutant and isogenic *acrAB*-wildtype strains were grown in LB, diluted to an optical density (OD_{600}) of 1.0 and diluted 500-fold, then added 1:1 into the cholic acid supplemented LB. OD_{600} of the cultures was assessed after 10 minutes and 6 hours of growth at 37°C. OD_{600} at 10 m was subtracted from OD_{600} at 6 h, and normalized to the OD_{600} of the strain grown in LB with 0 mM cholic acid (indicating maximal/normal growth).

Ex vivo intestinal content growth assay. For assessment of the relative contribution of bile levels and *acrAB* to *E. coli* JB2 growth in intestinal content of mice during malaria, whole content from the intestines of individual C57BL/6J mice both mock- and *Pyn*-infected (cecal and

whole small intestinal content) was collected at 7 dpp, homogenized in an equivalent volume of M9 minimal medium (1 mL/g content) and further diluted 1:1 with either more M9 or M9 with 2% (weight/volume) cholestyramine resin (CR), for a final concentration of 1% CR. 150 µL of content dilutions were aliquoted into individual wells and inoculated with 50 µL of M9 containing approximately $2.5x10^4$ CFU *E. coli* JB2 wildtype and $2.5x10^4$ CFU *E. coli* JB2 *acrAB*. Samples were incubated at 37°C in a flat-bottomed plate (aerobic, without shaking) and sampled at 4 h and 20 h for dilution and plating for CFUs on selective agar (MacConkey and LB+Carb).

Statistical analyses. The investigators were not blinded to animal allocation during experiments and outcome assessment. Sample sizes were estimated on the basis of effect sizes in previous studies, with a minimum of 3 animals per group used to allow for statistical analysis. All analyses were performed using Prism 9 (GraphPad Software, La Jolla, CA). The limit of detection while plating for *S.* Typhimurium loads was set to 100 CFU/g content, and the number of CFU per gram intestinal content was Log_{10}-transformed to normalize the data for statistical analysis. Significant differences in groups of normalized data were determined by unpaired *t* tests with Welch's correction, and significant differences between groups in non-normalized data were determined by Mann-Whitney tests (as indicated in figure legends). $P < 0.05$ was considered statistically significant, $P > 0.1$ was considered not significant, and P-values between 0.05-0.1 were indicated as such in the figures (though still considered not significant).

Software. Data was analyzed and plotted using Microsoft Excel for Mac (Microsoft) and Prism 9 for macOS (GraphPad Software).

REFERENCES

1. M. Adeolu, S. Alnajar, S. Naushad, S. G. R, Genome-based phylogeny and taxonomy of the 'Enterobacteriales': proposal for Enterobacterales ord. nov. divided into the families Enterobacteriaceae, Erwiniaceae fam. nov., Pectobacteriaceae fam. nov., Yersiniaceae fam. nov., Hafniaceae fam. nov., Morganellaceae fam. nov., and Budviciaceae fam. nov. *Int J Syst Evol Microbiol* **66**, 5575-5599 (2016).
2. M. Levy, A. A. Kolodziejczyk, C. A. Thaiss, E. Elinav, Dysbiosis and the immune system. *Nat Rev Immunol* **17**, 219-232 (2017).
3. C. Petersen, J. L. Round, Defining dysbiosis and its influence on host immunity and disease. *Cell Microbiol* **16**, 1024-1033 (2014).
4. C. R. Tiffany, A. J. Baumler, Dysbiosis: from fiction to function. *Am J Physiol Gastrointest Liver Physiol* **317**, G602-G608 (2019).
5. S. E. Winter *et al.*, Gut inflammation provides a respiratory electron acceptor for Salmonella. *Nature* **467**, 426-429 (2010).
6. S. E. Winter *et al.*, Host-derived nitrate boosts growth of E. coli in the inflamed gut. *Science* **339**, 708-711 (2013).
7. F. Rivera-Chavez, C. A. Lopez, A. J. Baumler, Oxygen as a driver of gut dysbiosis. *Free Radic Biol Med* **105**, 93-101 (2017).
8. B. M. Miller *et al.*, Anaerobic Respiration of NOX1-Derived Hydrogen Peroxide Licenses Bacterial Growth at the Colonic Surface. *Cell Host Microbe* **28**, 789-797 e785 (2020).
9. N. Gupta, B. M. Limbago, J. B. Patel, A. J. Kallen, Carbapenem-resistant Enterobacteriaceae: epidemiology and prevention. *Clin Infect Dis* **53**, 60-67 (2011).
10. H. Korach-Rechtman *et al.*, Intestinal Dysbiosis in Carriers of Carbapenem-Resistant Enterobacteriaceae. *mSphere* **5**, (2020).

11. E. E. Olsan *et al.*, Colonization resistance: The deconvolution of a complex trait. *J Biol Chem* **292**, 8577-8581 (2017).
12. A. Zhernakova *et al.*, Population-based metagenomics analysis reveals markers for gut microbiome composition and diversity. *Science* **352**, 565-569 (2016).
13. G. Bruno *et al.*, Proton pump inhibitors and dysbiosis: Current knowledge and aspects to be clarified. *World J Gastroenterol* **25**, 2706-2719 (2019).
14. M. Hojo *et al.*, Gut Microbiota Composition Before and After Use of Proton Pump Inhibitors. *Dig Dis Sci* **63**, 2940-2949 (2018).
15. F. Imhann *et al.*, Proton pump inhibitors affect the gut microbiome. *Gut* **65**, 740-748 (2016).
16. D. Jonkers, E. Stobberingh, R. Stockbrugger, Omeprazole inhibits growth of gram-positive and gram-negative bacteria including Helicobacter pylori in vitro. *J Antimicrob Chemother* **37**, 145-150 (1996).
17. S. Tomkovich *et al.*, The Proton Pump Inhibitor Omeprazole Does Not Promote Clostridioides difficile Colonization in a Murine Model. *mSphere* **4**, (2019).
18. C. Li, E. Seixas, J. Langhorne, Rodent malarias: the mouse as a model for understanding immune responses and pathology induced by the erythrocytic stages of the parasite. *Med Microbiol Immunol* **189**, 115-126 (2001).
19. B. W. Huang, E. Pearman, C. C. Kim, Mouse Models of Uncomplicated and Fatal Malaria. *Bio Protoc* **5**, (2015).
20. A. G. Craig *et al.*, The role of animal models for research on severe malaria. *PLoS Pathog* **8**, e1002401 (2012).
21. T. Taniguchi *et al.*, Plasmodium berghei ANKA causes intestinal malaria associated with dysbiosis. *Sci Rep* **5**, 15699 (2015).
22. A. M. Spees *et al.*, Streptomycin-induced inflammation enhances Escherichia coli gut colonization through nitrate respiration. *mBio* **4**, (2013).

23. E. Deriu *et al.*, Probiotic bacteria reduce salmonella typhimurium intestinal colonization by competing for iron. *Cell Host Microbe* **14**, 26-37 (2013).

24. M. Sassone-Corsi *et al.*, Microcins mediate competition among Enterobacteriaceae in the inflamed gut. *Nature* **540**, 280-283 (2016).

25. Y. Litvak *et al.*, Commensal Enterobacteriaceae Protect against Salmonella Colonization through Oxygen Competition. *Cell Host Microbe* **25**, 128-139 e125 (2019).

26. P. A. McLaughlin *et al.*, Inflammatory monocytes provide a niche for Salmonella expansion in the lumen of the inflamed intestine. *PLoS Pathog* **15**, e1007847 (2019).

27. J. E. Denny *et al.*, Differential Sensitivity to Plasmodium yoelii Infection in C57BL/6 Mice Impacts Gut-Liver Axis Homeostasis. *Sci Rep* **9**, 3472 (2019).

28. L. Balasubramanian *et al.*, Association of Plasmodium berghei With the Apical Domain of Hepatocytes Is Necessary for the Parasite's Liver Stage Development. *Front Cell Infect Microbiol* **9**, 451 (2019).

29. I. Brook, Aerobic and anaerobic microbiology of biliary tract disease. *J Clin Microbiol* **27**, 2373-2375 (1989).

30. M. Begley, C. G. Gahan, C. Hill, The interaction between bacteria and bile. *FEMS Microbiol Rev* **29**, 625-651 (2005).

31. S. Y. Wotzka *et al.*, Escherichia coli limits Salmonella Typhimurium infections after diet shifts and fat-mediated microbiota perturbation in mice. *Nat Microbiol* **4**, 2164-2174 (2019).

32. J. Y. Chiang, Bile acid metabolism and signaling. *Compr Physiol* **3**, 1191-1212 (2013).

33. J. M. Ferrell, S. Boehme, F. Li, J. Y. Chiang, Cholesterol 7alpha-hydroxylase-deficient mice are protected from high-fat/high-cholesterol diet-induced metabolic disorders. *J Lipid Res* **57**, 1144-1154 (2016).

34. G. Xu *et al.*, FXR-mediated down-regulation of CYP7A1 dominates LXRalpha in long-term cholesterol-fed NZW rabbits. *J Lipid Res* **44**, 1956-1962 (2003).

35. A. J. Cunnington, J. B. de Souza, M. Walther, E. M. Riley, Malaria impairs resistance to Salmonella through heme- and heme oxygenase-dependent dysfunctional granulocyte mobilization. *Nat Med* **18**, 120-127 (2011).

36. J. L. Boyer, Bile formation and secretion. *Compr Physiol* **3**, 1035-1078 (2013).

37. F. J. Lacroix *et al.*, Salmonella typhimurium acrB-like gene: identification and role in resistance to biliary salts and detergents and in murine infection. *FEMS Microbiol Lett* **135**, 161-167 (1996).

38. M. AbuOun *et al.*, Genome scale reconstruction of a Salmonella metabolic model: comparison of similarity and differences with a commensal Escherichia coli strain. *J Biol Chem* **284**, 29480-29488 (2009).

39. A. Gotz, E. Eylert, W. Eisenreich, W. Goebel, Carbon metabolism of enterobacterial human pathogens growing in epithelial colorectal adenocarcinoma (Caco-2) cells. *PLoS One* **5**, e10586 (2010).

40. P. Thiennimitr *et al.*, Intestinal inflammation allows Salmonella to use ethanolamine to compete with the microbiota. *Proc Natl Acad Sci U S A* **108**, 17480-17485 (2011).

41. R. W. Crawford *et al.*, Very long O-antigen chains enhance fitness during Salmonella-induced colitis by increasing bile resistance. *PLoS Pathog* **8**, e1002918 (2012).

42. J. P. Mooney *et al.*, Inflammation-associated alterations to the intestinal microbiota reduce colonization resistance against non-typhoidal Salmonella during concurrent malaria parasite infection. *Sci Rep* **5**, 14603 (2015).

43. N. van Best *et al.*, Bile acids drive the newborn's gut microbiota maturation. *Nat Commun* **11**, 3692 (2020).

44. A. M. Prouty, J. S. Gunn, Salmonella enterica serovar typhimurium invasion is repressed in the presence of bile. *Infect Immun* **68**, 6763-6769 (2000).

45. C. M. Theriot, A. A. Bowman, V. B. Young, Antibiotic-Induced Alterations of the Gut Microbiota Alter Secondary Bile Acid Production and Allow for Clostridium difficile Spore Germination and Outgrowth in the Large Intestine. *mSphere* **1**, (2016).

46. C. G. Buffie *et al.*, Precision microbiome reconstitution restores bile acid mediated resistance to Clostridium difficile. *Nature* **517**, 205-208 (2015).

47. R. A. Quinn *et al.*, Global chemical effects of the microbiome include new bile-acid conjugations. *Nature* **579**, 123-129 (2020).

48. M. D. Maines, J. C. Veltman, Phenylhydrazine-mediated induction of haem oxygenase activity in rat liver and kidney and development of hyperbilirubinaemia. Inhibition by zinc-protoporphyrin. *Biochem J* **217**, 409-417 (1984).

49. C. M. Roux *et al.*, Both hemolytic anemia and malaria parasite-specific factors increase susceptibility to Nontyphoidal Salmonella enterica serovar typhimurium infection in mice. *Infect Immun* **78**, 1520-1527 (2010).

50. I. Ali *et al.*, Ramadan Fasting Leads to Shifts in Human Gut Microbiota Structured by Dietary Composition. *Front Microbiol* **12**, 642999 (2021).

51. L. Li *et al.*, The effects of daily fasting hours on shaping gut microbiota in mice. *BMC Microbiol* **20**, 65 (2020).

52. T. H. Flo *et al.*, Lipocalin 2 mediates an innate immune response to bacterial infection by sequestrating iron. *Nature* **432**, 917-921 (2004).

53. V. E. Diaz-Ochoa, S. Jellbauer, S. Klaus, M. Raffatellu, Transition metal ions at the crossroads of mucosal immunity and microbial pathogenesis. *Front Cell Infect Microbiol* **4**, 2 (2014).

54. M. I. Hood, E. P. Skaar, Nutritional immunity: transition metals at the pathogen-host interface. *Nat Rev Microbiol* **10**, 525-537 (2012).

55. W. Jiang, M. Constante, M. M. Santos, Anemia upregulates lipocalin 2 in the liver and serum. *Blood Cells Mol Dis* **41**, 169-174 (2008).

56. M. Valdebenito, A. L. Crumbliss, G. Winkelmann, K. Hantke, Environmental factors influence the production of enterobactin, salmochelin, aerobactin, and yersiniabactin in Escherichia coli strain Nissle 1917. *Int J Med Microbiol* **296**, 513-520 (2006).

57. A. O. Mohammed *et al.*, Human neutrophil lipocalin: a specific marker for neutrophil activation in severe Plasmodium falciparum malaria. *Acta Trop* **87**, 279-285 (2003).

58. M. Shimada *et al.*, Upper gastrointestinal pathophysiology due to mouse malaria Plasmodium berghei ANKA infection. *Trop Med Health* **47**, 18 (2019).

59. J. C. van Velkinburgh, J. S. Gunn, PhoP-PhoQ-regulated loci are required for enhanced bile resistance in Salmonella spp. *Infect Immun* **67**, 1614-1622 (1999).

60. A. R. Hamoud, L. Weaver, D. E. Stec, T. D. Hinds, Jr., Bilirubin in the Liver-Gut Signaling Axis. *Trends Endocrinol Metab* **29**, 140-150 (2018).

61. B. W. Trotman, S. E. Bernstein, W. F. Balistreri, G. D. Wirt, R. A. Martin, Hemolysis-induced gallstones in mice: increased unconjugated bilirubin in hepatic bile predisposes to gallstone formation. *Gastroenterology* **81**, 232-236 (1981).

62. B. W. Trotman, S. E. Bernstein, K. E. Bove, G. D. Wirt, Studies on the pathogenesis of pigment gallstones in hemolytic anemia: description and characteristics of a mouse model. *J Clin Invest* **65**, 1301-1308 (1980).

63. R. W. Crawford *et al.*, Gallstones play a significant role in Salmonella spp. gallbladder colonization and carriage. *Proc Natl Acad Sci U S A* **107**, 4353-4358 (2010).

64. S. H. Kose, K. Grice, W. D. Orsi, M. Ballal, M. J. L. Coolen, Metagenomics of pigmented and cholesterol gallstones: the putative role of bacteria. *Sci Rep* **8**, 11218 (2018).

65. G. Gonzalez-Escobedo, J. S. Gunn, Identification of Salmonella enterica serovar Typhimurium genes regulated during biofilm formation on cholesterol gallstone surfaces. *Infect Immun* **81**, 3770-3780 (2013).

66. L. I. Dos Santos *et al.*, Disrupted Iron Metabolism and Mortality during Co-infection with Malaria and an Intestinal Gram-Negative Extracellular Pathogen. *Cell Rep* **34**, 108613 (2021).

67. M. L. Chen *et al.*, Resveratrol Attenuates Trimethylamine-N-Oxide (TMAO)-Induced Atherosclerosis by Regulating TMAO Synthesis and Bile Acid Metabolism via Remodeling of the Gut Microbiota. *mBio* **7**, e02210-02215 (2016).

FIGURES AND TABLES

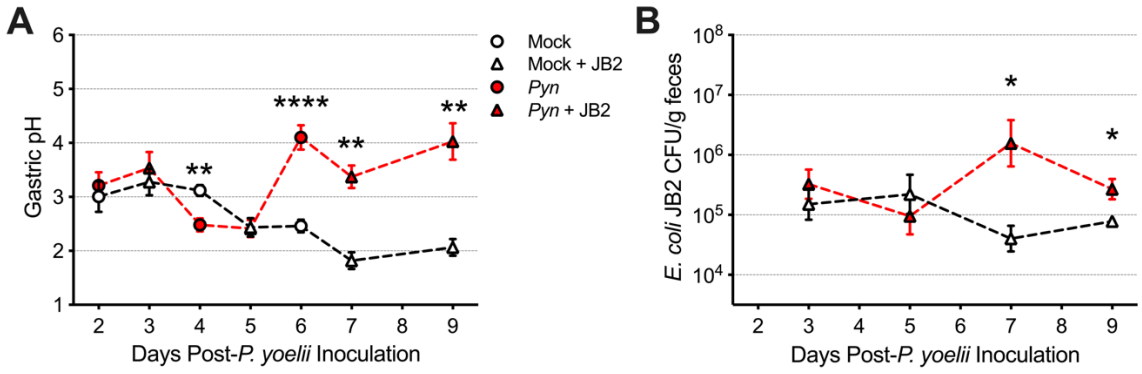

Figure 4.1. Gastric pH variability and intestinal *E. coli* burden with malaria. Groups of C57BL/6J mice, either pre-colonized for 4 days with commensal *E. coli* JB2 (triangles, n = 4 per group) or lacking commensal *E. coli* not (circles, n = 8 per group) were given either $1x10^7$ *Pyn*-iRBCs or an equivalent volume of diluted healthy mouse blood (Mock) by the intraperitoneal (i.p.) route. At the indicated time points (2-9 days after parasite inoculation), groups of mice were euthanized to assess gastric pH (A), and fecal *E. coli* burden (B) when applicable. Symbols and error bars represent the mean±SEM of the Log_{10}-normalized data (pH is already Log-normal); dashed lines connect similar groups (mock or *Pyn*) to better represent trends over time, but data at each time point do not come from the same set of mice. Statistical comparisons between data from groups euthanized at matched time points were made by

Welch's *t*-test, with significance indicated over time-matched groups. *P ≤ 0.05, **P ≤ 0.01, ****P ≤ 0.0001. No asterisk denotes differences between groups at that time point were not significant.

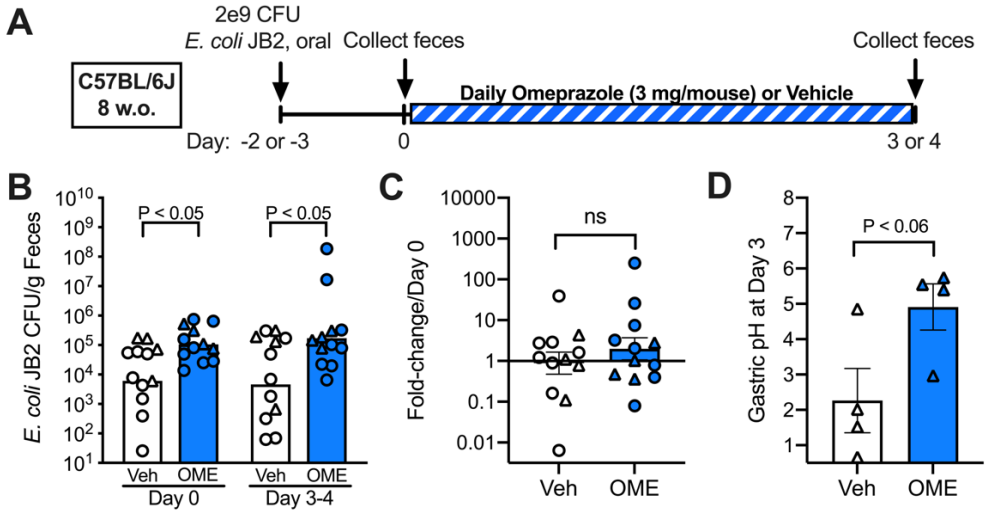

Figure 4.2. Omeprazole administration alone does not increase commensal *E. coli* loads. (A) Schematic outlining experiments to assess the impact of treatment with the proton pump inhibitor omeprazole on fecal *E. coli* levels. Groups of C57BL/6J mice were pre-colonized for 2 to 3 days with commensal *E. coli* JB2, then given daily treatments of either omeprazole (OME, 30 mg/mL suspended in 1% Tween-80/dPBS, 0.1 mL i.p.) or the vehicle (Veh). Fecal levels of *E. coli* were assessed by plating on selective MacConkey agar prior to treatment (Day 0) and after 3 days (triangles) or 4 days (circles) of omeprazole use. (B) *E. coli* JB2 CFU loads quantified in the feces of mice. (C) The fold-change (post-treatment/pre-treatment) in CFU *E. coli* JB2/g feces. (D) The gastric pH at necropsy in mice measured at day 3 of the treatment period. Data are combined from two separate experiments (n = 4 mice/treatment for Day 3 data in triangle symbols; n = 8 mice/treatment for Day 4 data in circle symbols) with similar results. P-values indicate statistical significance for comparisons between data from Veh and OME groups made by Welch's *t*-test. Ns, not significant (P > 0.1).

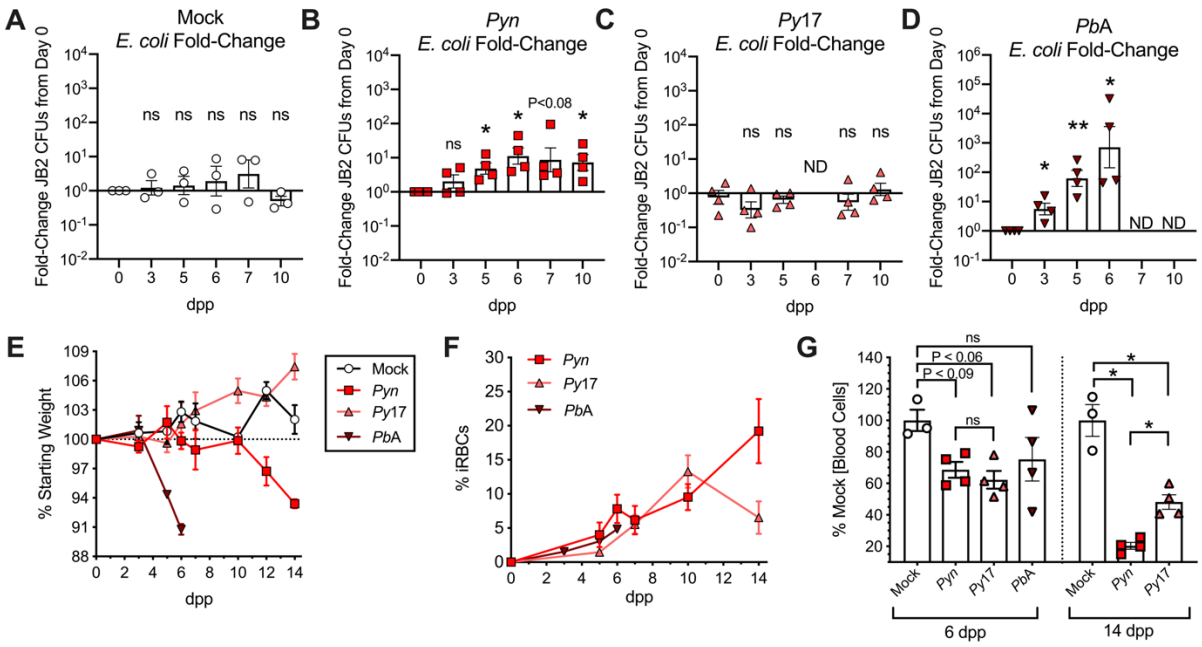

Figure 4.3. *Plasmodium* parasites vary in capacity to increase intestinal *E. coli* levels. Groups of C57BL/6J mice, pre-colonized for 10 days with commensal *E. coli* JB2 (n = 3-4 per group) were infected with 1x10^7 iRBCs of either *P. yoelii nigerienesis* (*Pyn*), *P. yoelii* 17XNL (*Py*17), *P. berghei* ANKA (*Pb*A) or an equivalent volume of diluted healthy mouse blood (Mock) by the intraperitoneal (i.p.) route. Fecal shedding of *E. coli* JB2 was tracked and compared to pre-infection (0 dpp) levels for (A) Mock, (B) *Pyn*-infected, (C) *Py*17-infected, and (D) *Pb*A-infected animals. (E) Weight changes through the parasite infections. (F) Circulating parasite burden through the infections. (G) Anemia (measured as total blood cell concentrations, normalized to the average Mock concentration) at 6 dpp and 14 dpp. Symbols in bar graphs indicate data from individual mice, while symbols in (E) and (F) indicate the mean±SEM. Statistically significant fold-change from 0 dpp was assessed by one-way *t* test. Anemia at each time point were compared by Welch's *t*-test. *P ≤ 0.05, **P ≤ 0.01. ns, not significant (P > 0.1).

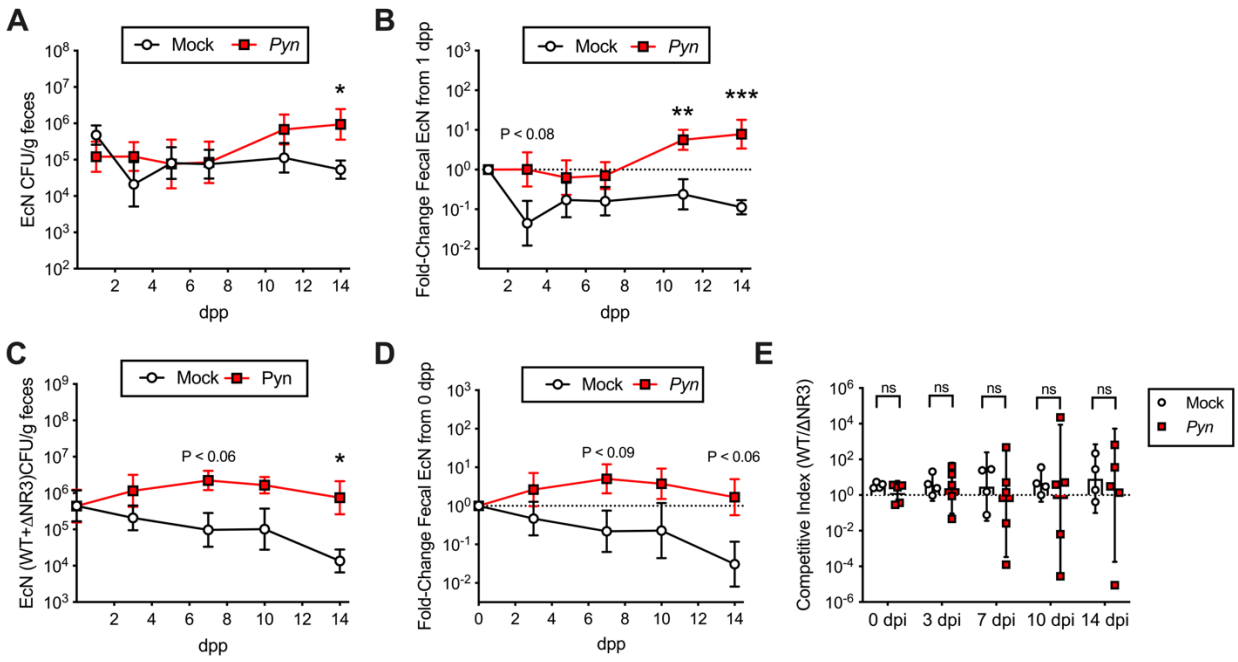

Figure 4.4. *E. coli* Nissle 1917 does not benefit from nitrate reductase utilization during *Pyn* infection. (A and B) C57BL/6J mice were inoculated with 1x10^7 CFU *E. coli* Nissle 1917 (EcN) by oral gavage on the same day they were infected with either 1x10^7 iRBCs *Pyn* or an equivalent volume of diluted healthy mouse blood (Mock) by the intraperitoneal (i.p.) route (n = 9 mice per group). (A) Fecal shedding of EcN tracked at indicated time points of infection. (B) Changing fecal EcN levels relative to levels 1 day post-inoculation tracked at indicated time points of infection. (C to E) C57BL/6J mice were co-inoculated with 5x10^7 CFU wildtype EcN and 5x10^7 CFU of a triple nitrate reductase mutant EcN Δ*narG* Δ*napA* Δ*narZ* (ΔNR3) by oral gavage. One day later, the mice were infected with either 1x10^7 iRBCs *Pyn* (n = 5 mice) or Mock-infected with diluted control blood (n = 4 mice), i.p. (C) Fecal shedding of combined wildtype EcN and EcN ΔNR3 tracked at indicated time points of infection. (D) Changing fecal EcN levels relative to levels at 0 dpp tracked at indicated time points of infection. (E) The competitive index of EcN WT:EcN ΔNR3 in the mice at indicated time points of infection. (A-D) Symbols represent the mean±SEM of Log_{10}-normalized data. (E) Symbols represent data from individual mice, bars and error bars represent the mean±SEM of Log_{10}-normalized competitive

indices. Group data at each time point were compared by Welch's *t*-test. *P ≤ 0.05, **P ≤ 0.01, ***P ≤ 0.001. ns, not significant (P > 0.1).

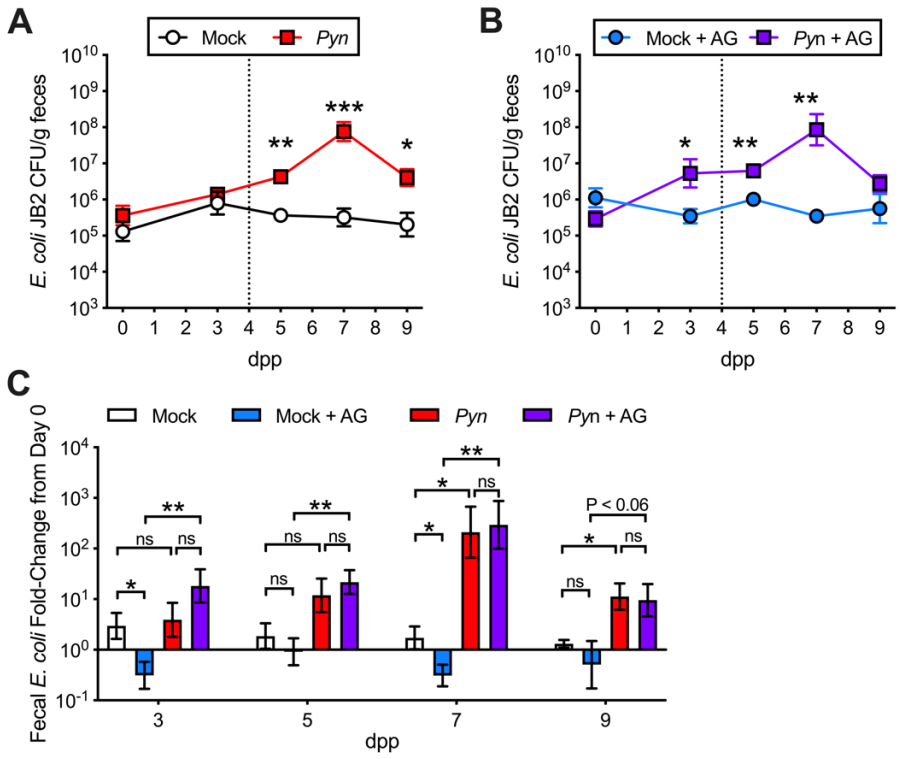

Figure 4.5. Inhibition of iNOS during *Pyn* infection does not prevent *E. coli* JB2 bloom. Mice (C57BL/6J) were pre-colonized with *E. coli* JB2 starting 10 days prior to infection with $1x10^7$ iRBCs *Pyn* or Mock-infected with diluted control blood, i.p. At 4 dpp (vertical line indicated in A and B), groups of mice were either maintained on their normal drinking water or had their water supplemented with 1 mg/mL of the iNOS inhibitor aminoguanidine chloride (AG). Fecal shedding of JB2 was tracked at indicated time points for mice (A) on normal drinking water, and (B) on AG-supplemented water. Symbols represent the mean±SEM of Log_{10}-normalized data. (C) The changing levels of JB2 relative to pre-infection (0 dpp) levels. Bars represent the mean±SEM of Log_{10}-normalized competitive indices. N = 3 mice in the Mock/normal water

group and n = 5 mice for all other groups. Group data at time points were compared by Welch's *t*-test. *P ≤ 0.05, **P ≤ 0.01, ***P ≤ 0.001. ns, not significant (P > 0.1).

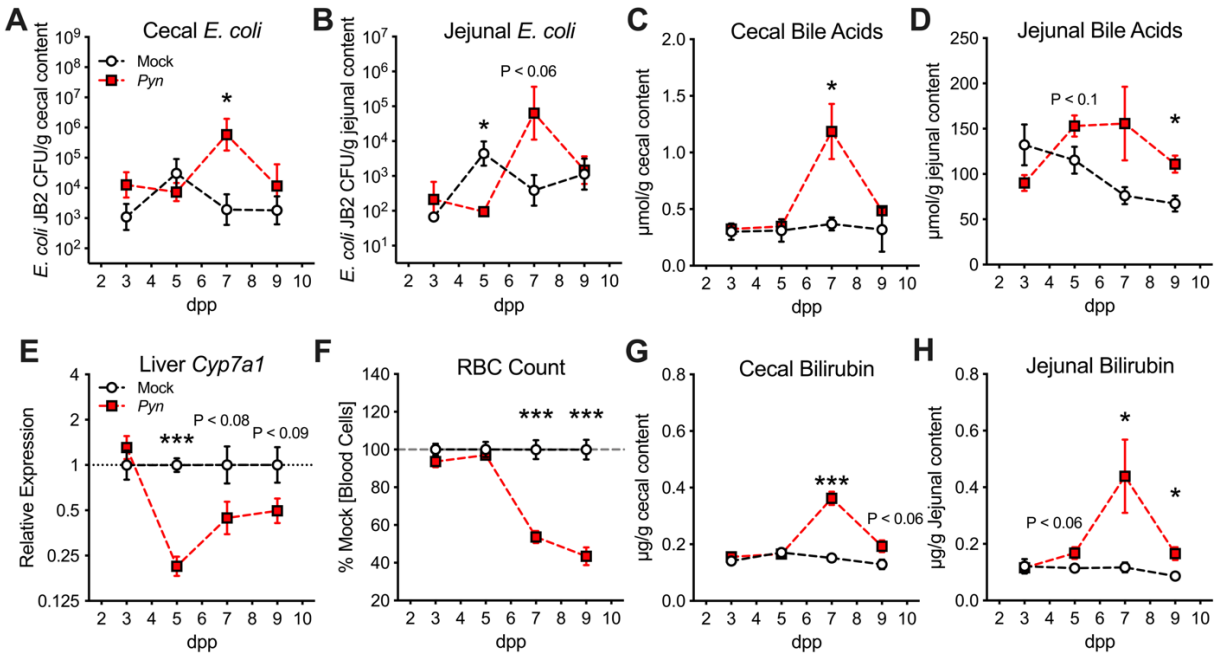

Figure 4.6. Impact of *Pyn* infection on levels of bile components in the intestinal lumen. Groups of mice (C57BL/6J) were pre-colonized with *E. coli* JB2 4 days prior to infection with $1x10^7$ iRBCs *Pyn* or Mock-infected with diluted control blood, i.p. Mice from each group (n = 4) were necropsied at indicated time points for collection of cecal content, small intestinal (jejunal) content, and liver tissues for measurements of: (A) JB2 levels in the cecal content, (B) JB2 levels in the jejunal content, (C) total bile acid levels in the cecal content, (D) total bile acid levels in the jejunal content, (E) relative expression of *Cyp7a1* transcripts in the liver tissues, (F) relative circulating blood cell counts, (G) bilirubin levels in the cecal content, and (H) bilirubin levels in the jejunal content. Symbols represent the group mean±SEM of data (Log_{10}-normalized for JB2 levels and Log_2-normalized for relative expression). Dashed lines connect similar groups (mock or *Pyn*) to better represent trends over time, but data at each time point do not come from the same set of mice. Statistical comparisons between data from groups euthanized at the

same time points were made by Welch's *t*-test, with significance indicated over time-matched data points. *P ≤ 0.05, ***P ≤ 0.001. No asterisk denotes differences between groups at that time point were not significant (P > 0.1).

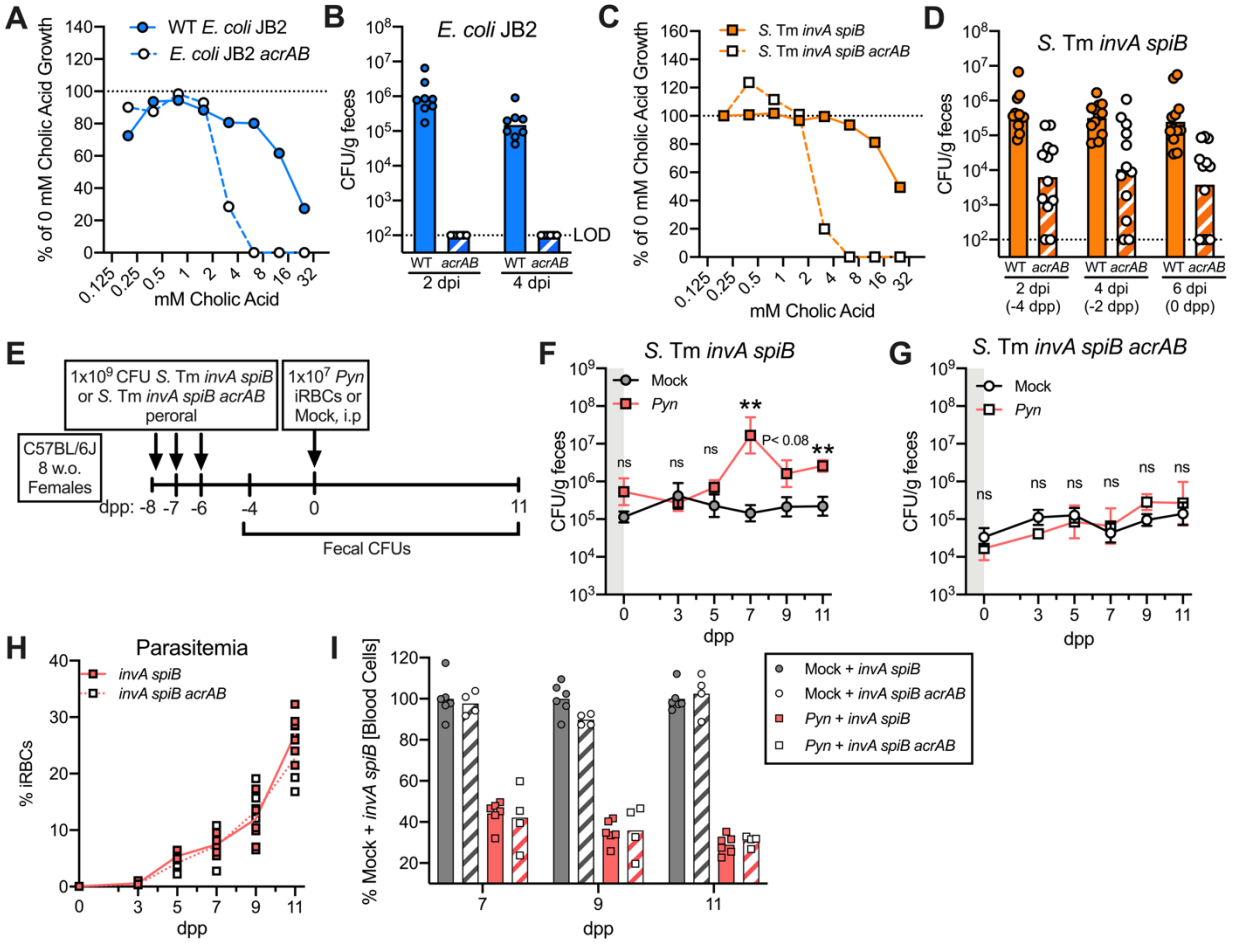

Figure 4.7. *Enterobacteriaceae acrAB* efflux pump mutants are sensitive to bile acids and do not expand in the gut during *Pyn* infection. (A) Growth of *E. coli* JB2 and an *E. coli* JB2 *acrAB* mutant after 6 h at 37°C in LB supplemented with cholic acid at indicated concentrations (0.195 mM to 25 mM) relative to the strain's growth in LB without cholic acid. (B) Fecal levels of *E. coli* JB2 and the *acrAB* mutant at 2- and 4-days post-inoculation (inoculation was 3 consecutive days of 1x10^9 CFU, peroral). Line labeled LOD indicates the limit of detection, 100 CFU/g content. (C) Growth of avirulent *S.* Typhimurium (*S.* Tm) *invA spiB* and a *S.* Tm *invA*

spiB acrAB mutant after 6 h at 37°C in LB supplemented with cholic acid at indicated concentrations (0.195 mM to 25 mM) relative to the strain's growth in LB without cholic acid. (D) Fecal levels of *S.* Tm *invA spiB* the *acrAB* mutant at 2-, 4-, and 6-days post-inoculation (inoculation was 3 consecutive days of $1x10^9$ CFU, peroral). Horizontal line labeled indicates the limit of detection, 100 CFU/g content. (E) Diagram of experiments presented in (D) through (I). Mice were orally inoculated on 3 consecutive days with $1x10^9$ CFU of either *S.* Tm *invA spiB* or the *S*. Tm *invA spiB acrAB* mutant, ending 6 days prior to infection with $1x10^7$ iRBCs *Pyn* or Mock-infected with diluted control blood, i.p. The *acrAB* was not detected in 4 mice (2 each from the mock- and *Pyn*-infected groups), which were subsequently removed from the analysis. (F) Fecal shedding of *S.* Tm *invA spiB* during mock or *Pyn* infection. Symbols represent the mean±SEM of Log_{10}-normalized data from n = 6 mice in each group. (G) Fecal shedding of *S.* Tm *invA spiB acrAB* during mock or *Pyn* infection. Symbols represent the mean±SEM of Log_{10}-normalized data from n = 4 mice in each group. (H) Parasite burden (percent *Plasmodium*-infected RBCs) in *Pyn* infected mice colonized with either the *S.* Tm *invA spiB* or *S.* Tm *invA spiB acrAB*. Symbols represent relative in individual mice. (I) Circulating blood cell counts relative to average levels in mock-infected mice colonized with *S.* Tm *invA spiB* at each time point (7, 9, and 11 dpp). Symbols in bar graphs represent data from individual mice, while bars indicate the means. For (F) and (G), statistical comparisons between data from groups at matched time points were made by Welch's *t*-test, with significance indicated over time-matched data points. **P ≤ 0.01, "ns" denotes differences between groups at that time point were not significant (P > 0.1).

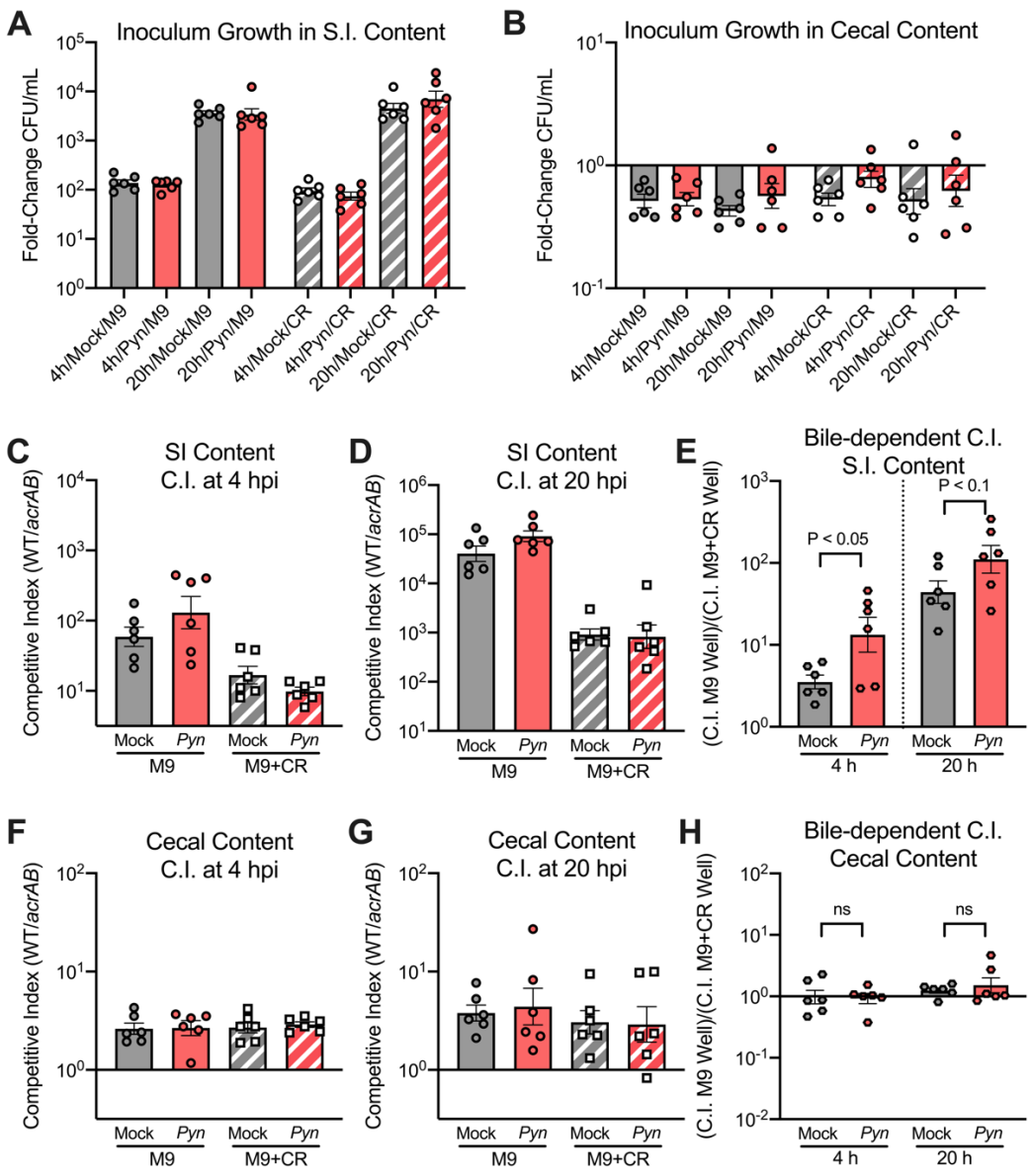

Figure 4.8. *Ex vivo* growth of wildtype *E. coli* and an *acrAB* mutant in intestinal contents of mock- and *Pyn*-infected mice. Intestinal content (cecal and whole small intestinal content) from individual mock- and *Pyn*-infected C57BL/6J mice was collected at 7 dpp and homogenized in either M9 minimal media or M9 with cholestyramine resin (CR, 1% w/v). Equivalently diluted content samples were inoculated with a competitive infection containing equal amounts of *E. coli* JB2 wildtype and *E. coli* JB2 *acrAB*, then incubated at 37°C and sampled at 4 h and 20 h to assess relative growth of the *E. coli* strains in the content *ex vivo*.

(A) Overall fold-change in wildtype JB2 CFUs in diluted small intestinal content. (B) Overall fold-change in wildtype JB2 CFUs in diluted cecal content. (C) Competitive index (wildtype JB2:*acrAB* mutant CFUs corrected to the inoculum ratio) in diluted small intestinal content sampled at 4 hour post-inoculation. (D) Competitive index (wildtype JB2:*acrAB* mutant CFUs corrected to the inoculum ratio) in diluted small intestinal content sampled at 20 hour post-inoculation. (E) The relative contribution of bile acids to the competitive index, calculated by dividing the competitive index in wells containing small intestinal content + M9 alone by the index from matched wells containing content from the same mouse treated with CR for bile sequestration. (F) Competitive index in diluted cecal content sampled 4 h post-inoculation. (G) Competitive index in diluted cecal content sampled at 20 h post-inoculation. (H) The relative contribution of bile acids to the competitive index, calculated by dividing the competitive index in wells containing cecal content + M9 alone by the index from matched wells containing content from the same mouse treated with CR for bile sequestration. Symbols represent data from diluted content collected from individual mice, while bars indicate the means of Log_{10}-normalized data. For (E) and (H), statistical comparisons between data from groups at matched time points were made by Welch's *t*-test. "ns" denotes differences between groups were not significant ($P > 0.1$).

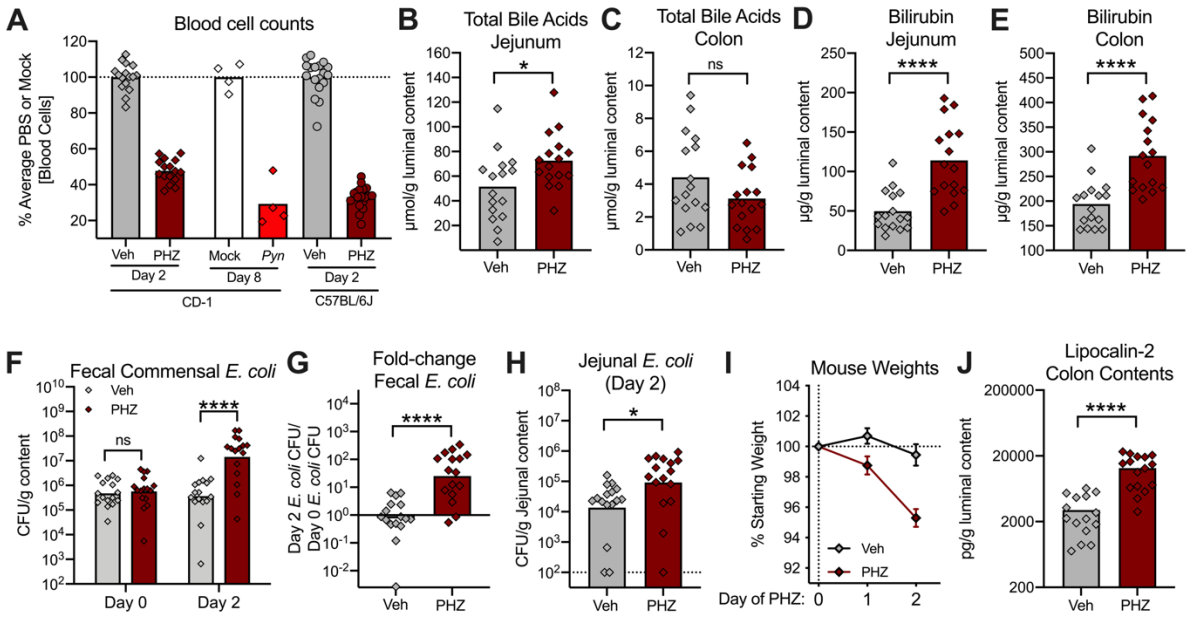

Figure 4.9. Phenylhydrazine treatment rapidly induces severe hemolytic anemia, changes in bile constituent levels, and gut *E. coli* expansion. (A) Circulating blood cell counts in CD-1 and C57BL/6J mice after either 2 days of phenylhydrazine administration (PHZ, 0.1 mL of 10 mg/mL in dPBS) or in CD-1 mice on day 8 of *Pyn* infection, relative to counts in control (vehicle or mock-treated) mice. Various measures were taken from the CD-1 mice during PHZ treatment, including: (B) total bile acids in jejunal content, (C) total bile acids in colon content, (D) bilirubin in the jejunum, (E) bilirubin in the colon, (F) endogenous *E. coli* in the feces before and after treatment, (G) calculated change in *E. coli* levels of each mouse after treatment, (H) endogenous *E. coli* in the jejunum after treatment, (I) mouse weights throughout the treatment, and (J) Lipocalin-2 levels in the colon content after treatment. PHZ data from CD-1 mice are combined from 2 separate experiments with n = 8 mice in each treatment group (n = 16 mice per group total). *Pyn* data from CD-1 mice are from a single experiment with n = 4 mice per group. PHZ data from C57BL/6J mice come from 2 separate experiments with a total of n = 18 mice total in each group; further data from this experiment is presented in Fig. 4.11. Symbols represent data from individual mice, and bars represent the mean, except in (I) where symbols represent the mean±SEM at different time points. Statistical comparisons between data were

made by Welch's *t*-test for Log-normalized data (F-H) and Mann-Whitney test for other types of data. *P ≤ 0.05, ****P ≤ 0.0001; "ns" denotes differences between compared groups were not significant (P > 0.1).

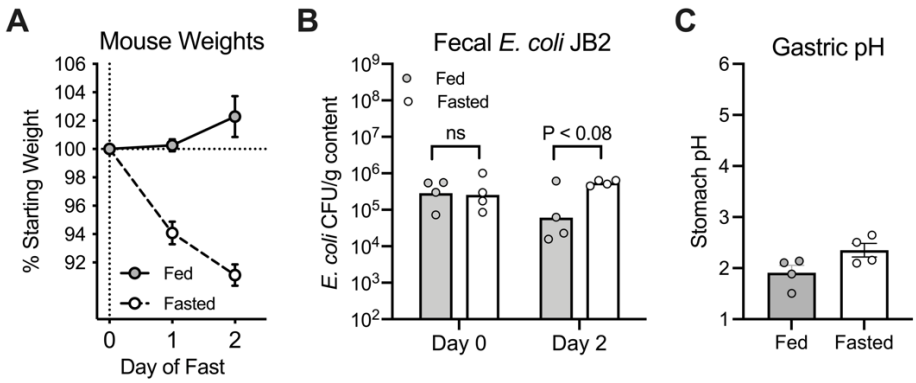

Figure 4.10. Impact of acute reduction in food intake on the gut *E. coli* load. C57BL/6J were pre-colonized for 9 days with *E. coli* JB2. One set of mice was fasted overnight, then given equivalent food to amounts consumed by *Pyn*-infected mice around 6 dpp (100 µg/g mouse/day) for one day. (A) Changes in mouse weights in fed and food-restricted ("Fasted") mice over the experiment. Symbols represent the mean±SEM at different time points (n = 4 mice per group). (B) Fecal shedding of *E. coli* JB2 before and after the fast. (C) Gastric pH of mice after the fast. Symbols represent data from individual mice, with bars representing the mean. Statistical comparisons between data were made by Welch's *t*-test, with P-values as indicated; "ns" denotes differences between compared groups were not significant (P > 0.1).

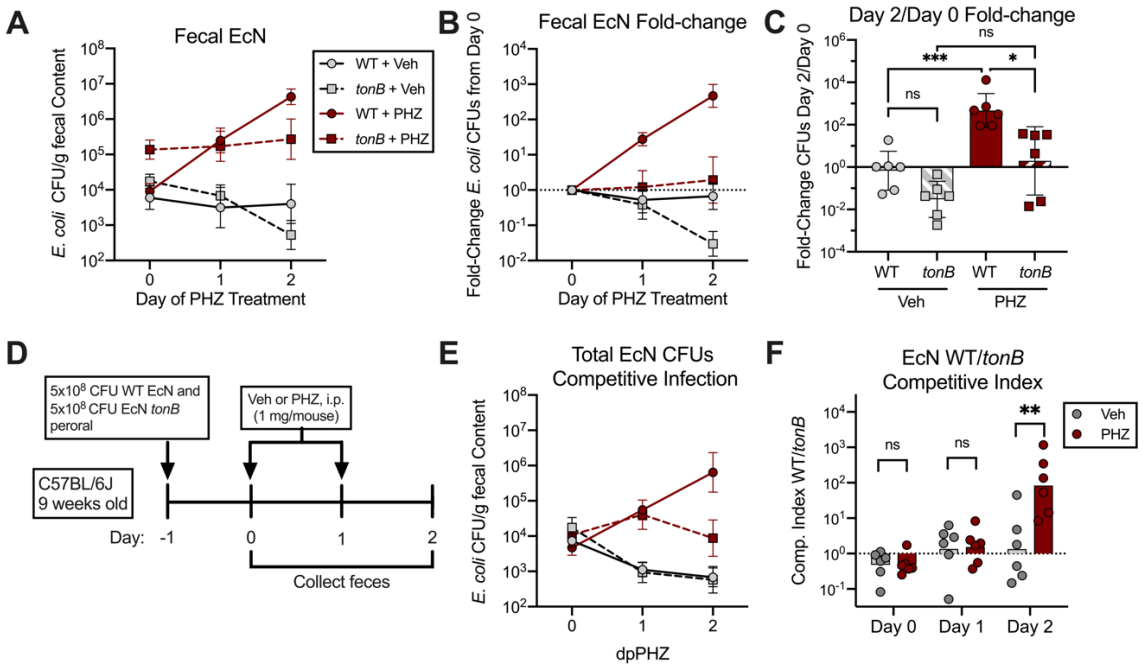

Figure 4.11. *E. coli* Nissle 1917 iron uptake mutants display deficiencies in the intestines during PHZ-induced severe anemia. (A to C) C57BL/6J mice (n = 6 per group) were orally inoculated with $1x10^9$ CFU of wildtype *E. coli* Nissle 1917 (WT) or an *E. coli* Nissle 1917 *tonB*-deficient siderophore uptake mutant (*tonB*) 1 day prior to treatment with either PHZ or vehicle (dPBS) for 2 days. (A) EcN levels detected in the feces through the treatment. (B) EcN levels relative to pre-PHZ treatment levels through the treatment. (C) Fold-change in EcN levels from Day 0 to Day 2 of PHZ treatment for comparisons. (D) Diagram outlining competitive infection of wildtype EcN and EcN *tonB* used for data in (E) and (F). (E) EcN WT (circles) and *tonB* (squares) detected in the feces of vehicle (gray) and PHZ-treated (red) mice at indicated time points. (F) Competitive index of EcN WT:EcN *tonB* in the feces at indicated time points. Symbols represent the mean±SEM of Log_{10}-normalized data for figures (A), (B), and (E). In (C) and (F), symbols represent data from individual mice and bars represent the mean of Log_{10}-normalized data. Statistical comparisons between groups were made by Welch's *t*-test. *P ≤ 0.05, **P ≤ 0.01, ***P ≤ 0.001; "ns" denotes differences between compared groups were not significant (P > 0.1).

Name in this study	Strain Designation	Genotype	Source or Reference
Escherichia coli JB2	JB2	Endogenous *E. coli* strain isolated from laboratory mice	PMID: 24508234
E. coli JB2 *acrAB*	GTW308	*acrAB*::*bla* ($Carb^R$)	This study
E. coli Nissle 1917	CAL225	pCAL62 ($Carb^R$ $Strep^R$)	PMID: 23820397
E. coli Nissle 1917 ΔNR3	CAL222	Δ*narG* Δ*napA* Δ*narZ* + pCAL61 (Kan^R $Strep^R$)	PMID: 23820397
E. coli Nissle 1917 *tonB*	ED50	Δ*tonB* (+230 to +1033)::Cm^R)	PMID: 23870311
S. Typhimurium *invA spiB*	FF459	Δ*invA* Δ*spiB phoN*::KSAC	Ch.2, Table 2.2
S. Typhimurium *invA spiB acrAB*	GTW61	IR715 Δ*invA* Δ*spiB phoN*::*Tn10d-Cm acrAB*::*bla* ($Carb^R$)	This Study

Table 4.1. Bacterial strains used in this study.

Chapter 5

Summary and Future Directions

In parts of sub-Saharan Africa, non-typhoidal *Salmonella* (NTS) serovars such as *S.* Typhimurium has been frequently isolated from disseminated infections and bacteremia, a comparatively rare outcome of NTS infection in western countries (*1, 2*). Common bloodstream isolates of *S.* Typhimurium in Africa appear to form a distinct clade (ST313) that displays significant antibiotic resistance as well as genetic and phenotypic hallmarks of adaptation to an invasive infection lifestyle that could be evidence of evolution towards human-restricted pathogenesis (*3, 4*). However, epidemiological research has also consistently identified HIV, malnutrition, and concurrent or recent malaria in children as significant risk factors for developing such "invasive" NTS disease (*2, 5, 6*).

Studies investigating how underlying risk factors contribute to iNTS risk have shown that heme oxygenase (HO-1) activation and IL-10 signaling during infection with the malarial parasite *Plasmodium* blunt innate anti-*Salmonella* immune responses and interfere with the ability of macrophages and neutrophils to clear extraintestinal *Salmonella* in mouse and non-human primate models (*7-9*). Additionally, intestinal responses to the bloodborne parasite can inhibit normal epithelial barrier functions producing a "leaky gut" and appear to yield compositional shifts in commensal gut microbial communities associated with reduced colonization resistance against potential enteric pathogens such as *S.* Typhimurium and *E. coli* in co-infected mice (*10-12*).

My dissertation research has focused on better understanding the latter impact of *Plasmodium* infection and hemolysis on the implantation of enteric infections and enrichment of endogenous *Enterobacteriaceae* in the gut. Through these studies, we found that *P. yoelii* infection reshapes the murine intestinal environment to the benefit of ingested pathogens and

endogenous *Enterobacteriaceae*. *P. yoelii* infection triggers a sustained, TNF-α-dependent hypochlorhydria that reduced the killing of inoculated *S.* Typhimurium in the stomach. However, reduced gastric acidity alone was insufficient to explain the bloom of endogenous *E. coli* in the intestine despite occurring in parallel to the onset of hypochlorhydria during the parasite infection. Instead, evidence point to hemolysis-associated changes in the intestinal environment- namely, alterations in bile composition or levels of bile acids and iron accessibility- providing benefits to *Enterobacteriaceae* with the ability to resist such antimicrobial defenses and better compete with the endogenous microbial flora. Taken together, these data suggest a model whereby immune responses to *Plasmodium* infection and the associated severe hemolysis can enhance susceptibility to the initial intestinal colonization of enteric pathogens while concurrently promoting the outgrowth of endogenous direct competitors for their preferred intestinal niches (modeled in Fig. 5.1). It seems possible that this situation selects for the evolutionary success of strains such as the ST313 lineages, better adapted to opt out of competition in the gut via rapid systemic dissemination and extraintestinal survival (*13, 14*).

Plasmodium-enhanced implantation of *S.* Typhimurium

The effects of *P. yoelii* on the C57BL/6 mouse intestinal environment were surveyed using a combination of 16S rRNA sequence microbiota analysis paired with untargeted metabolomics on soluble metabolites. Although a number of shifts in microbial abundance at day 6 of *P. yoelii* infection could be attributed to the parasite (Fig. 2.6 to 2.8), none appeared to strongly correlate with the relative levels of *S.* Typhimurium colonizing the intestine 24 hours later (Fig. 2.9). The untargeted metabolomics study yielded even fewer positive hits (Fig. 2.10). While an increased inflammatory tone to the intestine with *P. yoelii* infection had been previously reported (*12*), our hypothesis-driven approach found that molecules known to fuel *S.* Typhimurium colonization during inflammation (respiratory electron acceptors and iron) could not explain differential colonization of *P. yoelii*-infected mice (Fig. 2.11 and 3.1). Ultimately, it

became clear that the enhancement of implantation was independent of intestinal replication (Fig. 3.2) and was primarily due to parasite-related hypochlorhydria decreasing gastric killing (Fig. 3.3), since stimulation of gastric acid secretion using a H2R agonist rescued gastric acidity and limited *S.* Typhimurium colonization. TNF-α antibody blockade also abrogated hypochlorhydria and reduced implantation, linking the gastric effect to the cytokine response to *Plasmodium*.

It is still uncertain to what degree the observed changes in microbiota truly do contribute to increasing implantation. It seems that the effect might be fairly small, but notably, omeprazole treatment alone enhanced *S.* Typhimurium colonization levels but was not sufficient to fully mimic the impact of *P. yoelii* on *S.* Typhimurium implantation, suggesting there could be additional killing effects requiring *P. yoelii* co-infection to avoid. It is also unclear whether the development of gastric acidity impacts the parasite. Inducing gastric acid secretion directly did not have a notable impact on parasitemia, but TNF-α blockade increased circulating burden. Since TNF-α has been linked to limiting parasite replication, it seems that contributing to hypochlorhydria could be an off-target effect of the anti-*Plasmodium* response (*15*). Hypochlorhydria could rescue NTS transmission in malaria-endemic populations, where the lack of inflammation-driven intestinal growth might mean the pathogen is shed at significantly lower levels. As this response is also linked to a reduced consumption of food, it also suggests that while implantation of foodborne infections might be enhanced, overall behavioral changes could make ingesting contaminated food less likely. *S.* Typhimurium are actually known to encode virulence factors (SlrP) that counteract inflammatory responses inhibiting feeding behavior, which reduces *S.* Typhimurium virulence and enhance host survival to improve transmission (*16*). This suggests that reduced feeding behaviors during malaria could select for NTS modified for disseminated infection lifestyles, perhaps contributing to the generation of extraintestinal-adapted African bloodstream ST313 isolates.

Plasmodium*-associated expansion of endogenous *Enterobacteriaceae

The expansion of *Proteobacteria*, specifically members of the order *Enterobacterales*, has been identified as a microbial signature of gut dysbiosis linked to many intestinal diseases (*17, 18*). Mice infected with *P. yoelii* likewise developed higher levels of intestinal *E. coli* when colonized with it (Fig. 2.6 and 4.1), which could not be explained by the induction of hypochlorhydria (Fig. 4.2) or inflammatory production of nitric oxide generating nitrate for anaerobic respiratory growth in the gut lumen (Fig. 4.4 and 4.5) (*19*). Further characterization found that bile acids and bile pigment were often altered in intestinal concentration by the parasite infection (Fig. 4.6). A bile acid-sensitive *acrAB* mutant in a *S.* Typhimurium *invA spiB* background did not appreciably expand in the intestines of *P. yoelii* co-infected mice while the bile acid-resistant wildtype strain did (Fig. 4.7), and in an *ex vivo* competitive growth assay in intestinal content from healthy and *P. yoelii*-infected mice, an *E. coli* JB2 *acrAB* mutant displayed a slightly higher bile-dependent competitive defect in *P. yoelii*-associated small intestinal content (Fig. 4.8). Induction of hemolysis using phenylhydrazine also caused intestinal *E. coli* outgrowth and was associated with increasing concentrations of bile components (Fig. 4.9). Additionally, phenylhydrazine treatment was linked to the stimulation of Lipocalin-2 production and *E. coli* growth benefits from the treatment were found to depend on siderophore-related iron acquisition (Fig. 4.11). Although *P. yoelii* infection had also been found to increase intestinal Lcn2 levels (Fig. 2.11) and induce other metal-sequestration responses such as calprotectin (*12, 20*), it is still unknown whether these nutritional immunity responses contribute to the expansion of resistant *E. coli* during parasite infection. However, it seems probable that hemolytic anemia in both models is promoting iron sequestration responses, which suggests a shared mechanism generating *E. coli* blooms. Taken together, these results indicate that shifts in bile composition and iron levels or availability (Fe^{2+} versus Fe^{3+}) in the intestinal content could select for and contribute to the bloom of *Enterobacteriaceae* species during *P. yoelii* infection.

It is likely that systemic iron sequestration acute phase responses have evolved to protect the host during hemolytic crises by limiting the access of bloodborne extracellular bacterial pathogens to serum iron (*21*). However, iron-limiting responses by erythrophagocytic macrophages during *P. yoelii* infections in mice have been shown to benefit extraintestinal NTS inside iron-overloaded macrophages (*22*), suggesting such responses may be protective in some circumstances and actually detrimental in others. TonB-dependent enterobactin-Fe^{3+} or salmochelin-Fe^{3+} uptake by *Enterobacteriaceae* have been shown to only benefit the bacteria in iron-limited conditions (*23*), indicating hemolysis may generate sufficient iron limitation to promote this competitive edge. The impacts of hemolysis and *P. yoelii* on bile components are more variable but also seem to contribute to the outgrowth of resistant *Enterobacteriaceae*. The utilization of bile sequestrant in the mouse chow may help determine the relative influence of bile components on the bloom. It has actually been previously shown that endogenous *E. coli* can help protect from *S.* Typhimurium colonization when bile acid levels are heightened by competing for the bile-resistant niche in the gut (*24*), suggesting a bloom in *E. coli* could improve colonization resistance to related pathogenic bacteria.

Future Directions and Perspectives

These studies have broadened our understanding of the impact *Plasmodium* can have on a mammalian host that significantly enhances susceptibility to enteric bacterial infections. It is unclear whether successfully limiting the intestinal colonization of NTS during malaria would actually reduce iNTS incidents associated with the parasite, though. Once it gets past the gastric acid and AMP defenses of the stomach and upper small intestine, NTS would normally have to overcome microbiota-associated colonization resistance for luminal growth and transmission. However, NTS may better succeed in the *Plasmodium*-infected host by “opting out” and disseminating to systemic tissues, as a “leaky” gut epithelial barrier and immune suppression from the parasite may favor pathogen populations outside the gut. The genetic

changes displayed by ST313 isolates- increased disseminating potential, reduced immune activation, and degradation of components involved in intestinal metabolism- reflect this selective pressure for an extraintestinal lifestyle.

Whether the effects of *Plasmodium* on the gut environment apply to cases of human malaria remains to be evaluated. To our knowledge, clinical research has not associated malaria with increased stomach pH or significant changes in the gut microbiome, though few studies have attempted either (*25*). Based on the mechanisms we have uncovered in the mice, however, these physiological changes during human malaria seem plausible. TNF-α is a normal response to *P. falciparum* infection in humans, and SNPs in TNF-α and its promoter region can impact the outcomes of malaria (*15, 26*). Thus, it seems possible that the hypochlorhydria in response to TNF-α is also shared. Assuming reductions in gastric acidity can also occur in human malaria, precautionary treatment of the hypochlorhydria to prevent enteric infection is unlikely to be tested, as currently few pharmacological options for acidifying the stomach exist. Targeting the TNF-α response during malaria is complex, as it has been shown to be involved in both parasite killing and the development of severe disease (*15*). Additionally, TNF-α is critical in mucosal defense against NTS (*27, 28*), so blockade of this signaling pathway would likely promote invasive infections. Proton pump inhibitors are regularly prescribed for treatment of the overproduction of gastric acid, but proton pump stimulants are not generally used for hypochlorhydria, despite the known link between high gastric pH and enteric disease. In some trials, a supplement called betaine hydrochloride has been used to successfully transiently acidify the stomach to the uptake of weakly basic medications in volunteers with rabeprazole-induced hypochlorhydria (*29*), which could potentially be used prophylactically before meals during malaria. On the other hand, the hypochlorhydria response could ultimately be protective for the infected host- perhaps somehow limiting the severity of malaria for reasons that future studies could untangle.

These findings also suggest that utilizing probiotic competitors such as *E. coli* Nissle 1917 that can fill nutrient niches in the gut that open during malaria might be a viable method to limit colonization of pathogenic *Enterobacteriaceae* (*23, 30*). However, this strain has also been potentially linked to colibactin-associated genotoxicity and tumorigenicity (*31, 32*), though targeting of relevant mechanisms (i.e., siderophore uptake) could be a reasonable alternative approach (*33, 34*). This could also be beneficial as *Enterobacteriaceae* with significant antibiotic resistance, including to carbapenem antibiotics, circulate worldwide. In addition, human commensal *Enterobacteriaceae* may already fill this colonization resistance role of niche pre-emption, as they have been shown capable of doing in mouse models (*35*). Future studies could help characterize how the presence or absence of certain *Enterobacteriaceae* impacts colonization resistance against NTS during malaria or hemolysis over a longer period than 24 hours.

The use of antiretroviral therapy for HIV has successfully limited the co-occurrence of *Salmonella* bacteremia and mortalities (*36*), vitamin supplementation for micronutrient deficiencies shows promise in correcting immune dysfunction (*37*), and drops in malaria transmission have been correlated with a reduction in pediatric iNTS disease (*38-40*). Direct vaccination against relevant iNTS-associated strains has also been suggested, as the development of antibody responses to NTS is linked to reduced disease incidence (*2*). However, it is possible such vaccines will be less effective in patients with underlying HIV or malaria due to immune suppression (*41*). Rapid detection and resistance profiling of invasive bacterial infections when they occur can also help determine appropriate antibiotic regimens (*42*). Antimalarial drugs and upcoming vaccines with potentially high efficacy are likely to further reduce African malaria rates (*43*), which will hopefully reduce childhood iNTS burden. Better understanding the ways comorbidities contribute to iNTS and other invasive infections will allow for targeted approaches to treatments and prevention efforts that best fit the local demands.

REFERENCES

1. A. L. Walsh, A. J. Phiri, S. M. Graham, E. M. Molyneux, M. E. Molyneux, Bacteremia in febrile Malawian children: clinical and microbiologic features. *Pediatr Infect Dis J* **19**, 312-318 (2000).
2. J. J. Gilchrist, C. A. MacLennan, Invasive Nontyphoidal Salmonella Disease in Africa. *EcoSal Plus* **8**, (2019).
3. N. A. Feasey, G. Dougan, R. A. Kingsley, R. S. Heyderman, M. A. Gordon, Invasive non-typhoidal salmonella disease: an emerging and neglected tropical disease in Africa. *Lancet* **379**, 2489-2499 (2012).
4. C. V. Pulford *et al.*, Stepwise evolution of Salmonella Typhimurium ST313 causing bloodstream infection in Africa. *Nat Microbiol* **6**, 327-338 (2021).
5. R. N. Bronzan *et al.*, Bacteremia in Malawian children with severe malaria: prevalence, etiology, HIV coinfection, and outcome. *J Infect Dis* **195**, 895-904 (2007).
6. T. T. Ao *et al.*, Global burden of invasive nontyphoidal Salmonella disease, 2010(1). *Emerg Infect Dis* **21**, (2015).
7. A. J. Cunnington, J. B. de Souza, M. Walther, E. M. Riley, Malaria impairs resistance to Salmonella through heme- and heme oxygenase-dependent dysfunctional granulocyte mobilization. *Nat Med* **18**, 120-127 (2011).
8. K. L. Lokken *et al.*, Malaria parasite infection compromises control of concurrent systemic non-typhoidal Salmonella infection via IL-10-mediated alteration of myeloid cell function. *PLoS Pathog* **10**, e1004049 (2014).
9. J. P. Mooney *et al.*, The mucosal inflammatory response to non-typhoidal Salmonella in the intestine is blunted by IL-10 during concurrent malaria parasite infection. *Mucosal Immunol* **7**, 1302-1311 (2014).

10. J. Y. Chau *et al.*, Malaria-associated L-arginine deficiency induces mast cell-associated disruption to intestinal barrier defenses against nontyphoidal Salmonella bacteremia. *Infect Immun* **81**, 3515-3526 (2013).
11. R. A. Potts *et al.*, Mast cells and histamine alter intestinal permeability during malaria parasite infection. *Immunobiology* **221**, 468-474 (2016).
12. J. P. Mooney *et al.*, Inflammation-associated alterations to the intestinal microbiota reduce colonization resistance against non-typhoidal Salmonella during concurrent malaria parasite infection. *Sci Rep* **5**, 14603 (2015).
13. S. E. Carden *et al.*, Pseudogenization of the Secreted Effector Gene sseI Confers Rapid Systemic Dissemination of S. Typhimurium ST313 within Migratory Dendritic Cells. *Cell Host Microbe* **21**, 182-194 (2017).
14. D. L. Hammarlof *et al.*, Role of a single noncoding nucleotide in the evolution of an epidemic African clade of Salmonella. *Proc Natl Acad Sci U S A* **115**, E2614-E2623 (2018).
15. L. M. Randall, C. R. Engwerda, TNF family members and malaria: old observations, new insights and future directions. *Exp Parasitol* **126**, 326-331 (2010).
16. S. Rao *et al.*, Pathogen-Mediated Inhibition of Anorexia Promotes Host Survival and Transmission. *Cell* **168**, 503-516 e512 (2017).
17. N. R. Shin, T. W. Whon, J. W. Bae, Proteobacteria: microbial signature of dysbiosis in gut microbiota. *Trends Biotechnol* **33**, 496-503 (2015).
18. A. W. L. Rogers, R. M. Tsolis, A. J. Baumler, Salmonella versus the Microbiome. *Microbiol Mol Biol Rev* **85**, (2021).
19. S. E. Winter *et al.*, Host-derived nitrate boosts growth of E. coli in the inflamed gut. *Science* **339**, 708-711 (2013).
20. J. Z. Liu *et al.*, Zinc sequestration by the neutrophil protein calprotectin enhances Salmonella growth in the inflamed gut. *Cell Host Microbe* **11**, 227-239 (2012).

21. M. Nairz, G. Weiss, Iron in infection and immunity. *Mol Aspects Med* **75**, 100864 (2020).

22. K. L. Lokken, A. R. Stull-Lane, K. Poels, R. M. Tsolis, Malaria Parasite-Mediated Alteration of Macrophage Function and Increased Iron Availability Predispose to Disseminated Nontyphoidal Salmonella Infection. *Infect Immun* **86**, (2018).

23. E. Deriu *et al.*, Probiotic bacteria reduce salmonella typhimurium intestinal colonization by competing for iron. *Cell Host Microbe* **14**, 26-37 (2013).

24. S. Y. Wotzka *et al.*, Escherichia coli limits Salmonella Typhimurium infections after diet shifts and fat-mediated microbiota perturbation in mice. *Nat Microbiol* **4**, 2164-2174 (2019).

25. M. M. Ippolito, J. E. Denny, C. Langelier, C. L. Sears, N. W. Schmidt, Malaria and the Microbiome: A Systematic Review. *Clin Infect Dis* **67**, 1831-1839 (2018).

26. W. L. Mandala *et al.*, Cytokine Profiles in Malawian Children Presenting with Uncomplicated Malaria, Severe Malarial Anemia, and Cerebral Malaria. *Clin Vaccine Immunol* **24**, (2017).

27. P. Everest, M. Roberts, G. Dougan, Susceptibility to Salmonella typhimurium infection and effectiveness of vaccination in mice deficient in the tumor necrosis factor alpha p55 receptor. *Infect Immun* **66**, 3355-3364 (1998).

28. A. Vazquez-Torres, G. Fantuzzi, C. K. Edwards, 3rd, C. A. Dinarello, F. C. Fang, Defective localization of the NADPH phagocyte oxidase to Salmonella-containing phagosomes in tumor necrosis factor p55 receptor-deficient macrophages. *Proc Natl Acad Sci U S A* **98**, 2561-2565 (2001).

29. M. R. Yago *et al.*, Gastric reacidification with betaine HCl in healthy volunteers with rabeprazole-induced hypochlorhydria. *Mol Pharm* **10**, 4032-4037 (2013).

30. M. Sassone-Corsi *et al.*, Microcins mediate competition among Enterobacteriaceae in the inflamed gut. *Nature* **540**, 280-283 (2016).

31. S. Dubbert, B. Klinkert, M. Schimiczek, T. M. Wassenaar, R. V. Bunau, No Genotoxicity Is Detectable for Escherichia coli Strain Nissle 1917 by Standard In Vitro and In Vivo Tests. *Eur J Microbiol Immunol (Bp)* **10**, 11-19 (2020).

32. S. A. Cevallos *et al.*, Increased Epithelial Oxygenation Links Colitis to an Expansion of Tumorigenic Bacteria. *mBio* **10**, (2019).

33. M. Sassone-Corsi *et al.*, Siderophore-based immunization strategy to inhibit growth of enteric pathogens. *Proc Natl Acad Sci U S A* **113**, 13462-13467 (2016).

34. W. Neumann, M. Sassone-Corsi, M. Raffatellu, E. M. Nolan, Esterase-Catalyzed Siderophore Hydrolysis Activates an Enterobactin-Ciprofloxacin Conjugate and Confers Targeted Antibacterial Activity. *J Am Chem Soc* **140**, 5193-5201 (2018).

35. E. M. Velazquez *et al.*, Endogenous Enterobacteriaceae underlie variation in susceptibility to Salmonella infection. *Nat Microbiol* **4**, 1057-1064 (2019).

36. N. A. Feasey *et al.*, A reduction in adult blood stream infection and case fatality at a large African hospital following antiretroviral therapy roll-out. *PLoS One* **9**, e92226 (2014).

37. A. R. Stull-Lane *et al.*, Vitamin A supplementation boosts control of antibiotic-resistant Salmonella infection in malnourished mice. *PLoS Negl Trop Dis* **14**, e0008737 (2020).

38. G. Mackenzie *et al.*, A decline in the incidence of invasive non-typhoidal Salmonella infection in The Gambia temporally associated with a decline in malaria infection. *PLoS One* **5**, e10568 (2010).

39. J. A. Scott *et al.*, Relation between falciparum malaria and bacteraemia in Kenyan children: a population-based, case-control study and a longitudinal study. *Lancet* **378**, 1316-1323 (2011).

40. N. A. Feasey *et al.*, Modelling the Contributions of Malaria, HIV, Malnutrition and Rainfall to the Decline in Paediatric Invasive Non-typhoidal Salmonella Disease in Malawi. *PLoS Negl Trop Dis* **9**, e0003979 (2015).

41. J. P. Mooney *et al.*, Transient Loss of Protection Afforded by a Live Attenuated Non-typhoidal Salmonella Vaccine in Mice Co-infected with Malaria. *PLoS Negl Trop Dis* **9**, e0004027 (2015).

42. R. Krumkamp *et al.*, Classification of invasive bloodstream infections and Plasmodium falciparum malaria using autoantibodies as biomarkers. *Sci Rep* **10**, 21168 (2020).

43. M. S. Datoo, Magloire Natama, H., Somé, A., Traoré, O., Rouamba, T., Bellamy, D., Yameogo, P., Valia, D., Tegneri, M., Ouedraogo, F., Soma, R., Sawadogo, S., Sorgho, F., Derra, K., Rouamba, E., Orindi, B., Ramos-Lopez, F., Flaxman, A., Cappuccini, F., Kailath, R., Elias, S.C., Mukhopadhyay, E., Noe, A., Cairns, M., Lawrie, A., Roberts, R., Valéa, I., Sorgho, H., Williams, N., Glenn, G., Fries, L., Reimer, J., Ewer, K.J., Shaligram, U., Hill, A.V.S., and Tinto, H. (Available at SSRN: https://ssrn.com/abstract=3830681 or http://dx.doi.org/10.2139/ssrn.3830681, 2021).

FIGURES

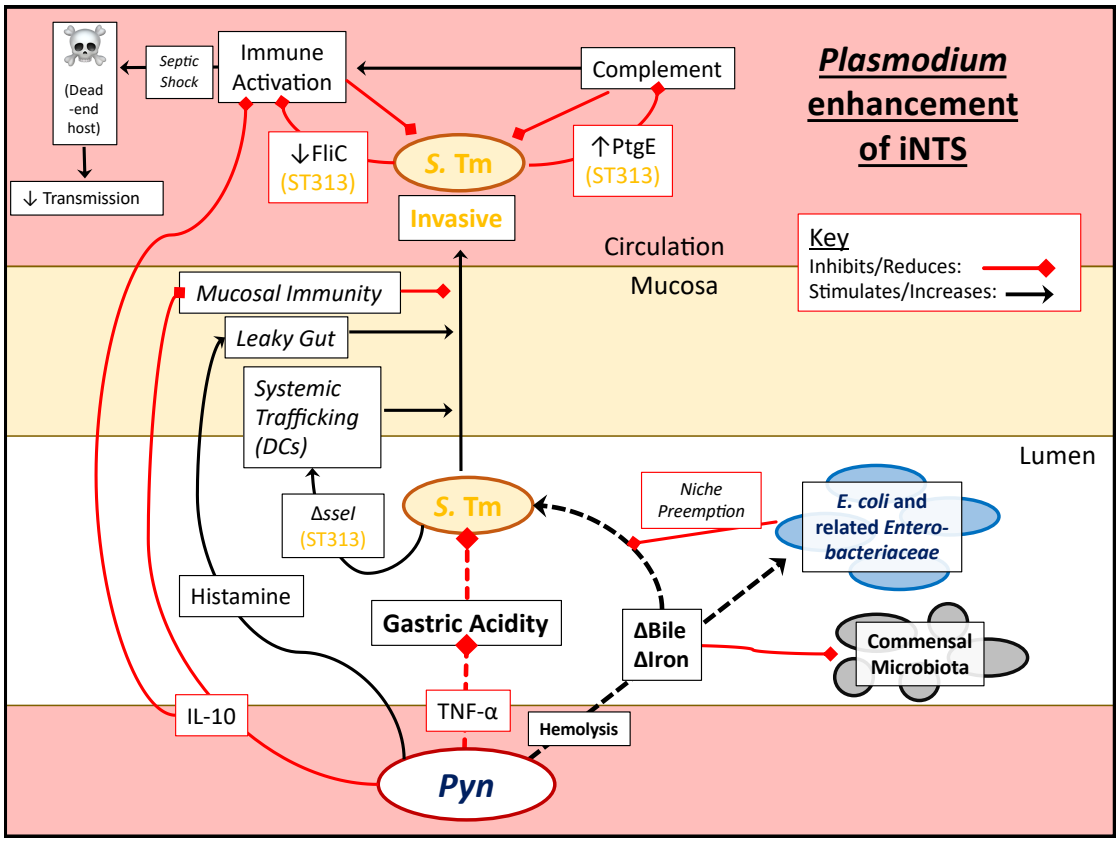

Figure 5.1. Model incorporating *Plasmodium yoelii*-associated susceptibility to NTS implantation and Enterobacteriaceae colonization into the context of enhanced iNTS infections. Dashed line interactions indicate mechanisms uncovered in this work, while whole lines indicate potential interactions with already published mechanisms. *Pyn*, *Plasmodium yoelii nigeriensis*. *S.* Tm, *Salmonella enterica* serovar Typhimurium.